

**SYNTHESIS AND CHARACTERIZATION OF β - CYCLODEXTRINE CAPPED
MAGNETIC NANOPARTICLES ANCHORED ON CELLULOSIC MATRIX
FOR REMOVAL OF HEXAVALENT CHROMIUM FROM MIMICKED
WASTEWATER**

LYNDA SAMATO MESOPPIRR

**RESEARCH THESIS SUBMITTED TO THE SCHOOL OF PURE AND APPLIED
SCIENCE IN PARTIAL FULFILLMENT FOR THE AWARD OF DOCTORATE
OF SCIENCE DEGREE IN CHEMISTRY.**

MAASAI MARA UNIVERSITY

2024

DECLARATION

This thesis is my original work and has not been presented for any degree in any other University.

Lynda Samato Mesoppirr

SP01/SP/MN/6448/2017

Signature..... Date.....

Declaration by supervisors:

This thesis has been submitted for examination with our approval as University supervisors.

Prof. OYARO NATHAN

Department of Mathematics and Physical Sciences,

Maasai Mara University, Kenya

Signature..... Date.....

Dr. OMWOYO WESLEY NYAIGOTI

Department of Mathematics and Physical Sciences,

Maasai Mara University, Kenya

Signature..... Date.....

Prof. SIMPHIWE NELANA

Biotechnology and Chemistry Department,

Vaal University of Technology

Signature..... Date.....

DEDICATION

I would like to dedicate this work to my beloved husband Roimen, parents Benson and Rosemary, my dear children Sancha, Ritei, Teyian and Meikan. Not forgetting my power siblings Senewa, Sankei, Mantai and Yiamiton.

ACKNOWLEDGMENTS

I would like to thank God for His mercies and the strength He granted me during this research.

Secondly, I would also like to acknowledge Maasai Mara University and Vaal University for the resources that enabled me carry this research.

My sincere gratitude goes to my supervisors Dr. Wesley Omwoyo, Prof. Nathan Oyaro, and Prof. Simphiwe Nelana for their encouragement, support and the immense knowledge they shared with me throughout this entire period.

I would also like to acknowledge my colleagues of Maasai Mara university: Patrick Odhiambo, Kenneth Rutto, Maxwell Gitonga, Evans Suter and Bakari Chaka for the different roles they played during this research.

I would also like to acknowledge Florence Sein, Justine Kisipan and the entire Namayiana for the encouragement and prayers they offered me during this period.

Lastly my sincere gratitude goes to my family: Mr and Mrs Benson Mesopirr, Mrs. Elizabeth Sukantet, husband Roimen Sukantet, siblings Senewa Lesere, Sankei Mesopirr, Mantai Mesopirr and Renei Yiamiton Lekina, my sister in love Siteyia and my children, Sancha, Ritei, Teyian and Meikan for their prayers, emotional and financial support.

ABSTRACT

Water is one of the most abundant features on Earth covering up to 70% of Earth's crust but only less than 1% of this water is fit for human consumption. Water can be polluted by both organic and inorganic matter. Hexavalent chromium (Cr(VI)) one of the inorganic pollutant is an important component in many industrial process finds its way into water bodies posing health problems which include lung cancer and inhibition of DNA and RNA in biological systems. This study thus focused on the preparation, characterization, and application of a novel nanocomposite adsorbent, CNC-Fe₃O₄NP-CD, for the removal of Cr(VI) from aqueous solutions. The cellulose used in this research was extracted from *Typha angustifolia* and hydrolized to cellulose nanocrystals (CNCs) using 32% H₂SO₄. The prepared and characterized cellulose nanocrystals, were incorporate onto iron oxide nanoparticles using co-precipitation method and functionalized with β -cyclodextrin by shear homogenization. Fourier Transform Infrared Spectroscopy (FTIR) identified the characteristic peaks of cellulose functional groups, including O-H stretching at 3309 cm⁻¹, C-H stretching at 2892 cm⁻¹, and C-O-C stretching at 1034 cm⁻¹. Transmission Electron Microscopy (TEM) revealed that the CNCs had nano-scale dimensions, with an average particle size of 98.57 \pm 2.54 nm. X-ray Diffraction (XRD) analysis confirmed the successful conversion to crystalline form, with a crystallinity index of 77.41%. The characterization of the nanocomposite (CNC-Fe₃O₄NP) with Scanning Electron Microscopy (SEM) and TEM analyses showed a uniform distribution of Fe₃O₄ nanoparticles, with an average particle size of 16.82 nm. The nanocomposite exhibited strong magnetic properties, as evidenced by Vibrating Sample Magnetometer (VSM) analysis, which recorded a magnetization value of 64.56 emu/g. Batch adsorption studies were conducted under varying conditions, including pH, adsorbent dosage, initial Cr(VI) concentration, contact time, and temperature. The optimal conditions for Cr(VI) removal were determined to be a pH of 2, an adsorbent dosage of 1.0 g, an initial Cr(VI) concentration of 20 mg/L, a contact time of 35 minutes at room temperature. Under these conditions, CNC-Fe₃O₄NP-CD achieved a maximum Cr(VI) removal efficiency of 97.45%. In the presence of competing ions such as Cu²⁺, Zn²⁺, and Pb²⁺ at a concentration of 20 mg/L, the Cr(VI) removal efficiency of CNC-Fe₃O₄NP-CD decreased to 30.22%, 30.22%, and 40.49% respectively. Regeneration studies demonstrated that CNC-Fe₃O₄NP-CD could be reused effectively over multiple adsorption-desorption cycles. Based on kinetic study, the experimental data fitted best with the pseudo-second-order kinetic model, which exhibited high linear regression coefficients ($R^2 > 0.98$) across all tested conditions. Equilibrium isotherm studies fitted well with the Langmuir isotherm model, indicating monolayer adsorption on a homogeneous adsorbent surface. The Freundlich and Temkin isotherms fitted to the experimental data. Thermodynamic studies revealed that the adsorption process was spontaneous, as indicated by negative Gibbs free energy (ΔG°) values. The enthalpy change (ΔH°) was also negative, suggesting that the adsorption process was exothermic. The positive entropy change (ΔS°) indicated an increase in randomness at the solid-liquid interface during adsorption. From the study, CNC-Fe₃O₄NP-CD presented a highly effective, sustainable, and reusable adsorbent for Cr(VI) removal, with excellent potential for real-world wastewater treatment applications.

TABLE OF CONTENTS

DECLARATION	ii
DEDICATION	iii
ACKNOWLEDGMENTS	iv
ABSTRACT	v
TABLE OF CONTENTS	vi
LIST OF FIGURES	xiii
LIST OF ABBREVIATIONS AND ACRONYMS	xvii
CHAPTER ONE	1
INTRODUCTION	1
1.1 Background of the Study	1
1.2 Problem Statement	10
1.3 Justification of the Study	12
1.4 Objectives	14
1.4.1 Broad Objective	14
1.4.2 Specific Objectives	14
1.5 RESEARCH QUESTIONS	15
1.6 SIGNIFICANCE OF STUDY	15
CHAPTER TWO	17
LITERATURE REVIEW	17
2.1 Narrow-leaf cattail grass (<i>Typha angustifolia</i>)	17
2.2 Cellulose	18
2.2.1 Cellulose nanomaterials	19

2.3 Functionalization of Cellulose Nanocrystals.....	23
2.4 Magnetic Nanoparticles.....	25
2.4.1 Iron Nanoparticles	26
2.4.2 Synthesis of Fe ₃ O ₄ Nanoparticles.....	29
2.4.3 Application of Magnetic Nanoparticles for Pollutant Removal	32
2.4.4 Functionalization/Coating of Magnetic Nanoparticles.....	33
2.5 Molecular Recognition Compounds.....	35
2.5.1 Cyclodextrin	37
2.5.2 Cross-Linking	40
2.6 Adsorption Process.....	43
2.6.1 Adsorption mechanism.....	44
2.6.2 Factors affecting adsorption	44
2.7 Adsorbents of Heavy Metal Ions Using Cellulose-Based Adsorbents.....	48
2.8 Modelling of Adsorption experimental data	60
2.8.1 Kinetic Models to Predict the Rate of Adsorption	60
2.8.2 Equilibrium Isotherm models	64
CHAPTER THREE	71
RESEARCH METHODOLOGY.....	71
3.1 EXPERIMENTAL DESIGN.....	71
3.1.1 Experimental Design	71
3.1.2 Sampling area and sample Size	71
3.1.3 Sampling Method	72
3.2 MATERIALS	73

3.2.1 Apparatus.....	73
3.2.2 Chemicals and Reagents.....	73
3.2.3 Equipment and Facilities	73
3.3 METHODS.....	74
3.3.1 Sample pretreatment.....	74
3.3.2 Dewaxing and Delignification.....	74
3.3.3 Chemical purification (bleaching).....	75
3.3.4. Synthesis of nanocellulose.....	75
3.3.5 Functionalization of Cellulose Nanocrystals with Fe ₃ O ₄ to form CNC-Fe ₃ O ₄ NP	77
3.3.6 Cross-linking of CNC-Fe ₃ O ₄ NP with β -Cyclodextrin to form CNC-Fe ₃ O ₄ NP- CD Nanocomposite.....	77
3.4 Characterization	78
3.4.1 Fourier Transform Infrared Spectroscopy (FTIR).....	78
3.4.2 Transmission Electron Microscopy (TEM).....	78
3.4.3 Scanning Electron Microscopy (SEM).....	79
3.4.4 Energy Dispersive X-ray Spectroscopy (EDS)	79
3.4.5 X-ray Diffraction (XRD).....	79
3.4.6 Thermogravimetric Analysis (TGA)	80
3.4.7 Brunauer-Emmett-Teller (BET) Analysis	80
3.4.8 Vibrating Sample Magnetometry (VSM).....	81
3.4.9 Zeta Potential.....	81
3.5 Batch Experiments	81

3.5.1 Determination of Effect of pH on adsorption	82
3.5.2 Effect of metal ions concentration on adsorption	82
3.5.3 Determination of effects of adsorbent weight on adsorption.	83
3.5.4 Determination of effects of contact time on adsorption.	83
3.5.6 Determination of effect of Temperature on adsorption	84
3.6 Spectrophotometric Analysis	85
3.7 Regeneration of the Adsorbents	85
3.8 Data Analysis	86
CHAPTER FOUR.....	87
RESULTS AND DISCUSSIONS.....	87
4.1 Characterization of <i>Typha angustifolia</i> , CPC and CNCs.....	87
4.1.1 Physical appearance.....	87
4.1.2 Functional group analysis (FTIR).....	88
4.1.3 Scanning electron microscopy (SEM).....	90
4.1.4 Elemental Analysis	92
4.1.5 Crystalline structure analysis X-ray diffraction.....	93
4.1.6 Thermal analysis.....	96
4.2 Characterization of Fe ₃ O ₄ NP, CNC-Fe ₃ O ₄ NP and CNC-Fe ₃ O ₄ NP-CD	98
4.2.1 Functional group analysis (FTIR).....	98
4.2.2 Scanning electron microscopy (SEM) Analysis.....	100
4.2.3 Energy Dispersive Spectroscopy (EDS).....	102
4.2.4 Transmission Electron Microscopy(TEM).....	104
4.2.5 Vibrating Sample Magnetometer (VSM)	107

4.2.6 Crystalline structure analysis X-ray diffraction (XRD) Analysis	108
4.2.7 Thermogravimetric Analysis (TGA)	110
4.2.8 (Brunauer-Emmett-Teller (BET) Analysis	114
4.2.9 Zeta Potential	115
4.3 Adsorption.....	116
4.3.1 Effect of pH on removal of Cr (VI) by CPC, CNC, CNC-Fe ₃ O ₄ NP and CNC- Fe ₃ O ₄ NP-CD.....	116
4.3.2 Adsorbent Dosage.....	120
4.3.3 Varying Pollutant Concentration	123
4.3.4 Varying Adsorption Time.....	126
4.3.5 The effect of Varying Adsorption Temperatures	130
4.4 Comparative Study on the Adsorbents.....	132
4.5 Kinetics studies of adsorption	135
4.5.1 Pseudo-first-order kinetic models.....	135
4.5.2 Pseudo-second-order kinetic model.....	136
4.5.3 Elovich model.....	137
4.5.4 Intra-particle diffusion model.....	138
4.6 Equilibrium isotherms	140
4.6.1 Langmuir isotherm model	140
4.6.2 Freundlich isotherm model.....	142
4.6.3 Temkin isotherm model.....	143
4.6.4 Dubinin–Radushkevich (D–R) model	145
4.7 Thermodynamics studies of adsorption	147

4.8 Effect of Competing Ions on Cr(VI) Adsorption	149
4.9 Regeneration of CNC-Fe ₃ O ₄ NP-CD	151
CHAPTER FIVE	154
CONCLUSIONS AND RECOMMENDATIONS	154
5.1 Conclusions	154
5.2 Recommendations for further research	156
REFERENCES	157
APPENDICES	196
Appendix 1: Calibration curve of Cr (VI) : time studies.....	196
Appendix 2: Calibration curve of Cr (VI) : time studies: concentration studies.....	196
Appendix 3: Prepared adsorbents for characterization	197
Appendix 4: Adsorption studies	197
Appendix 5: preparation of Iron oxide nanoparticles.....	198
Appendix 6: Published paper 1 abstract.....	199
Appendix 7: Puplished paper 2 abstract.....	200

LIST OF TABLES

Table 2. 1: Properties of natural cyclodextrins (Varan, 2023).....	38
Table 4.1: Crystallinity indices of Typha angustifolia grass powder, CPC, and CNCs. ..	95
Table 4.2: Thermal characteristics of Typha angustifolia grass powder, CPC and CNCs.	97
Table 4.3: Crystallinity indices of Fe ₃ O ₄ , CNC-Fe ₃ O ₄ NP, and CNC-Fe ₃ O ₄ NP-CD.....	110
Table 4.4: BET Surface area and pore properties	114
Table 4.5: Summary of kinetic model parameters	139
Table 4.6: Summary of Isotherms model parameters	146
Table 4.7: Thermodynamic parameters at various system temperatures	149
Table 4.8: Influence of competing ions on Cr(VI) removal efficiency	150

LIST OF FIGURES

Figure 2.1 <i>Typha angustifolia</i> grass (The picture was taken from Maasai Mara botanical garden).	17
Figure 2.2 Chemical structure of cellulose (4-O- β -D-Glucopyranosyl- β -D-glucopyranose	19
Figure 2.3: CN micrographs CN micrographs: (a) SEM of wood fibre, (b) SEM of microcrystalline cellulose (MCC), and (c) TEM of MCC. (d) TEM picture of TEMPO-CNFs, (e) TEM image of wood CNCs, (f) TEM image of tunicate CNCs, and (g) TEM image of algae CNCs and (h) An SEM picture of bacterial cellulose	21
Figure 2. 4 Schematics of (a) a single cellulose chain (b) a cellulose microfibril showing ordered (crystalline) and disordered (amorphous) regions and (c) CNCs after acid hydrolysis of the disordered	22
Figure 2.5 Schematic diagram illustrating the various types of chemical modifications on CNC surfaces	24
Figure 2.6: Magnetite-based iron oxide nanoparticles crystal arrangement	27
Figure 2.7: Structural features on pigment properties of α -Fe ₂ O ₃ haematite	28
Figure 2.8: Nano zero-valent iron particles	29
Figure 2.9: Schematic diagram for synthesising iron oxide nanoparticles	32
Figure 2. 10: Magnetoelectric reduction of chromium (VI) to chromium (III)	33
Figure 2.11: Magnetic nanoparticles featuring polyzwitterionic coatings	34
Figure 2.12: Chemical structure of alpha- (α -CD), beta- (β -CD) and gamma- (γ -CD) cyclodextrins	38
Figure 2.13: Chemical structure and shape of the β -cyclodextrin molecule	39

Figure 2.14: Cyclodextrin functionalized nanoparticles for hexavalent chromium removal	41
Figure 2.15: β -cyclodextrin-modified molybdenum disulfide for removal of Cr(VI)	42
Figure 2.16: Schematic representation of the adsorption process onto a solid adsorbent	44
Figure 2. 17: Behaviour of chromium in different pH environments	46
Figure 3.1: Sample collection area	72
Figure 3.2: Summarized schematic diagram for CPC isolation and synthesis of CNCs ..	76
Figure 4.1: Physical appearance of (a) Chopped <i>Typha angustifolia</i> , (b) Crushed <i>Typha angustifolia</i> , (c) Isolated cellulose and (d) Cellulose nanocrystals.....	88
Figure 4.2: FTIR spectra of <i>Typha angustifolia</i> , CPC, and CNCs	90
Figure 4.3: Scanning electron (SEM) images (a) <i>Typha angustifolia</i> , (b) CPC, and (c) CNCs.....	91
Figure 4.4: EDS spectrum of <i>Typha angustifolia</i> (a), CPC (b), and (c) CNCs.....	93
Figure 4.5: XRD pattern of <i>Typha angustifolia</i> , CPC and CNCs.....	96
Figure 4.6: (a). TGA and (b). DTG curve of <i>Typha angustifolia</i> , CPC, and CNCs.	98
Figure 4.7: FTIR spectra for $\text{Fe}_3\text{O}_4\text{NP}$, $\text{CNC-Fe}_3\text{O}_4\text{NP}$ and $\text{CNC-Fe}_3\text{O}_4\text{NP-CD}$ nanocomposites.....	100
Figure 4.8: SEM images for $\text{Fe}_3\text{O}_4\text{NP}$, $\text{CNC-Fe}_3\text{O}_4\text{NP}$, and $\text{CNC-Fe}_3\text{O}_4\text{NP-CD}$ nanocomposites.....	102
Figure 4.9: EDS data for (a). $\text{Fe}_3\text{O}_4\text{NP}$, (b). $\text{CNC-Fe}_3\text{O}_4\text{NP}$ and (c). $\text{CNC-Fe}_3\text{O}_4\text{NP-CD}$ nanocomposites.....	104
Figure 4.10: TEM images for $\text{Fe}_3\text{O}_4\text{NP}$, $\text{CNC-Fe}_3\text{O}_4\text{NP}$, and $\text{CNC-Fe}_3\text{O}_4\text{NP-CD}$	106
Figure 4.11: VSM for $\text{Fe}_3\text{O}_4\text{NP}$, $\text{CNC-Fe}_3\text{O}_4\text{NP}$, and $\text{CNC-Fe}_3\text{O}_4\text{NP-CD}$	108

Figure 4.12: XRD pattern of Fe ₃ O ₄ , CNC-Fe ₃ O ₄ NP, and CNC-Fe ₃ O ₄ NP-CD	109
Figure 4.13: (a).TGA graph and (b). DTG curve for Fe ₃ O ₄ , CNC-Fe ₃ O ₄ NP, and CNC-Fe ₃ O ₄ NP-CD.....	112_Toc182256811
Figure 4.15: Zeta potential for for Fe ₃ O ₄ , CNC-Fe ₃ O ₄ NP, and CNC-Fe ₃ O ₄ NP-CD.....	116
Figure 4.16: The effect of pH on the removal of hexavalent chromium using different adsorbents.	119
Figure 4.17: The influence of adsorbent mass on the removal of hexavalent chromium.	123
Figure 4.18: The influence of Cr(VI) concentration using different adsorbents.	126
Figure 4.19: The influence of contact time on the removal of hexavalent chromium using different adsorbents.....	129
Figure 4.20: The influence of temperature on the removal of hexavalent chromium using different adsorbents.....	131
Figure 4.21: Comparative study of the adsorbents at pH 2, Cr(VI) 20 mg/L, adsorbent mass of 1g, Contact time of 35 minutes at room temperature.	133
Figure 4.22: Pseudo-first-order kinetic model linear fit	135
Figure 4.23: Pseudo-second-order kinetic model linear fit.....	137
Figure 4.24: Elovich kinetic model linear fit	138
Figure 4.25: Intraparticle diffusion kinetic model linear fit	139
Figure 4.26: Langmuir linear fit isotherm models	142
Figure 4.27: Freundlich linear fit isotherm model	143
Figure 4. 28: Temkin Linear fit isotherm model.....	145
Figure 4.29: Dubinin–Radushkevich Linear fit isotherm model	146

Figure 4.30: Adsorption thermodynamic plots 149

Figure 4.31: Regeneration of the adsorbent (AD- adsorption and DP- desorption) 152

LIST OF ABBREVIATIONS AND ACRONYMS

AAS	Atomic Absorption Spectrophotometer
APTES	Aminopropyl Triethoxy Silane
BET	Brunauer–Emmett–Teller
BNC	Bacterial Nanocellulose
CD	Cyclodextrine
CM-CD-MNPs	Carboxymethyl- β -CD modified Fe ₃ O ₄ nanoparticles
CNC- Fe₃O₄NP	Cellulose Nanocrystals Iron Oxide Nanparticles
CNC- Fe₃O₄NP-CD	Cellulose Nanocrystals Iron Oxide Nanparticles Cyclodextrin
CNCs	Cellulose Nanocrystals
CNFs	Cellulose Nanofibers
DNA	Deoxyribonucleic acid
DTG	Derivative Thermogravimetric Analysis
ECNCs	electrostatically stabilized CNCs
EDX	Energy Dispersive X-ray analyzer
EPI	hexamethylene diisocyanate
Fe₃O₄	Magnetite

Fe₃O₄NP	Iron Oxide Nanoparticles
Fe-NP	iron nanoparticles
FTIR	Fourier transform Infrared
GTMAC	Glycidyl trimethyl ammonium chloride
HMDI	Hexamethylene Diisocyanate
KIPPRA	Kenya Institute for Public Policy Research and Analysis
KDHS	Kenya Demographic and Health Survey
MCC	Microcrystalline Cellulose
MF	Melamine-formaldehyde
MNP	Magnetic Nanoparticles
MRI	Magnetic Resonance Imaging
NaHCO₃	sodium bicarbonate
NaSCNCs	Sodium Sulfated cellulose nanocrystals
NCHs	Nanocrystal Hydrogels
NP	Nanoparticles
nZVI	Nano zero-valent iron
PD	Polydopamine

pH_{PZC}	Point of zero charge
PPMS	Physical Property Measurement System
RNA	Ribonucleic acid
SCNCs	Sulfated cellulose nanocrystals
SEM	Scanning Electron Microscopy
TAPPI	Technical Association of the Pulp and Paper Industry
TEM	Transmission Electron Microscopy
TEMPO	Periodate-chlorite, and 2,2,6,6-tetramethyl-1-piperidinyloxy
TGA	Thermal Gravimetric Analysis
T-β-CD-MNPs	Triazinyl- β -Cyclodextrin-modified magnetic nanoparticles
UNICEF	United Nations Children's Fund
US	United States
UV-VIS	Ultra-violet visible
VSM	Vibrating Sample Magnetometry
WHO	World Health Organization
XRD	X-ray Diffraction
A	Alpha

$\alpha\text{-Fe}_2\text{O}_3$	Hematite
$\alpha\text{-FeOOH}$	Goethite
B	Beta
$\beta\text{-CD}$	beta-Cyclodextrin
Γ	Gamma
$\gamma\text{-Fe}_2\text{O}_3$	Maghemite

CHAPTER ONE

INTRODUCTION

1.1 Background of the Study

Water is one of the most abundant features on Earth, covering up to 70% of Earth's crust (Scanlon et al., 2023). Unfortunately, less than 1% of this water is fit for human consumption (Barbier, 2019). Increasing population and human activities such as urbanization and industrialization have decreased water availability. In addition, the quality of water used is also deteriorating due to pollution (Liyanage & Yamada, 2017; Mishra, 2023). Water pollution can be defined as water contamination caused by foreign matter that deteriorates water quality (Liyanage & Yamada, 2017). Both organic and inorganic matter can pollute water; some inorganic pollutants include heavy metals, anions and ligands above permissible limits. Their primary sources are industrial effluents and agricultural runoffs (Breida et al., 2019).

Heavy metals are metals with a density of about $4-7.5\text{gml}^{-1}$ and are toxic even at trace concentrations (Gautam et al., 2016). They include mercury, lead, chromium, cadmium, copper, and arsenic amongst others. These metals are associated with bioaccumulation in biological organisms (Breida et al., 2019). These heavy metals get into water systems by both natural and anthropogenic methods. Natural methods include geochemical weathering of rocks and soils and volcanic eruptions (Akhtar et al., 2021). Heavy metal contamination exists in aqueous wastes of many industries, such as metal plating, mining operations, tanneries, radiator manufacturing, smelting, alloy industries and storage batteries industries (Pathak & Bhardwaj, 2021). Excessive release of heavy metals into

the environment due to industrialization and urbanization has posed a significant problem worldwide. Unlike organic pollutants, most susceptible to biological degradation, heavy metals do not degrade into harmless end products (Ali et al., 2021).

Diverse heavy metals have varying effects on humans; however, their presence in excess poses major concern due to their toxicity to many life forms. However beneficial to biological organisms, copper is harmful at high concentrations. Copper contamination in water streams occurred mainly from cleaning metal and plating baths, fertilizer, refineries, paper and pulp, and wood preservatives (Ali et al., 2021). In addition, high copper exposure causes breathing and oral irritations (Tripathi et al., 2021). Lead is one of the most toxic and is associated with kidney, reproduction and nervous disorders (Balali-Mood et al., 2021). It is a highly poisonous metal ion arising from coal burning, leaded fuels and gasoline, mining and other pyro-metallurgical works such as steel smelting (WHO, 2023.; Legge & Goadby, 2023). Typically, leaded products face bans due to their hazardous nature, minimizing lead emissions. Cadmium is an excellent electrode and is thus common in electrical works. It is widely used in electroplating, soldering, batteries, TV sets, insecticides and metal finishing industries (Chiroma et al., 2007). Cadmium, which is a prevalent heavy metal, is, however, known to cause renal dysfunction, bone degeneration, liver and blood damage (Ma et al., 2022). Zinc (Zn) mainly originates from mining, metallurgical works, as well as combustion of fossil fuels. Zinc plates are also used in batteries and significantly contribute to zinc emissions, especially if not properly disposed of (Okrikata & Nwosu, 2023). According to Hossini et al. (2022), chromium is common in most plastic, leather and tannery industries. Chromium (Cr), in its oxidation state of three, is an essential element in the human body,

and it is used in supplements and drugs. Cr (VI) can enter the human system through inhalation, ingestion or skin contact. However, Cr(VI) is very toxic and cause lung cancer, nasal irritation, nasal ulcers, hypersensitivity reactions e.g. asthma and dermatitis. It also inhibits DNA, RNA and protein synthesis in biological systems hence induces cell death (Hossini et al., 2022). This therefore calls for the need to develop water treatment technologies that are efficient and inexpensive that can eliminate these heavy metals especially chromium even at trace levels.

Wastewater treatment processes employing current traditional technologies have been developed to remove the toxic metallic elements from portable waters, and most known are distillation, chlorination, use of ion exchange resins (Saleh et al., 2022), filtration by use of membranes (N. Ahmed & Mir, 2021; Mahmoud & Mostafa, 2023), adsorption by use of highly porous materials like activated charcoal (Mariana et al., 2021). Other methods include biological and chemical advanced oxidation, Fenton process, and photodegradation etc (Nidheesh et al., 2022). Adsorption techniques using materials such as nanoparticles, polymers, simple organic compounds and inorganic clay materials have been employed for water treatment (Mariana et al., 2021). But these have been found to have drawbacks ranging from being effective only at high pollutant concentrations, low surface active sites, and high costs of operations to high activation energy of sorption and more so, they are only applicable for small-scale filtrations (Satyam & Patra, 2024). Ion exchange resins have also been used to remove pollutants from wastewater; however, these resins are easily contaminated by organic impurities in the wastewater, fouling their pollutant removal efficiency (Al-Asheh & Aidan, 2020). For membrane filtration, nanofiltration, ultra-filtration and reverse osmosis have been proven more efficient since

they rely on semi-permeable membranes to prevent the passage of pollutants. However, they are capital-intensive due to high maintenance costs since high pressures are required to operate the systems (Siddique et al., 2020). Chemical advanced oxidation, on the other hand, involves oxidative methods such as ozonation, ultraviolet irradiation and chlorination in waste removal. However, these methods are associated with high costs, incomplete removal or difficulties in recovery (Comninellis et al., 2008; Duan et al., 2020).

Biological systems can be used to treat water pollution through phytoremediation (A. U. Khan et al., 2022). In phytoremediation, some specific plants are planted in regions with high concentrations of water pollutants and used to harness these pollutants (Sharma & Malaviya, 2016; Tufail et al., 2021). Similarly, biological processes such as biologically active filtration, soil aquifer treatment, membrane bioreactors and river bank filtration, in which the decomposition of compounds using bacteria or enzymes are usually employed, remove minimal amounts of these pollutants (Ahmed et al., 2021). The contaminants are removed using activated sludge through several methods, such as sludge absorption, primary settling, precipitation, and aerating volatilization (Niehs, 2010). Several types of plants with a suitable biosorption mechanism are planted in polluted water. These plants absorb heavy metals from the contaminated water and use compounds of eutrophication (Nitrogen and Phosphates) as nutrients (Khan et al., 2022). Some of the aquatic plants include *Phragmites*, *Lemna* and *Typha* spp. (Sharma & Bhasin, 2011). The drawback of this method is that when herbivores or other animals ingest these plants, these pollutants might end up in human bodies (Mohan et al., 2021; Saxena et al., 2019). Thus, the best solution is to isolate bioactive compounds such as cellulose and cellulose nanocrystals

that can be used as adsorbents through volatilization. These materials are low-cost and abundant.

Over the past years, various research investigations have been conducted to examine low-cost adsorbents for the removal of heavy metal ions from water and wastewater (Bhatnagar et al., 2015; Iqbal et al., 2022; Lam & Hemraz, 2021; Yadav et al., 2018). An adsorbent can be classified as low-cost if it requires little processing, is abundant in nature, or is an industry by-product or waste material (Gupta et al., 2009). This study used *Typhaceae angustifolia* to isolate the bioactive cellulosic materials.

Cattail grass, *Typhaceae angustifolia* is an herbaceous grass that thrives in wetlands and belongs to the class Typha. The plant is perennial and known to have rhizomes with a well-developed aerenchyma system for survival in its wetland ecology (Yamauchi et al., 2013a). The morphology of Cattail grass is characterized by unique leaves that are pretty long, linear, and alternate (Liu et al., 2017). It has spiky flowers with numerous male flowers that form a narrow spike at the top of a vertical stem (Fahlgren, 2017). These species dominate over others in most wetland ecologies due to their dense matrix of canopy beneath the soil surface (Pandey & Verma, 2018a). Even non-living parts, such as the stem, have been reported to transmit oxygen beneath the soil surface (Wilcox et al., 2017). Cattail grass is widely available in tropical regions, especially in wetlands that experience water pollution. Moreover, the underneath encroaching system of its rhizomes acts as natural adsorbents (Zapata-Morales et al., 2023). The grass's fibrous and pulpy nature implies cellulosic content from this grass is speculated to be high.

Cellulose is the main structural constituent of all plant cell walls, which makes it the most abundant high-order polymer on Earth (Beg et al., 2020; Gupta et al., 2019; Klemm et al., 2005). Cellulose consists of cellobiose chains agglomerated by intermolecular hydrogen bonds between the hydroxyl groups of adjoining macromolecules (Gupta et al., 2019). It is a natural polysaccharide made up of glycosidic linked $\beta(1 \rightarrow 4)$ D-glucose units (Tapia-Orozco et al., 2016). This polysaccharide appears in nature as fibres in the micrometre scale and consists of four hierarchal levels. The molecular level is made up of -D-glucopyranose units with β -1 \rightarrow 4 glycosidic bonds bond linkages (Etale et al., 2023a). This study used cellulose nanomaterial (nanocellulose).

Nanocellulose is a cellulosic material with nanometer-scale dimensions (Ullah et al., 2021). The production of nanocellulose can be conducted using various methods from different lignocellulosic materials. There are three subcategories of nanocellulose, namely, cellulose nanocrystals (CNCs), cellulose nanofibers (CNF's) and bacterial nanocellulose (BNC) (Blanco et al., 2018). The type of nanocellulose produced depends on the source and the production method (Khalid et al., 2021). Different processes have been developed for the production of nanocellulose. The cellulose fibers can be separated by breaking the inter-fibrillar hydrogen bonds using chemicals, certain enzymes and mechanical methods (Fahma et al., 2021). Cellulose microfibrils contain amorphous regions and crystalline regions (Nagarajan et al., 2021). When acid hydrolysis treatments are used, amorphous regions of the cellulose microfibrils are selectively hydrolyzed, and the microfibrils break into smaller parts with a high degree of crystallinity; these crystalline parts are generally referred to as cellulose nanocrystals (Copenhaver et al., 2022). Cellulose nanofibers are produced by subjecting cellulose microfibrils to high

shear force; this results in cellulose nanofibers together with crystalline and amorphous regions (Rahimi et al., 2019).

Nanocellulose are known for effectively removing a variety of pollutants from aqueous solutions, making them promising efficient adsorbents for wastewater treatment (Li et al., 2016). Cellulosic-based materials with nano-scale properties such as large surface area, high aspect ratio and chemical accessibility can now be used as affordable adsorbents for wastewater treatment (Bhatnagar & Sillanpää, 2010; Gupta et al., 2009; Iqbal et al., 2022; Matsedisho et al., 2024; Nagarajan et al., 2021b; Shah et al., 2020; Zhang et al., 2024; Mautner, 2017). The adsorption phenomena in cellulosic materials are attributed to the significant hydrophilicity due to the hydroxyl groups and the excellent chemical reactivity of the other functional groups present in the material (Tapia-Orozco et al., 2016). In its unmodified form, the cellulosic-based material is known for its inadequate adsorption capacity and unstable physical stability (Hokkanen et al., 2016; Suter et al., 2024). According to a study conducted by Anirudhan et al. (2013), raw cellulose powder with a surface area of $18.2\text{m}^2.\text{g}^{-1}$ and a particle size of 0.069 mm showed an ion exchange capacity of 0.71 mequivg^{-1} . These results showed that raw cellulose was capable of ion exchange. However, its ion exchange capacity was low. The authors suggested that its ion exchange capacity could be enhanced by chemical modification as well as chemical grafting (Anirudhan et al., 2013). Some modifiers include metal nanoparticles, complexes, polymers, catalysts, hydrogels, etc. (Xiao et al., 2023).

Metal nanoparticles are preferred for their larger surface area to volume ratio, which enables them to adsorb more pollutants (Iqbal et al., 2022). These particles are also associated with high dispersion in solvents or materials, selectivity, self-assembly ability,

and high specific affinity (Visaveliya & Köhler, 2021). Synthesis of nanoparticles is also cost-effective and can be achieved under ambient laboratory conditions with few locally available solvents. Iron oxide nanoparticles are always ideal due to their magnetic properties, non-toxic, chemical inertness and biocompatibility (Karale & Game, 2022).

Magnetic nanoparticles are materials of a magnetic core and polymeric shell (Ansari et al., 2022). Magnetic nanoparticles have been recently applied in water and wastewater treatment because of their ease of synthesis, high surface area, large amounts of active sites for interaction with metallic and organic species, separation after use by an external magnetic field and the absence of internal diffusion resistance (Tee et al., 2022a). Magnetic nanoparticles can be reused after magnetic separation by desorbing the adsorbed contaminants (Rasheed, 2022).

Several types of iron magnetic particles, such as Fe_2O_3 , maghemite, Fe_3O_4 , CuFe_2O_4 and $\alpha\text{-Fe}_2\text{O}_3$, have been explored for their ability to perform as adsorbents for metallic and organic pollutants from water (Can et al., 2012; Jasim et al., 2022). These iron-based magnetic iron oxide nanoparticles are prone to agglomeration and iron leaching, and to prevent these, polymeric and ionic liquids have been proposed as stabilizers (Leonel et al., 2021).

Stabilizers refer to substances used in the nanoparticle preparation to prevent them from inter-particle interactions, thus preventing nanoparticle agglomerations (Shrestha et al., 2020). The size of the particles depends on the electron-donating capability of the stabilizing or capping agents (Aguilar et al., 2021). The stabilization of nanoparticles is carried out before their actual use in any technological application by their surface

modification with proper stabilizers whose choice depends upon the type of nanoparticles and their synthesis (Bae et al., 2011). According to (Jadhav et al., 2015), surface modification with stabilizers is crucial to achieve sufficient repulsive force between the particles, which prevents their aggregation and helps obtain a stable particle suspension. Various organic compounds are used to stabilize nanoparticles to reduce their surface energies and prevent them from aggregation, for example, simple surfactants, bifunctional organic compounds, natural polymers or biological materials, oligomers or polymers bearing different functional groups (Abdel-Halim et al., 2011). In this study, Beta-Cyclodextrine was used as a stabilizer.

Cyclodextrins (CDs) are a family of compounds made of sugar (starch) molecules bound together in a cyclic ring (Poulson et al., 2021a). They are a group of naturally cyclic oligosaccharides, with six, seven, or eight glucose sub-units linked by α -(1,4) glycosidic bonds in a torus-shaped structure and are denominated as α -, β -, and γ -CD, respectively (Poulson et al., 2021a). The three-dimensional structures formed in CD keep the hydroxyl groups on the outer edges, while hydrogen atoms and oxygen bridges exist in the internal cavity (Bao et al., 2024). This structure, therefore, makes cyclodextrin possess an external hydrophilic surface and a hydrophobic central cavity (Poulson et al., 2021; Bao et al., 2024). Non-polar pollutants can be trapped in the internal cavity while the outer surface remains hydrophilic (Bao et al., 2024). Cyclodextrin-based polymers could remove organic and inorganic pollutants from water to desirable levels because of their efficiency in pollutant removal from polycontaminated mixtures, even at low trace concentrations (Liu et al., 2024). Due to their unique sorption properties, much attention has recently focused on cyclodextrin-based polymeric materials in various applications.

Due to the cavity's properties and size, CDs can form inclusion complexes in solution or solid-state, with multiple guest molecules differing in chemical and physical properties (Bao et al., 2024). CDs represent an interesting and attractive alternative as adsorbents because of their particular structure, physicochemical characteristics, chemical stability, high reactivity and excellent selectivity towards aromatic compounds and metals, resulting from the presence of chemically reactive groups (hydroxyl, acetamido or amino functions) in polymer chains (Cova et al., 2021a).

Among the three types of cyclodextrin, β -CD has a relatively rigid structure, complete with a secondary belt formed by hydrogen bonds (Poulson et al., 2021a). β -CD has twenty one hydroxyl groups at the 2-, 3- and 6-positions in the glucose unit that are very reactive and available to form several linkages. Furthermore, β -CD shows excellent intermolecular interaction due to its hydrophobic cavity, which can accommodate and recognize various compounds (Liu et al., 2020). β -CD is the most commonly applied due to the relative ease of synthesis, low price and the presence of an internal cavity into which a large number of molecules will fit (Okasha et al., 2023).

This study aimed to develop a hybrid of agro-based adsorbent combined with magnetic iron oxide nanoparticles and β -CD that are chemically specific and capable of permanently sequestering hexavalent chromium metal ions even at trace levels, from drinking and wastewaters without fouling both for domestic and industrial wastewaters and that can be affordable both on operation and maintenance.

1.2 Problem Statement

Developing countries still suffer from water scarcity, and Kenya is no exception, with only 605 cubic metres of renewable freshwater and freshwater replenishment against a

population of over 40 million (Mulwa et al., 2021). This is mainly due to the country having about 83% of its total area being arid and semi-arid, leading to inadequate rainfall, poor management of the water resources and contamination of the available freshwater sources (Njora & Yilmaz, 2021). Access to clean and safe water in Kenya is currently estimated at 64.4% of the total population, leaving the rest of the population at risk of contaminated water from underground wells and rivers, many of which are polluted and sometimes even run dry in dry months (Mulwa et al., 2021). According to a 2022 KDHS report, 68% of Kenyans have access to clean and safe drinking water. However, other sources have different estimates, ranging from 59% to 60%. Regardless of the exact number, access to clean water is a challenge in Kenya, with 28–41 million people lacking access to safe water and improved sanitation (KIPPRA, 2024; UNICEF Kenya, 2020; Water.org, 2024).

Chromium (Cr) is a naturally occurring element found in the environment, including water, soil, and air. However, industrial activities such as leather tanning, electroplating, and dye production can release harmful levels of chromium into water bodies (Prasad et al., 2021). The most toxic form, hexavalent chromium (Cr(VI)), is a potent carcinogen and can cause severe health issues, including skin irritation, respiratory problems, and damage to the liver and kidneys (Hossini et al., 2022). In Kenya, the improper disposal of industrial waste has led to elevated chromium levels in some water sources, posing significant risks to human and animal health (Kinuthia et al., 2020). Contaminated water with chromium can lead to long-term environmental and health consequences, making it crucial to address and manage this issue effectively.

Existing adsorbents, such as macromolecular carbon materials, provide limited surface area for adsorption and are expensive, making them less practical for large-scale applications. Furthermore, many available nanocomposites are not biodegradable and have not been thoroughly tested for their effectiveness at trace levels of pollutants. Therefore, there is a critical need to develop efficient, cost-effective, and environmentally friendly adsorbents capable of removing heavy metals from aqueous media, even at very low concentrations.

This study, thus, aimed to fill this gap by developing a novel nanocomposite adsorbent that combines cellulose nanocrystals (CNC), iron oxide nanoparticles ($\text{Fe}_3\text{O}_4\text{NP}$) and β -cyclodextrin (CD). Each material is aimed to bring distinct advantages: CNC provides a renewable and biodegradable matrix with inherent adsorption properties; $\text{Fe}_3\text{O}_4\text{NP}$ offers a large surface area and magnetic properties for easy separation; and CD enhances selectivity and capacity for a wide range of pollutants. These materials were integrated to create a superior, eco-friendly adsorbent capable of achieving complete removal of Cr(VI) and other contaminants from aqueous media. This novel approach aims to improve water treatment efficiency and addresses the need for sustainable and accessible solutions in resource-limited settings.

1.3 Justification of the Study

The human populace and the need for clean and safe water are ever-increasing against constant water resources. Unfortunately, due to urbanization, industrialization, agricultural effluents and large volumes of industrial effluents are channeled into water bodies 'as a sink' with little or no pretreatment measures. These pollutants introduce heavy metals with varying effects on biological systems.

Typhaceae angustifolia's widespread availability, limited uses and the pulpy and fibrous nature of its stems and leaves have great potential for industrial cellulose production. Cellulose is an abundant, naturally occurring, and renewable resource that is both biocompatible and hydrophilic, making it ideal for producing nanocomposites.

Nanocomposites possess remarkable properties like high surface area to volume ratio giving, better adsorption capacities, high solvent dispersion, selectivity and high specific affinity. The use of nanoparticles increases the surface area of adsorbents, allowing pollutants to be trapped more effectively. Carbon nanotubes have been used in the recent past for the removal of water pollutants; the high aspect ratio that accompanies carbon nanotubes' (CN's) impressive mechanical properties is reminiscent of carbon nanotubes, but cellulose nanomaterials are an abundant, naturally occurring and renewable resource that is both biocompatible and hydrophilic due to the cellulose building blocks. Beta-cyclodextrin has the unique characteristic of having both hydrophobic and hydrophilic sites and hence, has the potential to be modified to adsorb a range of target pollutants.

The research contributes to the expanding literature of information on nanocomposite materials for environmental remediation. It explores cutting-edge techniques to enhance the properties of natural materials for valuable applications. The results may open up the possibility of more studies into other potential cellulose-based adsorbent modifications and uses.

1.4 Objectives

1.4.1 Broad Objective

To extract cellulosic materials from *Typhaceae angustifolia*, functionalize with magnetic iron oxide nanoparticle, β -cyclodextrin and characterize and employ it in batch experiments for removal of Cr (VI) and assess its effectiveness in competitive ion environments and re-usability.

1.4.2 Specific Objectives

- i. To extract cellulose from *Typhaceae angustifolia* and prepare cellulose nanocrystals (CNCs) from the cellulose through acid hydrolysis.
- ii. To prepare CNC-Fe₃O₄NP nanocomposite via in situ incorporation of Fe₃O₄NP onto cellulose nanocrystals.
- iii. To functionalize CNC-Fe₃O₄NP with β -cyclodextrin by shear homogenization to form CNC- Fe₃O₄NP-CD nanocomposite adsorbent.
- iv. To characterize CNC, CNC- Fe₃O₄NP and CNC-Fe₃O₄NP-CD for surface morphology using SEM, TEM, FTIR, XRD, BET, VSM, and TGA analytical techniques.
- v. To perform batch experiments with regard to varying pH, adsorbents dosage, contact time, temperature as well as initial concentration of Cr (VI) for the prepared adsorbents (CNC, CNC-Fe₃O₄NP and CNC-Fe₃O₄NP-CD and fit the batch experimental data in equilibrium and thermodynamic modes.

- vi. To evaluate the effect of competing ions on the removal of Cr (VI) by CNC-Fe₃O₄NP-CD in the presence of Zn²⁺, Pb²⁺, and Cd²⁺ and perform regeneration studies to ascertain the re-usability of the CNC- Fe₃O₄NP-CD adsorbent.

1.5 RESEARCH QUESTIONS

Water is a global resource whose demands are exponentially outdoing the supply. Use of technology for mass production in industries has led to pollution of water sources.

- I. Can the same technology be used to purify the effluents before discharge and consumption by humans?
- II. How effective are cellulose nanoparticles in water purification?
- III. Cellulose nanoparticles been fully optimized for removal of wastewater containing heavy metals?

1.6 SIGNIFICANCE OF STUDY

Many solutions to global challenges, such as environmental pollution, have been solved by increasing technology. One of these scientific advancements includes formulating chemical solvents from natural products and integrating them into other natural precursors to form more valuable compounds. Wastewater pollutants can thus be labelled, traced, and effectively removed before disposing of them in their natural sinks, where they are less harmful.

Adsorption is an effective tool for heavy metal removal. Metallic compounds especially heavy metals can be adsorbed using cellulose nanocomposites, leaving cleaner and safe

water. This reduces heavy metals in drinking water, significantly mitigating costs incurred in treating related ailments.

Advancements in adsorption technologies using polymers with multi-functional groups of adsorbing pollutants, such as cellulose nanocomposites, increase the efficiency of wastewater purification. Adsorption using cellulose is a relatively cheap method and the adsorbents can be packed in several readily available columns. Agglomeration of active sites is not quite enhanced; thus, the adsorbents can be regenerated. Electricity is not required in this method hence relatively cheap.

The use of nanoparticles ensures the optimization of surface activity, which increases the method's efficacy. Functionalization of cellulose ensures the adsorbents can withstand various chemical conditions. The resulting adsorbents can thus purify wastewater of both acidic and basic nature at a more comprehensive temperature range. Several types of wastewaters of different origins can be purified without adsorbent regeneration.

CHAPTER TWO

LITERATURE REVIEW

2.1 Narrow-leaf cattail grass (*Typha angustifolia*)

Typha comprises of approximately 30-species belonging to the Typhaceae family (Paniagua-Zambrana et al., 2024). *Typha angustifolia* is known in north America as narrow-leaf cattail but in other English speaking regions as reedmace or bulrush shown in Figure 2.1 (Pandey & Verma, 2018b). Wetlands are ideal habitats for the herbaceous *Typhaceae angustifolia* and according to Yamauchi et al. (2013), the plant is perennial and has rhizomes with a well-developed aerenchyma system, enabling survival in its particular wetland ecosystem (Yamauchi et al., 2013b). While *Typha angustifolia* L. can tolerate some salinity and is found in estuaries ,its preffered habitats typicly include meadow grass, fen, and marsh (Shapiro, 2022).



Figure 2.1 *Typha angustifolia* grass (The picture was taken from Maasai Mara botanical garden).

Typically, *T. angustifolia* L. is a macrophyte that has the ability to remove harmful metals and toxins by immobilizing them in the sediment and reintroducing them into the earth's geological cycle (Al-Baldawi, 2018). In addition, *Typha angustifolia* L. can emit exudates, promote phytovolatilization, carry oxygen into the rhizosphere, and provide donor surfaces that are absorbent and conducive to biofilm formation (Patro et al., 2023). Through phytoremediation, it can eliminate methylene blue dye and dichloroethane up to 100% in 42 days (El Amri et al., 2022; Namasivayam et al., 2023; Al-Baldawi, 2018). The plant's high biomass accumulation in its tissues and excellent resilience to stress makes it a popular choice for treating wastewater in wetland environments (Ievinsh, 2023). However, *T. angustifolia* L. has not been fully exploited extensively; people frequently overlook and disregard its presence.

2.2 Cellulose

Cellulose an ambigious fibre-forming polymer is a linear homopolymer of β -1,4-linked glucopyranose unit Figure 2.2 (Salim et al., 2021). Each glucopyranose unit consists of three hydroxyl groups, giving it properties like biodegradability, biocompatibility, robustness and insolubility in water (Bhaladhare & Das, 2022). It also serves as the protective wall for plant cells. The degree of polymerization in cellulose obtained from wood can reach 10,000 units, but that derived from cotton has 15,000 units (Siqueira et al., 2010; Trache et al., 2016a). Plant cell walls, such as those found in giant reed, sugarcane bagasse, cotton stalk waste, date seeds, roselle fibers, mengkuang (*Pandanus artocapus*) leaves, waste cotton textiles, and *Typha domingensis* plants, are the primary source of cellulose (Barragán et al., 2019; Evans et al., 2019; Kian et al., 2017; Li et al., 2019; Pandey & Verma, 2018b; Rani & Venkatachalam, 2022; Tlou et al., 2023; Trache

et al., 2016a). Other small sources of cellulose include marine creatures (tunicates), algae, bacteria, fungi, and anchovies (Ismail et al., 2023).

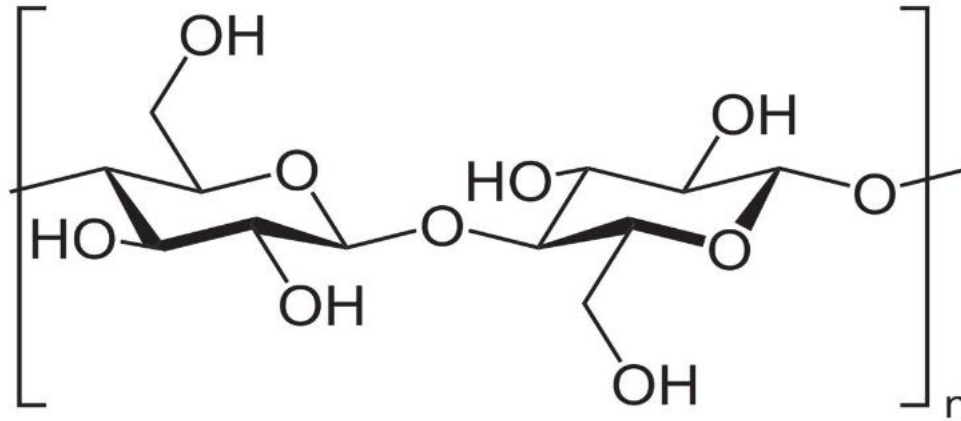


Figure 2.2 Chemical structure of cellulose (4-O- β -D-Glucopyranosyl- β -D-glucopyranose) (Md Salim et al., 2021).

2.2.1 Cellulose nanomaterials

Numerous processing methods have been employed to create cellulose nanoparticles (CNs) with a range of morphologies and physical characteristics (Tayeb et al., 2018a). Cellulose fibres comprise both densely packed highly crystalline domains and loosely packed amorphous areas (Kamali, 2022; Zimmermann et al., 2005). Many names for nanomaterials generated from cellulose have been proposed throughout the past ten years. These include cellulose nanocrystalline, microcrystalline, cellulose nanowhiskers, polysaccharide nanocrystals, cellulose nanocrystals, nanocellulose, cellulose nanofibrils, cellulose microfibrils, cellulose nanofibers, cellulose microfibers, nanofibrillated cellulose, microfibrillated cellulose, Avicel, bacterial cellulose and any combination of the aforementioned (Trache et al., 2020). To standardize the nomenclature, CNs have been divided into two primary groups: cellulose nanocrystals (CNCs) and cellulose

nanofibrils (CNFs) by the Technical Association of the Pulp and Paper Industry (TAPPI), the US Department of Agriculture, the US Forest Service and several Canadian organizations (Davis et al., 2015).

Although different cellulose sources may be used to make both nanomaterials, their manufacturing processes differ. Plant cellulose fibres are mechanically broken down into CNFs in an aqueous media using homogenization, extrusion, or grinding processes. This method of preparation yields CNFs that are only 60–80% crystalline and have lateral dimensions of 5-100 nm and lengths of 0.5–5 μm (Fernandes et al., 2023; Joseph et al., 2020; Tayeb et al., 2018a). In order to reduce the amount of mechanical energy needed to turn raw fibres into CNFs, cellulose fibres are frequently pre-treated with several chemicals, including glycidyl trimethyl ammonium chloride (GTMAC), periodate-chlorite, and 2,2,6,6-tetramethyl-1-piperidinyloxy (TEMPO) (Mohammed, 2017a; Mohammed et al., 2018). Some bacteria, such as *Gluconacetobacter xylinus* and *Acetobacter xylinum*, also known as bacterial cellulose, may be directly used to extract CNFs (Hamimed et al., 2022). By definition, bacterial cellulose falls under CNFs based on its dimensions, which are 10 nm on the sides and 1000 nm on the length (Hamimed et al., 2022). CNCs, on the other hand, are created by the acid hydrolysis of plant cellulose fibres (Mohammed et al., 2018). Figure 2.3 summarises several depictions of the many types of CNs. Figure 2.3 shows pictures from transmission electron microscopy (TEM) and scanning electron microscopy (SEM) of several types of CNCs.

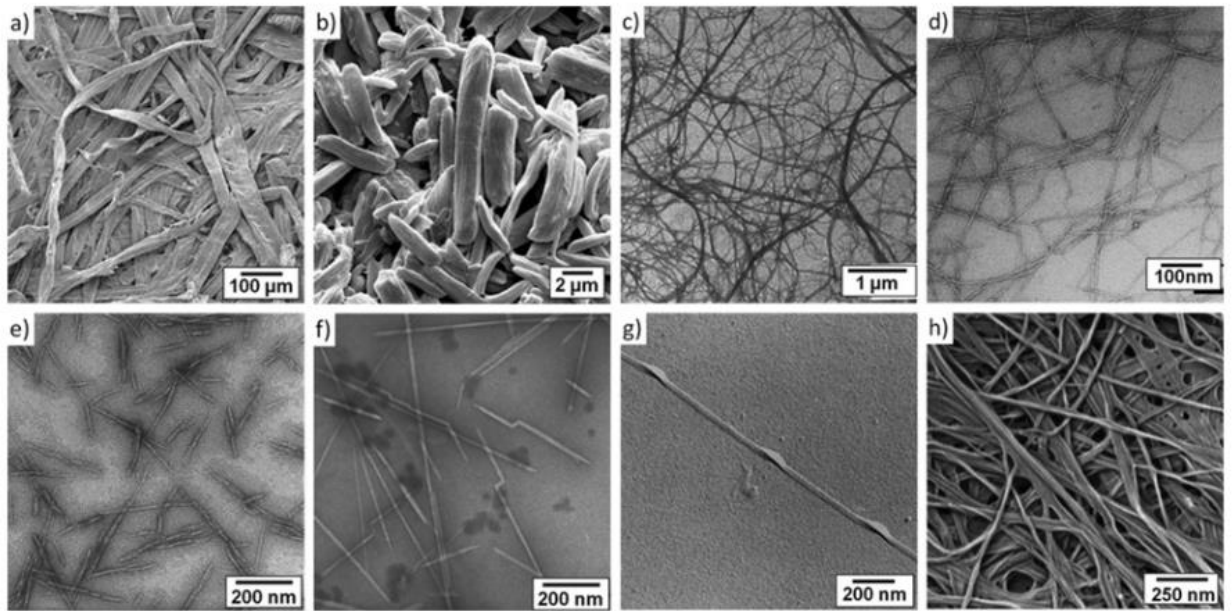


Figure 2.3: CN micrographs CN micrographs: (a) SEM of wood fibre, (b) SEM of microcrystalline cellulose (MCC), and (c) TEM of MCC. (d) TEM picture of TEMPO-CNFs, (e) TEM image of wood CNCs, (f) TEM image of tunicate CNCs, and (g) TEM image of algae CNCs and (h) An SEM picture of bacterial cellulose (Li et al., 2023).

2.2.1.1 Cellulose nanocrystals

CNCs are formed when cellulose fibres undergo acid hydrolysis, which separates the amorphous regions into discrete crystalline domains. CNCs from plant sources have lengths between 100 and 250 nm and lateral diameters between 5 and 70 nm (Hamad, 2017). The nanocrystals that are created when sulfuric acid (H_2SO_4) is hydrolyzed are adorned with negatively charged sulfate ester groups (Jasmania & Thielemans, 2018). These green nanoparticles are biodegradable and have a very large specific surface area, robust mechanical characteristics, and good surface functioning. They are stiffer than aluminum and perform more robustly than steel (Shchipunov & Postnova, 2018). They also have a high aspect-ratio (length/diameter), ranging from 30 to 150 depending on the

source (Mariano et al., 2016). CNCs derive their unique negative charge from the deprotonation of sulfate ester groups that are added to their surface during the hydrolysis of cellulose by H_2SO_4 . Due to the repulsion between these negatively charged sulfate ester groups on them, CNCs may create stable aqueous solutions (Zhang et al., 2023a). Additionally, these suspensions can form chiral nematic ordered phases beyond a threshold concentration in different solutions (Xu et al., 2020). An outline of the cellulose chain and its components is presented in Figure 2.4.

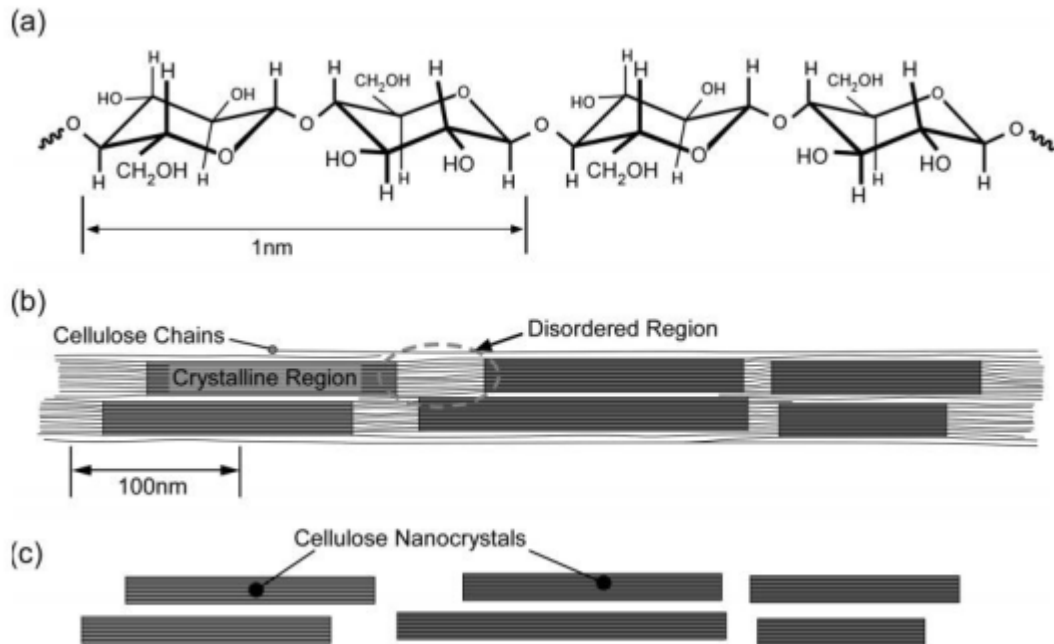


Figure 2. 4 Schematics of (a) a single cellulose chain (b) a cellulose microfibril showing ordered (crystalline) and disordered (amorphous) regions and (c) CNCs after acid hydrolysis of the disordered (Xie et al., 2018).

2.3 Functionalization of Cellulose Nanocrystals

Depending on the desired usage, CNCs' reactive surface, which is covered with many active hydroxyl groups, may also be employed for various functionalizations (Yadav et al., 2023). CNCs are often surface functionalized in order to enable their usage as reinforcing agents in composite materials or to fulfil specialized roles in innovative nanomaterials that have the potential to be used in a variety of industrial areas, including biomedical and personal care (Joseph et al., 2020; Xie et al., 2018). CNCs can be functionalized in various ways; among the most significant methods documented in the literature are esterification, cationization, carboxylation, silylation and polymer grafting (Roy et al., 2009). According to recent research, CNCs may also be surface functionalized with ease by coating them with melamine-formaldehyde (MF) and polydopamine (PD) (Tayeb et al., 2018b). Figure 2.5 shows a schematic illustration of the various chemical changes on the CNC surface.

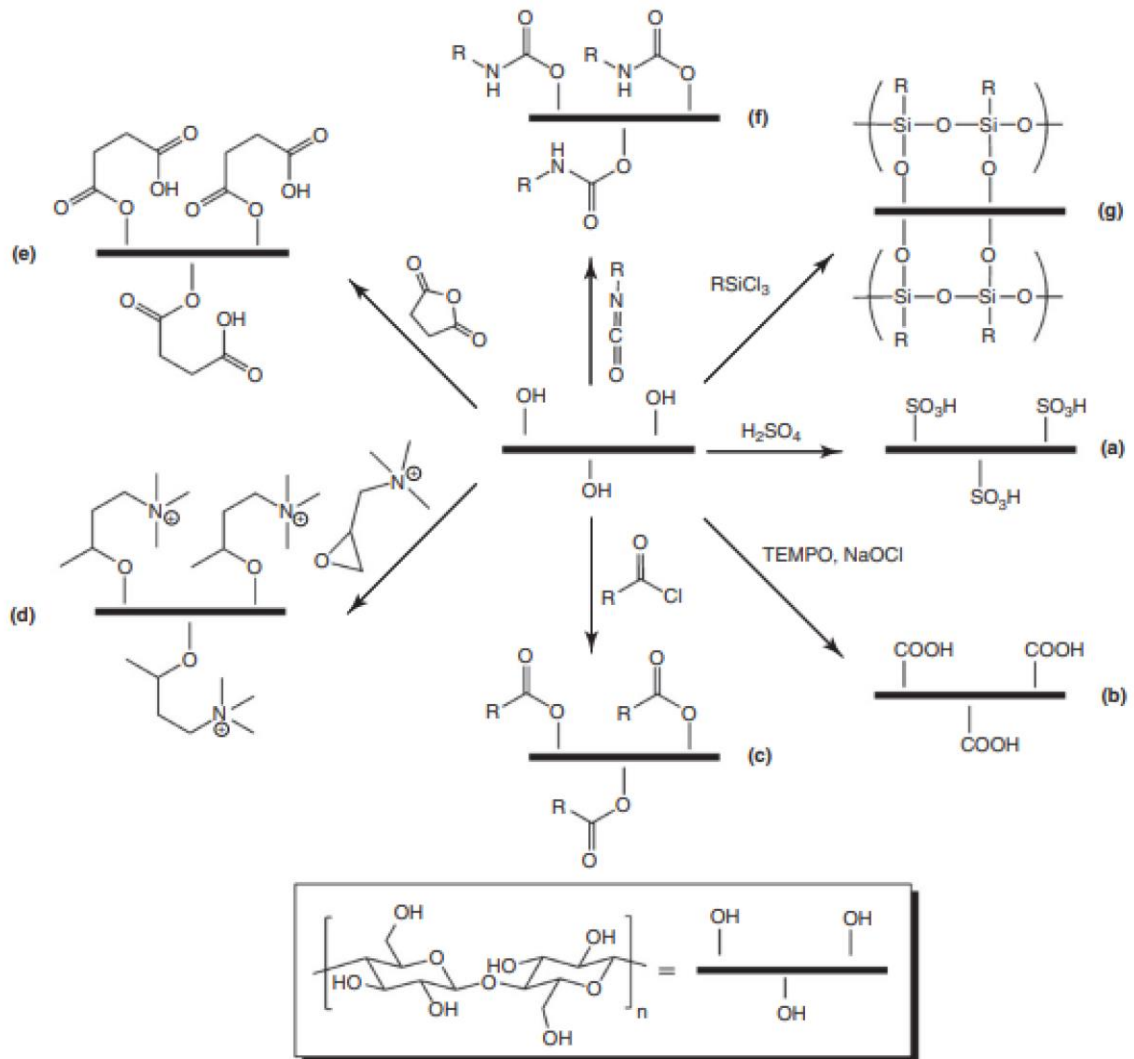


Figure 2.5 Schematic diagram illustrating the various types of chemical modifications on CNC surfaces (Norrurahim et al., 2022).

Furthermore, cellulose nanocrystal composites can also be obtained using cross-linked polymer network architectures that swell with water in the presence of nanoparticles or nanostructures. This can be achieved by forming nanocrystal hydrogels (NCHs) (Akteer et al., 2021; Alessandro et al., 2009). These NCHs contain nanoparticles that cross-link the hydrogel, adsorb or connect to polymer chains, or provide additional characteristics to the hydrogel by being entrapped inside the hydrogel network (Moini et al., 2019).

Polysaccharide nanocrystals, clay nanoparticles, hydroxyapatite nanoparticles, metallic nanoparticles, magnetic nanoparticles, colloidal nanoparticles such as micelles and nanogels, carbon nanotubes, and semiconducting nanoparticles are all examples of nanoparticles often employed in NCH (Karchoubi et al., 2023). Additionally, unique characteristics like synergistic features can be added to polymer hydrogels, depending on the type of nanoparticles used. This makes them promising materials for applications in many biotechnological fields, including electronics, optics, sensors, actuators, microfluidic sectors, catalysis, drug delivery, water treatment and separation devices (Kabir et al., 2018; Wahid et al., 2020). In this study, cellulose nanocrystals were functionalized with magnetic nanoparticles and Beta-cyclodextrine.

2.4 Magnetic Nanoparticles

Mourdikoudis et al. (2021) stated that magnetic nanoparticles comprise a polymeric shell and a magnetic core (Mourdikoudis et al., 2021). The utilisation of magnetic nanoparticles in the treatment of water and wastewater has become popular recently due to their ease of synthesis, high surface area, abundant active sites for interacting with organic and metallic species, ability to be separated after use by an external magnetic field, and lack of internal diffusion resistance (Aragaw et al., 2021). By desorbing the pollutants that have been adsorbed, magnetic nanoparticles can be reused during magnetic separation (Burks et al., 2013). Due to their many uses, iron magnetic particles have become increasingly popular in recent years (Ajinkya et al., 2020). Many forms of iron magnetic particles have been investigated for their potential as adsorbents for organic and metallic pollutants in water, including α -Fe₂O₃, CuFe₂O₄, Fe₂O₃, and maghemite (Can et al., 2012; Jasim et al., 2022). Fe⁰ nanoiron material (Fe⁰NPs), which

are active for remediating contaminants that are susceptible to reductive transformation, such as heavy metals of high valence, azo dyes, halogenated organics, and toxic inorganic anions, are present in these magnetic particles (Akter et al., 2022). According to Jain et al. (2018), nanomagnetic materials are advantageous because they are highly adsorbent due to their large surface to volume ratio, readily controlled by coating and functionalization, and harmless to the environment (Jain et al., 2018).

2.4.1 Iron Nanoparticles

The removal of heavy metals from wastewater using nanosized ferric oxides has been extensively explored. These oxides include goethite (α -FeOOH), hematite (α -Fe₂O₃), amorphous hydrous Fe oxides, maghemite (γ -Fe₂O₃), and magnetite (Fe₃O₄) (Can et al., 2012; Jasim et al., 2022). These nanoparticles, derived from iron's oxidation states, have various chemical characteristics. They are in an extensive range of hydration states and forms (polymorphs) (A. Ali et al., 2016). Iron oxides are nontoxic than other metal nanoparticles, have greater oxidative stability, and work well in nonaqueous environments (Tai et al., 2023). Many applications have found use for these iron nanoparticles, including drug carriers, hyperthermia, magnetic resonance imaging (MRI), proton exchange membrane, sensors, and cancer therapy (Anik et al., 2021; Farzin et al., 2020).

2.4.1.1 Magnetite (Fe₃O₄)

The magnetite (Fe₃O₄) phase is formed by an inverse spinel structure containing Fe(III) ions that are arbitrarily distributed across octahedral and tetrahedral sites, whereas Fe(II) ions are exclusively found in octahedral Figure 2.6 (Phan et al., 2016). It has distinct electrical and magnetic characteristics due to electron transport between Fe²⁺ and Fe³⁺ at

cubic sites (Guerra et al., 2023). Magnetite Fe_3O_4 has the most fascinating features of any iron oxide due to the existence of iron cations in two valence states, Fe^{2+} and Fe^{3+} , in the inverse spinel structure. Natural magnetite occurs as the black, ferromagnetic mineral known as lodestone. Despite this, magnetite nanoparticles are the most researched materials because of their high saturation magnetization and superparamagnetic behavior at room temperature in reaction to a magnetic field (Guerra et al., 2023; Nguyen et al., 2021a).

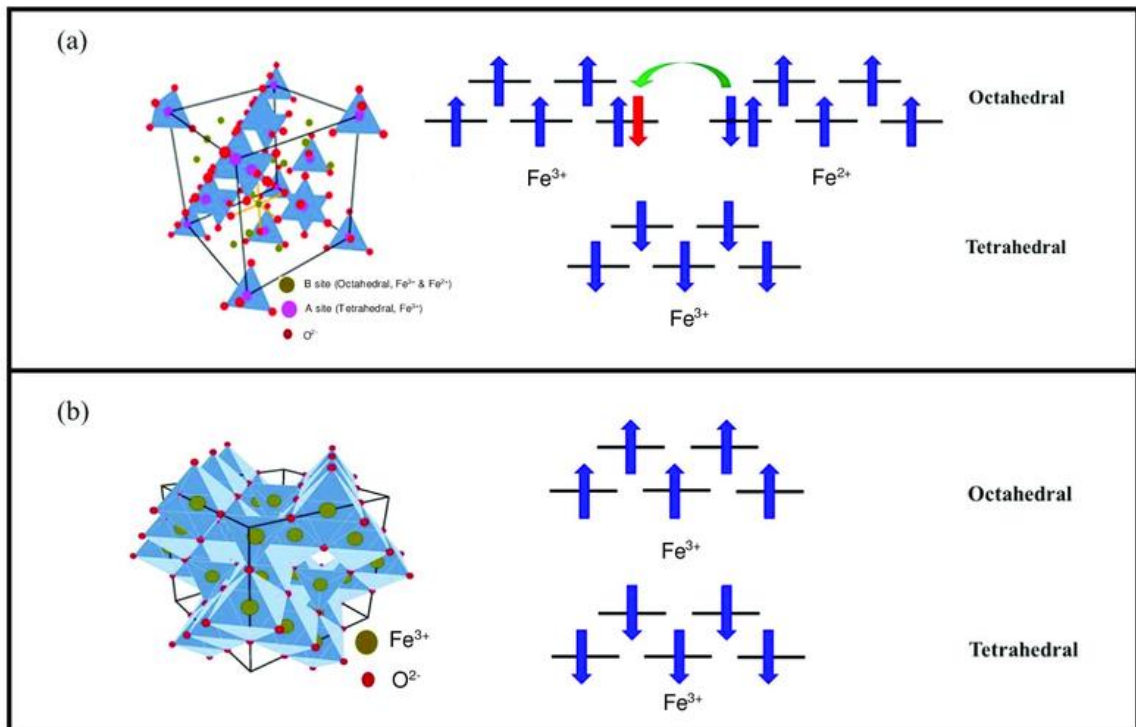


Figure 2.6: Magnetite-based iron oxide nanoparticles crystal arrangement (Phan et al., 2016).

2.4.1.2 Hematite ($\alpha\text{-Fe}_2\text{O}_3$)

Rocks and soils naturally contain the mineral hematite, which is ferric oxide. It has a corundum structure, with Fe(III) ions filling octahedral holes and oxide ions forming a

hexagonal tight packing lattice Figure 2.7 (Koemets, 2020; Pailhé et al., 2008). Fe(III) ions occupy two-thirds of the holes, resulting in Fe(O)₆ octahedra pairs. Each octahedron in the structure has three neighbours on the same plane as its edges, and another octahedron from a different plane shares its face (Koemets, 2020). According to Yin et al. (2024), hematite has been used to remove dyes and heavy metals from aqueous solutions (Yin et al., 2024).

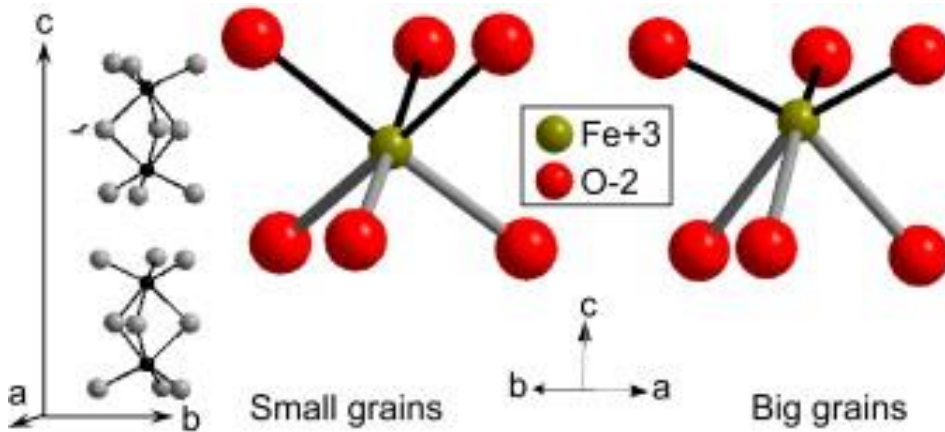


Figure 2.7: Structural features on pigment properties of α-Fe₂O₃ haematite (Pailhé et al., 2008).

2.4.1.3 Zero-valent iron

Numerous contaminants can be effectively removed from aqueous solutions using nano zero-valent iron (nZVI), a potent reducing agent. The nZVI may reportedly adsorb and co-precipitate chromium (III) in solution, as well as convert Cr(VI) to Cr(III) (Zhuang et al., 2023). Because nZVI particles have a high specific surface area and significant redox potential, they have also been utilized to treat a wide range of pollutants, such as textile wastewaters, nitrochlorobenzene, nitrites, chlorinated hydrocarbons, dyes, and nitrites

(Liu et al., 2023). Figure 2.8 shows the mechanism of iron uptake by nano zero-valent iron particles (Antony et al., 2021).

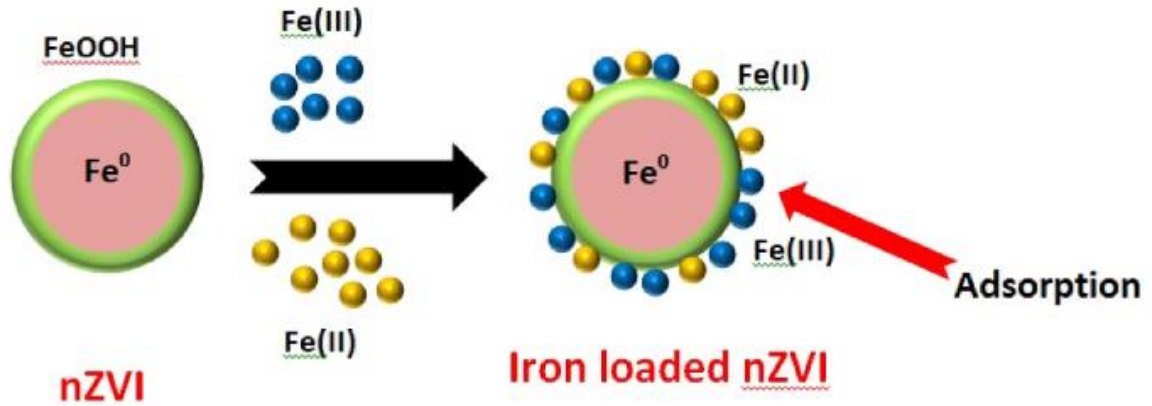


Figure 2.8: Nano zero-valent iron particles (Antony et al., 2021).

2.4.2 Synthesis of Fe_3O_4 Nanoparticles

Fe_3O_4 nanoparticles' distinct size, biocompatibility, minimal toxicity, and superparamagnetic characteristics, magnetic nanoparticles are becoming increasingly valuable instruments in various disciplines, including biology, physics, medicine, the environment, and material science (Stueber et al., 2021). Most of these applications need the nanoparticle to be evenly sized, shaped and evenly distributed throughout a solvent. Selecting the best synthesis technique or altering preparation circumstances might help optimize characteristics (Szczyglewska et al., 2023). The synthesis of iron oxide nanoparticles for diverse applications has been documented using a range of techniques, such as co-precipitation, thermal decomposition, sol-gel synthesis, hydrothermal reaction, micro emulsion synthesis, solvothermal synthesis, laser pyrolysis and high-temperature organic phase decomposition (Zadehnazari, 2024). For preparing Fe_3O_4 in various forms, these investigations offered several helpful preparation techniques. According to Mohsen

et al. (2014), chemical co-precipitation has been identified as the most promising approach among the presented techniques due to its simplicity, productivity, and ability to produce spherical-shaped Fe_3O_4 . In the section that follows, the most popular methods for preparing materials for use in metal removals are briefly described (Rezaei et al., 2024; Yaghoobi et al., 2023).

2.4.2.1 Micro emulsion method

A microemulsion is a thermodynamically stable isotropic dispersion of two immiscible liquids that contain nanosized domains of one or both liquids and is stabilized by an interfacial coating of surface-active molecules. Microemulsions are characterized as water-in-oil (w/o) or oil-in-water (o/w) based on the scattered and continuous phases (Roohinejad et al., 2018; Zielińska-Jurek et al., 2012). Water and oil (w/o) microemulsion is a process that uses nanosized water droplets distributed in an oil phase and stabilized by surfactant molecules at the water/oil interface. The main benefit of microemulsion systems is that the size of nanoparticles may be regulated by changing their composition and adjusting the size of the aqueous micellar core (Das et al., 2020). Utilizing microemulsions to create magnetic nanoparticles has a number of drawbacks, though. Largely aggregated nanoparticles are first produced frequently. In addition, because the process is typically carried out at a low temperature, the nanoparticles lack crystallinity (Liu et al., 2020). However, according to Ying et al. (2022), the yield of the nanoparticles is frequently relatively poor (Ying et al., 2022).

2.4.2.2 Hydrothermal

Aqueous hydrothermal reactions are conducted in autoclaves or high-pressure reactors, where temperatures exceeding 200°C and pressures up to 2000 psi can be reached (de

Conti et al., 2022). Tiny nanoparticles (NPs) are created when temperatures are high enough to cause rapid nucleation and quicker development of the newly generated particles. Magnetite may originate under hydrothermal circumstances in two significant ways: Two processes are involved in neutralizing mixed metal hydroxides: hydrolysis and oxidation. Except for the fact that the first approach uses solely ferrous salts, these two reactions are pretty similar. Reaction parameters, including temperature, duration, and solvent, often significantly impact the results in this process. Particle size in the hydrothermal process is primarily regulated by grain growth and nucleation rate mechanisms. While pH and precursor material reaction conditions affect the phase purity of the nanoparticles, time and temperature regulate the size and morphology of the products in hydrothermal reactions (A. Ali et al., 2021; Rashid et al., 2020).

2.4.2.3 Co-precipitation method

Co-precipitation is the most frequently utilized to create magnetic iron oxide nanoparticles shown in Figure 2.9 below. Using the co-precipitation technique, NaOH or NH₄OH is added as a precipitating agent, and magnetite nanoparticles are precipitated from a mixed ferrous and ferric salt solution. This technology has the benefit of being quick, easy, affordable, adaptable and diversified. It also allows for the simultaneous preparation of surface modification and synthesising of vast amounts of particles (Dudchenko et al., 2022). The kind of salts utilized (chlorides, sulphates, nitrates and perchlorates), temperature, pH of the solution, the ratio of Fe²⁺ to Fe³⁺, and the ionic strength of the precipitation medium all affect the size, composition and form of the nanoparticles. This technique has produced particles that range in size from 5 to 100 nm (A. Ali et al., 2021). The magnetite reaction may be expressed as shown in Equation 2.1.

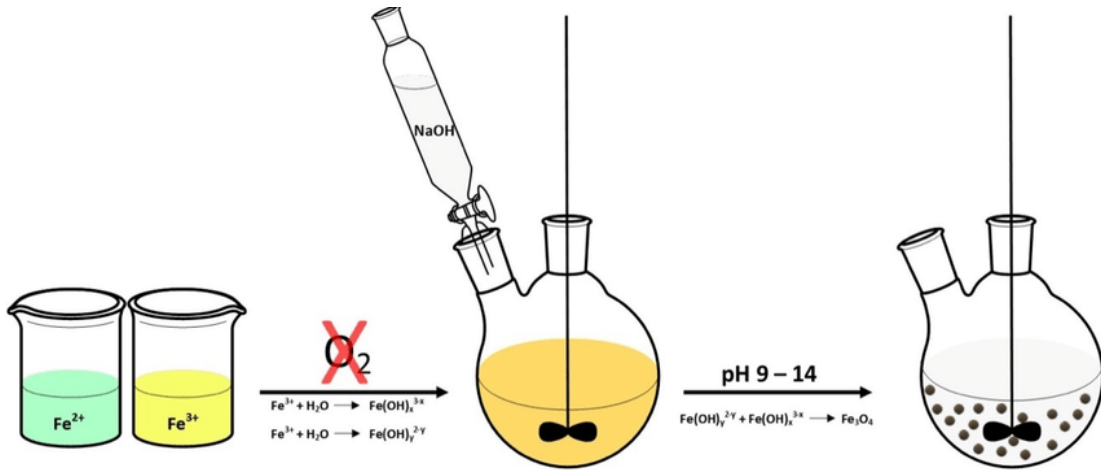
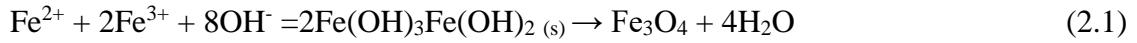


Figure 2.9: Schematic diagram for synthesising iron oxide nanoparticles (Zamani Kouhpanji & Stadler, 2020).

2.4.3 Application of Magnetic Nanoparticles for Pollutant Removal

The use of nanosized magnetic materials as adsorbents for removing pollutants has garnered significant interest recently because of its many benefits, including simplicity of functional modification, high separation efficiency, a straightforward manipulation method and benign operating conditions (Ali et al., 2021). Additionally, they have a large surface area and excellent magnetic qualities, which promote high adsorption efficiency, a high rate of contamination removal and simple, quick magnetic field separation of the adsorbent from the solution. After magnetic separation, hazardous substances that have been adsorbed can be removed, making magnetic nanoparticles reusable (Shen et al., 2023). Their fundamental characteristics, such as their minuscule size, high surface-area-to-volume ratio, and lack of internal diffusion resistance, offer superior adsorption kinetics for metal ions in aqueous solutions. Superparamagnetic magnetite nanoparticles are easily magnetized by an external magnetic field and quickly demagnetize when the

field is removed, losing all of their magnetism in the process (Ali et al., 2021). Because of their high specific surface energy and anisotropic dipolar attraction, magnetite nanoparticles combine to form more prominent clusters, which may result in a loss of superparamagnetism and restrict their uses. Magnetic nanoparticles are also vulnerable to air oxidation. The surface modification of MNPs imparts several benefits, including water solubility, biocompatibility, non-toxicity, nonspecific adsorption to cells, and bioconjugation, in addition to preventing aggregation/agglomeration and promoting colloidal stability Figure 2.10 (Manoj et al., 2024; Mushtaq et al., 2022).

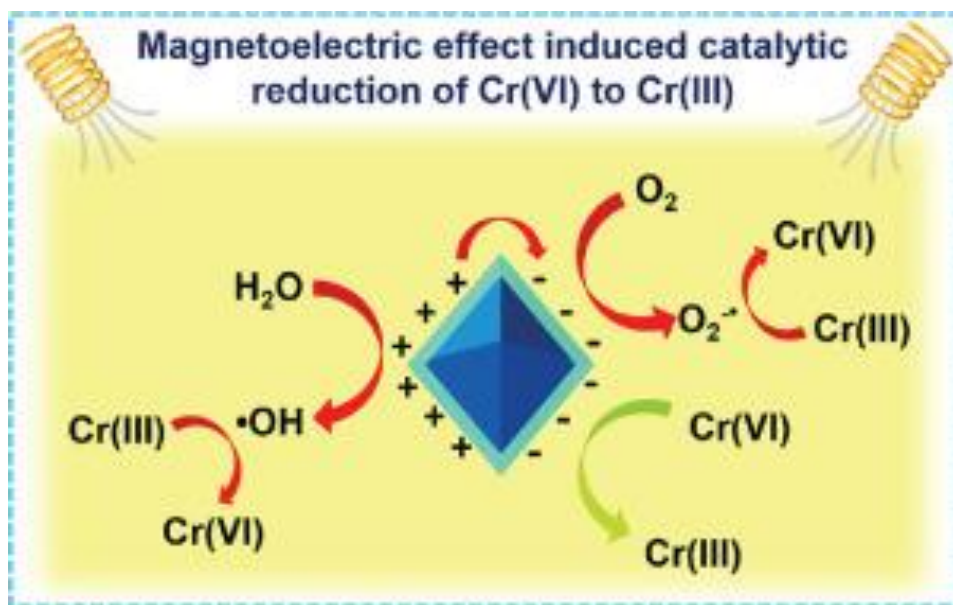


Figure 2. 10: Magnetoelectric reduction of chromium (VI) to chromium (III) (Mushtaq et al., 2022).

2.4.4 Functionalization/Coating of Magnetic Nanoparticles

Agglomeration is a significant problem when using nanoparticles, and it primarily results from direct interparticle interactions caused by Van der Waals forces and magnetic contact (Endres et al., 2021). According to Nedylakova et al. (2024), this aggregation

event lowers specific surface area, interfacial free energy, and particle reactivity (Nedylakova et al., 2024).

It is also known that iron magnetic nanoparticles, particularly Fe_3O_4 , exhibit poor selectivity and stability in acidic environments (Nedylakova et al., 2024). Determining the durability of nanoparticles under physiochemical circumstances so heavily relies on surface modification employing a stabilizer. These stabilizers can increase the dispersion of the nanoparticles by steric hindrance and electrostatic repulsion (Biehl et al., 2018) as shown in Figure 2.11. Magnetic nanoparticles can be added to a solid matrix made of polymers, silica, organic coating agents, carbon, zeolites, and biomaterials to facilitate separating wastewater from the solid matrix (Phouthavong et al., 2022).

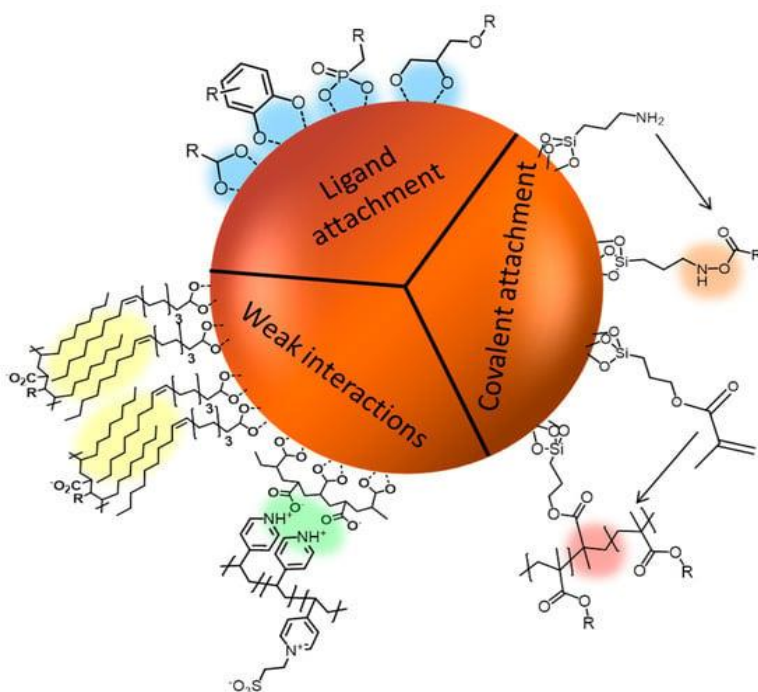


Figure 2.11: Magnetic nanoparticles featuring polyzwitterionic coatings (Biehl et al., 2018).

2.4.4.1 Coating of magnetic nanoparticles onto biomaterials

Adsorbents such as magnetic nanomaterials are typically injected straight into the effluent stream when used in water treatment. Separating the nanoparticles from the aqueous solution that follows can be challenging and time-consuming, and it can cause clogging in continuous systems (Phouthavong et al., 2022). Using biomaterials to coat magnetic nanoparticles combines the biomaterial's adsorption properties, which come from the presence of its functional groups with the comparatively high specific surface area, high number of active sites, and ease of separation provided by the magnetic species (Vallinayagam et al., 2021). Biological materials such as seaweed, orange peel powder, shellac, tea waste, orange peel pith, cross-linked pectin, polyacrylic acid, humic acid, gum arabic, and chitosan have been used to coat magnetic nanoparticles (Bardajee & Hooshyar, 2013; Manoj et al., 2024; Nasrollahzadeh et al., 2021; Nguyen et al., 2021; Rezaei et al., 2024; Rostami et al., 2024; Tang et al., 2017). The produced magnetic nanomaterial-biosorbents are used to extract organic contaminants and heavy metals from aqueous solutions. The size of the nanoparticles can be controlled by adding chelating organic anions, such as carboxylate ions (such as citric, gluconic, or oleic acid) or polymer surface complexing agents (such as dextran, carboxydextran, cyclodextrine, starch, or polyvinyl alcohol) during the magnetite formation process (Burke et al., 2002; Mohammed, 2017a; Mourdikoudis et al., 2021; Shchipunov & Postnova, 2018; Wahid et al., 2020). This can thus be achieved through molecular recognition of compounds.

2.5 Molecular Recognition Compounds

Molecular recognition pertains to a particular contact that occurs between two or more molecules through non-covalent bonding, such as van der Waals forces, electrostatic

effects, hydrophobic interaction, halogen bonding, metal coordination, and hydrogen bonding (Mahmudov et al., 2017; Schneider, 2009). When molecular recognition is used in separation processes, chemical separation is achieved by attaching a chemical molecule with robust species selectivity to a solid substrate. According to Mujahid et al. (2023), the recognition molecule known as the "host" has a high degree of recognition of particular elements or compounds known as the "guest". Even at low concentrations of the "guest" or when the guest is in intricate matrices, the compound's identification property ought to be successful (Beatty & Hof, 2021; Mujahid et al., 2023). Typically, the bigger molecule that encloses the smaller "guest" molecule is referred to as the "host" compound. Cyclodextrin, calixarenes, pillararenes, cucurbiturils, porphyrins, crown ethers, cryptophanes and so on are recognized "host" molecules. The theory that the interaction between host and guest molecules results in a decreased overall Gibbs free energy is the basis for the thermodynamic advantages of host-guest chemistry (Schneider, 2015). Cyclodextrin (CD), a cyclic oligosaccharide formed by D-glucopyranose monomers bound together by α -1,4-glycosidic linkages and closed in a ring to form a hollow structure of a truncated cone, is one crucial recognition compound used in water and wastewater treatment for host-guest interaction (Pholosi, 2019). Non-covalent interactions, such as van der Waals, hydrophobic, electrostatic, and charge transfer interactions, metal coordination, hydrogen bonding, and steric effects, are what drive host-guest supramolecular complexes comprising an amphiphilic molecule and a cyclodextrin ring (Liu et al., 2013).

2.5.1 Cyclodextrin

A class of compounds known as cyclodextrins (CDs) comprises molecules of sugar (starch) bonded to one another in a cyclic ring. α -, β -, and γ -CD refers to a class of naturally occurring cyclic oligosaccharides consisting of six, seven, or eight glucose subunits connected by α -(1,4) glycosidic linkages forming a torus-shaped structure (Poulson et al., 2021b). Hydrogen atoms and oxygen bridges are present in the interior cavity of the three-dimensional structures created during CD, with hydroxyl groups remaining on the outside borders. Because of this structure, Cyclodextrin has a hydrophobic centre chamber and an interior hydrophilic surface (Goyal et al., 2023). The interior cavity may retain non-polar pollutants while the external surface maintains hydrophilic properties. Because cyclodextrin-based polymers effectively remove pollutants from polycontaminated mixtures, even at low trace quantities, they can potentially bring both organic and inorganic contaminants from water down to acceptable levels (Liu et al., 2024). Because of their remarkable sorption capabilities, cyclodextrin-based polymeric materials have received attention recently in a wide range of applications. Due to the cavity's characteristics and dimensions, CDs may form inclusion complexes with a wide range of guest molecules with different chemical and physical characteristics in both the solid and solution states (Xu et al., 2023). Because of their unique structure, physicochemical properties, chemical stability, high reactivity, and excellent selectivity towards aromatic compounds and metals, all of which are caused by the presence of chemically reactive groups (hydroxyl, acetamido, or amino functions) in polymer chains, CDs offer an intriguing and alluring alternative as adsorbents (Liu et al.,

2024b). Table 2.1 illustrates the features of the α -, β -, and γ -CD chemical structures, shown in Figure 2.12 below.

Table 2. 1: Properties of natural cyclodextrins (Varan, 2023).

<i>Property</i>	α-Cyclodextrin	β-Cyclodextrin	γ-Cyclodextrin
Number of glucose units	6	7	8
Molecular weight	972	1134	1296
Approximate inner cavity diameter (pm)	500	620	800
Approximate outer diameter (pm)	1460	1540	1750
Approximate volume of cavity (10^6 pm^3)	174	262	427
Solubility in water at 25°C (g/100 mL)	14.5	1.85	23.2
Surface tension (MN/m)	71	71	71
Melting temperature range (°C)	255-260	255-265	240-245
Crystal water content (wt.%)	10.2	13-15	8-18
Water molecules in the cavity	6	11	17

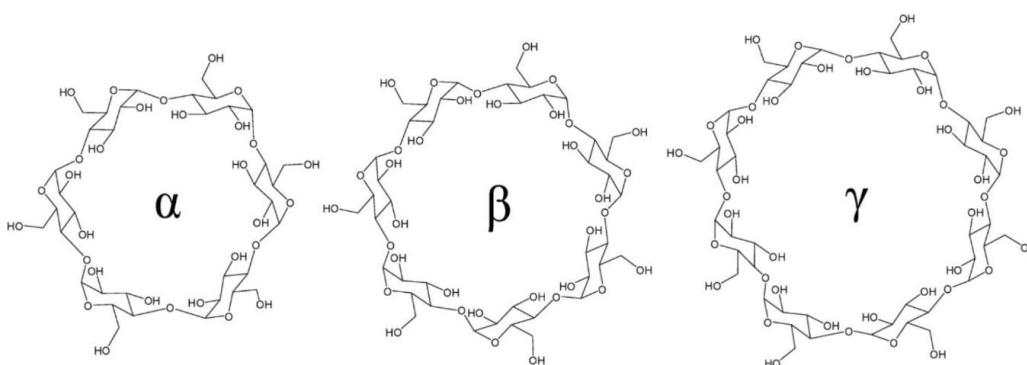


Figure 2.12: Chemical structure of alpha- (α -CD), beta- (β -CD) and gamma- (γ -CD) cyclodextrins (Li et al., 2007).

2.5.1.1 Beta-Cyclodextrin

β -CD, one of the three varieties of Cyclodextrin, has a quite stiff structure and includes a secondary belt made of hydrogen bonds (Poulson et al., 2021b). The glucose unit of β -CD has 21 hydroxyl groups at positions 2, 3, and 6, which are very reactive and can form multiple connections as shown in Figure 2.13 (Amanulla et al., 2018; Noreña-Caro & Alvarez-Láinez, 2016). Moreover, the hydrophobic cavity of β -CD allows it to identify and accept a wide range of chemicals, contributing to its outstanding intermolecular interaction. The most widely used type of CD is β -CD because of its inexpensive cost, simplicity of production and hollow interior that can accommodate many molecules (Cid-Samamed et al., 2022). However, the fact that they are highly soluble in water is their primary drawback, which restricts their use in the removal of contaminants from wastewater. Several investigations have been carried out to address the solubility issue by creating β -cyclodextrin polymer (β -CDP), which is water-insoluble (Urooj et al., 2024).

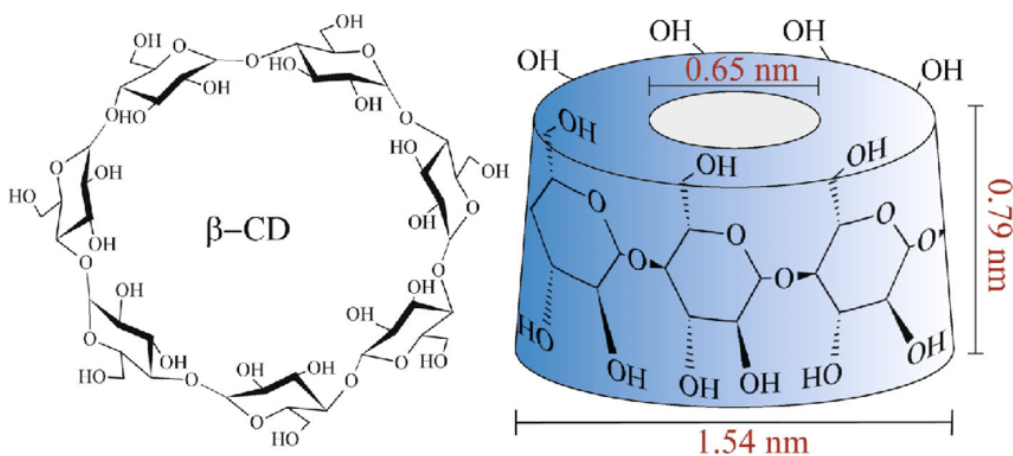


Figure 2.13: Chemical structure and shape of the β -cyclodextrin molecule (Amanulla et al., 2018; Noreña-Caro & Alvarez-Láinez, 2016).

2.5.2 Cross-Linking

To create a three-dimensional network, a cross-linking agent reagent must first induce cross-links and/or intermolecular bridges between polysaccharide macromolecules (Li & Lin, 2021). According to Dunky (2021), chemical cross-linkers for carbohydrates are polyfunctional substances with electrophilic properties that create covalent connections with the molecules' free reactive hydroxyl groups (Dunky, 2021). There have been studies and applications of several cross-linkers for carbohydrate molecules, such as diisocyanate, glutaraldehyde, epichlorohydrin (1-chloro-2,3-epoxypropane), and dicarboxylic acids (de Gimenez & Mota, 2023). After applying the cross-linker, the carbohydrate molecules typically branch out and form a three-dimensional network that changes their solubility in water to an insoluble, regenerative network-shaped polymer that can be used in various applications (de Gimenez & Mota, 2023).

Biomaterials and particular molecular recognition compounds have been linked together through cross-linkers. Examples of these include composites made of cotton and cyclodextrin (CD) that were cross-linked using vinyl monomer (Syeda et al., 2022); starch and cyclodextrin (CD) that were cross-linked using hexamethylene diisocyanate (HMDI) (Zhao & Sillanpää, 2020); and chitosan beads and Cyclodextrin that were linked together using hexamethylene diisocyanate (HMDI) (Zhao & Sillanpää, 2020). Lone pairs of electrons on the oxygen of $-OH$ on the carbohydrate and/or molecular recognition compound interact with the epoxide's electron-efficient carbon ($-CH_2^-$) in the instance of epichlorohydrin (EPI). β -CD molecules can form cross-linked networks because of their polyfunctionality and unique structure (Cova et al., 2021b). By directly reacting its hydroxyl groups with a coupling agent, β -CD can generate water-soluble or

water-insoluble polymeric structures by cross-linking. A heterogeneous mixture of several CD glyceryl ethers is the main byproduct of the reaction of CD with a coupling agent, such as epichlorohydrin (EPI) or hexamethylene diisocyanate (HMDI), in an alkaline media. The benefits of cross-linked beads include enhanced ease of use, quicker kinetics, and intriguing diffusion characteristics (Sun et al., 2022). The cross-linked materials are readily regenerable by solvent extraction or washing after adsorption. Even when crystallinity changes, cross-linked materials maintain their original characteristics and are unaffected by basic or acidic solutions (Pellicer et al., 2020). Figure 2.14 below shows an example of cross-linked with gold for adsorption of chromium ions (Amanulla et al., 2018).

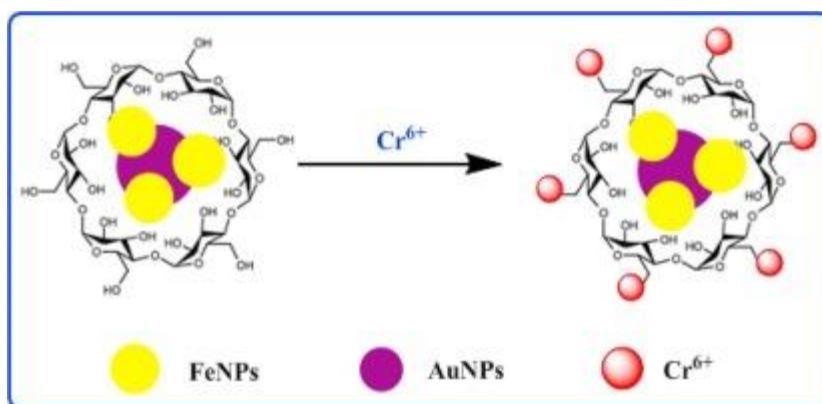


Figure 2.14: Cyclodextrin functionalized nanoparticles for hexavalent chromium removal (Amanulla et al., 2018).

2.5.2.1 Cross-linking Cyclodextrin to Magnetic Nanoparticles

Cross-linking or altering soluble Cyclodextrin with various materials to remove different contaminants from aqueous solution has been the subject of recent investigations. Adding magnetite-coated nanoparticles to Cyclodextrin would combine the benefits of both

materials and advance the development of better-quality adsorbents (Syeda et al., 2022). Using carboxymethyl- β -CD modified Fe_3O_4 nanoparticles (CM-CD-MNPs), Kaboudin et al. (2021) created a nano-sorbent for the removal of copper ions and methylene dye from aqueous solution (Kaboudin et al., 2021). It was hypothesized that CM- β -CD formed metal complexes crucial to its capacity to reduce metal toxicity. Methylene blue adsorption took 50 minutes to reach equilibrium, with 85–90% of the material adsorbed after 20 minutes of contact. Using triazinyl- β -CD-modified magnetic nanoparticles (T- β -CD-MNPs), Wadhawan et al. (2020) described a straightforward, economical, and ecologically friendly production of a new nanosorbent (Wadhawan et al., 2020). This study used hexamethylene diisocyanate to cross-link a new magnetite-coated pine cone to cyclodextrin and carboxymethyl cyclodextrin (Wu et al., 2021). Figure 2.15 below illustrates chromium adsorption performance and mechanism on β -cyclodextrin-modified molybdenum disulfide.

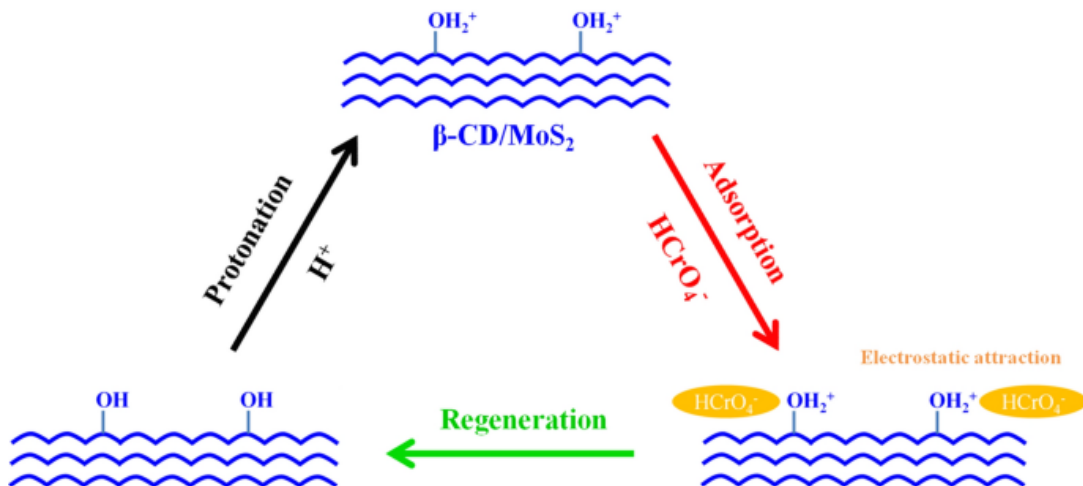


Figure 2.15: β -cyclodextrin-modified molybdenum disulfide for removal of Cr(VI) (Cheang et al., 2022).

2.6 Adsorption Process

Adsorption is a phase transfer process in which chemical species preferentially collect at the interface between two phases (Králík, 2014). These phases can be liquid-liquid, liquid-solid, gas-solid, or gas-liquid mixtures as shown in Figure 2.16. The adsorbing phase is the adsorbent, and the chemical species being adsorbed is the adsorbate. The driving force for adsorption is determined by the interaction between the adsorbate and the adsorbent and may vary between phases. Most adsorption processes fall into one of three categories: (a) physical adsorption, (b) chemical adsorption, and (c) electrostatic adsorption (Alaqrbeh, 2021). Whereas chemical adsorption involves the adsorption of an adsorbate to an adsorbent surface by the creation of a chemical bond, physical adsorption is driven by weak intermolecular interactions such as hydrogen bonding and van der Waals between the adsorbate and the surface of the adsorbent. The coulombic attraction between the adsorbate and adsorbent surface drives electrostatic adsorption or ion exchange (Pourhakkak et al., 2021). One method that is frequently used to remove impurities from water is adsorption. Of all the techniques used to treat water, adsorption produces the highest-quality treated water when used in conjunction with a carefully thought-out system. Furthermore, this method is better than others because of its straightforward construction and operation, cheap initial cost, efficiency and insensitivity to hazardous materials (Pillai, 2024; saad Algarni & Al-Mohaimed, 2022).

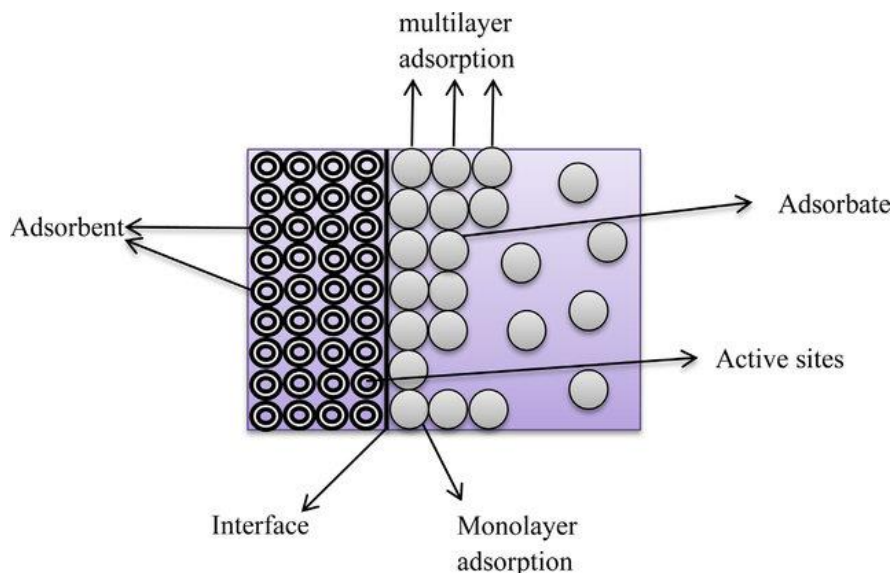


Figure 2.16: Schematic representation of the adsorption process onto a solid adsorbent (Soliman & Moustafa, 2020).

2.6.1 Adsorption mechanism

The adsorption mechanism is a complex process involving several mechanisms, such as chelation, chemisorption, complexation, adsorption on surfaces and pores, ion exchange, entrapment in inter- and intrafibrillar capillaries, and adsorption by physical forces, draws the metal ion species to the sorbent due to its strong affinity for them (de Castro-Alves et al., 2024; Manos & Kanatzidis, 2016).

2.6.2 Factors affecting adsorption

According to studies by Tee et al. (2022), the adsorption process is primarily influenced by several factors, such as the initial concentration of pollutants, solution pH, adsorbent surface area, temperature, ionic strength, competing ions, contact time, and adsorbent particle size (Tee et al., 2022b). According to various studies, when the adsorbent dosage, beginning concentration, contact duration, and stirring speed are increased, the percentage removal of the majority of different contaminants typically increases by 31%

(Ahmed et al., 2021b; Khan et al., 2022; Rout et al., 2021). The following subsections discuss the various variables influencing how adsorbents absorb pollutants.

2.6.2.1 Solution pH

According to earlier studies, one significant factor influencing the adsorption process is the pH of the solution (Rápó & Tonk, 2021). The degree of ionization, the metal chemistry, and the surface characteristics of the mineral are all strongly impacted by the pH of the solution (Chen, 2021). Figure 2.17 illustrates the effect of pH on Cr (VI) adsorption with Cr species distribution (Mancilla et al., 2022). Low solution pH causes the solution to be acidic and have a large concentration of H^+ ions, which will compete with the Cs^+ ions for adsorption sites and reduce the absorption of Cs^+ . On the other hand, the ionization of surface acid groups and the drop in H^+ ion concentration in the solution cause an increase in Cs^+ absorption when the solution pH rises (Priya et al., 2022). Zn(II) adsorption onto rice husk was investigated by Sanka et al. (2020) about the pH range of the solution, which was 2 to 8. According to their observations, Zn(II) was removed at a rate that increased with pH and peaked at pH 6 (Hossain et al., 2022; Sanka et al., 2020). Additionally, it has been shown that cation adsorption is higher at pH values greater than the point of zero charge (pHPZC) and lower at pH values lower than the point of zero charge (Al-Maliky et al., 2021). This results from the cation ions electrostatic interactions with the negative surface charge at higher pH values (Al-Maliky et al., 2021).

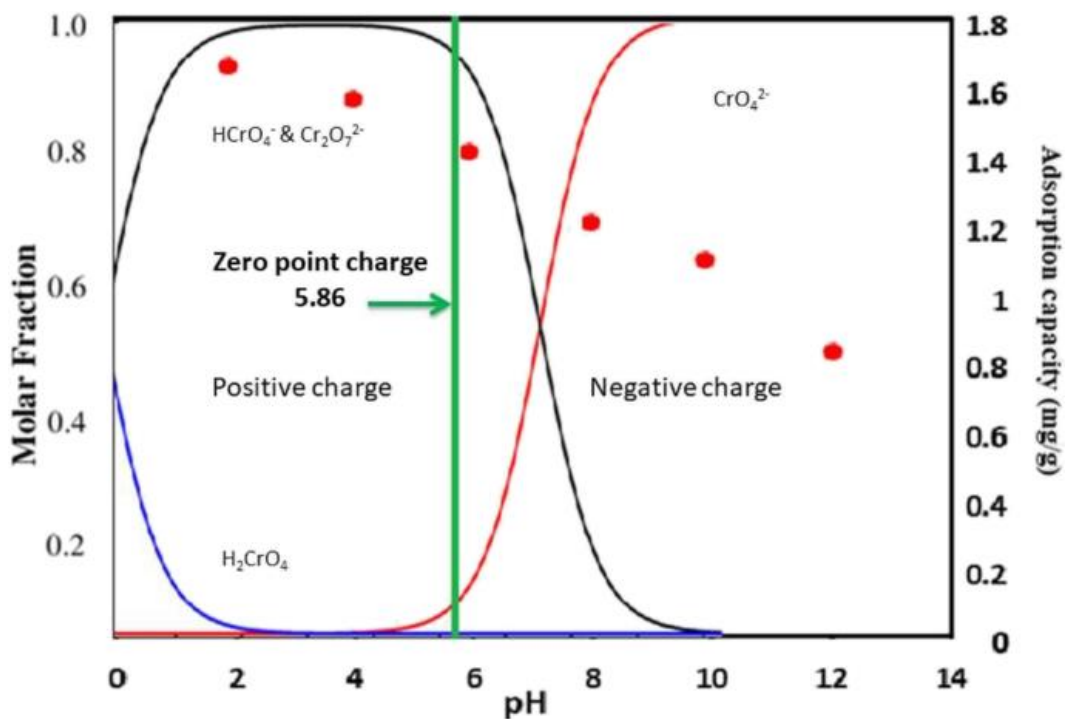


Figure 2. 17: Behaviour of chromium in different pH environments (Mancilla et al., 2022).

2.6.2.2 Adsorbent dose

The adsorbent dosage was shown to have a significant impact on the adsorption of heavy metals. Research has shown that increasing the dose of adsorbent causes an increase in the proportion of pollutants removed. This is significant given the increased number of adsorption sites at larger adsorbent dosages (Qasem et al., 2021a). Chakraborty et al., 2022; Syeda et al., 2022 investigated modified agricultural waste for metal ion adsorption; their research noted a significant surface area available, making the removal of metal ions rise as the adsorbent dosage increases.

2.6.2.3 Temperature

A number of scholars have also looked at how temperature affects adsorption experiments. Thermodynamic parameter changes are as a result of temperature variations.

Temperature-dependent changes in pollutant adsorption can produce an exothermic reaction by decreasing or increasing or cause an endothermic process by rising with temperature (Pourhakkak et al., 2021). According to several investigations, most contaminants or heavy metals have been shown to adsorb by an endothermic mechanism. The rate at which the adsorbate diffuses increases due to a temperature rise. High temperatures often cause molecules at the boundary layer contact to become more active, which might speed up the solute's diffusion (Raji et al., 2023).

The adsorbate's surface activity and kinetic energy both rise with temperature. Nonetheless, it has been suggested that the adsorbent's physical structure could be potentially impacted (Fomina and Gadd, 2014; Gautam et al., 2014; Wang et al., 2020). Agrahari et al. (2023) examined how Mosambi (Citrus limetta) peel absorbed Cr(VI) metal ions. They observed that Cr(VI) removal increased when the temperature rose, resulting in an endothermic reaction (Agrahari et al., 2023).

2.6.2.4 Initial concentration of pollutant

Research has indicated that the adsorption process is significantly impacted by the pollutant's initial concentration in the liquid phase (Pourhakkak et al., 2021). Adsorption is independent of starting concentration at low concentrations because the ratio of contaminants to adsorbent mass is low. More pollutants are accessible when the starting concentration is raised, and more pollutants are absorbed for a given adsorbent mass (Busetty, 2019). The need to overcome the mass transfer barrier for the contaminants to migrate from the bulk solution to the mineral surface rises with more significant starting concentrations (Ouyang et al., 1996; Sen & Khilar, 2006; Pourhakkak et al., 2021). It has

been discovered in several investigations that an increase in the starting concentration increases the percentage removal (Tee et al., 2022).

2.7 Adsorbents of Heavy Metal Ions Using Cellulose-Based Adsorbents

The most popular adsorbent for treating wastewater is activated carbon (El Gamal et al., 2018). However, the cost of activated carbon is increased by the energy needed for its creation and regeneration (El Gamal et al., 2018). Therefore, a strong incentive exists to create low-cost substitute adsorbents from industrial and agricultural waste (Bushra et al., 2021). Activated carbon has a higher carbon footprint during manufacture and regeneration than sustainable nanomaterials from cellulose. An estimated 8.5 pounds and 7.0 pounds of carbon dioxide (CO₂) are released annually during the production and regeneration of 1.0 pound of granular activated carbon, respectively (El Gamal et al., 2018; Vilén et al., 2022). Mechanical disintegration and sulfuric acid hydrolysis are also used to prepare the CNCs. Canada-based Celluforce Inc. produces about one ton of CNCs every day in their pilot plant, and they have already shown that it is feasible to recycle a significant amount of sulfuric acid during the manufacturing process (CelluForce Inc. 2024; Dunlop et al., 2021; Tang et al., 2022). Additionally, pulp waste from the paper sector is the raw material used in their manufacturing. As a result, the process as a whole is now sustainable and has far less carbon impact than with activated carbons. As per Celluforce Inc., the price of ultra-purified CNCs is around \$25/kg in the year 2024 (CelluForce, 2024). However, if CNC is produced commercially, this cost will drastically decrease. Also, wastewater treatment procedures are the only ones that need to use CNCs with lesser purity (CelluForce, 2024). Therefore, it is anticipated that the cost of CNCs will be competitive with that of the high-grade activated carbons that are now on the

market and are utilized in wastewater treatment procedures. These CNCs are also better than most of the current generation of ion exchange resins made from petroleum-based polymers in terms of environmental sustainability. Consequently, the notion of employing CNs, like CNCs and CNFs, to create adsorbents for removing pollutants has grown in acceptance among scientists throughout the globe (Jung et al., 2023).

Researchers from different groups have investigated the potential of CNs for the adsorption of various heavy metal ions from aqueous solutions. In the first investigation, Ag(I) was adsorbed from aqueous solutions using the two main types of CNs/CNCs and CNFs extracted from cellulose sludge by homogenizing cellulosic fibres and hydrolyzing it with H₂SO₄ (Kurniawan et al., 2023). Mohammed (2017) investigated the flocculation properties of both suspensions and carried out Ag⁺ adsorption studies with both kinds of CNs at different pH values. Following Ag⁺ treatment, the suspension of CNCs remained stable, but the suspension of CNFs was mostly sedimented and divided into discrete layers. This is consistent with the CNs' surface charge properties following the adsorption of Ag⁺ ions (Mohammed, 2017). Compared to CNFs that sedimented, CNCs had a larger specific surface area or percentage of adsorption sites accessible to bind Ag⁺ ions. Positively charged Ag⁺ ions and negatively charged functional groups of the CNs (sulfate ester groups on CNCs and carboxyl groups on CNFs) interact electrostatically to cause adsorption of Ag⁺ ions; the q_{\max} was calculated to be 34.4 and 15.45 mg/g on CNCs and CNFs, respectively (Kurniawan et al., 2023; Mohammed, 2017).

In a different study, the adsorption of Ag⁺, Cu²⁺, and Fe³⁺ from aqueous solutions was carried out in the second investigation using phosphorylated derivatives of CNCs and CNFs. The enhancement of metal sorption velocity and sorption capacity over virgin CNs

was facilitated by the addition of phosphate groups to their surface by enzymatic phosphorylation (Hamimed et al., 2022; Liu et al., 2015). It was discovered that the q_{max} for Ag^+ , Cu^{2+} , and Fe^{3+} for virgin CNCs was 56, 20 and 6.3 mg/g, respectively (Jawaid et al., 2017). For phosphorylated CNCs, it was 136, 117 and 115 mg/g; for phosphorylated CNFs, it was 120, 114 and 73 mg/g (Kurniawan et al., 2023). The large surface area of these CNs and the type and density of functional groups, such as phosphate groups (phosphorylated CNCs and CNFs), facilitate the adsorption of heavy metal ions and sulfonate groups (pristine CNCs). Furthermore, the demonstration was made about the possible utilization of these phosphorylated CNs in the elimination of Cu^{2+} and Fe^{3+} containing wastewater from the mirror-producing industry (Grishkewich et al., 2017; Kurniawan et al., 2023; Mohammed, 2017).

Yu et al. (2013) reported the adsorption of Pb(II) and Cd(II) from aqueous solution using surface functionalized CNCs, such as SCNCs and NaSCNCs (Yu et al., 2013). Following chemical modification with succinic anhydride to get carboxyl group-bearing SCNCs, the pure CNCs created by the hydrolysis of cotton with H_2SO_4 were treated with saturated sodium bicarbonate ($NaHCO_3$) to change the carboxyl groups into carboxylates, as in NaSCNCs (Hokkanen, Bhatnagar, & Sillanpää, 2016). Batch adsorption studies were used to thoroughly examine the adsorption capabilities of both of those types of CNCs. According to the results of adsorption investigations, Pb^{2+} and Cd^{2+} ions were adsorbed on SCNCs and NaSCNCs at rapid rates (Hokkanen, Bhatnagar, & Sillanpää, 2016). The calculated q_{max} values for SCNCs and NaSCNCs for Pb(II) and Cd(II) were 367.6, 259.7, and 465.1, 344.8 mg/g, respectively (Kurniawan et al., 2023). It was observed that NaSCNCs exhibited a greater adsorption capacity than SCNCs. In a comparable setting,

the adsorption of Cd^{2+} on NaSCNCs was superior to that of SCNCs, although both varieties of CNCs exhibited strong selectivity for Pb^{2+} in the presence of coexisting ions. Adsorption studies revealed that Pb^{2+} and Cd^{2+} ions adsorbed on SCNCs and NaSCNCs at extremely fast rates. The adsorption capacity for NaSCNCs approached equilibrium in 5 minutes, but it took 150 minutes for SCNCs. For Pb(II) and Cd(II), the estimated q_{max} values for SCNCs and NaSCNCs were 367.6, 259.7, and 465.1, 344.8 mg/g, respectively (Hokkanen, Bhatnagar, & Sillanpää, 2016). Compared to SCNCs, NaSCNCs were shown to have a higher adsorption capacity. In a similar environment, NaSCNCs were better at adsorbing Cd^{2+} than SCNCs were, but both types of CNCs showed good selectivity for Pb^{2+} when coexisting ions were present (Yu et al., 2013). Because of this, the superior adsorption qualities of NaSCNCs over SCNCs as a result of the ion exchange point to the significance of changing carboxyl groups into carboxylates for adsorbents that include carboxyl groups (Yu et al., 2013).

Researchers have also investigated the potential of both pure and a wide range of functionalized CNCs for the adsorptive removal of heavy metal ions in aqueous solutions, Cr(VI), Cd(II), Pb(II), and Ni(II) from aqueous solutions were adsorbed using CNCs made from rice straw fibres (Xu et al., 2021). Adsorption tests showed that these CNCs had more significant potential for adsorption than their parent materials, such as rice straw fibres and rice straw-derived cellulose. When CNCs are synthesized, amorphous domains in the cellulose chains are removed, which increases the number of primary hydroxyl groups available on the surface and may contribute to higher adsorption efficiency (Zhang et al., 2023). Moreover, negatively charged sulfate ester groups were added to the surface of CNCs during the acid hydrolysis of the cellulosic fibres used in

their production. These groups may serve as binding sites for cationic heavy metal ions. They also demonstrated the effective regeneration of these CNCs via three adsorption-desorption cycles with an eluent of 0.5M nitric acid (HNO_3), with estimated q_{max} values of 9.7, 9.42, and 8.55 mg/g for Cd(II), Pb(II), and Ni(II), respectively (Abouzeid et al., 2019; Kurniawan et al., 2023; Salama et al., 2021a). Through graft co-polymerization with different monomeric units, they were also able to enhance the adsorption performance of these CNCs toward Cd(II), Pb(II), Ni(II), and Cr(III) metal ions. CNCs' surface was modified via graft co-polymerization with monomeric acids such as acrylic acid, maleic acid, and itaconic acid, which increased the number of negatively charged carboxylate groups on the CNCs (Coudane et al., 2022; Zubair et al., 2022). On the surface of CNCs, however, graft co-polymerization with vinyl sulfonic acid added additional negatively charged sulfonate groups. These sulfonate and carboxylate groups on the graft copolymerized CNCs, as opposed to the pristine CNCs, function as extra active sites for heavy metal ion binding, increasing their adsorption capability. It was also discovered that, presumably as a result of their improved stability, the reusability of graft copolymerized CNCs was raised to five cycles as opposed to three cycles of pristine CNCs. In order to employ them for the decontamination of Cr(III) and Cr(VI), respectively (Etale et al., 2023b; T. S. Vo et al., 2020). CNCs were additionally functionalized using the succination and amination functionalization processes. According to a report, the enhanced surface area to volume ratio and quantum size effects of CNCs led to an increase in adsorption sites as well as the capacity to modify their surface properties through molecular tuning (Tang et al., 2017). This made CNCs perfect for surface functionalization, enriching the active adsorption sites. The hydroxyl groups

on CNCs underwent esterification when carboxyl groups were added by succinic anhydride, which increased the surface's ability to bind charged metal ions like Cr(III) (Zhang et al., 2023) positively. Cr(VI) could bind to CNCs due to the introduction of NH_3^+ cationic ligands on their surface by acrylamide and ethylenediamine amination. Over 40 minutes of contact time, the functionalized CNCs' adsorption capability approaches equilibrium. There were two different results for the q_{max} of the succinate CNCs/Cr(III) and aminated CNCs/Cr(VI) systems: 2.88 and 2.77 mg/g, respectively (Mohamed et al., 2022; Zhang et al., 2023). They also showed that 0.05M HNO_3 or 0.05M HCl eluent solutions could be used to successfully renew these CNCs for up to five regeneration cycles (Mohamed et al., 2022; Zhang et al., 2023).

Sheikhi & van de Ven (2017) produced electrostatically stabilized CNCs (ECNCs) for the adsorptive removal of Cu(II). It was hypothesised that the ECNCs, which were made from wood fibres by oxidizing them with periodate and chlorite, had dicarboxylated chains (DCC) sticking out of the crystalline domains (Mohamed et al., 2022; Sheikhi & van de Ven, 2017). The ECNCs are remarkably stable due to the high charge content imparted by these highly charged polyelectrolytes (Sheikhi & van de Ven, 2017). It was discovered that the processes by which ECNCs scavenge Cu^{2+} ions vary depending on the quantity of Cu(II). When the concentration of Cu(II) is low (≤ 200 ppm), ECNCs assemble into star-like particles that disintegrate into individual star-like entities via shear force and Brownian motion. At 300 or 400 ppm concentrations, these aggregation morphologies shift from star-like to raft-like, most likely due to projecting DCC chains collapsing and the ECNCs' charge being neutralized by copper adsorption (Mohamed et al., 2022). Unlike star-like agglomerates, these raft-like structures progressively expand

and are prone to sedimentation at Cu(II) concentrations (≥ 500 ppm), which facilitates their separation for wastewater treatment operations. The active sites for Cu²⁺ binding are highly charged DCC polyanions extending from ECNCs; the q_{\max} for this adsorption was determined to be 185 mg/g (Sheikhi et al., 2015; Sheikhi & van de Ven, 2017).

Bisphosphonate functionalized CNCs were developed by Voisin et al. (2017) to remove vanadium from aqueous solution. Wood cellulose fibres that had been periodate oxidized and sodium alendronate aminated were mechanically disintegrated to create the bisphosphonate functionalized CNCs (Voisin et al., 2017). Additionally, they discovered that adsorption was extremely effective at extremely low solution pH levels (2–3) (Voisin et al., 2017). The adsorption of vanadium onto these CNCs is most likely the result of electrostatic interactions between cationic vanadium species and anionic acid groups, as well as the complexation of vanadium with bisphosphonate groups. Vanadium's q_{\max} was 1.98 mmol/g (100.9 mg/g) (Salama et al., 2021; Voisin et al., 2017; Zhang et al., 2023).

Ma et al. (2012) discovered that radioactive UO₂²⁺ ions in water may be effectively removed by using ultrafine CNFs as adsorbents (H. Ma et al., 2012). The TEMPO/Sodium Bromide (NaBr)/Sodium Hypochlorite (NaClO) oxidation of wood pulp was employed to create the ultrafine CNFs used in this work. This procedure was followed by mechanical treatment. The interaction between the positively charged UO₂²⁺ ions and the negatively charged carboxylate groups eg on the CNFs caused a gel to develop as soon as the UO₂²⁺ ions were added to the suspension of CNFs. These ultrafine CNFs were shown to have a q_{\max} of 167 mg/g for UO₂²⁺ ions (Ma et al., 2012).

Furthermore, carboxylated CNFs were made by Sehaqui et al. (2014) to remove Cu(II), Cr(III), Ni(II) and Zn(II) from aqueous solutions adsorptively. They discovered that these carboxylated CNFs had a greater capacity for Cu(II) adsorption than pristine CNFs (Abou-Zeid et al., 2020; Sehaqui et al., 2014). This is because the additional carboxylate groups that were added to the CNF surface during the TEMPO oxidation of the parent cellulosic fibres serve as anionic binding sites for the Cu²⁺ ions' electrostatic attraction. Cu(II), Ni(II), Cr(III), and Zn(II) were predicted to have q_{max} values of 135, 58, 49, and 66 mg/g, respectively (Abou-Zeid et al., 2020; Sehaqui et al., 2014). Additionally, they showed that after three adsorption-desorption cycles, this adsorbent could be efficiently regenerated with an eluent of acidic HCl solution and more than 90% adsorption capacity (Abou-Zeid et al., 2020; Sehaqui et al., 2014). For the adsorptive removal of Cu(II) from aqueous solution, Zhang et al. (2006) produced TEMPO-oxidized CNFs modified with polyethyleneimine (PEI), a highly functionalized adsorbent (S. Zhang et al., 2006). The CNFs were changed by oxidizing them using a TEMPO reagent and then grafting PEI using a glutaraldehyde cross-linking technique. The q_{max} was calculated to be 52.3 mg/g (Vo et al., 2020; Zhang et al., 2006; Zhang et al., 2023b). This alteration added a large number of carboxyl and amino functional groups to CNFs, which might serve as active sites for the binding of Cu²⁺ ions in aqueous solution. Furthermore, the adsorption capacity was consistent throughout four adsorption-desorption cycles following regeneration with 1M HCl eluent, suggesting the high regeneration capability of this adsorbent (Mohammed, 2017; Zhang et al., 2006).

Hokkanen et al. (2014) created various functionalized CNFs to adsorb heavy metals from water. CNFs modified with aminopropyl triethoxy silane (APTES) were made to adsorb

Ni(II), Cu(II), and Cd(II) from aqueous solutions (Hokkanen et al., 2014). They claimed that the adsorption capacity of APTES-modified CNFs is much greater than that of unmodified CNFs. Meanwhile, in APTES-modified CNFs, the amino groups added by the amino silane functionalization offer extra functional groups for metal ion binding. In unmodified CNFs, metal ion binding is caused by electrostatic interaction with only the carboxyl groups on their surface (Hokkanen et al., 2014; Hokkanen et al. 2016). The q_{max} of these APTES-modified CNFs for Ni(II), Cu(II), and Cd(II) ions was calculated to be 2.734 mmol/g (160.5 mg/g), 3.150 mmol/g (200.2 mg/g), and 4.195 mmol/g (471.6 mg/g), respectively (Hokkanen et al., 2014; Hokkanen et al. 2016). These CNFs are easily regenerable using 0.1M NaOH eluent. For the purpose of eliminating Zn(II), Ni(II), Cu(II), Co(II), and Cd(II) from aqueous solutions, 119 modified CNFs containing succinic anhydride were created (Hokkanen et al., 2014; Hokkanen et al. 2016). The q_{max} for Zn(II), Ni (II), Cu(II), Co(II), and Cd(II) was estimated to be 1.610 mmol/g (105.3 mg/g), 0.744 mmol/g (43.7 mg/g), 1.900 mmol/g (120.7 mg/g), 1.338 mmol/g (81.8 mg/g), and 2.062 mmol/g (231.8 mg/g), respectively (Hokkanen et al., 2014; Hokkanen et al. 2016). These heavy metal ions adsorb on the carboxyl groups on the surface of these modified CNFs. Using 1M HNO₃ eluent and ultrasonic treatment, it was also demonstrated that the succinic anhydride-modified CNFs could be successfully regenerated. Ni(II) and Cd(II) adsorption from aqueous solution was achieved by manufacturing 120 carbonated hydroxyapatite (CHA) modified CNFs. Here, the ion exchange process or the dissolution-precipitation mechanism may cause the adsorption of Ni(II) and Cd(II) ions. Both heavy metals may be efficiently regenerated using weaker acid (0.01M HNO₃), according to regeneration tests employing different strengths of

HNO₃. The adsorption capacity for Ni²⁺ ions decreased with each cycle, but that of Cd²⁺ ions remained constant even after four cycles. For Ni(II) and Cd(II), the calculated q_{max} of these adsorbents were 2.021 mmol/g (118.62 mg/g) and 1.224 mmol/g (137.6 mg/g), respectively (Hokkanen, Bhatnagar, & Sillanpää, 2016; Hokkanen et al., 2014; Mohammed, 2017b).

Zhao et al. (2023) actuated CNFs by magnetic nanoparticles to remove As(V) from aqueous solution via adsorptive means (Zhao et al., 2023). In this case, the oxidized states of Fe³⁺ from iron nanoparticles (Fe-NP) in the adsorbent form inner-sphere complexes that lead to the adsorption of arsenic species. Therefore, the adsorption capabilities are influenced by the presence of OH²⁺, OH⁻, and O⁻ functional groups on the surface of the adsorbent. They calculated the q_{max} to be 2.460 mmol/g (184.31 mg/g), which took around 75 minutes for their adsorption capacity to achieve equilibrium (Zhao et al., 2023). Additionally, they discovered that this adsorbent could be efficiently regenerated using 1M NaOH eluent after three cycles, showing a regeneration efficiency of over 98% (Zhao et al., 2023). To recover Au(III) in its ionic, nanoparticulate, and metallic forms, sulfonated CNFs were synthesized. These anionic CNFs were created by oxidizing CNFs with periodate and then sulfonating them with sodium metabisulfite (Dwivedi et al., 2014). Comparing CNFs to pure CNFs, adding more anionic sulfonated functional groups to their surface can increase their adsorption capability (Zhang et al., 2023b). These anionic sites may function as extra locations where cationic metal ion species are bound during adsorption. These sulfonated CNFs were shown to have a q_{max} of 60 mg/g for Au(III). Additionally, they discovered that the competing heavy metal ions, such as Cd(II), Co(II), Cr(VI), Ni(II), and As(V), present in an aqueous environment had little

effect on Au(III) adsorption (Musumba et al., 2020; Zhang et al., 2023b). The regeneration using a strong complexing eluent, such as 0.5M thiourea in 1M HCl, successfully recovered more than 83–99% of the adsorbed Au(II) ions from the adsorbent (Dwivedi et al., 2014). Sulfonated CNFs were also employed by Suopajarvi et al. (2015) to remove Pb(II) adsorptively from aqueous solutions. These sulfonated CNFs were calculated to have a q_{max} of 1.2 mmol/g (248.6 mg/g) (Suopajarvi et al., 2015).

Employing Pb(II) adsorbents, Zhou et al. (2014) used magnetic chitosan hydrogel beads packed with carboxylated CNFs. In this instance, the hydrogel beads were created by an instantaneous gelation procedure. A nanocomposite solution including carboxylated CNFs, amine-functionalized magnetite nanoparticles, and PVA blended chitosan was put into a NaOH gallant bath (Xu et al., 2021; Zhou et al., 2014). Composite hydrogel beads with and without carboxylated CNFs differed in their adsorption capability, with the former performing better across the board for all pH ranges. This may be explained by the carboxyl groups on CNFs, which strengthen the adsorbent's electrostatic interaction with Pb^{2+} ions. After 200 minutes, their adsorption capacity reached equilibrium, and they calculated the q_{max} to be 171 mg/g (Xu et al., 2021). They also showed that these composite hydrogel beads are reusable by maintaining their adsorption efficacy at 90% even after four adsorption-desorption cycles with 0.01 HNO₃ eluent (Xu et al., 2021).

Yi et al. (2022) recently created carboxylated CNFs with PVA hybrid aerogels with high metal ion adsorption capabilities. These hybrid aerogels were produced by freeze-drying the cross-linked carboxylated CNFs/PVA composite gel (Chen et al., 2021; Yi et al., 2022). These hybrid aerogels with CNFs demonstrated superior adsorption performance compared to aerogels without CNFs in terms of their metal ion adsorption capabilities.

This improved performance could be attributed by the fact that the TEMPO oxidation procedure produced more carboxyl groups on the surface of CNFs, which added additional active sites for metal ion binding (Y. Chen et al., 2021; Yi et al., 2022). These hybrid aerogels have adsorption capabilities of 157.5, 110.6, 151.3, and 114.3 mg/g for Hg^{2+} , Pb^{2+} , Cu^{2+} , and Ag^+ , respectively (Yi et al., 2022).

Hamimed et al. (2022) created CNC-based nanocomposites that are useful for the adsorptive removal of heavy metal ions from wastewater from industrial processes. In the first study, they made a composite of itaconic acid-grafted magnetite CNCs modified with 2-mercaptobenzamide that may be utilized to selectively adsorb Hg(II) from aqueous solutions (Kumari et al., 2021). This adsorbent was made via graft copolymerization of itaconic acid onto magnetite CNC composite employing potassium sulfate as a free radical initiator and ethylene glycol dimethacrylate as a cross-linking agent. It was further modified with 2-mercaptobenzamide. (Kumari et al., 2021). Ionized carboxyl and sulfhydryl groups attached the adsorbent's surface by electrostatic attraction, which allowed Hg^{2+} ions to be adsorbed onto it selectively. They calculated the q_{max} to be 240 mg/g, which took 60 minutes for their adsorption capacity to achieve equilibrium (Rostami et al., 2024). Additionally, it was shown that even after five adsorption-desorption cycles, the adsorption capacity remained above 85% and that wasted adsorbent can be efficiently regenerated using 0.1M HCl eluent (Hamimed et al., 2022). In their second study, they created a composite of poly(itaconic acid/methacrylic acid)-grafted CNCs and nano bentonite that may be effectively employed to remove Co(II) from aqueous solutions (Hamimed et al., 2022). This adsorbent was created by radical polymerizing methacrylic acid, cross-linking with ethylene glycol dimethacrylate,

and then ionic cross-linking CNCs/nano bentonite with itaconic acid. With their adsorption capacity reaching equilibrium after 120 minutes, they calculated the q_{max} to be 350.8 mg/g (Hamimed et al., 2022). Furthermore, it was shown that even after six adsorption and desorption cycles, the adsorption capacity remained above 85% and that wasted adsorbent can be efficiently regenerated using 0.1M HCl eluent (Rostami et al., 2024).

2.8 Modelling of Adsorption experimental data

The most crucial aspects of designing an adsorption system are estimating the adsorption rate for a particular system and comprehending the interactions between adsorbates and adsorbents (Dąbrowski, 2001). The residence duration of adsorbate uptake at the solid–solution interface is governed by the kinetic parameters, which also characterize the solute uptake rate (Rudzinski & Plazinski, 2007). Furthermore, kinetics relies on predicting the rate at which contaminants are removed from aqueous solutions since this knowledge is crucial for process modelling and design. However, the adsorption isotherms are extremely important to maximise the utilisation of adsorbents. Thus, the practical design and operation of adsorption systems depend on the correlation of equilibrium data using theoretical or empirical equations (Al-Ghouti & Da'ana, 2020). Several kinetic equations and isotherms are well described and used to fit experimental data in the following sub-sections.

2.8.1 Kinetic Models to Predict the Rate of Adsorption

The study of adsorption kinetics examines how quickly contaminants are transferred from an aqueous solution onto an adsorbent surface, which in turn regulates how long the adsorbate takes to absorb at the interface between solid and liquid solutions (Guo &

Wang, 2019). In essence, it offers insightful information on the mechanisms and reaction pathways of the adsorption processes. Many kinetic models have been developed to explain the reaction sequence of adsorption systems depending on solution concentration as well as the process of solute adsorption onto adsorbent (Ho et al., 2000; Lach & Okoniewska, 2024; Lima et al., 2015; Musah et al., 2022; Revellame et al., 2020). The diffusion chemisorption model, Lagergren's first-order and pseudo-second-order expression, equation are examples of reaction orders dependent on the adsorbent's capacity (Revellame et al., 2020).

2.8.1.1 Lagergren Pseudo first Order Model

In 1898, Lagergren introduced the first order rate equation for the adsorption of malonic and oxalic acids onto charcoal (Bujdák, 2020; Huang, 2022). Lagergren differentiated a kinetics equation depending on the solids' adsorption capacity and solution concentration (Revellame et al., 2020). Since then, various contaminants, including heavy metals and organic chemicals, have been adsorbed using this kinetic equation on a large scale. Adsorption kinetics, described by diffusion over a barrier and may be followed, can be followed using the nonlinear form of the pseudo-first-order model given in Equation 2.2 (Tseng et al., 2010).

$$\frac{dq_t}{dt} = k_1(q_e - q_t) \quad (2.2)$$

Where q_t is the amount of adsorbate adsorbed at time t (mg/g), q_e is the equilibrium adsorption capacity (mg/g), while k_1 is the rate constant of pseudo-first-order adsorption (min^{-1}). To determine the rate constant and evaluate the model's applicability, the Lagergren pseudo-first-order model can be linearized, as shown in Equation 2.3.

$$\ln(q_e - q_t) = \ln q_e - k_1 t \quad (2.3)$$

In the pseudo-first-order kinetic model, k_1 represents the first order rate constant (min^{-1}) while q_t and q_e denote the quantity adsorbed at time t and equilibrium, respectively. A straight line represents pseudo-first-order kinetics when plotting $\ln(q_e - q_t)$ vs t ; k_1 and q_e may be calculated from the graph's slope and intercept, respectively.

2.8.1.2 Pseudo second order reaction model

The pseudo-second-order model describes the adsorption processes for surface chemisorption (Musah et al., 2022). According to Ho and McKay (2000), the pseudo-second-order model is predicated on the possibility that chemical adsorption, which involves valence forces through the sharing or exchange of electrons between the adsorbent and adsorbate may be the rate-limiting phase (Ho et al., 2000). Equation 2.4 represents the pseudo-second-order model.

$$\frac{dq_t}{dt} = k_2 (q_e - q_t)^2 \quad (2.4)$$

where q_e is the quantity adsorbed at equilibrium (mg.g^{-1}), q_t is the amount adsorbed on the surface of the adsorbent at any given time, t , and k is the adsorption rate constant ($\text{g.mg}^{-1}.\text{min}^{-1}$). After being integrated and rearranged, Equation 2.4 becomes Equation 2.5 below.

$$\frac{t}{q_t} = \frac{1}{k_2 q_e^2} + \frac{1}{q_e} \quad (2.5)$$

Plotting $\frac{t}{q_t}$ against t should result in a linear relationship. The slope of the resulting line is

$\frac{1}{q_e}$ and the intercept is $\frac{1}{k_2 q_e^2}$. From this plot, the values of q_e and k_2 can be determined.

The equilibrium adsorption capacity q_e can be obtained from the slope. The rate constant k_2 can be calculated using the intercept and the value of q_e .

2.8.1.3 Intraparticle diffusion model

The intraparticle diffusion model is based on Weber and Morris' approach to determining the adsorption mechanism (Wu et al., 2009). The graph of q_t vs $t^{0.5}$ should produce a straight line passing through the origin. The weber and Morris equation is given in Eqn .2.6 below.

$$q_t = k_{id}t^{0.5} + C \quad (2.6)$$

Where q_t is the amount of solute adsorbed at any time, t , k_{id} is the intraparticle diffusion rate constant ($\text{mg/g} \cdot \text{min}^{0.5}$), C , the intercept, is a constant that gives an idea about the boundary layer thickness (mg/g),

2.8.1.4 Diffusion chemisorption model

The diffusion chemisorption model is an empirical kinetic model developed to mimic heavy metal adsorption onto heterogeneous surfaces (Lach & Okoniewska, 2024). Equation 2.7 gives the Sutherland's expression (Sutherland & Venkobachar, 2010).

$$q_t = k \left(\frac{1}{t + \frac{1}{k_c}} \right) \quad (2.7)$$

where q_t (mg/g) is the amount of adsorbate adsorbed at time t (mg/g), and k is a constant related to the adsorption capacity (mg/g). k_c is the chemisorption rate constant (min^{-1}).

Eq.2.7 can be linearized to Equation 2.8 below to enhance its applicability.

$$\frac{1}{q_t} = \frac{1}{k} + \frac{1}{k_c t} \quad (2.8)$$

A plot of $\frac{1}{q_t}$ against $\frac{1}{t}$ can help determine whether the process is diffusion-controlled or chemisorption-controlled. The intercept and slope of this plot can provide values for k and kc , respectively. If chemisorption is the rate-limiting step, the adsorption rate will be relatively fast and slow as the surface sites become occupied. If diffusion is the rate-limiting step, the adsorption rate will gradually approach equilibrium, dominated by the slow diffusion process (Shahrabadi et al., 2022).

2.8.2 Equilibrium Isotherm models

To maximize the utilization of adsorbents, it is essential to understand how solutes interact with them through the use of adsorption isotherms (Basu et al., 2022; Ehiomogbe et al., 2021; Musah et al., 2022). When the solute concentration stays constant due to a net zero transfer of solute that has been adsorbed and desorbed from the adsorbent surface, equilibrium is reached. In addition to proposing the interactive forces involved in the process, the equilibrium adsorption isotherms describe the relationships between the equilibrium concentration of the adsorbate in the solid and liquid phases at constant temperature (Musah et al., 2022). The general equation states that an adsorption isotherm may characterize the process at constant temperature:

$$q = \frac{(C_o + C_e).V}{m} \quad (2.9)$$

where C_o is the initial adsorbate concentration (mg/dm^3), and q is the equilibrium sorption capacity (mg/g). V is the solution volume (dm^3), m is the mass of the adsorbent (g), and C_e is the equilibrium adsorbate concentration (mg/dm^3). The following Eqn. 2.10 is used to determine the percentage removal.

$$\% \text{ Removal} = \frac{(C_o + C_e)}{C_o} \times 100 \quad (2.10)$$

A number of adsorption isotherms were presented in light of the possibility of a more complicated adsorption process. Among them, Langmuir and Freundlich's models are the most often employed to explain the process in water and wastewater applications (Ho, 2004; Basha et al., 2008). Additionally, experimental data have been modelled using equilibrium isotherms such the Temkin, Tooth, Redlich-Peterson, Langmuir-Freundlich (Sips isotherm), and Dubinin-Radushkevich.

2.8.2.1 Freundlich isotherm

Freundlich's isotherm is among the earliest empirical equations to explain equilibrium data (Ao et al., 2012; Ehiomogue et al., 2021). In the isotherm model, the total quantity of material adsorbed is the sum of the adsorption on all sites, and the surface is assumed to be heterogeneous with a non-uniform distribution of heat of adsorption (Musah et al., 2022). Freundlich's isotherm does not only suggest monolayer formation but also about reversible adsorption. With a rise in the proportion of occupied sites, the enthalpy of biosorption should drop logarithmically (Appel, 1973; Musah et al., 2022). The Freundlich isotherm model is given in Equation 2.11 below.

$$q_e = K_f C_e^{\frac{1}{n}} \quad (2.11)$$

where K_f and n are the system's Freundlich constants, representing the biosorption intensity and capacity, respectively. $\frac{1}{n}$ is a dimensionless constant that relates to the adsorption intensity and shows the energy distribution of the adsorption sites as well as the surface heterogeneity. By linearizing Eq. (2.11) in logarithmic form, one may obtain Eq. (2.12) and ascertain the Freundlich constants.

$$\log q_e = \log K_f + \frac{1}{n} \log C_e \quad (2.12)$$

A plot of $\log q_e$ versus $\log C_e$ should yield a straight line, the slope of the line corresponds to $\frac{1}{n}$, which gives insight into the heterogeneity of the adsorbent surface. If $\frac{1}{n} = 1$, the adsorption is homogeneous; if $\frac{1}{n} < 1$, it suggests favourable adsorption. The intercept corresponds to $\log K_f$, from which the Freundlich constant K_f can be determined. A higher K_f value indicates a greater adsorption capacity of the adsorbent. The value of $\frac{1}{n}$, ranges between 0 and 1, indicating the favorability and heterogeneity of the adsorption process. When $0 < \frac{1}{n} < 1$, it suggests that the adsorption is favourable and that the adsorbate is readily adsorbed at low concentrations but more difficult at higher concentrations (Kalam et al., 2021).

2.8.2.2 Langmuir isotherm

To relate the quantity of gas adsorbed on a surface due to the gas's pressure, Langmuir invented the Langmuir isotherm in 1916 (Beebe, 2024). This theoretical isotherm represents the most basic process for monolayer adsorption onto a surface with a limited number of identical sites. Metal ions in bulk solution and those retained on the biosorbent will be balanced at constant temperature (Ayawei et al., 2017; Ehiomogue et al., 2021). When the adsorption process has an identical activation energy, the equation may be used for homogeneous adsorption. The underlying presumptions of this model are as follows: (i) Adsorption cannot continue beyond monolayer coverage; (ii) All sites are equivalent, and the surface is uniform, meaning it is perfectly flat at the microscopic level; and (iii) A molecule's capacity to adsorb at a particular site is independent of the occupying of

nearby sites (Ayawei et al., 2017). Next, the saturated monolayer isotherm may be given (Eq.2.13).

$$q_e = \frac{q_m K_L C_e}{1 + K_L C_e} \quad (2.13)$$

Where q_m is the maximum adsorption capacity corresponding to complete monolayer coverage (mg/g), K_L is the Langmuir constant related to the affinity of the binding sites and the adsorption/desorption energy (dm^3/mg), and q_e is the number of metal ions adsorbed ($\text{mg}\cdot\text{g}^{-1}$).

The Langmuir isotherm (Eq.2.14) can be linearized in several ways to facilitate the determination of the model parameters.

$$\frac{1}{q_e} = \frac{1}{q_m K_L} \times \frac{1}{C_e} + \frac{1}{q_m} \quad (2.14)$$

In this form, plotting $\frac{1}{q_e}$ against $\frac{1}{C_e}$ yields a straight line. The slope is $\frac{1}{q_m K_L}$ and the intercept is $\frac{1}{q_m}$.

2.8.2.3 Temkin Isotherm

According to the Temkin isotherm model, adsorption is characterized by a uniform distribution of binding energies up to a maximum binding energy, and the adsorption energy decreases linearly with surface coverage as a result of adsorbent–adsorbate interactions (Ao et al., 2012; Lima et al., 2015; Sheha & Metwally, 2007). Equations 2.15 and 2.16 represent the Temkin isotherm model.

$$q_e = B \ln(AC_e) \quad (2.15)$$

or

$$q_e = \frac{RT}{b} \ln(AC_e) \quad (2.16)$$

q_e is the amount of adsorbate adsorbed at equilibrium (mg/g), C_e is the equilibrium concentration of the adsorbate in the solution (mg/L), and A is the Temkin isotherm constant (dm^3/g) related to the maximum binding energy. B is a constant associated with the heat of adsorption (J/mol), often expressed as $B = \frac{RT}{b}$, R is the universal gas constant (8.314 J/mol·K), T is the absolute temperature (K), and b is a constant related to the adsorption energy. The linearized equation is given in Equation 2.17.

$$q_e = B \ln(C_e) + B \ln(A) \quad (2.17)$$

By plotting q_e against $\ln(C_e)$, a linear relationship is obtained, where the slope of the line is B, and the intercept is $B \ln(A)$ where A is the Temkin isotherm constant (dm^3/g).

The Temkin isotherm assumes that the heat of adsorption of all the molecules in the layer decreases linearly with coverage due to adsorbate-adsorbent interactions. It applies to adsorption processes where adsorption energy decreases with increasing surface coverage due to repulsive interactions between adsorbed molecules (Chu, 2021).

2.8.2.4 Dubinin-Radushkevich

The Dubinin-Radushkevich model is commonly utilized to describe biosorption's physical and chemical characteristics (Basu et al., 2022). The response mechanism can be linked to the size of E in a Dubinin-Radushkevich isotherm. The adsorption is likely to involve stronger chemical interactions, such as covalent bonding, and may be less reversible (Ion exchange controls sorption) if E is between 8 and 16 kJ/mol (Ao et al., 2012). When E is less than 8 kJ/mol, the sorption process may be impacted by physical

forces such as van der Waals forces and is reversible (Ehiomogue et al., 2021). The linear version of the Dubinin–Radushkevich (D–R) isotherm is shown in Equation 2.18.

$$q_{\varepsilon} = q_m \exp(-\beta\varepsilon^2) \quad (2.18)$$

Here, ε is the Polanyi potential, which is connected to the equilibrium concentration as

$$\varepsilon = RT \ln\left(1 + \frac{1}{C_{\varepsilon}}\right) \quad (2.19),$$

where R is the gas constant (8.314 J/mol.K) and T is the absolute temperature.

q_m is the Dubinin–Radushkevich monolayer biosorption capacity (mg/g), and β , sometimes denoted as B, is a constant related to biosorption energy (mol^2/kJ^2). When 1 mol of an ion is moved from infinity in the solution to the surface of the solid, the mean free energy change, or E (kJ/mol), is given by the constant β , which can be calculated using the relationship (Eq.2.20).

$$E = \frac{1}{\sqrt{\beta}} \quad (2.20)$$

2.8.2.5 Langmuir-Freundlich (Sips)

The Langmuir-Freundlich (Sips) model was created by Sips in 1948 and combines the Freundlich and Langmuir models (Ehiomogue et al., 2021). The model is generated by adding a power law representation of the Freundlich isotherm into the Langmuir isotherm and is mostly used to explore the equilibrium of multicomponent systems (De Vargas Brião et al., 2023). Equation 2.21 represents the Sips isotherm model's non-linearized form.

$$q_{\varepsilon} = \frac{q_m(KC_{\varepsilon})^n}{1 + (KC_{\varepsilon})^n} \quad (2.21)$$

where the Sips isotherm constant, K (L/mg), represents the energy of adsorption or the strength of the interaction between the adsorbate and the adsorbent and q_m (mg/g) is the

theoretical maximum adsorption capacity, analogous to the monolayer capacity in the Langmuir isotherm. The Sips isotherm equation simplifies to the Langmuir equation when $\beta = 1$ or nearer to 1, and to the Freundlich isotherm when the value of either C_e or n approaches 0. Additionally, n is the heterogeneity index, which accounts for the system's heterogeneity. When $n=1$, the system behaves as per the Langmuir model, implying homogeneous adsorption, while when $n<1$, it indicates heterogeneity in the adsorption sites.

The linearized form of the model is given in Equation 2.22.

$$\ln\left(\frac{q_e}{q_m - q_e}\right) = n \ln K + n \ln C_e \quad (2.22)$$

In this linearized form, a plot of $\ln\left(\frac{q_e}{q_m - q_e}\right)$ versus $\ln C_e$ can be used to determine the parameters K and n . The Langmuir-Freundlich (Sips) isotherm is widely used in cases where the adsorption process is influenced by surface heterogeneity and a range of adsorbate affinities.

CHAPTER THREE

RESEARCH METHODOLOGY

3.1 EXPERIMENTAL DESIGN

3.1.1 Experimental Design

An Independent Measures Experimental design was employed in this study. The process began with the collection of Cattail grass samples using a Randomized Block Design. These samples were then subjected to consistent treatments across all stages, including pretreatment, sample preparation, dewaxing, delignification, purification, and nanoparticle synthesis. The treatment levels were maintained uniformly throughout these processes with the conditions carefully controlled to ensure reliability and accuracy of the results.

3.1.2 Sampling area and sample Size

Typha angustifolia grass was harvested from Maasai Mara University botanical garden, Narok Kenya (1° 41' 5.2872" N and 37° 20' 27.096" E), altitude of 1827 M above sea level (**Figure 3:1**). A total of five batches of cattail grass, each weighing 20 kg (wet mass), were collected individually at the sampling point. This quantity ensured an adequate supply of raw material for subsequent processing and experimental analyses.

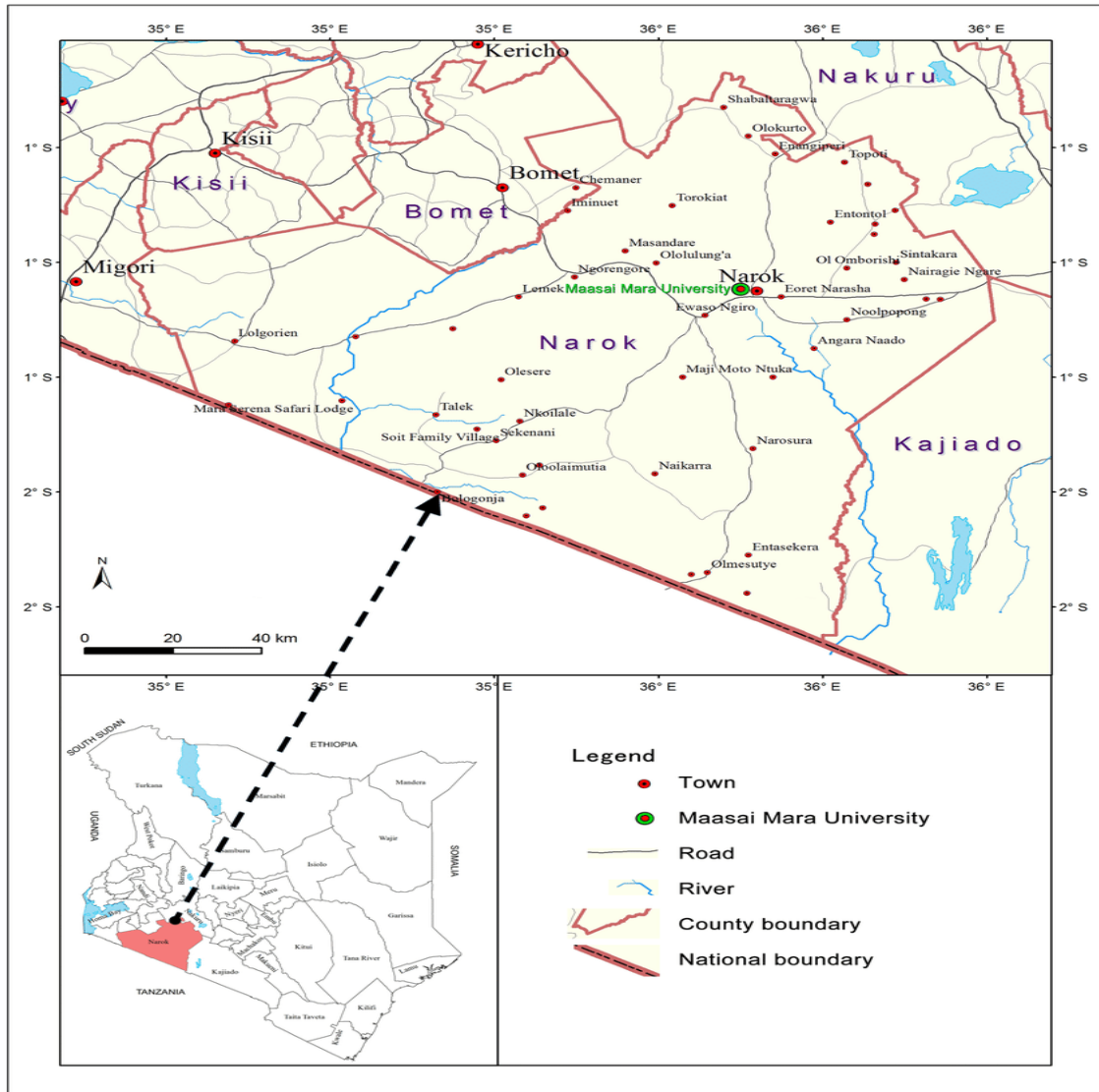


Figure 3.1: Sample collection area (Onyango et al., 2020).

3.1.3 Sampling Method

A Randomized Block design was used, where the Cattail grass was randomly collected from the sample regions specified above before pooling the samples together (for each strata) and removal of physically contaminated grass done. Physical contamination included cuts and grass with exposed stem flesh. Weighing was then done before moving on to the next sampling strata.

3.2 MATERIALS

3.2.1 Apparatus

Liebig's condenser, Erlenmeyer's flask, measuring cylinders, volumetric flasks, Wash bottle with distilled water, kitchen knives, glass beakers (50,100,250,500 mL), shredder, thermometer, soxhlet extraction apparatus, visking tubing, centrifuge, and vials were used in this study.

3.2.2 Chemicals and Reagents

Sodium hydroxide ($\text{NaOH} \geq 98\%$), sulfuric acid ($\text{H}_2\text{SO}_4, >98\%$), acidified sodium hypochlorite ($\text{NaOCl}, \geq 75\%$), acetic acid ($\geq 99\%$), acetone ($\geq 99.9\%$), ammonium hydroxide (25%, NH_4OH), Iron (III) chloride hexahydrate ($\text{FeCl}_3 \cdot 6\text{H}_2\text{O}$) ($\geq 99\%$), ferrous sulfate heptahydrate ($\text{FeSO}_4 \cdot 7\text{H}_2\text{O}$) ($\geq 99.5\%$), methanol ($\geq 99.85\%$), distilled water, β -Cyclodextrin, potassium dichromate ($\text{K}_2\text{Cr}_2\text{O}_7 >99\%$), sodium chloride solution, hydrochloric acid ($\text{HCl} \geq 32\%$), nitric acid ($\text{HNO}_3 \geq 55\%$). All the chemicals used were analytical grade.

3.2.3 Equipment and Facilities

Analytical weighing balance, temperature programmable Centrifuge (Shimadzu), Fourier Transform Infra-Red spectrophotometer (Perkin Elmer), Scanning Electron Microscope, Transmission Electron Microscope, X-Ray Diffractometer, Thermal Gravimetric Analyzer, Water bath sonicator, pH meter and UV-Vis Spectrometer (Shimadzu).

3.3 METHODS

3.3.1 Sample pretreatment

The collected cattail grass was washed and air-dried. The grass samples were then cut into small pieces, with cylindrical samples approximately 3 cm in diameter and 5 mm in height, and cubical samples measuring 5 mm on each side. These samples were air-dried for 6-8 days to remove moisture, then shredded into smaller pieces and further air-dried for an additional 2 days. Finally, the samples were dried in an oven at 60°C for 6 hours.

3.3.2 Dewaxing and Delignification

Figure 3.2(a-f) illustrates the dewaxing and delignification of *Typha angustifolia* ground powder to obtain cellulose fibres. The dewaxing and delignification began by soaking the dried grass powder in 10% nitric acid; this was aimed at effectively breaking down lignin, a complex organic polymer in the cell walls of plants that makes them rigid and woody. The soaking temperature was set at 80 °C for 2 hours to achieve this. Similarly, this step also helped in the removal of waxes and other extractives that are not part of the cellulose structure. This step was followed by thorough washing with deionized water to remove residual acid and dissolved components. Following this, the material underwent alkaline pre-treatment with 1.0M sodium hydroxide (NaOH); this was aimed at breaking down hemicellulose and residual lignin further that were still present after the acid treatment. The resulting cellulose fibres were then quenched with cold deionized water and washed until a neutral pH. This step was performed to ensure that the material was ready for the subsequent purification without any chemical residues that might interfere with further treatments.

3.3.3 Chemical purification (bleaching)

The chemical bleaching process and the resultant chemically purified cellulose are shown in Figure 3.2 (e–d). The obtained cellulose fibres were refluxed with 350 mL (7.35% (w/v)) sodium hypochlorite, 2% (w/v), followed by 4 mL acetic acid. The reaction mixture was agitated for 3 hours at 80°C with constant stirring at 900 rpm. The sodium hypochlorite, a strong oxidizing agent, aided in the breakdown of pigments and impurities like lignin. Acetic acid was added to improve the bleaching effect and regulate the pH. The resultant chemically refined cellulose was next filtered using a Büchner funnel attached to a vacuum pump to separate the liquid phase from the solid cellulose effectively. The chemically purified cellulose was further washed to remove any remaining contaminants. The washing was thoroughly performed with deionized water until it achieved a neutral pH of 7. Further purification was made by using acetone in a Soxhlet chamber to effectively remove organic impurities such as waxes and lipids. The process of soxhlet extraction allowed for constant washing with fresh acetone. This was then followed by three days of room-temperature drying to ensure that the CPC was free of acetone. The resulting pure cellulose was kept for characterization and further experiments.

3.3.4. Synthesis of nanocellulose

Figure 3.2(g-i) illustrates a schematic process for synthesizing CNCs through acid hydrolysis. Briefly, in a 500 mL conical flask, 20 g of chemically purified cellulose (CPC) was combined with 400 mL (32% w/v) sulfuric acid. The synthesis process involved using a 1:20 (g: mL) cellulose-to-acid ratio; the mixture was heated in a water bath for 45 minutes. The solution was first heated to 45 °C, then to 55 °C with constant

stirring at 600 rpm. The hydrolysis process was stopped by carefully quenching it with 200 mL of 10-fold deionized water five times. The resultant suspension was homogenized using a centrifuge for 40 minutes at 10000 rpm. This process was repeated five times, each time removing the supernatant from the sediment and replacing it with new distilled water until the supernatant's pH was neutral. After three days of room temperature drying, the resulting CNCs were packaged for characterization.

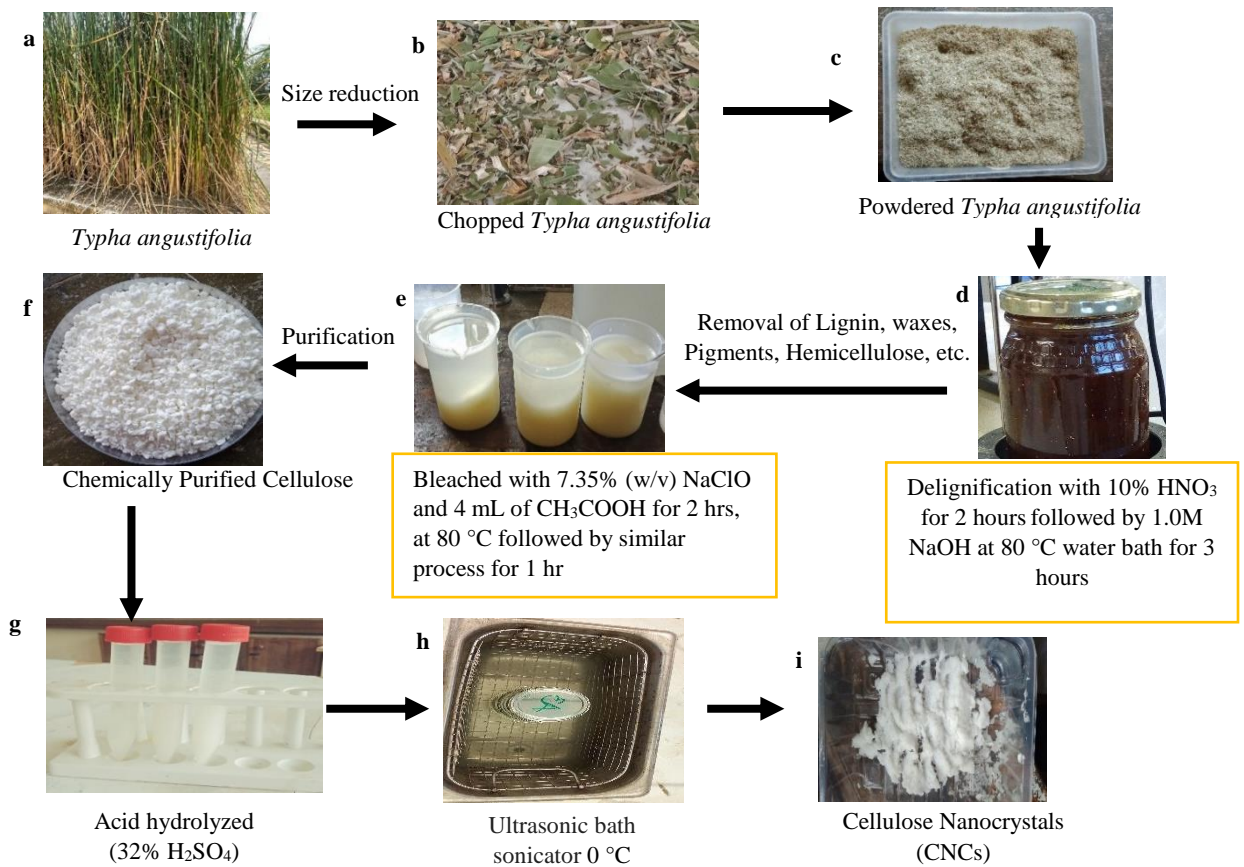


Figure 3.2: Summarized schematic diagram for CPC isolation and synthesis of CNCs

3.3.5 Functionalization of Cellulose Nanocrystals with Fe₃O₄ to form CNC-Fe₃O₄NP

For the synthesis of Fe₃O₄ nanoparticles, a co-precipitation method by (Ba-Abbad et al., 2022) was adopted with small modifications. First, an aqueous solution containing FeCl₃·6H₂O and FeCl₂·4H₂O in a 2:1 molar ratio was prepared. The solution was heated to 80°C under nitrogen gas, and a 25% ammonia solution was added dropwise until the pH reached 10, resulting in the formation of Fe₃O₄ nanoparticles. The black precipitate was washed with deionized water and ethanol, and then dried. To functionalize CNC with Fe₃O₄NP, a suspension of CNCs was mixed with the Fe₃O₄ nanoparticles under ultrasonic agitation for one hour to ensure uniform coating. The mixture was then stirred continuously at room temperature for four hours. The resulting CNC-Fe₃O₄ nanoparticles (CNC-Fe₃O₄NP) were separated using a magnet, washed with deionized water, and dried in a vacuum oven at 60°C.

3.3.6 Cross-linking of CNC-Fe₃O₄NP with β -Cyclodextrin to form CNC-Fe₃O₄NP-CD Nanocomposite

The formed CNC-Fe₃O₄NP was further functionalized with beta-cyclodextrin (β-CD) to enhance its adsorption capacity for pollutants. First, a solution of β-CD was prepared by dissolving β-CD in deionized water at a concentration of 10 mg/ml. The solution was stirred at room temperature until fully dissolved. To cross-link β-CD with CNC-Fe₃O₄NP, the CNC-Fe₃O₄NP was dispersed in deionized water and sonicated for 30 minutes to ensure a homogeneous suspension. The β-CD solution was then added to the CNC-Fe₃O₄NP suspension under continuous stirring. To facilitate the cross-linking, 0.1M NaOH was added dropwise to the mixture. The reaction was maintained at 70°C for 6 hours under constant stirring. After the cross-linking reaction, the mixture was cooled to

room temperature. The CNC-Fe₃O₄NP-CD nanocomposite was separated using a magnet and washed several times with deionized water to remove any unreacted β-CD and other impurities. The CNC-Fe₃O₄NP-CD was then dried in a vacuum oven at 60°C. The resulting CNC-Fe₃O₄NP-CD nanocomposite was stored in an airtight container for subsequent characterization and application in the adsorption studies.

3.4 Characterization

3.4.1 Fourier Transform Infrared Spectroscopy (FTIR)

FTIR spectra were recorded in the range of 4000 to 500 cm⁻¹ using Perkin Elmer Fourier Transform Infra-Red spectrometer equipped with an attenuated total reflectance (ATR) accessory. The resolution was set to 4 cm⁻¹, and 32 scans were accumulated for each spectrum. The spectrum was then base line corrected, normalized, smoothed and the key absorption peaks were analyzed to confirm the presence of specific functional groups such as hydroxyl, carboxyl, and Fe-O bonds.

3.4.2 Transmission Electron Microscopy (TEM)

TEM was used to observe the size and morphology of the prepared samples. A small amount of the sample was dispersed in ethanol and sonicated to achieve a well-dispersed solution. A drop of the dispersion was placed on a carbon-coated copper grid and allowed to dry at room temperature. TEM images were obtained using a JEOL JEM-2100 microscope operated at an accelerating voltage of 200 kV. The images provided detailed information on the particle size, shape, and distribution, as well as the degree of crystallinity of the CNC-Fe₃O₄NP and CNC-Fe₃O₄NP-CD nanocomposites.

3.4.3 Scanning Electron Microscopy (SEM)

SEM was employed to analyze the surface morphology. The samples were first coated with a thin layer of gold using a sputter coater to enhance conductivity. SEM images were captured using a JEOL IT-7500LA instrument, operated at an accelerating voltage of 15-20 kV. The micrographs provided insights into the surface texture, particle agglomeration, and overall morphology of the grass powder, CPC, CNC, Fe₃O₄NP, CNC-Fe₃O₄NP, and CNC-Fe₃O₄NP-CD samples. The magnification range used varied from 1,000x to 50,000x.

3.4.4 Energy Dispersive X-ray Spectroscopy (EDS)

EDS was performed in conjunction with SEM to determine the elemental composition of the nanocomposites. The samples were prepared similarly to SEM analysis. The EDS detector, integrated into the SEM system, was used to identify and quantify the elemental constituents. Spectra were collected at an accelerating voltage of 15 kV, and peaks corresponding to elements such as carbon, oxygen, iron, and others were analyzed.

3.4.5 X-ray Diffraction (XRD)

XRD was utilized to examine the crystalline structure of the materials. The powdered samples were placed on a sample holder, and XRD patterns were recorded using a Shimadzu XRD-7000 diffractometer. The diffractometer operated with Cu K α radiation ($\lambda = 1.5406 \text{ \AA}$) at 40 kV and 30 mA. The scanning range (2θ) was set from 10° to 80° at a scanning rate of $2^\circ/\text{min}$. The obtained diffraction patterns were analyzed to identify crystalline phases and calculate the average crystallite size using the Scherrer equation (Eq.3.1) (Hassanzadeh-Tabrizi, 2023).

$$\text{Crystal size (D)} = \frac{K\lambda}{\beta \cos \theta} \quad (3.1)$$

From the equation, the crystal structure has a K factor of 0.89, λ is the length of a light wave (1.54056 Å), β is the Full Width at Half Maximum (FWHM) in radians, and θ is the angle of diffraction in degrees

The crystallinity index (CrI) was calculated using Equation 3.2 below. Where I_{002} and I_{am} represent the intensity of the peak of crystalline and amorphous regions.

$$C_r I(\%) = \frac{I_{002} - I_{am}}{I_{002}} \times 100 \quad (3.2)$$

3.4.6 Thermogravimetric Analysis (TGA)

TGA was conducted to study the thermal stability and decomposition behavior of the prepared materials and the nanocomposites. Approximately 10 mg of each sample was placed in a platinum pan, and the analysis was carried out using a PerkinElmer TGA 4000 system. The samples were heated from room temperature to 1000°C at a rate of 10°C/min under a nitrogen atmosphere. The weight loss was recorded as a function of temperature, providing information on thermal stability, decomposition temperatures, and the composition of the materials.

3.4.7 Brunauer-Emmett-Teller (BET) Analysis

The surface area, pore volume, and pore size distribution of the nanocomposites were determined using BET analysis. The samples were degassed at 120°C under vacuum for 12 hours prior to analysis to remove adsorbed gases and moisture. Nitrogen adsorption-desorption isotherms were measured at 77 K using a Micromeritics ASAP 2020 surface area analyzer. The BET surface area was calculated from the linear portion of the

adsorption isotherm, while the Barrett-Joyner-Halenda (BJH) method was used to analyze pore size distribution and total pore volume.

3.4.8 Vibrating Sample Magnetometry (VSM)

VSM was used to measure the magnetic properties of the Fe₃O₄NP, CNC-Fe₃O₄NP and CNC- Fe₃O₄NP-CD nanocomposites. Approximately 50 mg of the sample was placed in a VSM sample holder, and magnetic measurements were conducted using a Quantum Design PPMS VSM. The magnetic hysteresis loops were recorded at room temperature, applying a magnetic field ranging from -15,000 Oe to +15,000 Oe. The saturation magnetization, coercivity, and remanence were determined to assess the magnetic behavior and potential for magnetic separation.

3.4.9 Zeta Potential

Zeta potential measurements were performed to determine the surface charge and colloidal stability of the nanocomposites in aqueous suspension. A dilute suspension of the sample was prepared in deionized water, and the pH was adjusted to the desired value. The suspension was then sonicated for 10 minutes to ensure proper dispersion. Zeta potential measurements were carried out using a Malvern Zetasizer Nano ZS instrument. The results provided information on the electrostatic interactions between particles.

3.5 Batch Experiments

To evaluate the batch experiments, a succession of bottles containing chromate ions and varying volumes of the prepared adsorbents were shaken to assess the efficacy of the adsorbents. A 2.485g (0.02M) oven-dried, moisture-free potassium dichromate powder

was dissolved in 1000ml of deionized water to create stock solutions for hexavalent chromium.

3.5.1 Determination of Effect of pH on adsorption

To investigate the effect of pH on the adsorption efficiency of the functionalized cellulose nanocomposite, a 100 mL solution of wastewater was prepared with a known initial concentration of Cr(VI) and fixed mass of the adsorbent. The pH of the solution was measured and then adjusted to specific pH levels from 1.0 to 12.0, to adjust the pH of the solution 1M NaOH and 1M HNO₃ were used. The adjusted solutions were placed in plastic beakers, each containing a fixed mass of the functionalized cellulose nanocomposite adsorbent. The mixtures were agitated on a magnetic stirrer at a room temperature for 35 minutes to ensure thorough interaction between the adsorbent and the metal ions. After agitation, the mixtures were filtered, and the filtrates were collected for analysis. The concentration of Cr(VI) in each filtrate was measured using UV-Vis spectroscopy. The optimum pH for the removal of Cr(VI) was determined by calculating the percentage removal at each pH level. The one with the highest removal efficiency was chosen as the optimal pH for adsorption.

3.5.2 Effect of metal ions concentration on adsorption

To study the effect of metal ion concentration on the adsorption capacity of the functionalized cellulose nanocomposite, aqueous solutions containing Cr(VI) at varying concentrations (10 ppm, 20 ppm, 30 ppm, 40 ppm, 50 ppm, and 60 ppm) were prepared. The optimal pH, as determined from the previous experiment, was adjusted for each solution using 1M NaOH or 1M HNO₃. After adjusting the pH, each Cr(VI) solution was

then placed in a separate plastic beaker, and a fixed mass of the functionalized cellulose nanocomposite adsorbent was added. The mixtures were stirred using a magnetic stirrer at a room temperature for 2 hours, allowing sufficient contact time for adsorption to occur. After stirring, the solutions were filtered to separate the adsorbent from the aqueous phase. The concentration of Cr(VI) in each filtrate was analyzed using UV-VIS spectroscopy. The adsorption capacity of the adsorbent at different initial Cr(VI) concentrations was calculated by determining the difference between the initial and final metal ion concentrations. The percentage removal of Cr(VI) at each concentration level was also calculated to assess the adsorption efficiency of the nanocomposite.

3.5.3 Determination of effects of adsorbent weight on adsorption.

To determine the optimum weight of the functionalized cellulose nanocomposite for Cr(VI) adsorption, varying amounts of adsorbent (0.1 g to 1.0 g) were tested with 100 ml of 20 ppm Cr(VI) solution at the optimal pH. The solutions were stirred for 2 hours, then filtered. The remaining Cr(VI) concentration in the filtrates was measured using UV-VIS spectroscopy to calculate the percentage removal. The adsorbent weight that achieved the highest removal efficiency was identified as the optimal dosage, providing valuable data for efficient water treatment applications.

3.5.4 Determination of effects of contact time on adsorption.

To determine the optimal contact time for adsorption, a fixed mass of functionalized cellulose nanocomposite was added to a fixed concentration and volume of Cr(VI) solution. The mixtures were stirred for pre-determined time intervals of 0, 5, 10, 15, 20, 25, 30, and 35 minutes. At each time point, the mixture was filtered, and the residual concentration of metal ions in the solution was measured using UV-VIS spectroscopy.

This process was carried out to assess the rate of adsorption and to determine the time required to reach equilibrium, ensuring maximum removal efficiency.

3.5.6 Determination of effect of Temperature on adsorption

To determine the effect of temperature on adsorption, batch experiments were conducted using a fixed mass of functionalized cellulose nanocomposite. The experiments were performed at a specific predetermined pH. Aqueous solutions containing a fixed concentration and volume of Cr(VI) were prepared. The solutions were placed in separate beakers, each maintained at different pre-determined temperatures (25°C, 25°C, 35°C, 45°C, and 55°C). The mixtures were stirred for a set duration to ensure thorough contact between the adsorbent and the metal ions. After the incubation period, the mixtures were filtered, and the residual concentration of Cr(VI) in the filtrates was measured using UV-VIS spectroscopy. The temperature that resulted in the highest adsorption efficiency was identified, helping to understand the thermal influence on the adsorption process and the thermodynamics involved.

3.5.7 Effect of Competing Ions on Adsorption

To study the effect of competing ions on the adsorption of Cr(VI) by the functionalized cellulose nanocomposite, batch experiments were conducted with aqueous solutions containing a fixed concentration of Cr(VI) and varying concentrations of other metal ions, such as Cd^{2+} , Pb^{2+} and Zn^{2+} . A fixed mass of the adsorbent was added to each solution, and the mixtures were adjusted to the optimal pH for Cr(VI) adsorption. The samples were then stirred at a controlled temperature for a pre-determined contact time. After stirring, the solutions were filtered, and the concentrations of Cr(VI) and the

competing ions in the filtrates were measured using UV-VIS spectroscopy and atomic absorption spectroscopy (AAS).

3.6 Spectrophotometric Analysis

Following tests on adsorption and desorption, the UV-Vis was used to spectrophotometrically measure the amounts of Cr(VI) in the treated water solutions. The total amount of hexavalent chromium ions that were not adsorbed was measured using the Diphenyl-Carbazide (DPC) technique at 540 nm in wavelength. In order to perform the Diphenyl-Carbazide process, 0.01M of DPC solution (2.0g of DPC dissolved in 100 mL acetone) and 10% sulfuric acid were prepared (Warmiati & Wijayanti, 2024). For UV-Vis analysis, 2 mL of each hexavalent chromium solution before and after adsorption was combined with 2mL of 0.01M DPC and 0.1mL of 10% sulfuric acid in 15mL test tubes, followed by 10mL of deionized water. The study was performed at a wavelength of 540 nm.

3.7 Regeneration of the Adsorbents

To evaluate the regeneration capability of the functionalized cellulose nanocomposite, adsorption-desorption cycles were performed. After the initial adsorption of Cr(VI) from a solution of 20mg/L concentration of Cr(VI), the used adsorbent was separated from the solution and washed with deionized water to remove loosely bound ions. The adsorbent was then treated with a desorbing agent, such as 0.1M HCl or 0.1M NaOH, and stirred for 1 hour to release the adsorbed Cr(VI) ions. The desorbed Cr(VI) was quantified, and the adsorbent was thoroughly rinsed with deionized water until neutral pH was achieved. The regenerated adsorbent was dried at 60°C in an oven and reused in a new batch of Cr(VI) solution under the same conditions as the initial adsorption experiment. This

process was repeated for multiple cycles to assess the stability and reusability of the adsorbent. The adsorption efficiency after each regeneration cycle was calculated to determine the extent of performance retention over repeated uses.

3.8 Data Analysis

Data analysis was performed using OriginLab software. The software was used to plot various graphs, including XRD, TGA, FTIR, TDG, VSM, Zeta potential, adsorption isotherms, kinetics, and temperature effects. Derivative curves were generated to analyze the rate of adsorption, while smoothing techniques were applied to reduce noise in the data. Stacking was utilized to compare multiple data sets, such as the effect of competing ions and different regeneration cycles. Particle size distribution was analyzed using histogram plots, and statistical analysis was conducted to calculate the mean and standard deviation, providing insights into the consistency and reliability of the experimental results.

CHAPTER FOUR

RESULTS AND DISCUSSIONS

4.1 Characterization of *Typha angustifolia*, CPC and CNCs.

4.1.1 Physical appearance

Figures 4.1(a-d) show the physical characteristics of the raw chopped *Typha angustifolia* as collected from the field without any chemical treatments, the powdered *Typha angustifolia*, and the chemically purified cellulose before and after acid hydrolysis. The chemical alteration caused the *Typha angustifolia* to become whiter in colour. The raw and powdered *Typha angustifolia* were green and brown, as seen in Figure 4.1a and b. The cellulose (white powder) was formed by treating *Typha angustifolia* powder with HNO₃, NaOH, and sodium hypochlorite (Figure 4.1c). Whiter and gel, hairy-like material (cellulose nanocrystals) was obtained by hydrolyzing the recovered cellulose with H₂SO₄ acid and then washing it with acetone (Figure 4.1d). It was established that chemical treatment with NaOH and purification (bleaching with NaOCl) makes the fibre change colour from brown to white. This was also observed by Evans et.al. (2019) and Johar et al. (2012) while working on sugarcane bagasse and rice husks respectively. The observed changes were all associated with eliminating wax and pigments like chlorophyll, lignin and hemicelluloses (Trache et al., 2017).



Figure 4.1: Physical appearance of (a) Chopped *Typha angustifolia*, (b) Crushed *Typha angustifolia*, (c) Isolated cellulose and (d) Cellulose nanocrystals

4.1.2 Functional group analysis (FTIR)

The functional groups for the *Typha angustifolia*, chemically purified cellulose (CPC) and cellulose nanocrystals (CNC) are illustrated in Figure 4.2. The major absorption bands corresponding to different groups for the *Typha angustifolia*, CPC and CNC were observed from 500 cm^{-1} to around 3600 cm^{-1} . The broad peak at around 3309 cm^{-1} is linked to intramolecular hydrogen bond O-H stretching, and was observed in all the three materials. Similarly, all materials exhibit the C-H stretching, with only minor shifts and variations in intensity, at peaks around 2892 and 2915 cm^{-1} as also suggested by Dantas and Botaro (2012) as an indication of C-H stretching. The wavenumber around 898 cm^{-1}

is observed in all the three materials is due to C-H rocking vibration of cellulose. The bands at 1034 cm^{-1} , 1730 cm^{-1} and 1632 cm^{-1} represent the C-O-C of the pyranose ring and carboxyl groups that are found in esters and acids that are primarily found in lignin and O-H bending vibrations, respectively. Similar observations were observed by Suter et al. (2024) and Zhang & Zou (2019) in their respective studies on cellulose. The peak at 1730 cm^{-1} associated with esters and acids of lignin as reported by Zhang and Zou, (2019) was only observed in the *Typha angustifolia* grass powder. This peak was not seen in chemically purified cellulose and cellulose nanocrystals samples, which is a clear indication that the esters and acids were successfully removed. The peak at 1157 cm^{-1} , represents O-H associated with C-O-H which was present in all the three materials but was more extensive and well-defined in chemically purified cellulose and cellulose nanocrystals, an indication of a purer material, this was also noted by Suter et al. (2024) in cellulose from sugarcane bagasse. The O-H peak associated with absorbed water at around 1632 cm^{-1} was present in all the samples.

The peak at around 1245 cm^{-1} ; was attributed to C=C of aromatic rings, and this may be due to the presence of other organic compounds which are aromatic in nature such as phenols and lignin. The peak 1245 cm^{-1} was not present in the delignified grass and the chemically purified cellulose, indicating that lignin was completely removed.

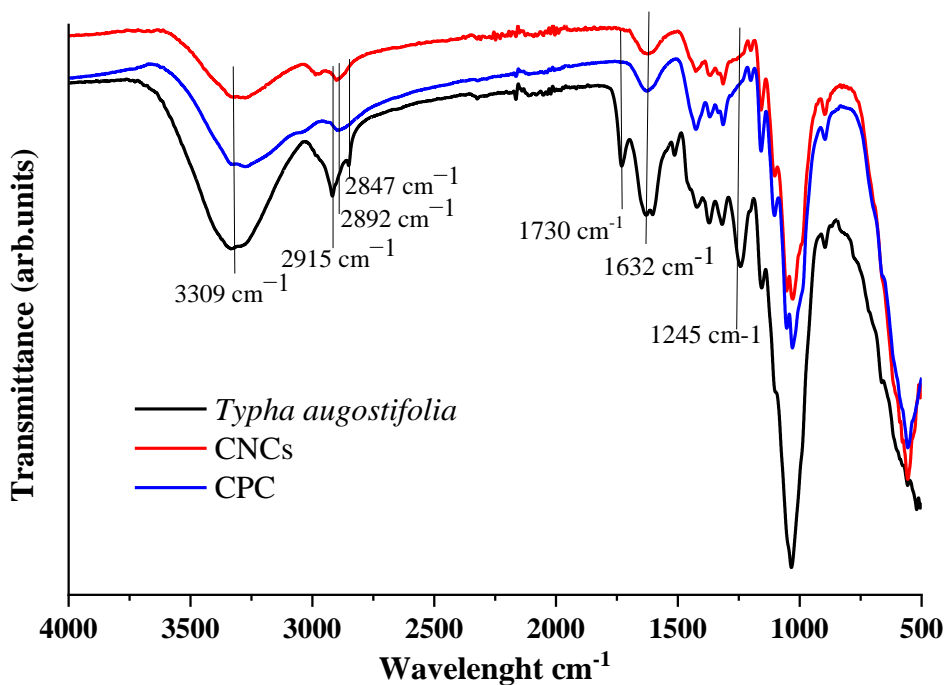


Figure 4.2: FTIR spectra of *Typha angustifolia*, CPC, and CNCs

4.1.3 Scanning electron microscopy (SEM)

Using scanning electron microscopy, the shape and diameter of the CPC and CNCs were determined as seen in Figure 4.3 a-c. From the SEM images, the *Typha angustifolia* display regular rod-like structures that are not chemically connected with spongy-like and the loose materials stuck on its rough surface indicates that the materials were of different composition as seen in Figure 4.3a. On dewaxing and delignification, it can be seen that the CPC structures are not fused despite having a lengthy, uneven form as seen in Figure 4.3b.

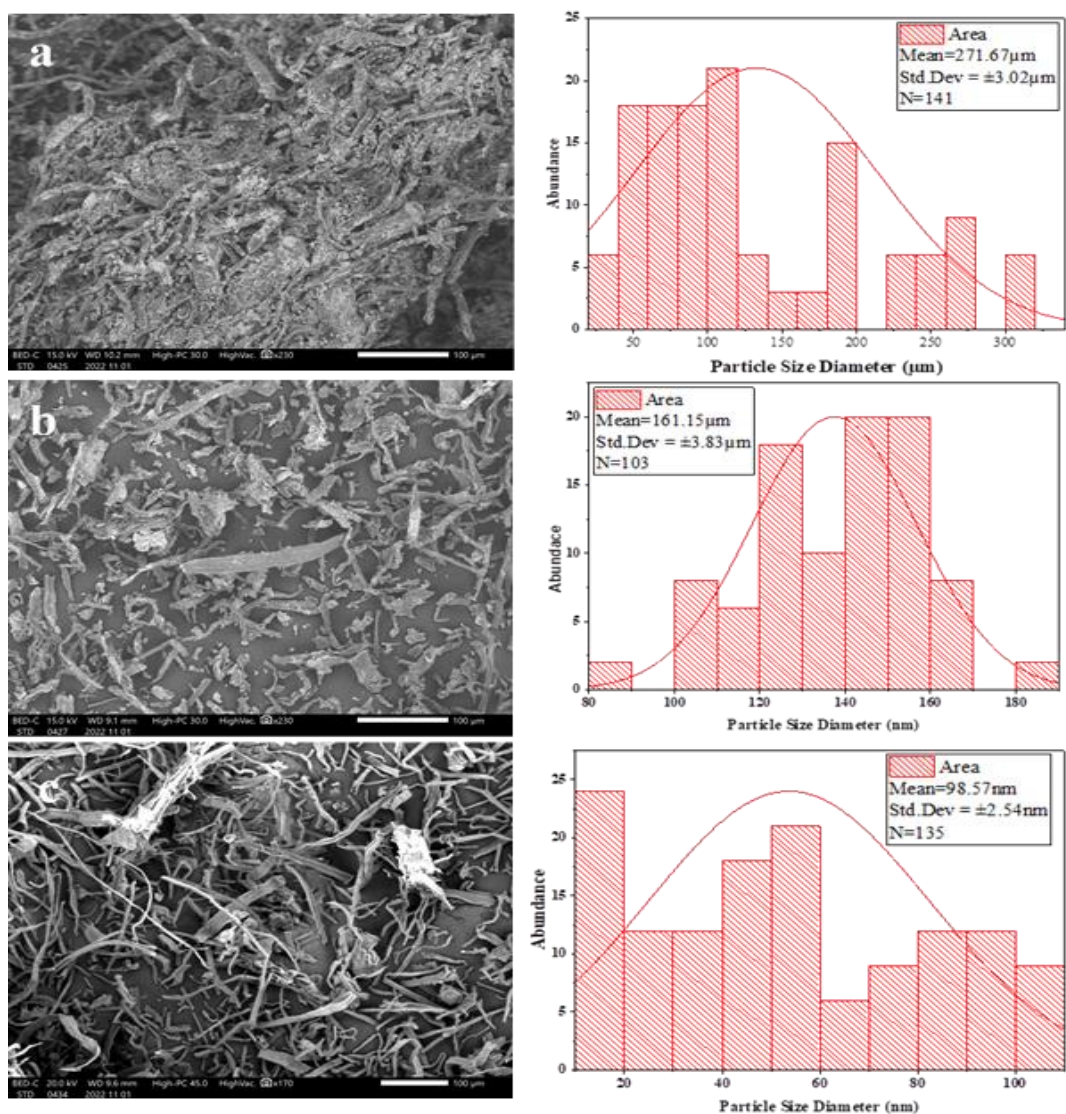


Figure 4.3: Scanning electron (SEM) images (a) *Typha angustifolia*, (b) CPC, and (c) CNCs

The smooth surface of the cellulose results from lignin and hemicellulose being completely removed from the powdered *Typha angustifolia* (Tarchoun et al. 2019). The amorphous and crystalline portions of microcrystalline cellulose are still fused together, resembling a continuous thread, which was also reported by Adawiyah and Suryanti (2022); Patro et al. (2023) and Trache et al. (2016b) in their respective studies on

cellulose. The size of the powdered *Typha angustifolia*, the chemically purified cellulose and cellulose nanocrystals were $271.67 \pm 3.02 \mu\text{m}$, $161.15 \pm 3.83 \mu\text{m}$, and $98.57 \pm 2.54 \text{ nm}$ respectively. After H_2SO_4 hydrolysis, the formed CNCs (Figure 4.3c) show smoother and smaller particles an indication that the crystalline regions remained as the amorphous regions were broken by the acid hydrolysis.

4.1.4 Elemental Analysis

The quantification of the composition of elements present in the *Typha angustifolia* and the prepared cellulosic materials was done using Electron Diffraction Spectroscopy (EDS). The results obtained are shown in Figure 4.4 a-c. The analysis was performed to further investigate the composition of the isolated cellulose and the synthesized CNCs Figure 4.4 b and c. From the *Typha angustifolia* EDS spectrum, C and O, the main building blocks of cellulose, were quantified to be $44.40 \pm 0.11\%$, and $55.42 \pm 0.31\%$. While traces of Ca and Fe were found to be $0.13 \pm 0.02\%$, and $0.06 \pm 0.02\%$, respectively. These trace elements could be attributed to nutrients initially present in the *Typha angustifolia* grass. However, for the cellulosic materials carbon and oxygen atoms constituted $44.26 \pm 0.22\%$ and $55.74 \pm 0.59\%$ respectively for CPC and $52.71 \pm 0.16\%$ and $47.29 \pm 0.41\%$ respectively for CNCs. The elemental analysis showed the purity of the cellulose formed and was purely carbons and oxygens. On hydrolysis using H_2SO_4 , it was noted that there was an increase in C percentage with decrease in that of O and this was due to the breakdown of cellulose into smaller components (cellulose nanocrystals) which results in the removal of oxygen-containing functional groups as reported by Khili et al. (2019) in their study. This observation therefore confirmed that the isolation of cellulose and synthesis of its nanocrystals was successful.

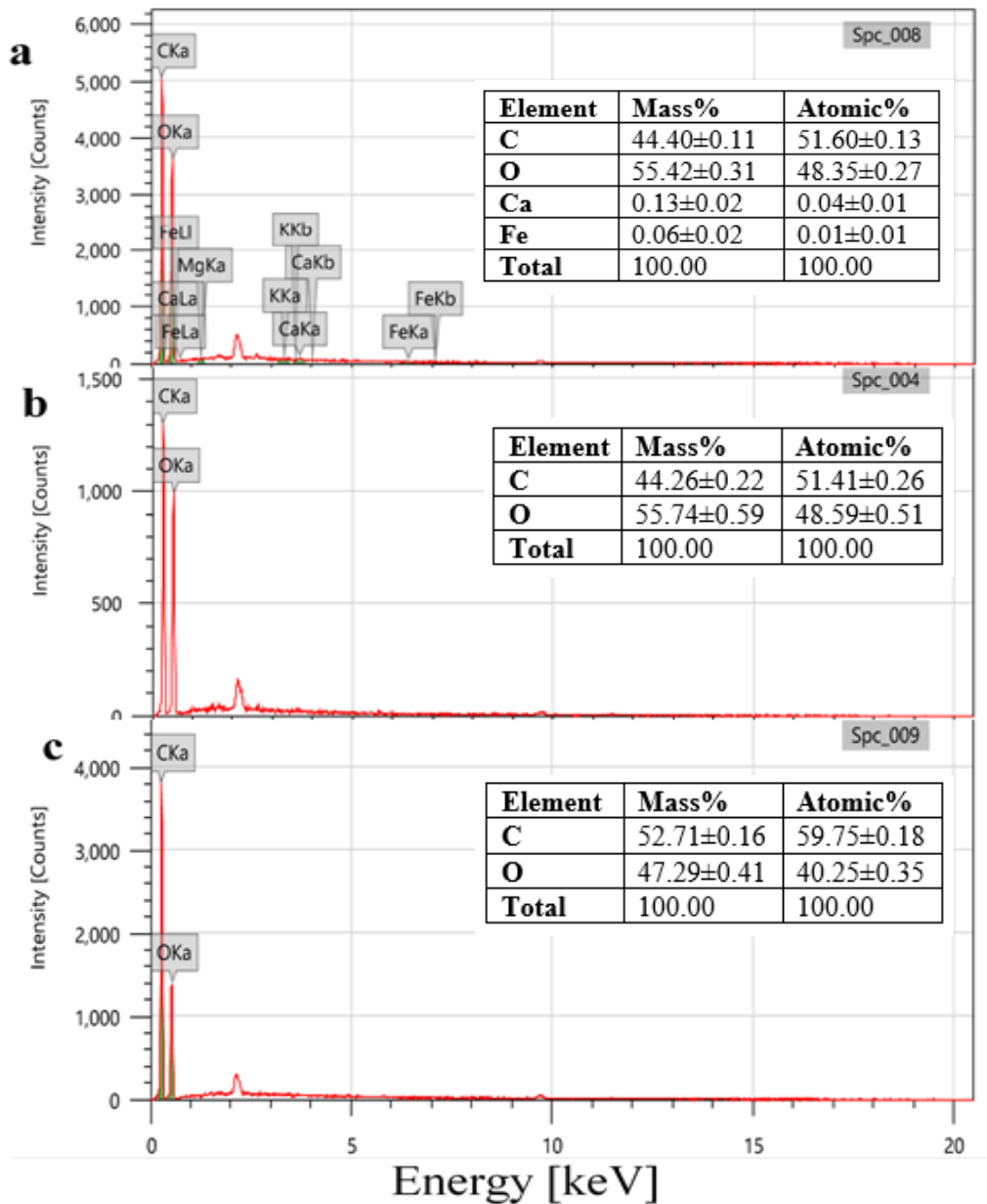


Figure 4.4: EDS spectrum of *Typha angustifolia* (a), CPC (b), and (c) CNCs

4.1.5 Crystalline structure analysis X-ray diffraction

Figure 4.5 shows the crystal structures and Table 4.1 shows the crystallinity indices of *Typha angustifolia* powder, CPC and CNCs. While the peaks in each sample varied in intensity, they all displayed similar patterns except for *Typha angustifolia* grass powder.

Cellulose polymorphs I and II correspond to either CNCs or CPC. High amounts of NaOH added to *Typha angustifolia* grass powder might have changed the cellulose properties from cellulose I to cellulose II. The (101) crystalline planes of hemicellulose are thought to be responsible for the first XRD peak as previously reported by Guna et al., (2019). The (002) planes from the monoclinic structure of cellulose I are referred to as the second peak (Rouhou et al., 2018). Similarly, the third XRD reflex, which appears as a blurred band, confirms the presence of the (004) crystal faces from the amorphous areas (primarily lignin and hemicellulose) as it was earlier reported by Tarchoun et al. (2019), that for cellulose I and cellulose II, the peak intensity values of crystal cellulose are $2\theta = 22.5^\circ$ and $2\theta = 20.1^\circ$, respectively. The highest intensity value of amorphous cellulose is $2\theta = 18^\circ$ for cellulose I and $2\theta = 16.3^\circ$ for cellulose II. From Figure 4(a) the cellulose's post-hydrolysis peak pattern shows that crystalline cellulose I, have a typical structure on the peak of 2θ at 22.64° . In contrast, amorphous cellulose II has a typical structure on the peak of 2θ at 15.83° . Crystalline cellulose II, and crystalline cellulose I showed peaks at intensity values of 2θ of 16.23° and 22.58° , respectively, prior to hydrolysis of cellulose. The powdered *Typha angustifolia* showed peaks with intensity values of 2θ of 16.11° , 21.00° , and 22.89° representing amorphous cellulose I, amorphous cellulose II, and crystalline cellulose II, this was similar to what was reported by Chilukoti and Mandapati (2022) and Tarchoun et al. (2019) in their respective studies.

Table 4.1: Crystallinity indices of *Typha angustifolia* grass powder, CPC, and CNCs.

Sample	2θ (Amorphous) ($^{\circ}$)		2θ (002) ($^{\circ}$)		Crystallinity Index (CrI %)
	Degree	Intensity, I_{am}	Degree	Intensity, I_{002}	
<i>Typha angustifolia</i>	21.00	376	34.97	658	42.86
CPC	22.58	287	34.73	868	66.94
CNCs	22.64	211	34.84	934	77.41

Following hydrolysis, the crystallinity of CNCs is better than that of CPC and *Typha angustifolia* as shown from each sample peak intensity. Additionally, it is evident from the peak heights of each sample that upon hydrolysis, cellulose nanocrystals had a greater peak than the other two an indication of well defined crystals. The crystallinity index and the size of the powdered *Typha angustifolia*, the chemically purified cellulose and cellulose nanocrystals were 42.86% and 308.3 μm , 66.94% and 280.9 μm , and 77.41% and 87.3 nm respectively.

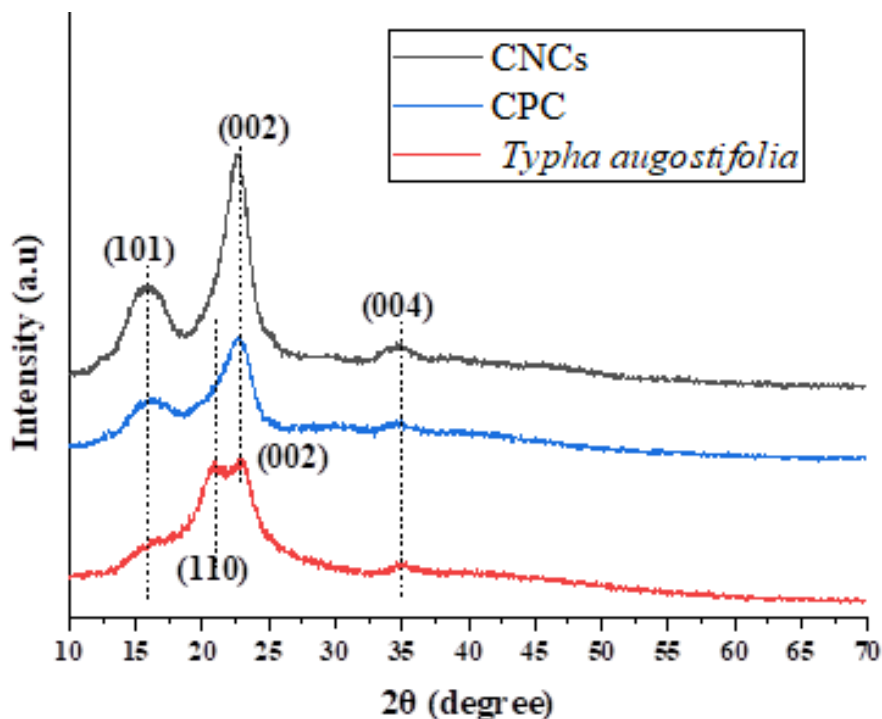


Figure 4.5: XRD pattern of *Typha angustifolia*, CPC and CNCs.

4.1.6 Thermal analysis

Figure 4.6 a and b alongside Table 4.2 provide TGA/DTG data from the thermal degradation mechanisms of powdered *Typha angustifolia*, CPC, and CNCs. It can be seen that the breakdown of hemicellulose happens between 200–260°C while lignin breakdowns at 280–500°C, and cellulose at 340–350°C, this is similar to findings reported by Adewale et al. (2022) and Adeniyi et al. (2022) in their respective studies on the thermal stability of cellulose. The TGA and DTG curves for the samples shown in Figures 4.6 a and b display two main peaks for CPC and CNCs, while *Typha angustifolia* displays three. Evans et al. (2019) and Tarchoun et al., (2019) noted that, the emission of water, volatile chemicals, polysaccharides, and other low molecular weight molecules peaked between 70 and 150 °C which is similar to the findings of this study. For *Typha*

angustifolia powder, CPC and CNCs, the percentage weight loss from the first peak in this temperature range was 14.23%, 8.31% and 8.98% respectively. This demonstrated that *Typha angustifolia* powder had a greater water content than CNC and CPC. The existence of the absorption band at a peak of 1630 cm⁻¹ from the FTIR spectrum Figure 4.2 on the water's hydrogen bond supports this observation. The second peak, which ranged from 250 to 350 °C, indicated the presence of cellulose degradation, by polymer and carboxylate elimination, dehydration, and glycosyl breakdown. At this temperature range (250 to 350 °C) weight loss was found to be 68.76% of the CNCs, 44.62% of the CPC, and 35.04% of the powdered *Typha angustifolia*. The final degradation at the range of 400 and 1000 °C involves an oxidation process and residue breakdown with a weight loss of 14.29% for powdered *Typha angustifolia*, 2.16% for CPC, and 2.68% for CNCs. As can be seen from the TGA and DTG curves, *Typha angustifolia* powder has the highest heat degradation which can be attributed to benzene rings of the aromatic polycyclics of lignin, hemicelluloses, and other noncellulosic molecules (Abu-Thabit et al., 2020). *Typha angustifolia* powder breaks down at 229.28°C and has the lowest thermal stability (Table 4.2), as compared to CPC and CNCs even though CNCs take the longest decomposing time.

Table 4.2: Thermal characteristics of *Typha angustifolia* grass powder, CPC and CNCs.

Temperature	<i>Typha angustifolia</i> (°C)	CPCs (°C)	CNC (°C)
T _{onset}	229.28	239.01	253.24
T _{endset}	354.06	344.45	339.56
T _d	298.32	315.18	315.19

The increased thermal stability of CNCs can be attributed to the use of acid in hydrolysis (Adawiyah & Suryanti, 2022). The greatest amount of cellulose residue was observed in CNCs and the breakdown of the β -1,4-glycosidic linkages, generation of levoglucosan and charcoal was probably the order of cellulose degradation at higher temperatures according to Adawiyah and Suryanti (2022), for *Typha angustifolia* powder, CPC and CNCs.

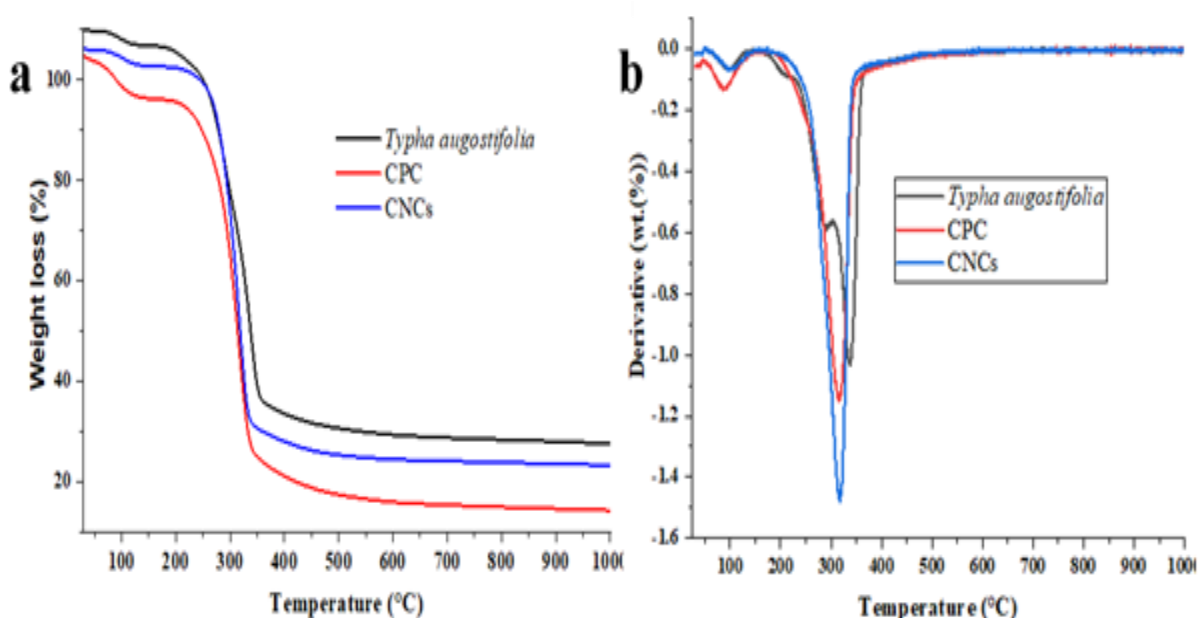


Figure 4.6: (a). TGA and (b). DTG curve of *Typha angustifolia*, CPC, and CNCs.

4.2 Characterization of Fe₃O₄NP, CNC-Fe₃O₄NP and CNC-Fe₃O₄NP-CD

4.2.1 Functional group analysis (FTIR)

Figure 4.7 illustrates the FTIR spectroscopy for Fe₃O₄NP, CNC-Fe₃O₄NP and CNC-Fe₃O₄NP-CD nanocomposites. The characteristic bands observed in the FTIR spectra provide evidence of successful functionalization and incorporation of various functional groups. From this study, the three FTIR spectra for Fe₃O₄NP, CNC-Fe₃O₄NP and CNC-

Fe₃O₄NP-CD, the spectrum exhibited a significant band at 546 cm⁻¹, corresponding to the Fe-O stretching vibrations of Fe₃O₄NP. This band confirmed the presence of magnetic Fe₃O₄NP within the nanocomposite as earlier reported by Abdulwahid et al. (2023) in a similar research on iron oxide nanocomposites. Additionally, the spectrum of CNC-Fe₃O₄NP and CNC-Fe₃O₄NP-CD nanocomposites showed peaks around 1421 cm⁻¹ and 892 cm⁻¹, associated with the cellulose structure, indicating that the cellulose backbone remained intact after nanoparticle incorporation as also reported by Kadam et al. (2022) in their study. In addition, the peaks at around 3323 cm⁻¹ is linked to intramolecular hydrogen bond O-H stretching. The peaks at around 2895 and 2976 cm⁻¹ represents C-H stretching of the cellulosic materials, with only minor shifts and variations in intensity as compared with that of CNCs. When functionalized with β-cyclodextrin (CD), the FTIR spectrum of CNC-Fe₃O₄NP-CD displays new peaks at 1022 cm⁻¹ and 1155 cm⁻¹, corresponding to C-O-C and C-H bending vibrations from CD as suggested by Gala (2015) in an earlier research. These peaks, 1022 cm⁻¹ and 1155 cm⁻¹, confirm the successful attachment of β-cyclodextrin to the CNC-Fe₃O₄NP nanocomposite. The inclusion of CD enhances the nanocomposite's capability to form host-guest complexes with various pollutants, improving its adsorption efficiency for hexavalent chromium (Tian et al., 2021).

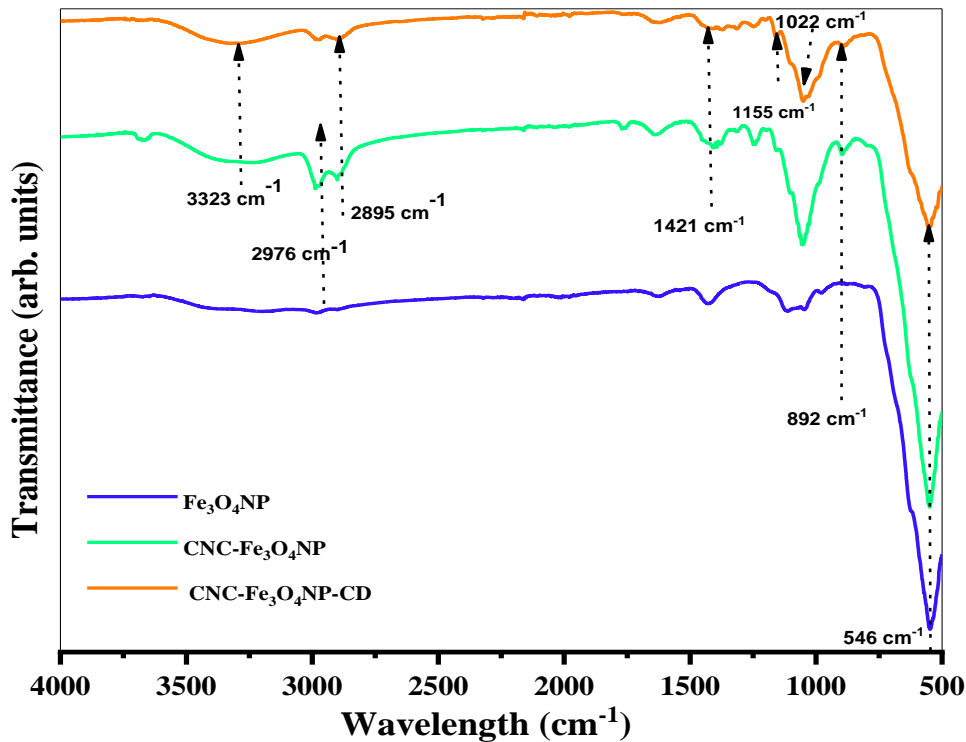


Figure 4.7: FTIR spectra for Fe₃O₄NP, CNC-Fe₃O₄NP and CNC-Fe₃O₄NP-CD nanocomposites

4.2.2 Scanning electron microscopy (SEM) Analysis

Figure 4.8 a-c presents SEM images showing the surface morphology of Fe₃O₄NP, CNC-Fe₃O₄NP, and CNC-Fe₃O₄NP-CD nanocomposites. The SEM analysis provides crucial insights into the structure and distribution of the components within these materials. In the case of Fe₃O₄NP Figure 4.8a, the image reveals the presence of large aggregates, which are common due to the magnetic nature of Fe₃O₄, that causes its particles to attract each other and form clusters. This agglomeration reduces the surface area available for adsorption, potentially limiting the efficiency of the nanoparticles in capturing from aqueous solutions as reported by Falciglia et al. (2022) in their study on nanoparticles. For the CNC-Fe₃O₄NP nanocomposites, Figure 4.8(b), the SEM images display a

significant reduction in agglomeration, with the particles forming more uniform attachment to the CNCs rod-like structures. The introduction of cellulose nanocrystals (CNCs) appears to help disperse the Fe₃O₄ nanoparticles more evenly. CNCs, being naturally fibrous and possessing abundant hydroxyl groups, interact with the nanoparticles, providing a steric hindrance that mitigates their tendency to clump together (Katiyar & Dhar, 2020). This improved dispersion increases the overall surface area and exposes more active sites, enhancing the material's adsorption capacity (Katiyar & Dhar, 2020).

The further modification to CNC-Fe₃O₄NP-CD, Figure 4.8(c) shows an even more homogeneous dispersion without significant aggregation. The presence of β-cyclodextrin appears to enhance this dispersion further. CDs, with their unique toroidal structure and the ability to form inclusion complexes, contribute to stabilizing the nanoparticles hence preventing them from agglomerating. The uniform distribution observed in these nanocomposites indicates a higher availability of active sites, which enhances the efficiency of adsorption. The presence of β-CD also provides additional functional groups that interact with metal ions, potentially increasing their adsorption capacity and selectivity of contaminants (Chan et al., 2021).

The enhanced dispersion and reduced agglomeration observed in CNC-Fe₃O₄NP and CNC-Fe₃O₄NP-CD suggest that these materials could be highly effective in removing heavy metals from wastewater. The increased surface area and uniform distribution of active sites mean more effective adsorption of metal ions, leading to higher removal efficiencies (Marcelo et al., 2021 and Zhao et al., 2011).

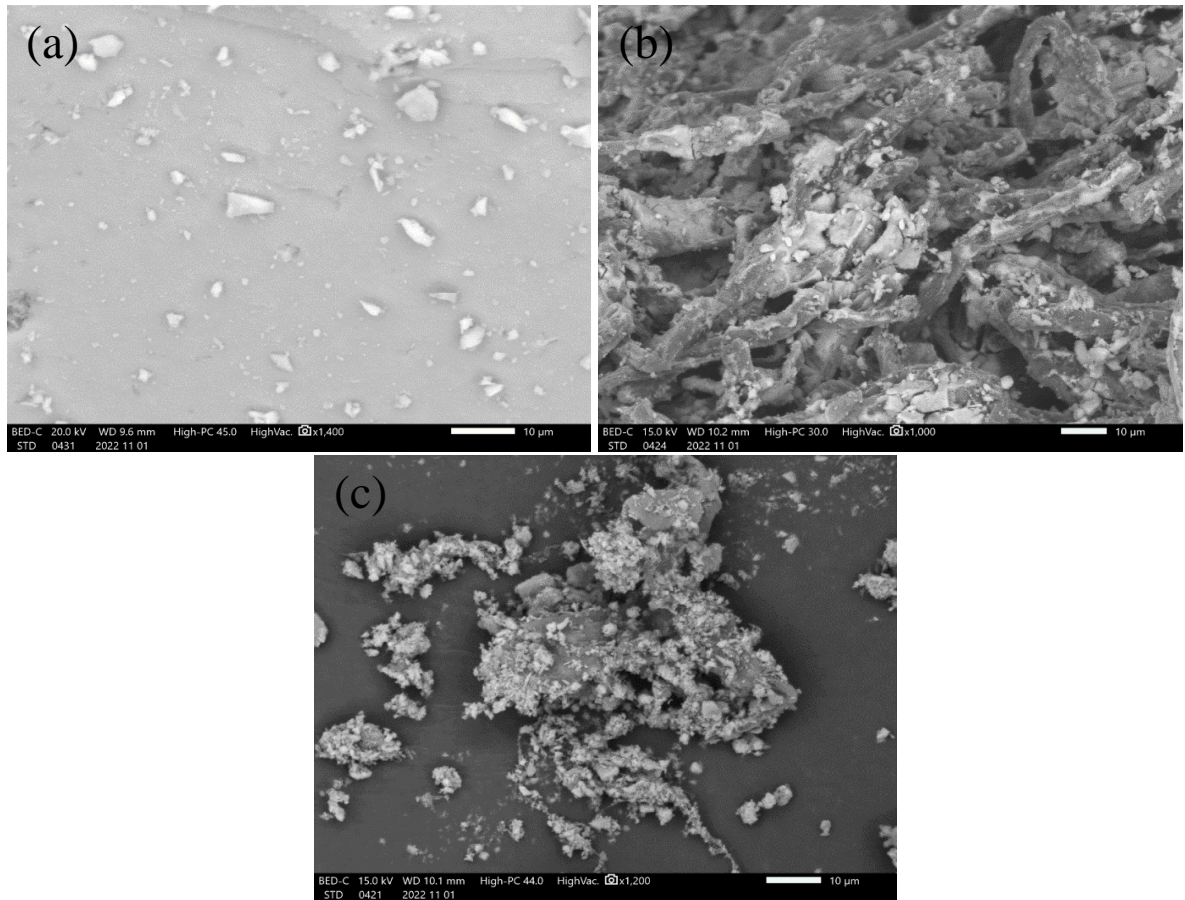


Figure 4.8: SEM images for Fe₃O₄NP, CNC-Fe₃O₄NP, and CNC-Fe₃O₄NP-CD nanocomposites

4.2.3 Energy Dispersive Spectroscopy (EDS)

To further confirm the structure of Fe₃O₄NP, CNC-Fe₃O₄NP, and CNC-Fe₃O₄NP-CD nanocomposites, Energy dispersive spectroscopy (EDS) was employed to analyze the elemental composition of the materials Figure 4.9 (a-c). The data reveal significant changes in the elemental composition as a result of the addition of Fe₃O₄ and β -cyclodextrin to cellulose nanocrystals. The EDS analysis of Fe₃O₄NP showed predominant presence of iron (Fe) and oxygen (O) with mass percentages of $70.41 \pm 0.21\%$ and $11.77 \pm 0.33\%$, respectively Figure 4.9a. This high concentration of iron

is as a result of Fe_3O_4 which is primarily composed of iron and oxygen. The carbon (C) content is relatively low, indicating minimal contamination or presence of organic material in the sample (Clarina et al., 2018). The atom percentages reflected a similar distribution, with iron being the dominant component, essential for the magnetic properties of the nanoparticles (Clarina et al., 2018). With the addition of Fe_3O_4 to CNC to form CNC- Fe_3O_4 NP, the EDS data revealed an increase in the carbon content, indicated by a mass percentage of 25.32%. This increase in carbon content is attributed to the cellulose nanocrystals, which are organic in nature. The oxygen content also increased greatly from 11.77% to 36.75%, which is associated with both the CNCs and the Fe_3O_4 nanoparticles. Notably, the iron content decreases to 37.70% from 70.41%, reflecting the partial coating of the nanoparticles with CNCs, which is consistent with the reduction in the surface density of iron due to the presence of the organic CNC matrix as was suggested by Ruiz-Caldas et al. (2020) in a similar study. Further functionalization with β -cyclodextrin to form CNC- Fe_3O_4 NP-CD resulted in additional changes in elemental composition. The EDS spectra for this composite revealed an increase in carbon content from 25.32 to 39.78%, highlighting the organic nature of β -cyclodextrin. The iron content decreased further to 21.90% from 37.70% as the introduction of β -cyclodextrin contributes more organic material, reducing the relative amount of iron detected. These trends in elemental composition reveals the successful incorporation of Fe_3O_4 nanoparticles and CD into the CNCs, leading to the formation of the CNC- Fe_3O_4 NP and CNC- Fe_3O_4 NP-CD composites.

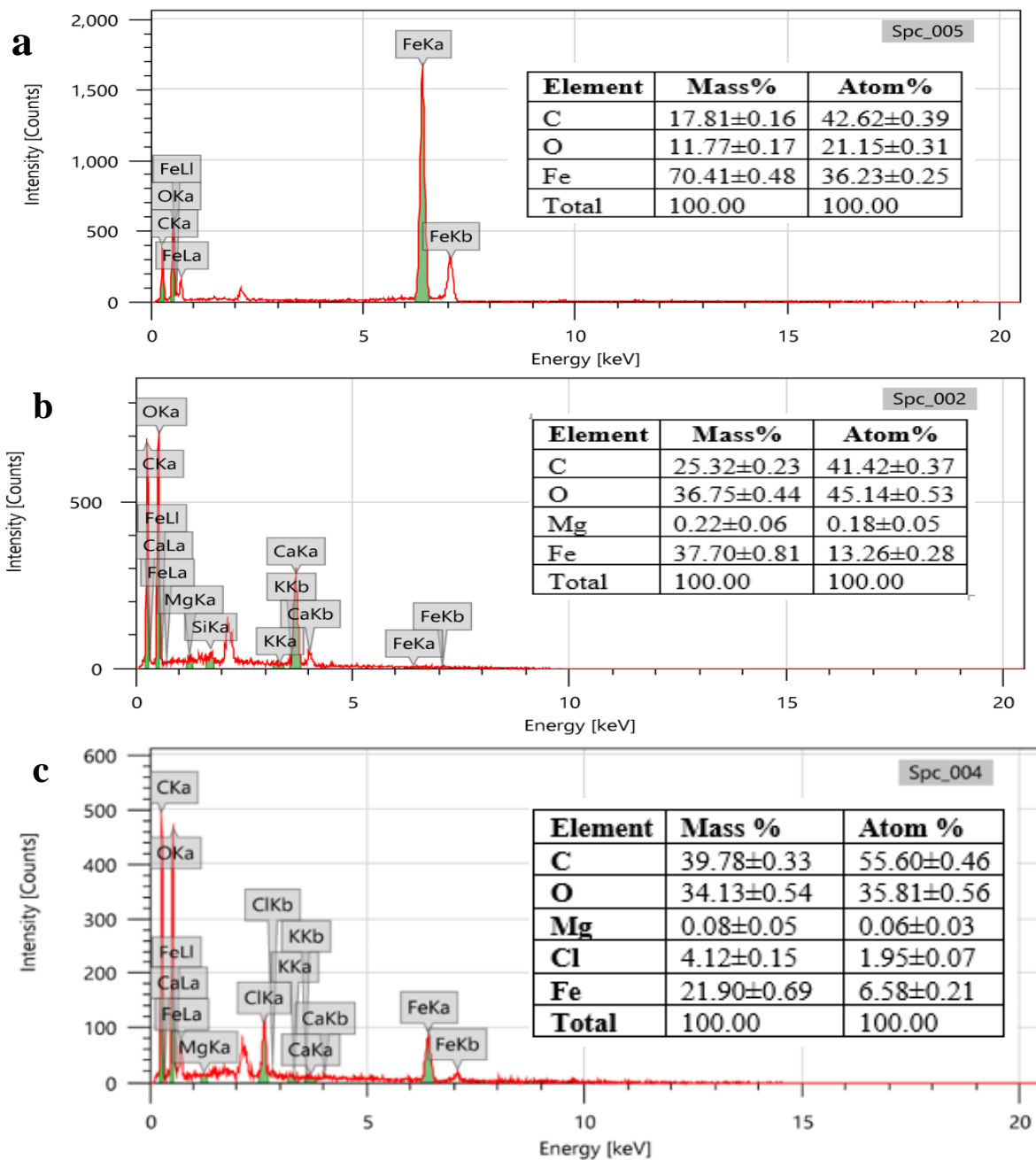


Figure 4.9: EDS data for (a). Fe₃O₄NP, (b). CNC-Fe₃O₄NP and (c). CNC-Fe₃O₄NP-CD nanocomposites

4.2.4 Transmission Electron Microscopy(TEM)

TEM analysis was performed to establish the particle size and morphology of the prepared adsorbents (Fe₃O₄NP, CNC-Fe₃O₄NP, and CNC-Fe₃O₄NP-CD). The analysis

data is presented in Figure 4.10(a-c). From this study, TEM analysis revealed an increase in particle size following the modifications of Fe₃O₄ nanoparticles with cellulose nanocrystals (CNC) and further with β-cyclodextrin. The initial Fe₃O₄ nanoparticles exhibited significant agglomeration, forming larger grains with particle size of 12.76 nm. To reduce agglomeration and optimize particle size distribution, surface functionalization was employed by incorporating CNCs. Where Fe₃O₄ nanoparticles incorporates onto CNC, the average particle size increased to approximately 16.82 nm, but with less agglomerations demonstrating improved dispersion. When CNC-Fe₃O₄NP nanocomposite was functionalization with β-cyclodextrin the particle size increased to 27.76 nm. Various research studies have shown similar observations that surface functionalization affects particle size (Nguyen et al., 2021). Functionalization with CNC typically results in improved dispersion and a slight increase in size due to the coating effect of the CNC. This effect is observed in the decrease in agglomeration and the formation of a more stable nanoparticle suspension. While smaller nanoparticles typically offer higher surface area-to-volume ratios, the functionalization process enhances the surface chemistry, which can significantly improve adsorption efficiency despite an increase in size (Irshad et al., 2023).

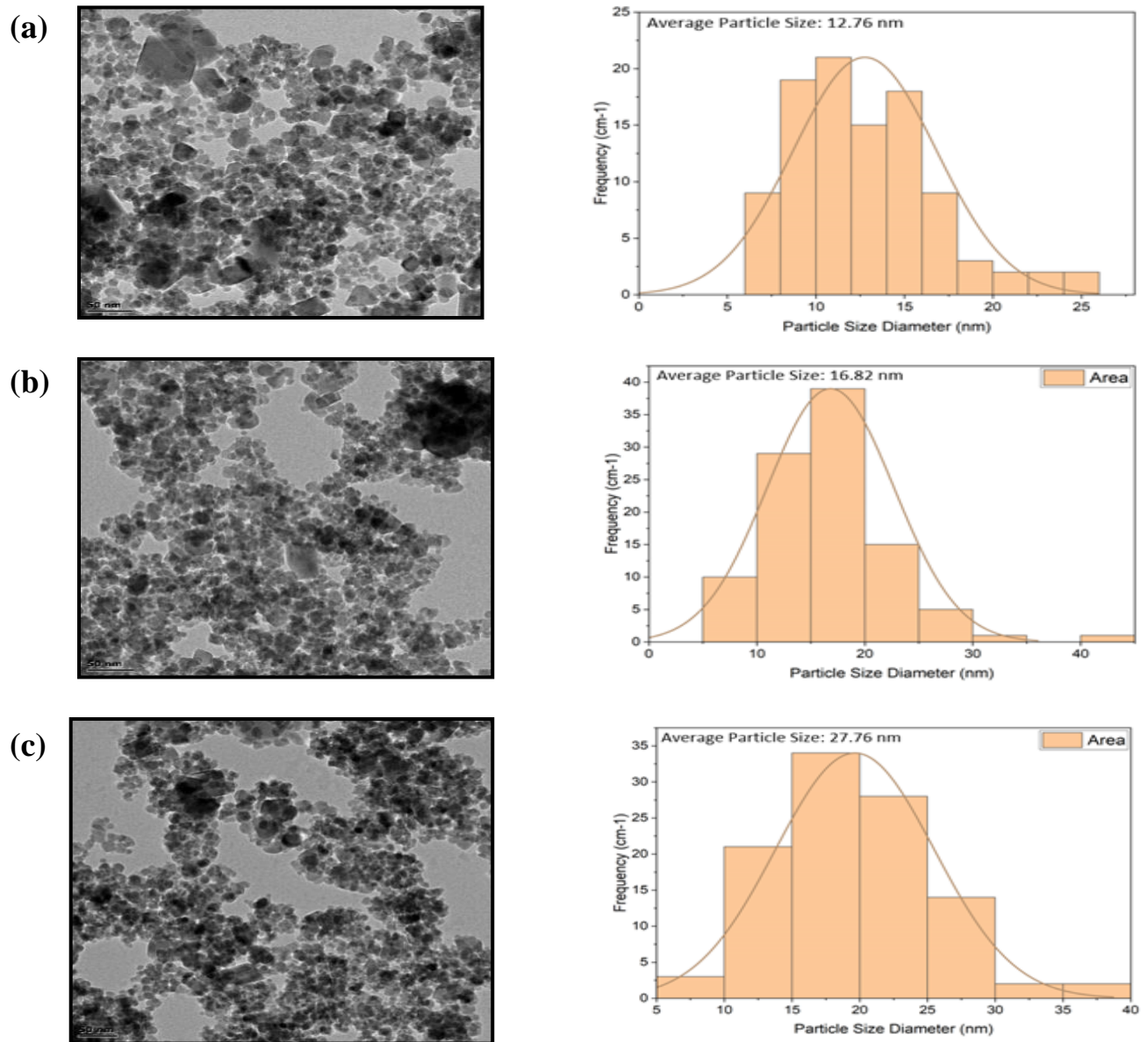


Figure 4.10: TEM images for Fe₃O₄NP, CNC-Fe₃O₄NP, and CNC-Fe₃O₄NP-CD

For CNC-Fe₃O₄NP nanocomposites, the improved dispersion and reduction in agglomeration provide more uniform and accessible active sites for metal ions adsorption as earlier observed by Xu et al. (2012) working on nanocomposites. With the further functionalization to form CNC-Fe₃O₄NP-CD, the additional β -cyclodextrin molecules introduce more hydroxyl groups and binding sites, which can interact with metal ions.

Although the particle size increases, the enhanced surface functionality compensates for the reduced surface area per unit mass as suggested by Qu et al. (2020) in their study.

4.2.5 Vibrating Sample Magnetometer (VSM)

The magnetic properties of Fe₃O₄NP, CNC-Fe₃O₄NP, and CNC-Fe₃O₄NP-CD nanocomposites were studied using a vibrating sample magnetometer (VSM) at room temperature. The hysteresis loops reveal significant insights into the magnetic behavior of these materials, confirming their superparamagnetic nature Figure 4.11. The VSM data indicates that pure Fe₃O₄ nanoparticles exhibit high magnetization values, reaching up to 77.14239 emu/g at an applied magnetic field (H) of ±15,000 Oe. This high magnetization is expected for Fe₃O₄ nanoparticles, which are well-known for their strong magnetic properties. The coercivity and remanence values are close to zero, indicating superparamagnetic behavior, which is advantageous for applications requiring quick magnetic response and easy redispersion once the external magnetic field is removed. Upon incorporation of Fe₃O₄ nanoparticles into cellulose nanocrystals to form CNC-Fe₃O₄NP, a magnetization value of 64.56152 emu/g was observed which was slightly lower than that of Fe₃O₄ nanoparticles at the same applied field of ±15,000 Oe. This reduction can be attributed to the dilution of magnetic Fe₃O₄ content by the non-magnetic CNC matrix. Despite the reduction in magnetic property of the composite, it still retains a significant portion of its magnetic properties, which is beneficial for applications like targeted adsorption and separation in wastewater treatment. Further functionalization with β-cyclodextrin to form CNC-Fe₃O₄NP-CD results in a further reduction in magnetization, with values reaching 34.97082 emu/g at ±15,000 Oe. The additional layer of β-cyclodextrin contributed to this decrease as it introduces more non-magnetic

material into the composite (Hu et al., 2023). Despite this reduction, the CNC-Fe₃O₄NP-CD nanocomposite remains superparamagnetic as evidenced by the low coercivity and remanence values. This superparamagnetic property ensures that the composite can still respond quickly to an external magnetic field and be easily separated from aqueous solutions.

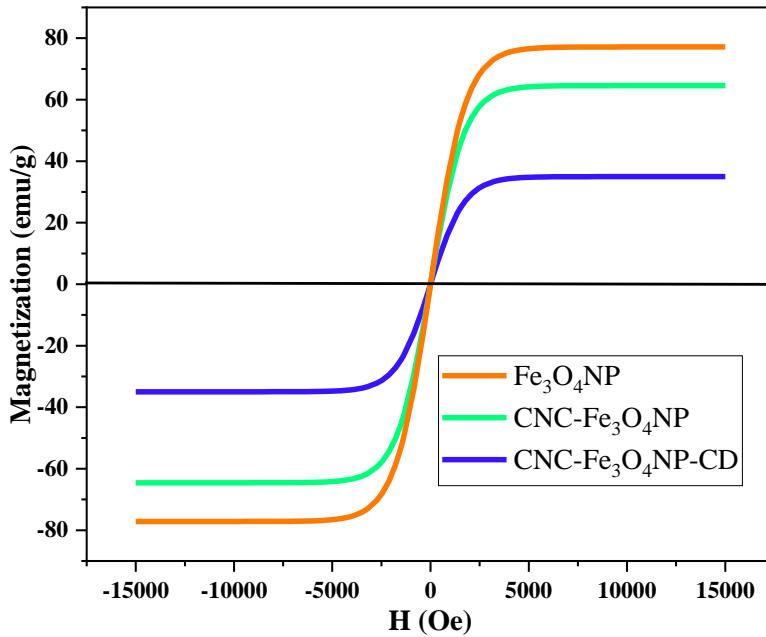


Figure 4.11: VSM for Fe₃O₄NP, CNC-Fe₃O₄NP, and CNC-Fe₃O₄NP-CD

4.2.6 Crystalline structure analysis X-ray diffraction (XRD) Analysis

XRD analysis was used to determine the crystalline structure of the Fe₃O₄NP and the nanocomposites Figure 4.12. For CNC-Fe₃O₄NP, the XRD patterns exhibit peaks corresponding to both cellulose and Fe₃O₄, confirming the presence of magnetic nanoparticles. The distinct peaks at 2θ values of around 30.37°, 35.74°, 43.51°, 53.83°, 57.46° and 63.07° correspond to the (220), (311), (400), (422), (511) and (440) reflections of Fe₃O₄, respectively as quoted by Nguyen et al. (2021b) in their study. The

functionalization with β -cyclodextrin resulted in XRD patterns that show additional broad reflection profiles centered at 22.39° and is attributed to the amorphous nature of CD. These results indicate that the crystalline structure of the Fe_3O_4 nanoparticles is retained while introducing the amorphous CD, enhancing the nanocomposite functionality for Cr(VI) adsorption. This finding is consistent with that reported by Ding et al. (2015), who highlighted the importance of XRD in verifying the crystalline phases of incorporated nanoparticles. The presence of both crystalline and amorphous components in the nanocomposite ensures a balance between structural features and functional flexibility, which might enhance CNC- Fe_3O_4 NP-CD removal efficiency for heavy metals.

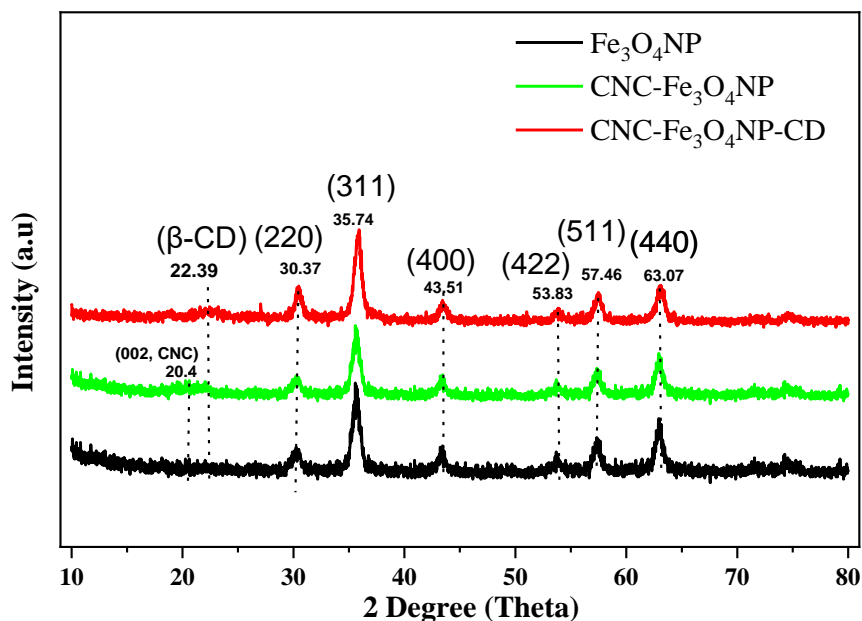


Figure 4.12: XRD pattern of Fe_3O_4 , CNC- Fe_3O_4 NP, and CNC- Fe_3O_4 NP-CD

Furthermore, the crystallinity indices (CrI) for Fe_3O_4 NP, CNC- Fe_3O_4 NP, and CNC- Fe_3O_4 NP-CD nanocomposites reveal significant trends and changes that correlate with their structural modifications and material composition Table 4.3. Fe_3O_4 NP itself does

not have a defined crystallinity index in this context, as it lacks the distinct amorphous and crystalline regions found in cellulose-based composites. The CNC-Fe₃O₄NP nanocomposite, with a CrI of 77.65%, shows a slight increase in crystallinity compared to pure CNCs, attributed to the integration of Fe₃O₄ nanoparticles, which enhances the crystalline regions within the cellulose matrix. This suggests a more ordered structure due to the interaction between CNCs and Fe₃O₄. When β-cyclodextrin is introduced to form CNC-Fe₃O₄NP-CD, the CrI further increased to 84.37%. This increase is attributed to the formation of additional crystalline structures facilitated by CD, Bizymis et al. (2022) which enhances the regular arrangement within the composite. The higher CrI in CNC-Fe₃O₄NP-CD could suggest a more structured and stable composite for adsorption applications as it implies a greater degree of order and potentially more efficient interaction sites for pollutants.

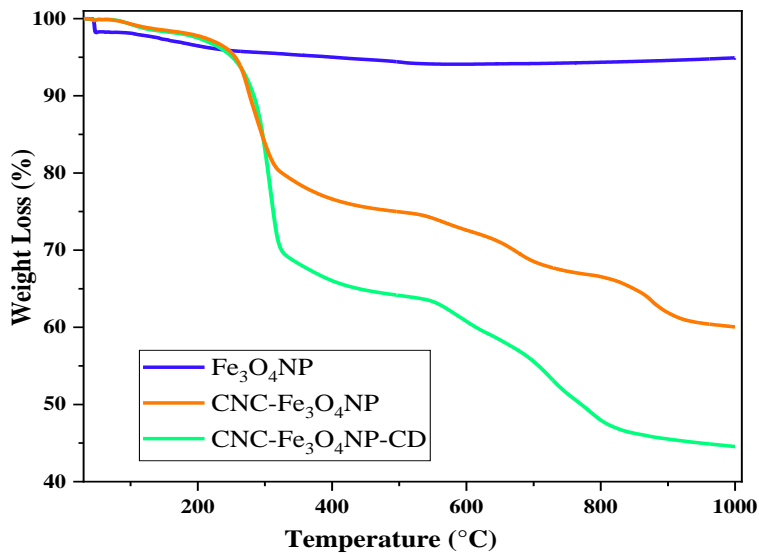
Table 4.3: Crystallinity indices of Fe₃O₄, CNC-Fe₃O₄NP, and CNC-Fe₃O₄NP-CD.

Sample	2θ (Amorphous) (°)		2θ (002) (°)		Crystallinity Index (CrI %)
	Degree	Intensity, I_{am}	Degree	Intensity, I_{002}	
Fe ₃ O ₄ NP	-	-	35.74	-	-
CNC-Fe ₃ O ₄ NP	20.04	34.63	35.59	154.95	77.65
CNC-Fe ₃ O ₄ NP-CD	22.39	39.61	35.70	253.40	84.37

4.2.7 Thermogravimetric Analysis (TGA)

The incorporation of Fe₃O₄NP into CNCs to form CNC-Fe₃O₄NP nanocomposite significantly alters the thermal degradation profile. The TGA thermogram and DTA curve of CNC-Fe₃O₄NP shows enhanced thermal stability as compared to that of pure CNCs Figure 4.13 a, b. The presence of Fe₃O₄NP contributed to the increased stability by

providing a thermal barrier and enhancing the structural integrity of the nanocomposite. From the TGA analysis of CNC-Fe₃O₄NP the first step, occurring between 50°C and 100°C, corresponded to the loss of adsorbed water and volatile substances, similar to pure CNCs, but the mass loss is slightly reduced due to the presence of Fe₃O₄NP. The second significant mass loss step, occurring between 250°C and 400°C, represents the degradation of the cellulose matrix. In CNC-Fe₃O₄NP, this step is shifted to higher temperatures, around 350°C, indicating improved thermal stability. The third step, occurring above 400°C, corresponds to the oxidation and decomposition of the iron oxide nanoparticles (Kumar et al., 2020).



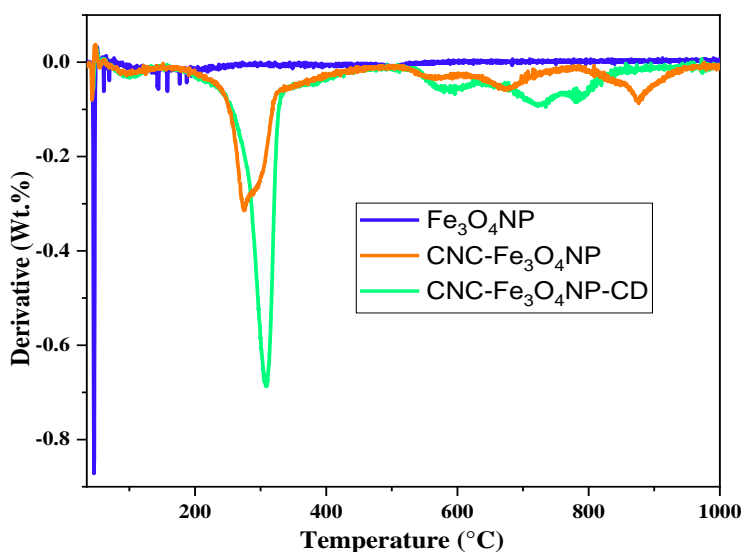


Figure 4.13: (a).TGA graph and (b). DTG curve for Fe_3O_4 , CNC- $\text{Fe}_3\text{O}_4\text{NP}$, and CNC- $\text{Fe}_3\text{O}_4\text{NP-CD}$

In terms of mass loss, CNC- $\text{Fe}_3\text{O}_4\text{NP}$ showed a reduced overall mass loss compared to pure CNCs. Typically, the total mass loss for CNC- $\text{Fe}_3\text{O}_4\text{NP}$ up to 500°C is around 50-60%, which is lower than the 60-70% observed for CNCs Figure 4.14 (a), (b). This reduction could be attributed to the thermal stability imparted by the $\text{Fe}_3\text{O}_4\text{NP}$. The DTG curve for CNC- $\text{Fe}_3\text{O}_4\text{NP}$ reveals a peak around 350°C , which is higher than the peak for CNCs, this confirms the enhanced thermal stability due to the incorporation of $\text{Fe}_3\text{O}_4\text{NP}$, Kumar et al. (2020) also reported similar observations.

The functionalization of CNC- $\text{Fe}_3\text{O}_4\text{NP}$ with β -cyclodextrin (CD) to form CNC- $\text{Fe}_3\text{O}_4\text{NP-CD}$ introduced additional complexity to the thermal degradation behavior. The TGA thermogram of CNC- $\text{Fe}_3\text{O}_4\text{NP-CD}$ reveals a slightly reduced thermal stability compared to CNC- $\text{Fe}_3\text{O}_4\text{NP}$ due to the presence of CD, which decomposes at lower temperatures. However, the nanocomposite still maintains considerable thermal stability, essential for practical applications. From the TGA analysis of CNC- $\text{Fe}_3\text{O}_4\text{NP-CD}$, it

shows three main degradation steps. The first step, occurring between 50°C and 100°C, corresponds to the loss of adsorbed water and volatile components, similar to CNC and CNC-Fe₃O₄NP. The mass loss in this step is slightly higher, around 10-15%, due to the presence of CD, which has a higher moisture content. The second step, occurring between 200°C and 350°C, corresponds to the decomposition of β-cyclodextrin and partial degradation of the cellulose matrix, similar observations were also reported by Hădărugă et al. (2006) and Trotta et al. (2000) in their respective studies. This step exhibited a significant mass loss, around 40-50%, due to the combined degradation of CD and cellulose. The third step, occurring between 350°C and 500°C, corresponds to the further degradation of the cellulose matrix and the oxidation of Fe₃O₄NP. The overall mass loss for CNC-Fe₃O₄NP-CD up to 500°C is around 60-70%, which is higher than CNC-Fe₃O₄NP but still lower than pure CNCs.

The DTG curve for CNC-Fe₃O₄NP-CD reveals two prominent peaks. The first peak occurs around 300°C, corresponding to the degradation of β-cyclodextrin, and the second peak occurs around 350°C, corresponding to the further degradation of the cellulose matrix and the oxidation of Fe₃O₄NP. The shift in the degradation peaks to lower temperatures compared to CNC-Fe₃O₄NP indicates the influence of CD on the thermal stability of the nanocomposite.

Addition of β-cyclodextrin to the nanocomposites resulted in a slight decrease in thermal stability due to the lower decomposition temperature of CD, Qin et al. (2024) also reported similar findings. The high thermal stability of CNC-Fe₃O₄NP and CNC-Fe₃O₄NP-CD ensures that these nanocomposites can withstand varying environmental conditions without significant degradation.

4.2.8 (Brunauer-Emmett-Teller (BET) Analysis

The BET (Brunauer-Emmett-Teller) analysis provides crucial insights into the surface area, pore volume, and pore diameter of Fe₃O₄NP, CNC-Fe₃O₄NP, and CNC-Fe₃O₄NP-CD nanocomposites (Table 4.4).

Table 4.4: BET Surface area and pore properties

Parameters	Adsorbents		
	Fe ₃ O ₄	CNC-Fe ₃ O ₄ NP	CNC-Fe ₃ O ₄ NP-CD
Surface area (m ² .g ⁻¹)	7.335	8.786	6.961
Pore volume (cm ³ .g ⁻¹)	0.0089	0.0037	0.0079
Average pore diameter (nm)	3.453	2.758	1.976

The BET surface area, a measure of the total available surface for adsorption, is directly related to the number of active sites available for interaction with pollutants. Fe₃O₄ nanoparticles (NPs) exhibit a surface area of 7.335 m²/g, indicating a significant number of active sites for adsorption. However, when these nanoparticles are incorporated into cellulose nanocrystals (CNCs) to form CNC-Fe₃O₄NP, the surface area slightly increases to 8.786 m²/g an indication that it offers more space for adsorption. Functionalization with β-cyclodextrin (CD) in CNC-Fe₃O₄NP-CD nanocomposites results in a slight decrease in surface area of 6.961 m²/g. However, the prepared nanocomposite CNC-Fe₃O₄NP-CD, had a higher pore volume (0.0079 cm³.g⁻¹) as compared to CNC-Fe₃O₄NP which had a pore volume of 0.0037 cm³.g⁻¹ an indication that CNC-Fe₃O₄NP-CD can hold more of the adsorbate. CNC-Fe₃O₄NP-CD also had the smallest pore diameter of 1.976nm as compared to both CNC-Fe₃O₄NP and Fe₃O₄ nanoparticles which had pore

diameters of 2.758nm and 3.453nm respectively. This characteristic might help CNC-Fe₃O₄NP-CD to adsorb even smaller adsorbate molecules.

4.2.9 Zeta Potential

Figure 4.14 shows the Zeta potential data for three adsorbents; Fe₃O₄NP, CNC-Fe₃O₄NP, and CNC-Fe₃O₄NP-CD across various pH levels. The zeta potential, a measure of surface charge, is crucial as it dictates the electrostatic interactions between adsorbent particles and charged contaminants (Gopmandal and Duval, 2022). In this study, lower pH levels exhibited positive zeta potentials for all three adsorbents, which promote the electrostatic attraction of the negatively charged Cr(VI) oxyanions (such as CrO₄²⁻). Typically, CNC-Fe₃O₄NP-CD showed a remarkably high positive zeta potential of 31 mV at pH 2, suggesting it may be particularly effective in acidic conditions due to strong electrostatic attractions, thereby enhancing Cr(VI) adsorption efficiency. As the pH increased, the zeta potential of all adsorbents decreased, eventually becoming negative, with CNC-Fe₃O₄NP-CD demonstrating the highest decline, reaching -32.79 mV at pH 12. This shift to negative values indicates potential electrostatic repulsion between the adsorbents and the Cr(VI) ions, reducing adsorption efficiency at higher pH levels. Moreover, a zeta potential near zero, observed around neutral pH for these adsorbents, could lead to particle aggregation, diminishing the available surface area for adsorption and further lowering the removal efficiency. Thus, the most effective Cr(VI) removal is expected at lower pH levels where the adsorbents are positively charged, with CNC-Fe₃O₄NP-CD being particularly promising due to its higher positive zeta potential, indicating better stability and less propensity for aggregation in acidic conditions.

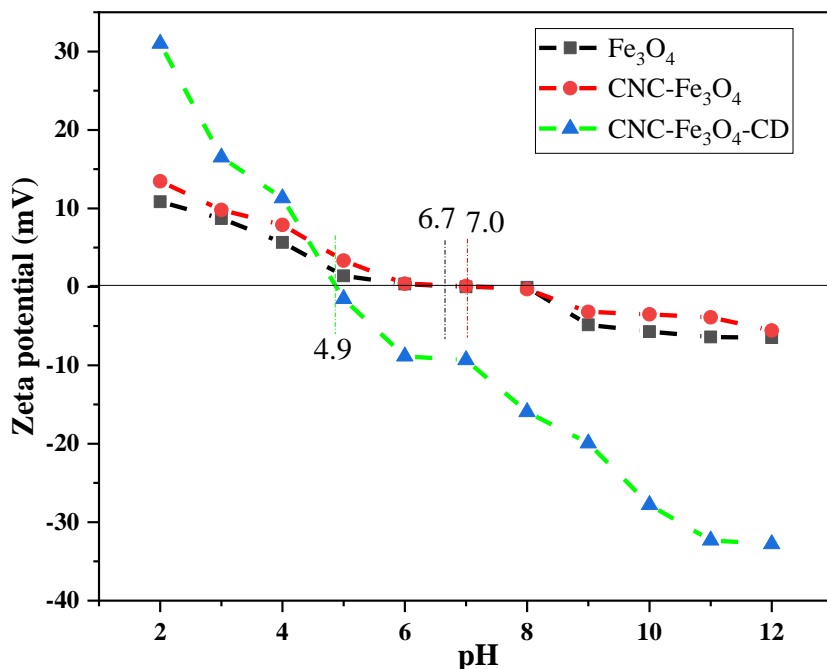


Figure 4.15: Zeta potential for for Fe₃O₄, CNC-Fe₃O₄NP, and CNC-Fe₃O₄NP-CD

4.3 Adsorption

4.3.1 Effect of pH on removal of Cr (VI) by CPC, CNC, CNC-Fe₃O₄NP and CNC-Fe₃O₄NP-CD

Figure 4.16 displays the removal efficiency of hexavalent chromium using CPC, CNC, CNC-Fe₃O₄NP and CNC-Fe₃O₄NP-CD adsorbents under various pH values. The effectiveness of adsorbents on the removal of Cr (VI) was investigated in solutions with pH values ranging from 1 to 12. The results indicate that the pH significantly influenced the adsorption capacity of these materials and the removal efficiency varied widely based on the nature of the adsorbent and the solution pH. The removal efficiency increased from pH 1 to 2 then decrease as the pH increased to 8 where the removal efficiency became constant for all the adsorbents. Contrary to the findings of this study, Rahaman

et.al. (2021) using modified cellulose and chitosan reported low adsorption of heavy metals at low pH which maximized at pH 4.

At pH 1, the removal efficiencies were 60.21% for CPC, 68.45% for CNC, 80.45% for CNC-Fe₃O₄NP, and 94.45% for CNC-Fe₃O₄NP-CD. The high removal efficiency at this low pH can be attributed to the protonation of the adsorbent surface, which increases the positive charge density on the surface (Yuan et al., 2023). This protonation enhances the electrostatic attraction between the negatively charged Cr(VI) species (HCrO₄⁻ and Cr₂O₇⁻) and the positively charged adsorbent surfaces, facilitating higher adsorption (Yuan et al., 2023) when using polypyrrole based adsorbents. The presence of iron oxide nanoparticles in CNC-Fe₃O₄NP enhances this effect due to their inherent magnetic properties and high surface area, which provides more active sites for adsorption (Wang et al., 2013). The incorporation of β-cyclodextrin in CNC-Fe₃O₄NP-CD improved the adsorption efficiency, likely due to the inclusion complex formation capability of β-cyclodextrin, which can encapsulate Cr(VI) ions, enhancing their removal from the aqueous solution.

At pH 2, the removal efficiency increased for all adsorbents, with CNC-Fe₃O₄NP-CD achieving the highest efficiency of 97.45%. The other adsorbents CNC-Fe₃O₄NP, CNC and CPC achieved removal efficiencies of 95.45%, 78.12% and 69.19% respectively. This increase can be explained by the optimal balance between the positively charged surface sites and the concentration of Cr(VI) species. This observation is in agreement with that made by Sun et. al. (2014) studying Cr(VI) removal using amino functionalized magnetic cellulose whereby they found the best adsorption pH for Cr(VI) to be 2. At this pH, the predominant species, HCrO₄⁻, are effectively attracted to the adsorbent surface

enhancing the removal of Cr(VI) from solution by CNC-Fe₃O₄NP and CNC-Fe₃O₄NP-CD as compared to CNC, this is thought to be due to the synergistic effects of magnetic nanoparticles and β -cyclodextrin, which increase surface area and provide additional binding mechanisms. At pH 2 the increased protonation on the adsorbent surface favors both electrostatic and ion exchange between the adsorbent and the adsorbate (Sun et.al., 2014).

As the pH increased from 3 to 4, a slight decrease in removal efficiency was observed across all adsorbents. This can be attributed to the decreasing availability of H⁺ ions, reducing the positive charge density on the adsorbent surfaces, thus decreasing the electrostatic attraction between Cr(VI) species and the adsorbents (Yuan et al., 2023). At pH 4, the removal efficiencies were 55.25%, 60.65%, 88.98%, and 90.12% for CPC, CNC, CNC-Fe₃O₄NP, and CNC-Fe₃O₄NP-CD, respectively. The drop in efficiency for CPC and CNC indicates their lower capacity for maintaining positive charge at this pH, compared to CNC-Fe₃O₄NP and CNC-Fe₃O₄NP-CD. The removal efficiency of CPC and CNC in this study was comparable to that found by Rahaman et.al. (2021) who achieved a removal efficiency of 56% of hexavalent chromium using modified cellulose.

At pH 5 to 8, the removal efficiencies continued to decline for all adsorbents. For instance, at pH 5, the efficiencies were 53.98%, 59.89%, 70.36%, and 88.24% for cellulose, CNC, CNC-Fe₃O₄NP, and CNC-Fe₃O₄NP-CD, respectively. This decline is more pronounced in the adsorbents CPC and CNC, indicating their lesser stability and lower availability of active sites at higher pH levels and it might also be due to the start of precipitation of metal ion as hydroxides or oxides as reported by Rahaman et al. (2021) in their study.

The removal efficiencies at pH 12 were 39.01%, 40.11%, 55.61% and 64.76% for CNC, CNC-Fe₃O₄NP, and CNC-Fe₃O₄NP-CD respectively. These adsorptions are far much less as compared to the lower pHs. This can be attributed to decreased protonation on the surface of the adsorbents leading to less electrostatic interaction and increased competition for active sites by OH⁻ and hexavalent chromium (Yuan et.al., 2023; Sun et.al. 2014). At pH 12 CNC-Fe₃O₄NP-CD had a high removal efficiency 64.76% as compared to CNC and CNC-Fe₃O₄NP, this can be attributed to the presence of β-cyclodextrin which enhances the adsorbent resistance to pH changes and complexation abilities of β-cyclodextrin which can still effectively attract Cr(VI) species even as the adsorbent surface charge becomes less positive Liu et. al. (2011), or even neutral or negative.

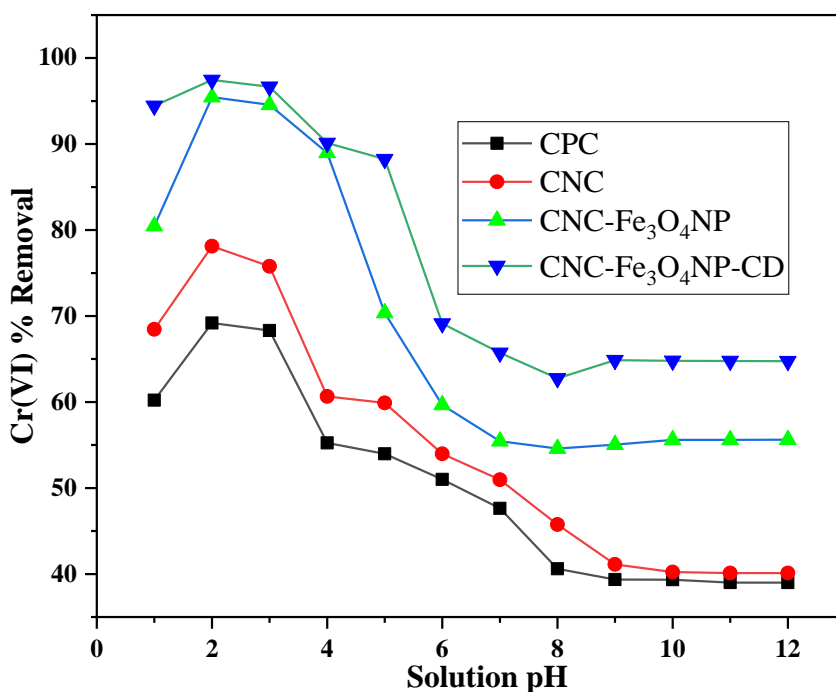


Figure 4.16: The effect of pH on the removal of hexavalent chromium using different adsorbents.

4.3.2 Adsorbent Dosage

The effect of adsorbent mass on the removal efficiency of Cr(VI) was evaluated by varying the mass of the adsorbents (CPC, CNC, CNC-Fe₃O₄NP, and CNC-Fe₃O₄NP-CD) from 0.2 g to 1.4 g, keeping all other parameters constant. The results indicated a general trend of increasing removal efficiency with an increase in adsorbent mass for all the adsorbents as shown in Figure 4.17.

At a lower adsorbent mass of 0.2 g, the removal efficiencies were relatively low across all adsorbents, with CPC showing a 16.45%, CNC at 18.43%, CNC-Fe₃O₄NP at 27.94%, and CNC-Fe₃O₄NP-CD had the highest removal at 35.67%. This trend can be attributed to the limited availability of active sites for adsorption as suggested by Rahaman et al. (2021) and the ease of saturation of these sites at lower adsorbent masses, which restricts the capacity to adsorb Cr(VI) ions from the solution (Qasem et al., 2021b). As the adsorbent mass increased from 0.4 g to 0.6 g, the percentage removal also increased where CNC-Fe₃O₄NP-CD showed a substantial increase in removal efficiency, from 49.7% to 68.45%, 38.10% to 50.65% for CNC-Fe₃O₄NP, 26.65% to 31.20% for CNC and 24.87% to 26.65% for CPC. This indicated that increase in adsorbent mass leads to an increase in the number of available adsorption sites, enhancing the adsorptive capacity as also observed by Syeda et al. (2022) in their study. Chakraborty et al. (2022) investigated modified agricultural waste for metal ion adsorption and they noted a significant surface area available, making the removal of metal ions rise as the adsorbent dosage increases (Chakraborty et al., 2022).

The presence of Fe₃O₄ nanoparticles and β-cyclodextrin in CNC-Fe₃O₄NP-CD likely provided additional surface area and functional groups, contributing to the higher adsorption efficiency compared to the other adsorbents. Similar suggestions were made by Vo et al. (2024) using chitosan-graphene oxide- magnetite nanocomposite for removal of Pb from water.

At 0.8 g, CNC-Fe₃O₄NP-CD achieved a removal efficiency of 97.98%, while CNC-Fe₃O₄NP also showed an increase, reaching 64.61%. This continued increase in efficiency with higher adsorbent mass suggests that, up to this point, the adsorption process is not limited by the availability of active sites (Vo et al., 2024 ;\\ Chakraborty et al., 2022).

CPC and CNC also showed pronounced improvements, with maximum removals of 37.87% and 40.19%, indicating fewer active sites and possibly lower surface area. When the adsorbent mass was further increased to 1.0 g, the maximum removal efficiencies were observed: 98.34% for CNC-Fe₃O₄NP-CD, 82.62% for CNC-Fe₃O₄NP, 40.44% for CNC, and 38.76% for cellulose. This trend indicates that, at this dosage, the adsorbents, particularly the CNC-Fe₃O₄NP and CNC-Fe₃O₄NP-CD, had sufficient active sites to adsorb nearly all available Cr(VI) ions in the solution. Similar observations that an increase in adsorbent dosage results in an increase in adsorption were made by Zaimie et al. (2021) and Chakraborty et al. (2022) in their study using different adsorbents.

Beyond 1.0 g, at 1.2 g and 1.4 g, the increase in removal efficiency plateaued, particularly for CNC-Fe₃O₄NP and CNC-Fe₃O₄NP-CD. The percentage removal for CNC-Fe₃O₄NP-CD slightly increased from 98.45% at 1.2 g to 98.61% at 1.4 g,

suggesting that the adsorption process reached equilibrium Akiode et al. (2023), where additional adsorbent mass did not significantly enhance the removal efficiency. This plateau indicates that at higher adsorbent dosages, most of the Cr(VI) ions were already adsorbed, and additional adsorbent did not lead to a proportional increase in adsorption due to the saturation of available active sites and more so due to possible repulsion resulting from the adsorbate crowding (Akiode et al., 2023).

The results demonstrate that CNC-Fe₃O₄NP-CD is the most effective adsorbent among the tested materials, having achieved the highest removal efficiency across all dosages. This superior performance is likely due to the enhanced surface area, magnetic properties, and the presence of β -cyclodextrin, which offers additional mechanisms for Cr(VI) ion binding. The functionalization of CNC with Fe₃O₄ nanoparticles and β -cyclodextrin not only increases the number of adsorption sites but also improves the dispersibility and accessibility of these sites Akiode et al. (2023), facilitating efficient adsorption.

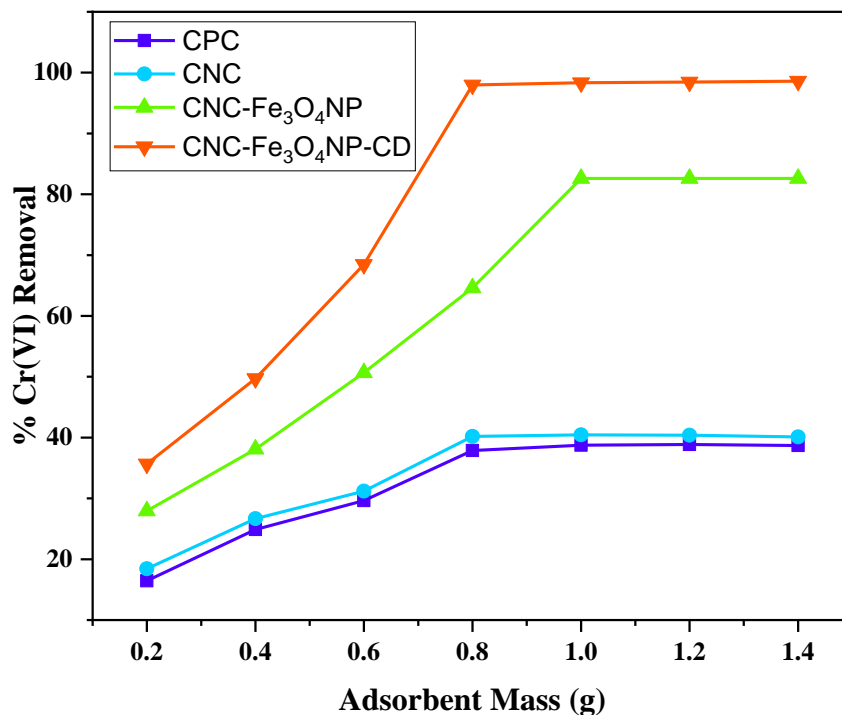


Figure 4.17: The influence of adsorbent mass on the removal of hexavalent chromium.

4.3.3 Varying Pollutant Concentration

The effect of adsorbate concentration on the removal efficiency of Cr(VI) was investigated by varying the initial concentration of Cr(VI) in the mimicked wastewater, using the adsorbents cellulose, CNC, CNC-Fe₃O₄NP, and CNC-Fe₃O₄NP-CD (Figure 4.18). The concentrations evaluated ranged from 10 mg/L to 60 mg/L.

From the findings, the removal efficiency varied significantly depending on both the type of adsorbent and the initial concentration of Cr(VI). At the lowest concentration of 10 mg/L, the removal efficiencies were highest across all adsorbents. CNC-Fe₃O₄NP and CNC-Fe₃O₄NP-CD demonstrated exceptional removal capabilities, achieving 97.21% and 97.31% respectively. The high efficiency at low concentration can be attributed to the availability of abundant active sites relative to the number of Cr(VI) ions present

Chakraborty et al. (2022) and this ensured that a large proportion of the ions are adsorbed. CPC and CNC, on the other hand, showed lower efficiencies, 40.98% and 43.69%, respectively, indicating fewer active sites and potentially lower affinity for Cr(VI) ions compared to the functionalized nanocomposites which is in agreement with the observations reported by Syeda et al. (2022) in their study.

As the concentration increased to 20 mg/L, a notable decrease in removal efficiency was observed across all adsorbents. CNC-Fe₃O₄NP-CD still maintained a relatively high removal efficiency of 87.56%, while CNC-Fe₃O₄NP showed 84.67% removal. The decline in efficiency is likely due to the saturation of active sites, as the number of Cr(VI) ions in solution begins to exceed the available adsorption sites (Syeda et al. 2022). This is a common trend where, at higher concentrations, the adsorbent's capacity to adsorb ions reduced because the active sites become fully occupied. The efficiency of CPC and CNC further decreased from 40.98% to 36.21% and from 43.69% to 36.78%, respectively, highlighting their limited capacity compared to the modified composites.

At an initial Cr(VI) concentration of 30 mg/L, the removal efficiencies continued to decline further. CNC-Fe₃O₄NP and CNC-Fe₃O₄NP-CD removed 80.57% and 83.54% of Cr(VI), respectively. This slight drop compared to the 20 mg/L concentration indicates that the active sites are approaching full occupancy, and the competition for these sites becomes more intense as similarly suggested by Alrowais et al. (2024) using activated carbon for adsorption. Further increases in Cr(VI) concentration to 40 mg/L and beyond resulted in more pronounced decline in removal efficiency. The removal efficiency dropped for CNC-Fe₃O₄NP (60.19%) and CNC-Fe₃O₄NP-CD (60.95%), this high reduction highlights the limitation in the number of adsorption sites available, as the

system reaches a saturation point where additional Cr(VI) ions cannot be effectively adsorbed, this observation is agreement with that of Tee et al. (2022) using magnetic biosorbent to remove pollutants from aqueous media. At the highest tested concentration of 60 mg/L, the removal efficiencies of CNC-Fe₃O₄NP and CNC-Fe₃O₄NP-CD were 60.32% and 61.53% respectively, which was almost identical to that of 40mg/L. This suggests that both materials reached a near-saturation point where their adsorption capacities were fully utilized, and no further significant adsorption could occur despite the increased availability of Cr(VI) ions, this was also suggested by Yuan and Lu (2024) in their study adsorption study. In contrast, CPC and CNC maintained removal efficiencies close to 40%, indicating a stable but low performance across the concentration range.

The results indicate that CNC-Fe₃O₄NP-CD consistently outperformed the other adsorbents, particularly at lower concentrations, due to its enhanced surface area, higher number of active sites, and improved dispersibility provided by the incorporation of Fe₃O₄ nanoparticles and β -cyclodextrin (Kauli et. al., 2020). The decline in removal efficiency with increasing concentration highlights the challenge of maintaining high adsorption efficiency as the pollutant load increases, which is critical for practical applications in wastewater treatment. This scineraio was also observed by Obayomi et al. (2020) who evaluated the statistical analyses on effective removal of cadmium and hexavalent chromium ions by multiwall carbon nanotubes (MWCNTs).

These findings suggest that while functionalized cellulose nanocomposites like CNC-Fe₃O₄NP and CNC-Fe₃O₄NP-CD are highly effective at lower concentrations, their efficiency reduces at higher concentrations due to site saturation. Therefore, optimizing

adsorbent dosage and regeneration strategies becomes crucial for maintaining efficiency in real-world applications, where pollutant concentrations can vary widely (Mudhoo et al., 2021).

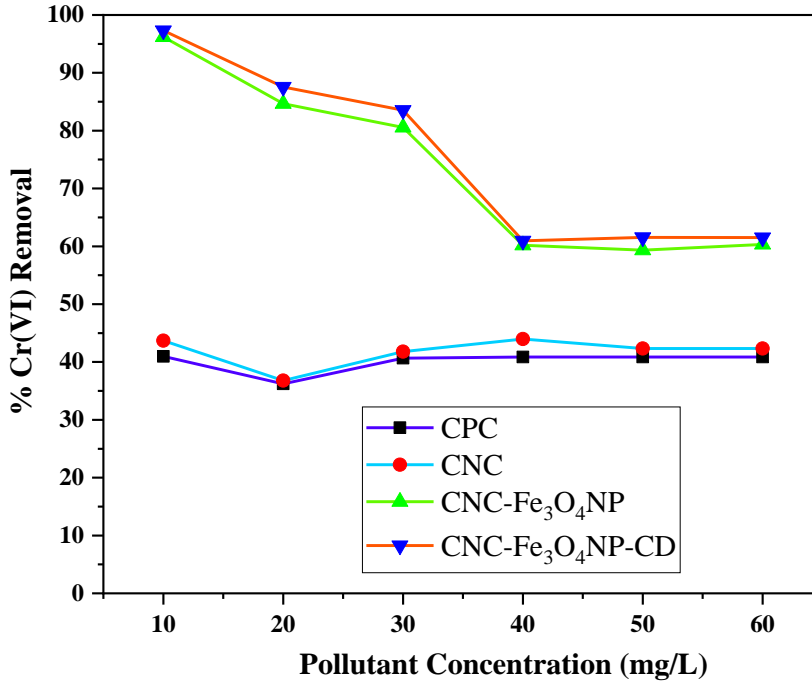


Figure 4.18: The influence of Cr(VI) concentration using different adsorbents.

4.3.4 Varying Adsorption Time

The effect of contact time on the adsorption of Cr(VI) using cellulose, CNC, CNC-Fe₃O₄NP, and CNC-Fe₃O₄NP-CD was evaluated, and the results show a significant variation in removal efficiency over time for each adsorbent. The percentage removal of Cr(VI) was measured at various time intervals ranging from 1 to 35 minutes Figure 4.19.

Within the first minute, a slight adsorption was observed across all adsorbents, with CNC-Fe₃O₄NP-CD demonstrating the highest removal efficiency (10.56%), followed closely by CNC-Fe₃O₄NP (10.23%). CNC and CPC showed lower efficiencies, with 6.7% and 2% removal, respectively. This rapid initial adsorption can be attributed to the

availability of abundant active sites on the adsorbents surfaces, which readily adsorb the Cr(VI) ions. A similar case was reported by Yuan and Lu (2024) who investigated the adsorption of Cr (VI) from aqueous solutions using inorganic clays modified magnetic chitosan adsorbent.

As contact time increased to 5 minutes, the removal efficiencies significantly improved. CNC-Fe₃O₄NP-CD achieved a 40.56% removal, indicating its superior adsorption capacity due to the presence of Fe₃O₄ nanoparticles and β-cyclodextrin, which enhance the surface area and active site availability. CNC-Fe₃O₄NP followed with 31.98% removal, while CNC and CPC showed lesser efficiency, with 17.99% and 15% removal, respectively. The increase in adsorption is probably due to the diffusion of Cr(VI) ions into the interior active sites of the adsorbents as more contact time allows for greater interaction as also suggested by Masuku et al. (2024) using pinecone biochar to adsorb hexavalent chromium.

At the 10-minute mark, CNC-Fe₃O₄NP-CD continued to demonstrate the highest removal efficiency at 60.89%, followed by CNC-Fe₃O₄NP at 50.56%. The removal efficiency of CNC reached 20.55%, while CPC achieved 18%. This period marked a significant increase in removal for the composite adsorbents, suggesting that the adsorption process was still progressing toward equilibrium as earlier reported by Villabona et al. (2022) in their study. Between 15 to 20 minutes, the adsorption efficiency further increased, with CNC-Fe₃O₄NP-CD reaching 69.87% and 89.23% at the respective time points. CNC-Fe₃O₄NP also showed substantial improvement, reaching 60.65% and 70.56% at 15 and 20 minutes respectively. CNC and CPC, however, showed a more gradual increase, reaching 30.67% and 35.44% respectively at 20 minutes. The increase in removal

efficiency for CNC-Fe₃O₄NP-CD and CNC-Fe₃O₄NP during this period indicates a high availability of more adsorption sites and efficient ion binding facilitated by the functional groups on the composites as confirmed by the FTIR results. Yang et al. (2019) also reported that surface functional groups of carbon-based adsorbents improves the removal of heavy metals from aqueous solutions.

At 25 minutes, CNC-Fe₃O₄NP-CD achieved a high removal efficiency of 92.56%, while CNC-Fe₃O₄NP reached 78.56%, The removal efficiency of CNC and CPC, however, remained lower, at 36.98% and 23.45%, respectively. This suggests that the maximum adsorption capacity of CNC-Fe₃O₄NP-CD and CNC-Fe₃O₄NP was being approached, as indicated by the smaller increases in percentage removal compared to earlier time intervals. By the 30-minute mark, the removal efficiencies plateaued, with CNC-Fe₃O₄NP-CD reaching 93.01% and CNC-Fe₃O₄NP achieving 78.88%. CNC and CPC showed negligible increases in removal efficiency, suggesting that equilibrium had been nearly reached. At 35 minutes, CNC-Fe₃O₄NP-CD and CNC-Fe₃O₄NP maintained high removal efficiencies at 93.2% and 78.95%, respectively, while CNC and CPC displayed stable, lower removal efficiencies of 36.76% and 21.84% this probably due to active sites of the adsorbent being almost saturated hence additional time did not give a significant difference. The results indicate that the composite adsorbents, particularly CNC-Fe₃O₄NP-CD, exhibited rapid initial adsorption followed by a gradual approach to equilibrium, demonstrating high removal efficiency within a short period. The superior performance of CNC-Fe₃O₄NP-CD can be attributed to the enhanced surface area and functional group availability, providing more active sites for Cr(VI) adsorption as suggested by Lim et al. (2019), who reported that composites mineral adsorbents

perform efficiently and reaches equilibrium faster in the removal of metal ions from polluted water.

These findings suggest that the contact time significantly influences the adsorption efficiency, with optimal adsorption occurring within the first 25 minutes for CNC-Fe₃O₄NP-CD, CNC-Fe₃O₄NP, CNC and CPC which is comparable to that of Yuan et al. (2024) who reported an optimal removal within the first 30 minutes using magnetic chitosan to remove hexavalent chromium. Villabona et al. (2022), reported a maximum removal of pollutants at 120 minutes using modified cellulose. For practical applications, this implies that using CNC-Fe₃O₄NP-CD can achieve efficient removal of Cr(VI) in a relatively short contact time, making it an effective adsorbent for rapid water treatment processes.

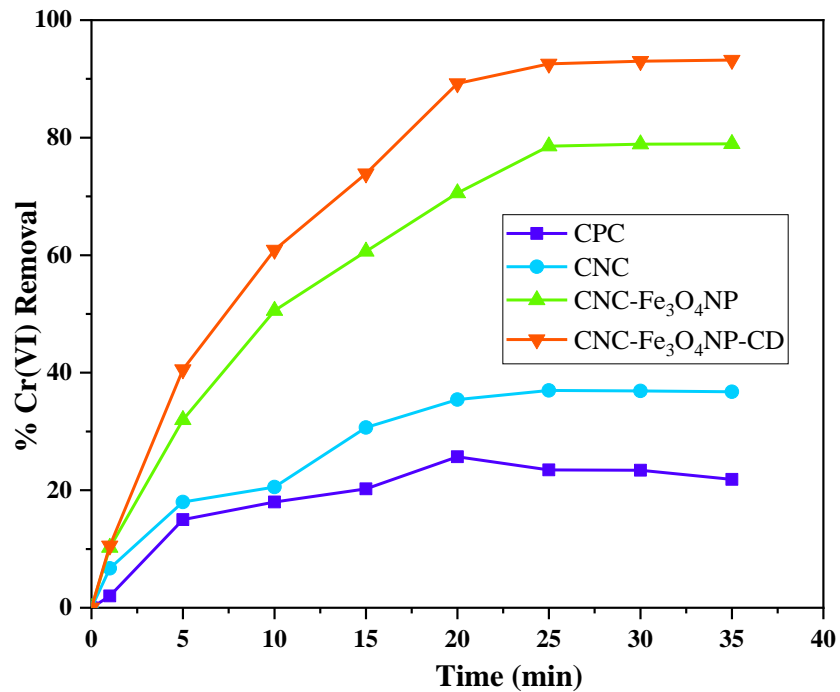


Figure 4.19: The influence of contact time on the removal of hexavalent chromium using different adsorbents

4.3.5 The effect of Varying Adsorption Temperatures

The effect of varying temperature on the removal efficiency of the CNC-Fe₃O₄NP-CD, CNC-Fe₃O₄NP, CNC and CPC adsorbents for Cr(VI) adsorption were evaluated and the findings presented in Figure 4.20. The temperatures investigated ranged from 298 K to 318 K. The results demonstrate a clear trend where the efficiency of the adsorbents in this study slightly decreased with increasing temperature.

The removal percentage for CNC-Fe₃O₄NP-CD was 97.33% at 298 K and 96.76% at 303 K, respectively. The removal efficiency decreased with increasing temperature, reaching 93.86% at 308 K, 92.26% at 313 K, and 89.36% at 318 K. Similarly, the percentage removal of hexavalent chromium using CNC-Fe₃O₄NP were 91.45%, 89.89%, 86.30%, 84.21% and 83.10% at 298K, 303K, 308K, 313K and 318K respectively. A similar trend was observed with CNC and CPC where the percentage removal were 60.13% and 55.44% respectively at 298K, which further decreased to 57.22% and 53.25% at 303K. As the temperature further increased to 308K, the percentage removal decreased to 55.65% for CNC and 51.12% for CPC. This pattern indicates that the adsorption process is exothermic, as rising temperatures have a significant effect on the capacity for adsorption as earlier suggested by Budnyak et al. (2020); Dabizha and Kersten, 2020 and Hu et.al. (2011) in their studies of adsorption of hexavalent chromium using different adsorbents.

The weakening of the adsorptive interactions between Cr(VI) ions and the active sites of the nanocomposite could be attributed to the reduction in removal effectiveness with increasing temperatures. Adsorption effectiveness is decreased by higher temperatures

because the molecules have greater kinetic energy to resist the adsorptive forces as suggested by Mabungela et al. (2022) and also as the kinetic energy of ions increases, the oscillating radii become large hence repelling ions in solution this finding is consistent with the research done by Keke et al. (2021) that used chitosan and activated carbon-based adsorbents and found that temperature had a detrimental effect on adsorption. Leyva-Ramos et al. (2008) and Pakade et al. (2019) reported that higher temperatures may encourage the desorption of Cr(VI) ions that have already been adsorbed, reducing efficiency even further.

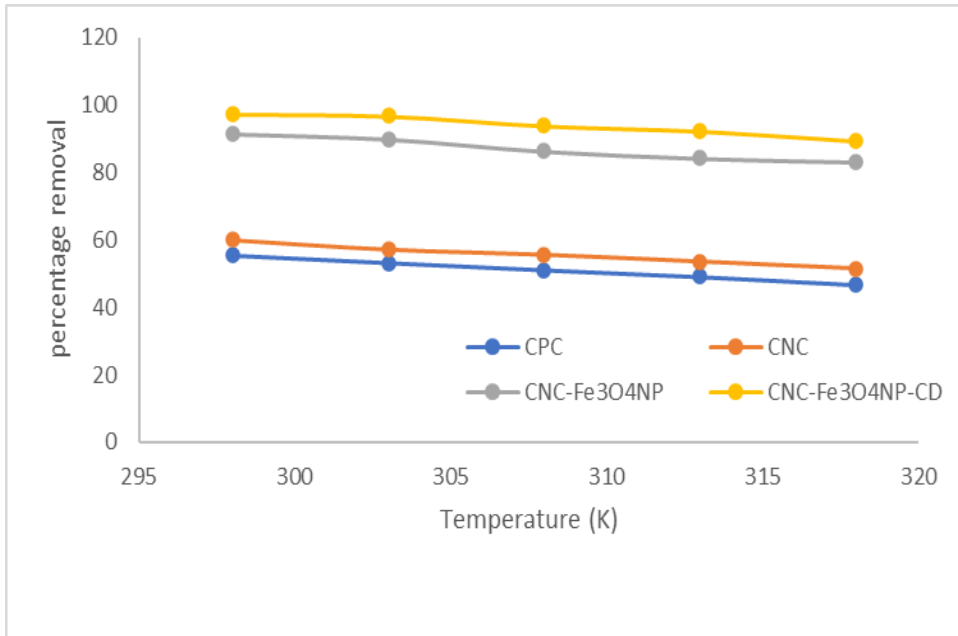


Figure 4.20: The influence of temperature on the removal of hexavalent chromium using different adsorbents

4.4 Comparative Study on the Adsorbents

The effectiveness of CPC, CNC, Fe₃O₄NP, CNC-Fe₃O₄NP, and CNC-Fe₃O₄NP-CD adsorbents towards the removal of hexavalent chromium (Cr(VI)) from mimicked waste water was assessed under a range of experimental conditions, including temperature, pH, adsorbent dose, pollutant concentration, and contact time (Figure 4.21). The results consistently demonstrated the superior performance of CNC-Fe₃O₄NP-CD, particularly at low pH levels, which is critical for efficient Cr(VI) removal due to the positive charge on the adsorbent surface that enhances electrostatic attraction with negatively charged Cr(VI) species. The incorporation of Fe₃O₄ nanoparticles and β-cyclodextrin in CNC-Fe₃O₄NP-CD not only increased the surface area and provided additional active sites for adsorption but also enhanced the material's stability and dispersibility, leading to higher removal efficiencies compared to the other adsorbents.

In terms of adsorbent dosage, CNC-Fe₃O₄NP-CD achieved nearly complete removal at lower masses, indicating a higher number of accessible active sites and efficient binding mechanisms, which were further supported by the functional groups present as evidenced by FTIR analysis. At varying initial Cr(VI) concentrations, CNC-Fe₃O₄NP-CD maintained high removal efficiencies, particularly at lower concentrations, demonstrating its capacity to effectively adsorb Cr(VI) even as the pollutant load increases. The study also highlighted the rapid adsorption kinetics of CNC-Fe₃O₄NP-CD, reaching equilibrium quickly, which is advantageous for practical water treatment applications where time efficiency is crucial.

Furthermore, the adsorption capacity of CNC-Fe₃O₄NP-CD decreased with increase in temperature, suggesting an exothermic adsorption. This thermodynamic favorability

makes CNC-Fe₃O₄NP-CD an excellent candidate for adsorption studies even at room temperature.

Given these findings, CNC-Fe₃O₄NP-CD stands out as the most effective adsorbent for Cr(VI) removal, offering high efficiency, rapid kinetics, and stability across various conditions. Its unique composition, combining the benefits of cellulose nanocrystals, Fe₃O₄NP nanoparticles, and β-cyclodextrin, provides multiple interaction mechanisms, making it ideal for equilibrium and thermodynamic studies. CNC-Fe₃O₄NP-CD was therefore, chosen for isotherms, kinetics and thermodynamic studies. This adsorbent efficiency was also compared with other adsorbents from other works of hexavalent chromium removal. The comparison is tabulated in table 4.9

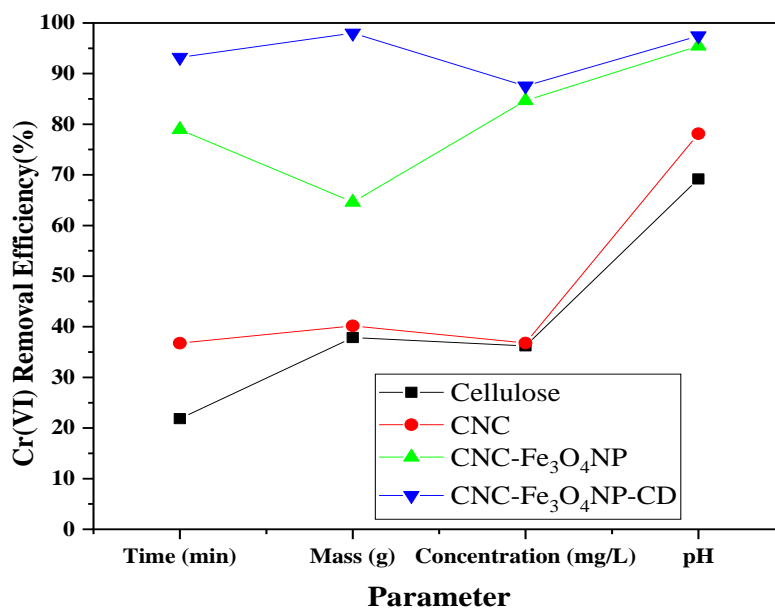


Figure 4.21: Comparative study of the adsorbents at pH 2, Cr(VI) 20 mg/L, adsorbent mass of 1g, Contact time of 35 minutes at room temperature.

Table: 4.9 Comparison of Several materials and methods related to the adsorption of Cr(VI)

Adsorbent	% Removal Efficiency	Reference
CNC-Fe₃O₄NP-CD	97.45%	Current work
Polypyrrole magnetic nanocomposite	99.2%	(Aigbe et al., 2018)
Sodium carboxymethyl cellulose stabilized zerovalent iron nanoparticles	88.5%	(Yu et al., 2020)
Iron Oxide Particles	82%	(Kitkaew et al., 2018)
Cellulose Nanocrystal–Magnetic Iron Oxide Nanocomposite	91.78%	(Suter et al., 2024)
Cellulose biochar supported iron nanoparticles	97.23%	(Ali et al., 2017)
Chitosan-coated superparamagnetic iron oxide nanoparticles	>92%	(Samrot et al., 2018)
Stabilized iron sulfide nanoparticles	82.23%	(Wang et al., 2019)
Bio-based iron oxide nanoparticles	98.71%	(Jawed et al., 2024)
Carboxymethyl Cellulose–Stabilized Sulfidated Nano Zerovalent Iron	85.08%	(Zhao et al., 2019)

As shown in Table 4.9 above, CNC-Fe₃O₄NP-CD showed comparable removal percentage to both cellulose biochar and Bio-based iron oxide nanoparticles which had 97.23% and 98.71% (Jawed et al., 2024 ; Ali et al., 2017) . It however outdid many other adsorbents like Carboxymethyl Cellulose–Stabilized Sulfidated Nano Zerovalent Iron (85.08%) and stabilized iron sulfide nanoparticles (82.23%) as shown in table 4.9. Polypyrrole magnetic nanocomposite on the other had was reported to have 99.2% removal which is higher than the removal percentage of the current study (Aigbe et al., 2018).

4.5 Kinetics studies of adsorption

4.5.1 Pseudo-first-order kinetic models

To investigate the kinetic behavior and mechanism of Cr(VI) on the CNC-Fe₃O₄NP-CD nanocomposite adsorbent, the linear regression coefficient (R^2) was used to demonstrate the applicability of the pseudo-first-order kinetic model across several experimental data sets. The study findings are provided in Figure 4.22 and Table 4.5.

The results gave linear regression coefficients (R^2) ranging from 0.555 to 0.94783. This indicates that the model was fairly appropriate given the current adsorption system on the CNC-Fe₃O₄NP-CD nanocomposite adsorbent. Low values of (q_{cal}) was obtained due to low linear regression coefficient (R^2) further confirm the model less applicability. The less applicability of this model to fit in the PFO was also reported by Sun et. al. (2014) and Chen et. al. (2011) working on different adsorbent for Cr(VI) removal.

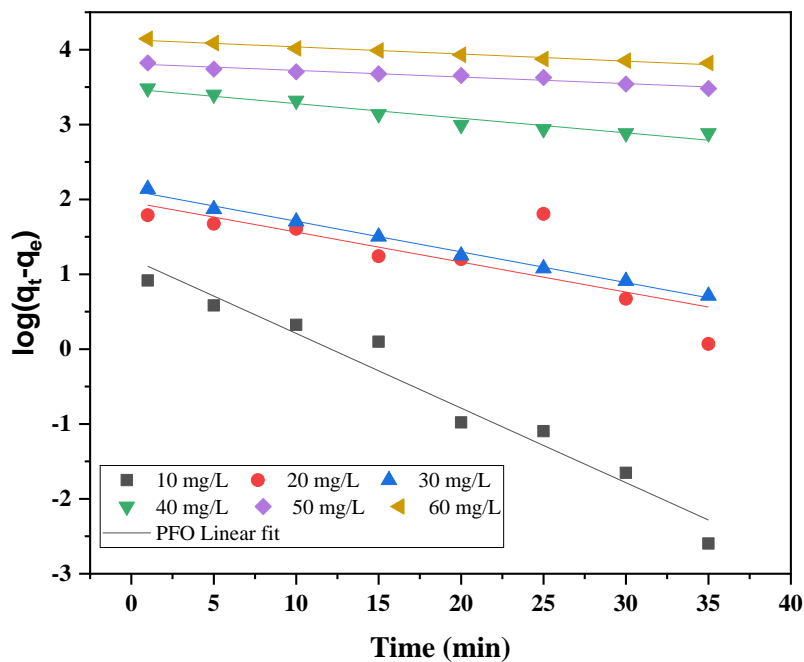


Figure 4.22: Pseudo-first-order kinetic model linear fit

4.5.2 Pseudo-second-order kinetic model

The findings on the applicability of the pseudo-second-order kinetic model for the study are presented in Figure 4.23 and Table 4.5. Through the use of the linear regression coefficient (R^2) and the applicability of the kinetic model on the batch adsorption experimental data was evaluated. The experimental data under various physio-chemical conditions conform well to the second-order kinetic linear model. The model displayed high linear regression coefficient values ($R^2 > 0.98$). Application of the PSO model demonstrates that electron sharing between the solute and adsorbent occurred (Sun et al., 2014). Furthermore, because there was less competition between the metal ions and the adsorption site at the higher initial concentration, lower values of the second-order kinetic constant K_2 were obtained. Numerous studies on the removal of heavy metals, including zinc (Zn^{2+}), copper (Cu^{2+}), and nickel (Ni^{2+}), demonstrated that these systems also followed pseudo-second-order kinetics (Biswas et al., 2019 and Singh & Mishra, 2021). These results further imply that regulating the metal ion adsorption on the CNC- Fe_3O_4 NP-CD nanocomposite adsorbent is governed by a single-step process and entails several steps as also suggested by Salehi et al. (2021) in their study.

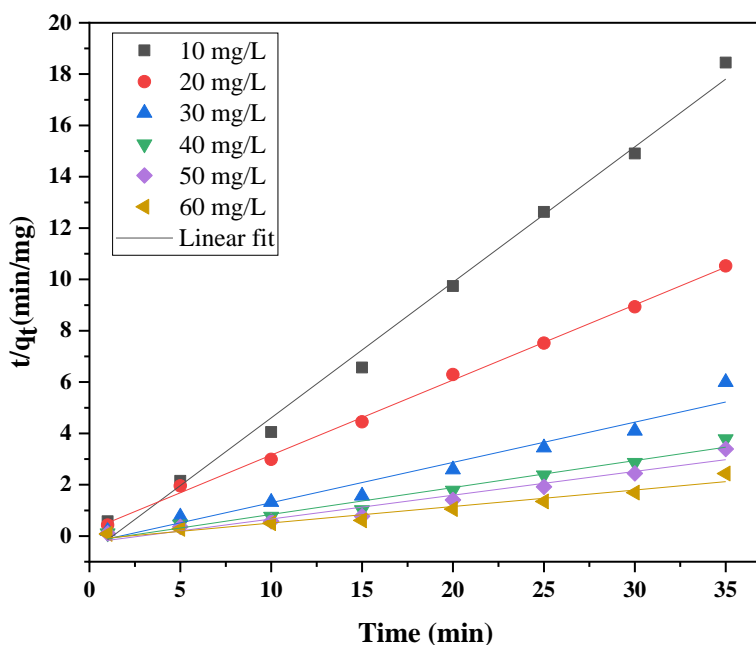


Figure 4.23: Pseudo-second-order kinetic model linear fit

4.5.3 Elovich model

The kinetics of chemisorption on heterogeneous adsorbents were quantified using the Elovich model. The model predicts the existence of heterogeneous active surface sites with various activation energies (Wang & Guo, 2023). Figure 4.24 and Table 4.5 illustrate how the model linear fit to the experimental data allowed for the derivation of the Elovich constants and linear correlation coefficient. According to the Elovich model adsorbent coefficient of determination, sorption onto the nanocomposite adsorbent was chemically guided ($R^2 > 0.93$). The CNC-Fe₃O₄NP-CD nanocomposite adsorbent effectively adsorbed the metal ion because the initial sorption rates exceeded the corresponding desorption constants as also found by Chaudhary et al. (2019) in their study. In the Elovich model, active surface sites are assumed to be heterogeneous and to have a range of activation energies. The linear model fit to the experimental data (Table

4.5) was used to determine the Elovich constants. The adsorbent utilized had initial sorption rate alpha that were greater than the desorption constant beta, proving that they were all suitable for the adsorption of metal ions, similar results were reported by Rani et al. (2022) in their kinetics studies.

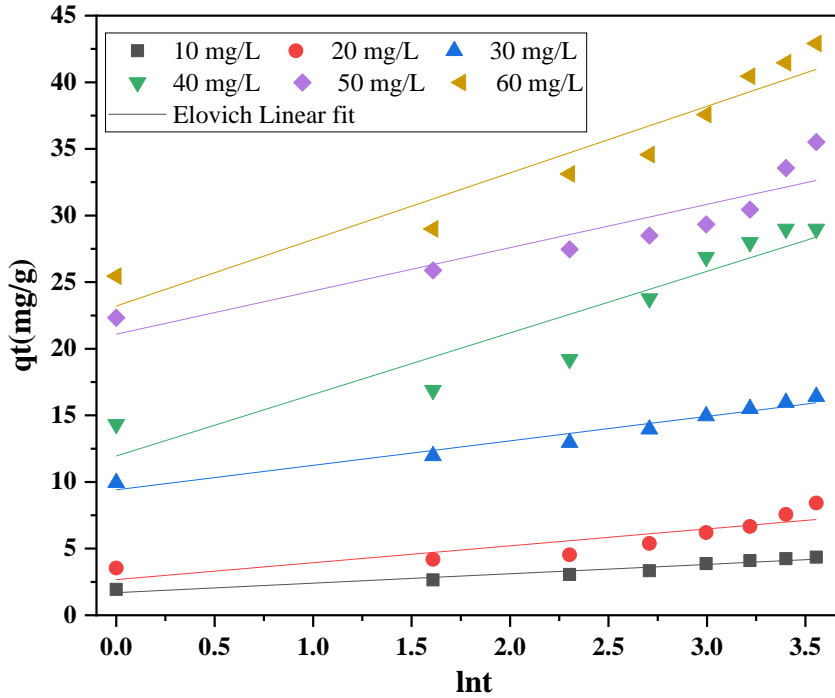


Figure 4.24: Elovich kinetic model linear fit

4.5.4 Intra-particle diffusion model

The intraparticle diffusion model, sometimes referred to as the Webber-Morris model, is crucial for understanding the behavior of any adsorption process (Biswas et al., 2019). Understanding the adsorption mechanism and how it underlies the system apparent dynamic behavior is crucial for designing and controlling any large-scale adsorption system. According to the results of this study, as shown in Figure 4.25 and Table 4.5, the Cr^{6+} ions adsorb pretty quickly at first before slowing down. The rate-limiting step is

frequently predicted using this model for an adsorption system involving porous materials. The model states that an entire system is controlled by intraparticle diffusion when the plot between q_t and $t^{0.5}$ results in a straight line that goes through the origin. However, the plot in this study did not result in a single straight line passing through the origin. As a result of the observation, the adsorption mechanisms can be listed as metal ion transport from the bulk solution to the adsorbent surface, diffusion across the adsorbent surface boundary layer, adsorption on the adsorbent surface active site and through intra-particle diffusion into the adsorbent pores. Pholosi et al. (2020) suggested that the slowest step, external film diffusion, or pore diffusion, regulates the total adsorption rate. Even the rate-controlling step itself might be split into two. External film diffusion can heavily influence adsorption.

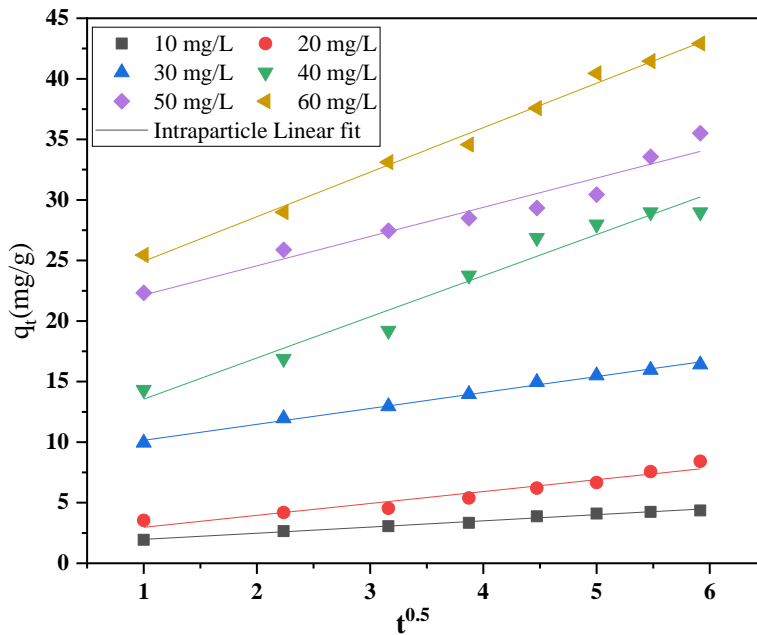


Figure 4.25: Intraparticle diffusion kinetic model linear fit

Table 4.5: Summary of kinetic model parameters

Kinetic model/ Adsorbate	Parameters				
	10 mg/L	20 mg/L	30 mg/L	40 mg/L	60 mg/L
<i>Pseudo-first kinetic model</i>					
q _e (exp)(mg/g)	4.361	8.426	16.412	28.983	35.509
q _e (model) (mg/g)	4.234	7.897	15.028	27.671	34.280
k ₁ (mg/g)	0.00814	0.01284	0.00127	0.00196	0.01205
R ²	0.91513	0.55538	0.93332	0.9333	0.94783
<i>Pseudo second kinetic model</i>					
q _e (model) (mg/g)	4.154	7.3043	15.419	26.881	34.114
K ₂ (g/mg.min)	0.52803	0.29292	0.15689	0.10498	0.09251
R ²	0.9925	0.99747	0.98417	0.99781	0.98051
<i>Elovich kinetic model</i>					
β(mg/g)	0.07228	0.27979	0.1101	0.15705	0.69519
α(mg/g.min)	0.19591	0.75835	0.42567	1.88423	1.52761
R ²	0.93083	0.9362	0.95093	0.96044	0.93083
<i>Intraparticle kinetic model</i>					
K _{id} (mg/g.min ^{0.5})	0.50892	0.98097	0.5805	1.3161	3.39731
C	1.46329	1.99285	8.83463	10.15689	19.73795
R ²	0.98776	0.92505	0.99342	0.95541	0.98776

4.6 Equilibrium isotherms

4.6.1 Langmuir isotherm model

The model assumes that all active sites in this model limiting reaction step have the same adsorption activation energy, and it is a surface reaction equivalent to a heterogeneous catalytic reaction. Additionally, the model assumes that there will not be any interaction

between the metal ions and previously adsorbed molecules. The Langmuir isotherm model plot (C_e vs. C_e/q_e) produced a straight line from the experimental fitting of the batch adsorption investigation, as shown in Figure 4.26. According to the graphical plots, the Langmuir model better matches the experimental data with ($R^2 > 0.99$) as shown in Table 4.6, indicating that the monolayer adsorption proceeds on a homogeneous adsorbent surface.

The dimensionless separation factor R_L was further determined to further understand the adsorption process favorability. The separation factor for the dimensionless parameter may be computed as given in equation 4.1 below.

$$R_L = \frac{1}{(1 + K_L C_o)} \quad (4.1)$$

where C_o is the initial metal ion concentration (mg/L) and K_L is the Langmuir constant (L/mg). If ($R_L > 1$ or $R_L = 1$), then the system is unfavorable; the system is favorable if ($0 < R_L < 1$); however, if the system is linear, $R_L = 1$, and when $R_L = 0$, the system is irreversible.

According to the results presented in Table 4.6, the separation constant for the adsorbate adsorbent system examined in this study was within the expected range ($0 < R_L < 1$), thus confirming that the adsorption process was favorable (Sun et al., 2014; Mishra et al., 2021).

Table 4.6: R_L Values for isotherm systems

Metal ions	R_L values				
	298 K	303K	308K	313K	318K
Cr^{6+}	0.9359	0.9521	0.9484	0.9402	0.9453

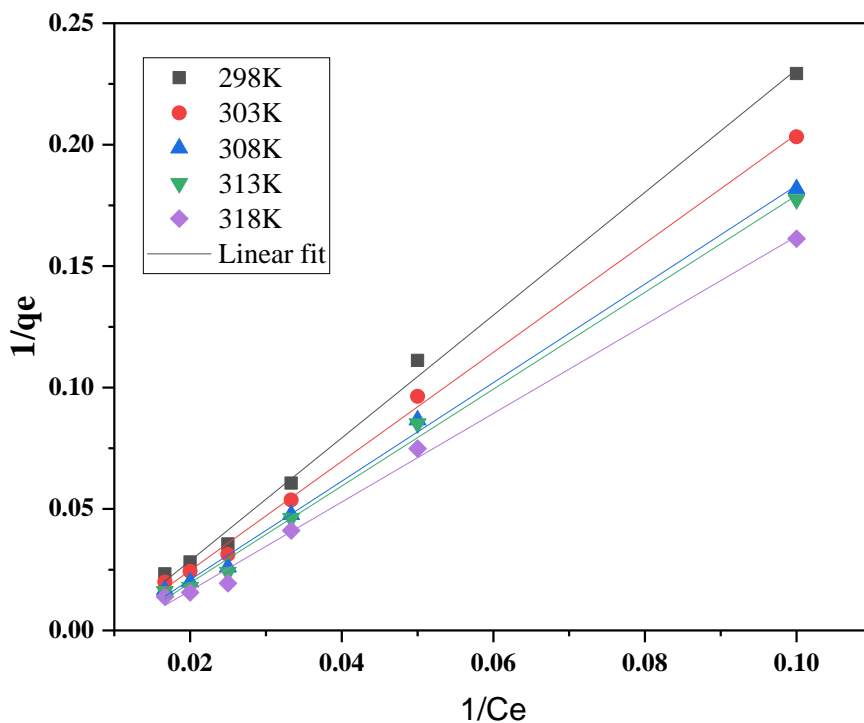


Figure 4.26: Langmuir linear fit isotherm models

4.6.2 Freundlich isotherm model

According to the Freundlich isotherm model, multilayer adsorption occurs on the adsorbent heterogeneous surface. The model also predicts that as adsorbate concentration increases, so does the absorbed quantity. The Freundlich isotherms linear fit plot of ($\ln q_e$ vs. $\ln C_e$) produced a straight line Figure 4.27. The graphical representation demonstrates that the Freundlich model for the metal ion has a linear regression value ($R^2 > 0.97$), as given in Table 4.7. It was assumed that the multilayer adsorption process occurred on the nanocomposite adsorbent because of the relatively large regression coefficient. The adsorption process on the nanocomposite adsorbent is believed to be effective if the Freundlich constant value is between 1 and 10. According to the analysis of experimental

data obtained under various experimental conditions, the Freundlich constants for the metal ion on the nanocomposite adsorbent ranged from 1.132 to 1.657, which is within an acceptable range and suggests that the adsorption process was effective, thus making the nanocomposite adsorbent a good choice for the adsorption of Cr(VI) from aqueous media. This agrees with the findings of Sigh and Mishra (2021), Sun et al. (2014) who found their adsorbent data to fit the Freundlich model as well.

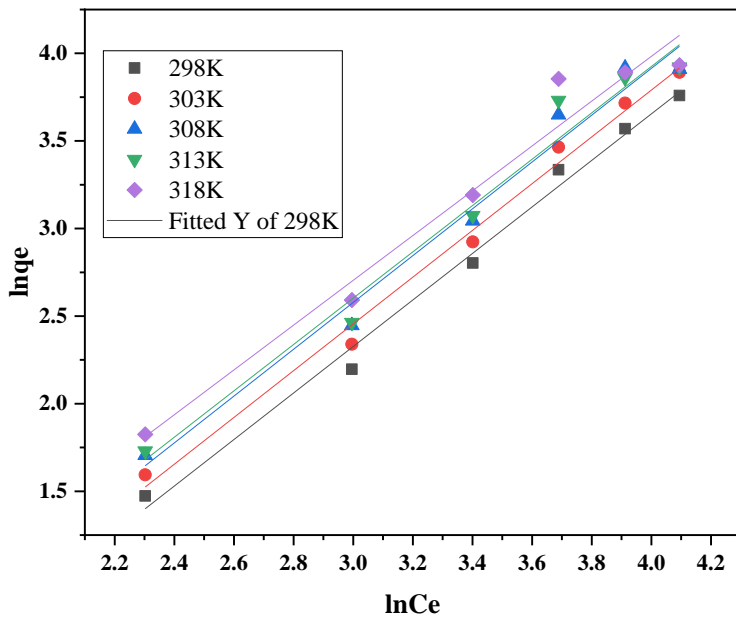


Figure 4.27: Freundlich linear fit isotherm model

4.6.3 Temkin isotherm model

The Temkin isotherm model was developed to account for the influence of indirect adsorbent-adsorbate interactions on adsorption; according to this hypothesis, these interactions would cause the layer heat of adsorption to drop linearly with coverage (Temkin, 1941). While disregarding extremely low and very high concentrations, the Temkin isotherm assumes a linear rather than a logarithmic reduction in the heat of

adsorption. Homogeneous distribution of bonding energy up to a specific maximum bonding energy is assumed. From the equation $q_e = B \ln(AC_e)$, B and A may be determined from the slopes (B) and intercepts (BlnA) of the plot of q_e vs. $\ln C_e$ Figure 4.28. The interaction between the hexavalent chromium and CNC-Fe₃O₄NP-CD nanocomposite adsorbent was strong, as evidenced by the B values, which ranged from 12.9 to 20.94 J/mole, which could have been attributed to the intense heat of adsorption. The linear correlation coefficient ($R^2 > 0.96$) further demonstrated the strong interaction, indicating that the model fitted the experimental data. The adsorption energy recorded ($E > 8.0$ J/mole) and high R^2 value suggest that the Temkin isotherm is a suitable model for describing the adsorption process of the prepared adsorbent as also reported by Xing et. al. (2022). The Temkin isotherm model suited the experimental data relatively well, indicating an intense contact between the adsorbate and the surface of the CNC-Fe₃O₄NP-CD nanocomposite adsorbent. This is in agreement with Sun et al. (2011) and Villabona et al. (2022) who found the Temkin isotherm to fit their experimental data.

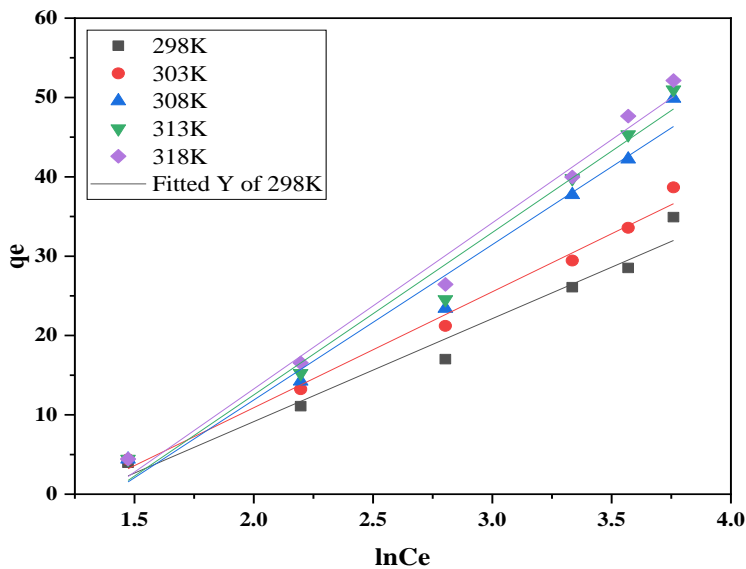


Figure 4. 28: Temkin Linear fit isotherm model

4.6.4 Dubinin–Radushkevich (D–R) model

This isotherm model was introduced to determine the typical porosity and the apparent free energy of adsorption. This isotherm model, however, does not presuppose a uniform surface or a constant sorption potential.

The linear version of the Dubinin–Radushkevich (D–R) isotherm is $q_{\epsilon} = q_m \exp(-\beta\epsilon^2)$ where, ϵ is the Polanyi potential, which is connected to the equilibrium concentration (C_e) as $\epsilon = RT \ln(1 + \frac{1}{C_e})$ where R is the gas constant (8.314 J/mol.K), T is the absolute temperature in K.

The Dubinin Radushkevich isotherms linear fit plot of ($\ln q_e$ vs. ϵ^2 (KJ²/mol²) resulted in a straight line Figure 4.29. The values of mean free energy $E = \frac{1}{\sqrt{-2K_{DR}}}$ are used in predicting the adsorption mechanisms; if $E < 8$ kJ/mol, the adsorption process is physical in nature, and if E is between 8 and 16 kJ/mol, the adsorption process is due to ion exchange. In the present study, the numerical values of adsorption of the mean free energy for Cr⁶⁺ as shown in Table 4.6 were found to be between 10.20 and 14.26 kJ/mol, which correspond to the chemical process. This is similar to the the findings of Islam et. al. (2019) and Oskui et al. (2019) who reported a chemical process in their respective adsorption studies.

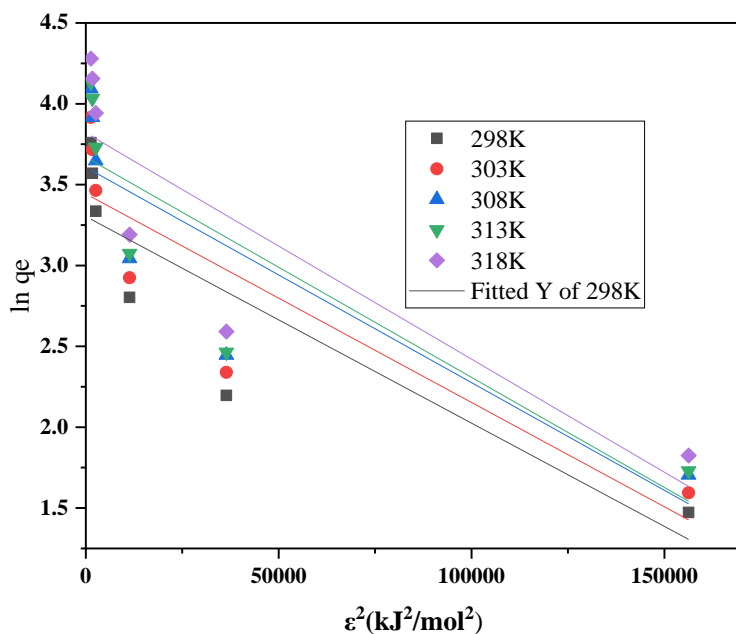


Figure 4.29: Dubinin–Radushkevich Linear fit isotherm model

Table 4.6: Summary of Isotherms model parameters

Isotherms/Adsorbate	Parameters				
	298K	303K	308K	313K	318K
Langmuir isotherm					
qm (mg/L)	17.4804	17.3361	16.765	17.879	18.581
K_L (L/mg)	0.00342	0.00251	0.00272	0.00318	0.00289
R^2	0.99633	0.99749	0.9964	0.99489	0.99496
Freundlich isotherm					
N	1.32794	1.33463	1.33644	1.3224	1.2787
K_f	1.65764	1.54842	1.43125	1.36509	1.13216
R^2	0.98907	0.98989	0.97544	0.97134	0.98907
Temkin isotherm					
B (J/mol)	12.97575	14.61523	19.59557	20.47952	20.94192

Bln(A) (L/mg)	16.79723	18.32456	27.32356	28.4412	28.61598
R ²	0.96414	0.98664	0.96692	0.97383	0.96414
<hr/>					
<i>Dubinini-Radushkevich</i>					
<i>isotherm</i>					
B	0.0000127	0.0000128	0.0000133	0.0000136	0.000014
E	10.60676	12.5085	10.20424	11.16307	14.26124
ε (mol ² /J ²)	3.30269	3.44307	3.60739	3.66965	3.81993
R ²	0.71985	0.71857	0.70271	0.69256	0.71985
<hr/>					

4.7 Thermodynamics studies of adsorption

In adsorption, thermodynamic characteristics such as the Gibbs free energy change (ΔG°) (kJ/mole), enthalpy change (ΔH°) (kJ/mole), and entropy change ΔS° (J/mol.K) are crucial in determining whether the process is exothermic or endothermic (Al-Harby et al., 2021; Saha & Chowdhury, 2011). Equations 4.2-4.5 below provide solutions to various thermodynamic parameters,

$$K_c = \frac{q_e}{c_e} \quad (4.2)$$

$$\Delta G^\circ = -RT \ln K_c \quad (4.3)$$

$$\Delta G^\circ = \Delta H^\circ - T \Delta S^\circ \quad (4.4)$$

$$\ln K_c = \frac{\Delta S^\circ}{RT} - \frac{\Delta H^\circ}{RT} \quad (4.5)$$

Where T is the temperature in K, R is the universal gas constant (8.314 J/mol.K), q_e is the solid-phase equilibrium concentration (in mg/L), K_c is the equilibrium constant and c_e is the equilibrium solution concentration (in mg/L). The values of ΔH° and ΔS° ,

represents the slope and the intercept, which can be determined from the linear plot of $\ln K_c$ vs. $1/T$ (K^{-1}).

Figure 4.30 illustrates the thermodynamic plots of adsorption for hexavalent chromium. To understand the nature of any form of adsorption system, whether endothermic or exothermic, chemical or physical, requires studying and quantifying several thermodynamic parameters. The current study investigated various thermodynamic parameters, including the Gibbs free energy change (ΔG°), system entropy change (ΔS°), and system enthalpy change (ΔH°). Table 4.7 displays the thermodynamic parameters obtained. It is reported that when $\Delta G^\circ < 0$, the process is thermodynamically favored. Table 4.7 shows a negative value of ΔG° , suggesting that the CNC- Fe_3O_4 NP-CD nanocomposite adsorbent adsorbed hexavalent chromium ion well and spontaneously, demonstrating the thermodynamic favorability of the adsorption process without the requirement for additional energy. The adsorption was exothermic, as shown by the negative values of ΔH° . The positive values of ΔS° demonstrate the adsorbent affinity for the Cr^{6+} and a rise in sorbate concentration at the solid-liquid interface. This confirms the increasing randomness at the solid solution interface during sorption. With increasing temperature, a slight change in the negative value of ΔG° suggests that the adsorption process is less advantageous at high temperatures and adsorption is preferable at low temperatures (Mennas et al., 2023 ; Munagapati et al., 2022).

From this study, it is clear that thermodynamic characteristics demonstrated that the system is exothermic with ΔH° of -826.521 kJ/mole and that the adsorption is chemisorption and spontaneous.

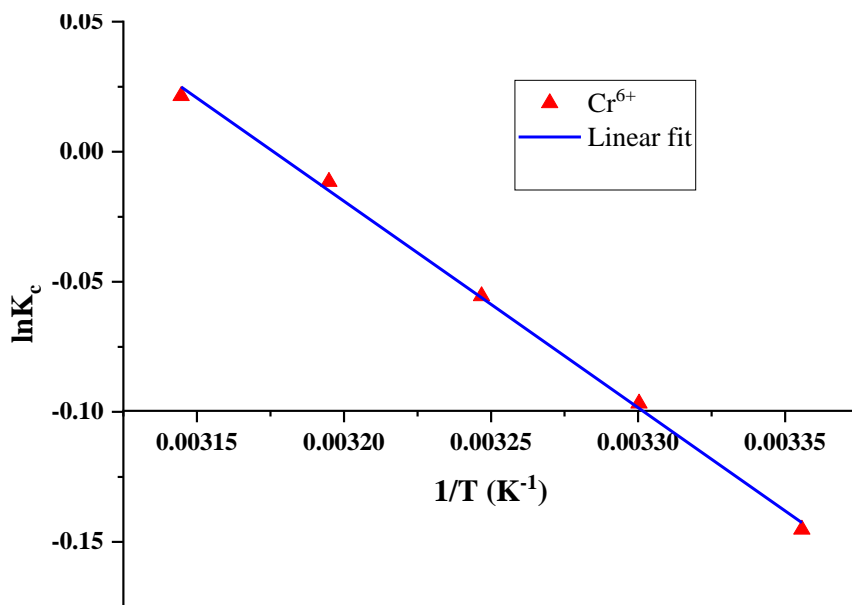


Figure 4.30: Adsorption thermodynamic plots

Table 4.7: Thermodynamic parameters at various system temperatures

ΔH° (kJ/mole)	ΔS° (kJ/mole)	ΔG° (kJ/mole)				
		298K	303K	308K	313K	318K
-826.521	2.585	-1596.85	-1609.78	-1622.7	-1635.63	-1648.55

4.8 Effect of Competing Ions on Cr(VI) Adsorption

Effect of competing ions on Cr(VI) adsorption efficiency was analysed and the data tabulated in Table 4.8. From this study in a solution containing 20 mg/L of Cd^{2+} , Zn^{2+} , and Pb^{2+} along with Cr(VI), the removal efficiency dropped to $35.32 \pm 0.13\%$ in presence of Cd^{2+} , $30.22 \pm 0.32\%$ in presence of Zn^{2+} , and $40.49 \pm 0.15\%$ in presence of Pb^{2+} . This can be attributed to the difference in the atomic radii of the competing ions (Mekatal et al., 2012). The presence of competing ions in aqueous solutions can significantly impact the adsorption efficiency of an adsorbent. This effect is particularly important when

considering real-world wastewater treatment, where multiple ionic species coexist (Mudhoo et al., 2021). The competitive adsorption between Cr(VI) and other ions can be influenced by several factors, including the charge, ionic radius, and concentration of the competing ions as reported by Zhang et al. (2020) and Abu-Dabeez et al. (2023) in their respective studies. In this study, the removal of chromium in presence of Cd^{2+} , Zn^{2+} , and Pb^{2+} resulted to an interaction with the adsorption sites on the CNC- Fe_3O_4 NP-CD nanocomposite, thereby inhibiting the binding of Cr(VI) to the adsorption sites as had been earlier reported by Abu-Dabeez et al. (2023) when investigating several metal ion competing for the adsorption sites. Divalent ions like Cd^{2+} , Zn^{2+} and Pb^{2+} , due to their higher charge, are particularly effective in occupying available active sites, thereby reducing the adsorption efficiency for Cr(VI) (Mohamad et al., 2023 ; Zhang et al., 2020). These ions are thought to have a stronger electrostatic attraction to the adsorbent surface, which can outcompete the Cr(VI) ions, leading to a reduction in removal efficiency. Zn^{2+} having a lesser influence to hexavalent chromium adsorption as compared to Cd^{2+} and Pb^{2+} can be due to its small ionic radius of 0.83\AA resulting to high charge density therefore having increased hydrated radius of 4.30\AA , this therefore limits the Zn^{2+} from reaching the adsorption sites of the adsorbent effectively hence giving chance to Cr(VI) to be adsorbed.

Table 4.8: Influence of competing ions on Cr(VI) removal efficiency

Adsorbate	Adsorption efficiency (%) of Cr(VI) in presence		
	Cd^{2+}	Zn^{2+}	Pb^{2+}
Cr^{2+}	$35.32\pm 0.13\%$	$30.22\pm 0.32\%$	$40.49\pm 0.15\%$

4.9 Regeneration of CNC-Fe₃O₄NP-CD

Figure 4.31 illustrates the desorption efficiencies achieved using different eluents across multiple cycles. The regeneration of the CNC-Fe₃O₄NP-CD nanocomposite is a crucial aspect of its practical application in water treatment. Effective regeneration allows for multiple cycles of use, thereby reducing operational costs and enhancing sustainability. The regeneration process typically involves the desorption of adsorbed metal ions or pollutants, which can be achieved through various eluent solutions. The effectiveness of the regeneration process depends on the choice of eluent and the regeneration conditions. The eluents used for desorption in this study were deionized water, HCl, and NaOH. These eluents work by altering the pH or ionic strength of the solution, disrupting the interactions between the adsorbate and the adsorbent. The very acidic solution HCl can protonate the functional groups on the CNC-Fe₃O₄NP-CD surface, and occupy the active sites hence limiting space for chromium adsorption hence encouraging release of adsorbed Cr(VI) ions. NaOH, on the other hand, increases the pH and increases the the repulsion of the negatively charged surface and the anion hexavalent chromium, facilitating desorption.

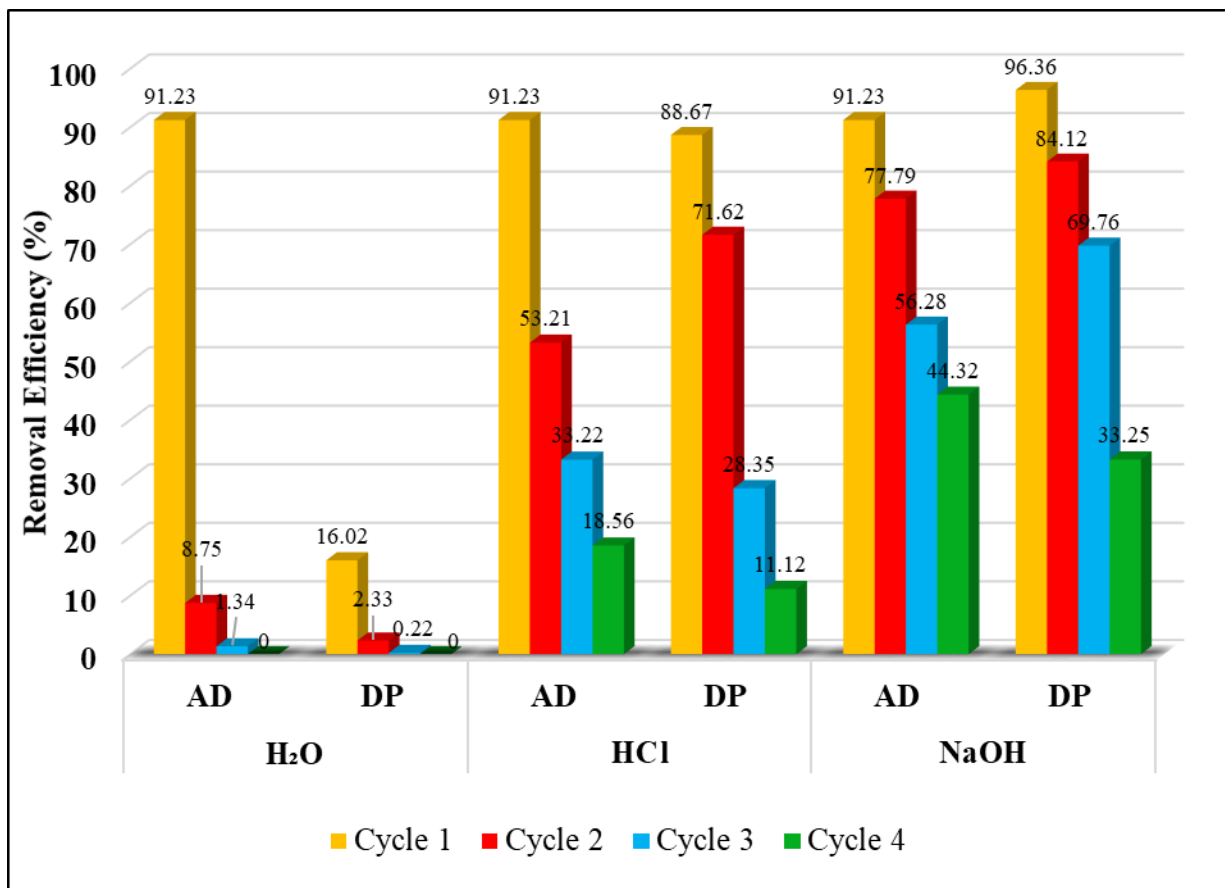


Figure 4.31: Regeneration of the adsorbent (AD- adsorption and DP- desorption)

From the findings of this study, using 20mg/L concentration of Cr(VI), the regeneration process efficiency decreased with subsequent cycles due to potential surface modification or fouling of the adsorbent. Initially, HCl and NaOH achieved desorption efficiencies of 96.36% and 88.67% but this efficiency dropped with each cycle. For instance it dropped to 71.62% for HCl and dropped to 84.12% for NaOH by the second cycle. As indicated in Figure 4.31, the desorption efficiency decreased with each cycle, with NaOH generally providing the highest desorption efficiency over multiple cycles. The decrease in efficiency is likely due to changes in the surface chemistry of the CNC-Fe₃O₄NP-CD,

such as the possible formation of insoluble complexes (Zhang et al., 2020) or the irreversible binding of some ions.

The CNC-Fe₃O₄NP-CD nanocomposite exhibits good potential for reuse in multiple adsorption-desorption cycles, especially when using NaOH as an eluent. However, the gradual decline in efficiency suggests that periodic regeneration and potential chemical treatments may be necessary to maintain high performance as was also noted by Sun et. al., (2014) using magnetic cellulose for removal of Cr(VI). The material stability under various pH conditions and its ability to maintain significant adsorption capacity make it a promising candidate for practical water treatment applications, where cost-effectiveness and sustainability are critical considerations.

CHAPTER FIVE

CONCLUSIONS AND RECOMMENDATIONS

5.1 Conclusions

This research work prepared and characterized chemically purified cellulose, cellulose nanocrystals, CNC-Fe₃O₄NP and a novel cellulose-based nanocomposite (CNC-Fe₃O₄NP-CD) for the effective removal of hexavalent chromium (Cr(VI)) from mimicked wastewater. The success of these preparations were confirmed by the characterization done using FTIR, TEM, SEM, XRD, BET and VSM.

Batch adsorption experiments were conducted under varying conditions of pH, adsorbent dosage, contact time, and initial Cr(VI) concentration. The CNC-Fe₃O₄NP-CD nanocomposite exhibited the highest adsorption efficiency, particularly at pH 2, where it achieved a removal efficiency of 97.45%. The optimal adsorbent dosage was found to be 1.0 g, with a maximum removal efficiency of 98.61%. This efficiency was significantly higher than that of other adsorbents, such as CNC and CNC-Fe₃O₄NP, which achieved 68.56% and 73.45% respectively. The high efficiency of CNC-Fe₃O₄NP-CD at low pH can be attributed to the protonation of the adsorbent surface, which increased the positive charge density and enhanced the electrostatic attraction between the adsorbent and the negatively charged Cr(VI) species, a characteristic that makes CNC-Fe₃O₄NP-CD particularly suitable for treating acidic wastewater.

Pollutant concentration also played a significant role in determining the adsorption efficiency. At a Cr(VI) concentration of 10 mg/L, CNC-Fe₃O₄NP-CD maintained a high removal efficiency of 97.31%, demonstrating its exceptional capacity to handle lower

pollutant loads. This efficiency was higher than those of CNC and Fe₃O₄NP, which managed 43.69% and 84.67%, respectively. However, as the Cr(VI) concentration increased, the removal efficiency gradually declined across all adsorbents, indicating that the active sites were nearing saturation. Despite this, CNC-Fe₃O₄NP-CD consistently outperformed the other adsorbents, underscoring its robustness and efficiency in various concentration ranges.

The study also highlighted the importance of contact time in the adsorption process. CNC-Fe₃O₄NP-CD exhibited rapid initial adsorption, with a removal efficiency of 93.2% within 35 minutes, indicating that the adsorbent quickly reached equilibrium. This rapid adsorption rate is crucial for practical water treatment applications where time is often a limiting factor. The superior performance of CNC-Fe₃O₄NP-CD can be attributed to its enhanced surface area and the availability of functional groups that provide more active sites for Cr(VI) adsorption.

The study further found that the adsorption capacity of CNC-Fe₃O₄NP-CD decreased with increase in temperature, achieving a removal efficiency of 97.33%. This trend suggests that the adsorption process is exothermic and spontaneous as indicated by the negative values of ΔG° .

In the regeneration study, CNC-Fe₃O₄NP-CD nanocomposite showed good potential for reuse across multiple adsorption-desorption cycles, particularly when NaOH was used as an eluent. Initial desorption efficiencies were above 90%, though the efficiency gradually declined with each cycle, indicating the need for periodic regeneration treatments. Despite this, the material stability under various pH conditions and its ability to maintain

significant adsorption capacity make it a promising candidate for sustainable water treatment applications.

The ability of the adsorbent to maintain high efficiency across various parameters, coupled with its potential for regeneration, makes it an attractive option for large-scale environmental remediation.

5.2 Recommendations for further research

The prepared adsorbents in this study proved to be adsorbents that could be relied on for removal of hexavalent chromium. However I would recommend the the following

- I. That more research on the adsorbent CNC-Fe₃O₄NP-CD be done to check how well it would work in the removal of organic pollutants eg EDC and PAHs in water.
- II. More research s be done to modify further the nanocomposite prepared in this study to be able to remove pollutants more effectively at neutral pH for easy applicability in domestic water purification.
- III. Investigate the long-term stability and performance of CNC-Fe₃O₄NP-CD in continuous flow wastewater treatment systems.
- IV. Preparation of cartridges to be used for continous flow waste water treatment.
- V. More studies to be done on regeneration of the nanocomposite to find the best solution mixture to achived more regeneration cycles.
- VI. Explore the adsorption mechanisms of other heavy metals using CNC-Fe₃O₄NP-CD to assess its broader environmental remediation potential.

REFERENCES

- Abdel-Halim, E. S., El-Rafie, M. H., & Al-Deyab, S. S. (2011). Polyacrylamide/guar gum graft copolymer for preparation of silver nanoparticles. *Carbohydrate Polymers*, 85(3), 692–697. <https://doi.org/10.1016/j.carbpol.2011.03.039>
- Abdulwahid, F. S., Haider, A. J., & Al-Musawi, S. (2023). Effect of laser parameter on Fe₃O₄ NPs formation by pulsed laser ablation in liquid. *AIP Conference Proceedings*, 2769(1). <https://pubs.aip.org/aip/acp/article-abstract/2769/1/020039/2884814>
- Abouzeid, R. E., Khiari, R., El-Wakil, N., & Dufresne, A. (2019). Current State and New Trends in the Use of Cellulose Nanomaterials for Wastewater Treatment. *Biomacromolecules*, 20(2), 573–597. <https://doi.org/10.1021/acs.biomac.8b00839>
- Abou-Zeid, R. E., Salama, A., Al-Ahmed, Z. A., Awwad, N. S., & Youssef, M. A. (2020). Carboxylated cellulose nanofibers as a novel efficient adsorbent for water purification. *Cellul. Chem. Technol*, 54, 237–245.
- Abu-Daabes, M. A., Abu Zeitoun, E., & Mazi, W. (2023). Competitive adsorption of quaternary metal ions, Ni²⁺, Mn²⁺, Cr⁶⁺, and Cd²⁺, on acid-treated activated carbon. *Water*, 15(6), 1070.
- Abu-Thabit, N. Y., Judeh, A. A., Hakeem, A. S., Ul-Hamid, A., Umar, Y., & Ahmad, A. (2020). Isolation and characterization of microcrystalline cellulose from date seeds (*Phoenix dactylifera* L.). *International Journal of Biological Macromolecules*, 155, 730–739. <https://doi.org/10.1016/j.ijbiomac.2020.03.255>
- Adawiyah, R., & Suryanti, V. (2022). Preparation and characterization of microcrystalline cellulose from lembang (*Typha angustifolia* L.). *Journal of Physics: Conference Series*, 2190(1), 012007. <https://iopscience.iop.org/article/10.1088/1742-6596/2190/1/012007/meta>
- Adeniyi, A. G., Adeyanju, C. A., Emenike, E. C., Otoikhian, S. K., Ogunniyi, S., Iwuozor, K. O., & Raji, A. A. (2022). Thermal energy recovery and valorisation of *Delonix regia* stem for biochar production. *Environmental Challenges*, 9, 100630.
- Agrahari, S., Singh, A. K., Gupta, M. K., Afroz, M., Pandey, V., Singh, H., & Tandon, P. K. (2023). Valorization of waste pulp of Citrus limetta for decontamination of chromium from polluted water. *Materials Today: Proceedings*. https://www.sciencedirect.com/science/article/pii/S2214785323050290?casa_token=nluhbvhcK0AAAAA:NO8P0JBuWcSwyntwpQ3mxn7gqNNGwSmCXc7aaa01YiDNORV1Ek6aKwnw82J_DVpIWBL8OK9tpWY

- Ahmed, N., & Mir, F. Q. (2021). Chromium(VI) removal using micellar enhanced microfiltration (MEMF) from an aqueous solution: Fouling analysis and use of ANN for predicting permeate flux. *Journal of Water Process Engineering*, *44*, 102438. <https://doi.org/10.1016/j.jwpe.2021.102438>
- Ahmed, S. F., Mofijur, M., Nuzhat, S., Chowdhury, A. T., Rafa, N., Uddin, M. A., Inayat, A., Mahlia, T. M. I., Ong, H. C., & Chia, W. Y. (2021a). Recent developments in physical, biological, chemical, and hybrid treatment techniques for removing emerging contaminants from wastewater. *Journal of Hazardous Materials*, *416*, 125912.
- Ahmed, S. F., Mofijur, M., Nuzhat, S., Chowdhury, A. T., Rafa, N., Uddin, M. A., Inayat, A., Mahlia, T. M. I., Ong, H. C., & Chia, W. Y. (2021b). Recent developments in physical, biological, chemical, and hybrid treatment techniques for removing emerging contaminants from wastewater. *Journal of Hazardous Materials*, *416*, 125912.
- Ajinkya, N., Yu, X., Kaithal, P., Luo, H., Somani, P., & Ramakrishna, S. (2020). Magnetic Iron Oxide Nanoparticle (IONP) Synthesis to Applications: Present and Future. *Materials (Basel, Switzerland)*, *13*(20), 4644. <https://doi.org/10.3390/ma13204644>
- Akhtar, N., Syakir Ishak, M. I., Bhawani, S. A., & Umar, K. (2021). Various natural and anthropogenic factors responsible for water quality degradation: A review. *Water*, *13*(19), 2660.
- Akiode, O. K., Adetoro, A., Anene, A. I., Afolabi, S. O., & Alli, Y. A. (2023). Methodical study of chromium (VI) ion adsorption from aqueous solution using low-cost agro-waste material: Isotherm, kinetic, and thermodynamic studies. *Environmental Science and Pollution Research*, *30*(16), 48036–48047.
- Akter, M., Bhattacharjee, M., Dhar, A. K., Rahman, F. B. A., Haque, S., Rashid, T. U., & Kabir, S. F. (2021). Cellulose-based hydrogels for wastewater treatment: A concise review. *Gels*, *7*(1), 30.
- Akter, M., Tajuddin Sikder, Md., & Atique Ullah, A. K. M. (2022). Zero-Valent Iron and Some Other Nanometal Particles for Environmental Remediation. In S. Tanaka, M. Kurasaki, M. Morikawa, & Y. Kamiya (Eds.), *Design of Materials and Technologies for Environmental Remediation* (Vol. 115, pp. 539–568). Springer Nature Singapore. https://doi.org/10.1007/698_2021_821
- Alaqrabeh, M. (2021). Adsorption phenomena: Definition, mechanisms, and adsorption types: short review. *RHAZES: Green and Applied Chemistry*, *13*, 43–51.

- Al-Asheh, S., & Aidan, A. (2020). A comprehensive method of ion exchange resins regeneration and its optimization for water treatment. *Promising Techniques for Wastewater Treatment and Water Quality Assessment*, 163–176.
- Al-Baldawi, I. A. (2018). Removal of 1, 2-Dichloroethane from real industrial wastewater using a sub-surface batch system with *Typha angustifolia* L. *Ecotoxicology and Environmental Safety*, 147, 260–265.
- Alessandro, S., Demitri, C., & Madaghiele, M. (2009). Biodegradable Cellulose-based Hydrogels: Design and Applications. *Materials*, 2. <https://doi.org/10.3390/ma2020353>
- Al-Ghouthi, M. A., & Da'ana, D. A. (2020). Guidelines for the use and interpretation of adsorption isotherm models: A review. *Journal of Hazardous Materials*, 393, 122383.
- Al-Harby, N. F., Albahly, E. F., & Mohamed, N. A. (2021). Kinetics, isotherm and thermodynamic studies for efficient adsorption of Congo Red dye from aqueous solution onto novel cyanoguanidine-modified chitosan adsorbent. *Polymers*, 13(24), 4446.
- Ali, A., Shah, T., Ullah, R., Zhou, P., Guo, M., Ovais, M., Tan, Z., & Rui, Y. (2021). Review on recent progress in magnetic nanoparticles: Synthesis, characterization, and diverse applications. *Frontiers in Chemistry*, 9, 629054.
- Ali, A., Zafar, H., Zia, M., Ul Haq, I., Phull, A. R., Ali, J. S., & Hussain, A. (2016). Synthesis, characterization, applications, and challenges of iron oxide nanoparticles. *Nanotechnology, Science and Applications, Volume 9*, 49–67. <https://doi.org/10.2147/NSA.S99986>
- Ali, M. M., Hossain, D., Al-Imran, A., Khan, M. S., Begum, M., & Osman, M. H. (2021). Environmental pollution with heavy metals: A public health concern. *Heavy Metals-Their Environmental Impacts and Mitigation*, 771–783.
- Al-Maliky, E. A., Gzar, H. A., & Al-Azawy, M. G. (2021). Determination of point of zero charge (PZC) of concrete particles adsorbents. *IOP Conference Series: Materials Science and Engineering*, 1184(1), 012004. <https://iopscience.iop.org/article/10.1088/1757-899X/1184/1/012004/meta>
- Alrowais, R., Bashir, M. T., Khan, A. A., Bashir, M., Abbas, I., & Abdel Daiem, M. M. (2024). Adsorption and Kinetics Modelling for Chromium (Cr6+) Uptake from Contaminated Water by Quaternized Date Palm Waste. *Water*, 16(2), 294.
- Amanulla, B., Subbu, H. K. R., & Ramaraj, S. K. (2018). A sonochemical synthesis of cyclodextrin functionalized Au-FeNPs for colorimetric detection of Cr6+ in different industrial waste water. *Ultrasonics Sonochemistry*, 42, 747–753.

- Anik, M. I., Hossain, M. K., Hossain, I., Mahfuz, A. M. U. B., Rahman, M. T., & Ahmed, I. (2021). Recent progress of magnetic nanoparticles in biomedical applications: A review. *Nano Select*, 2(6), 1146–1186. <https://doi.org/10.1002/nano.202000162>
- Anirudhan, T. S., Nima, J., & Divya, P. L. (2013). Applied Surface Science Adsorption of chromium (VI) from aqueous solutions by glycidylmethacrylate-grafted-densified cellulose with quaternary ammonium groups. *Applied Surface Science*, 279, 441–449. <https://doi.org/10.1016/j.apsusc.2013.04.134>
- Ansari, M. J., Kadhim, M. M., Hussein, B. A., Lafta, H. A., & Kianfar, E. (2022). Synthesis and Stability of Magnetic Nanoparticles. *BioNanoScience*, 12(2), 627–638. <https://doi.org/10.1007/s12668-022-00947-5>
- Antony, J., Meera, V., & Raphael, V. P. (2021). Investigations on the capacity and mechanism of iron uptake by nano zero-valent iron particles. *Bulletin of Materials Science*, 44(1), 3. <https://doi.org/10.1007/s12034-020-02274-5>
- Ao, D., AP, L., & AM, O. (2012). Langmuir, Freundlich, Temkin and Dubinin–Radushkevich isotherms studies of equilibrium sorption of Zn²⁺ onto phosphoric acid modified rice husk. *IOSR Journal of Applied Chemistry*, 3(1), 38–45.
- Appel, J. (1973). Freundlich's adsorption isotherm. *Surface Science*, 39(1), 237–244.
- Aragaw, T. A., Bogale, F. M., & Aragaw, B. A. (2021). Iron-based nanoparticles in wastewater treatment: A review on synthesis methods, applications, and removal mechanisms. *Journal of Saudi Chemical Society*, 25(8), 101280.
- Ayawei, N., Ebelegi, A. N., & Wankasi, D. (2017). Modelling and Interpretation of Adsorption Isotherms. *Journal of Chemistry*, 2017, 1–11. <https://doi.org/10.1155/2017/3039817>
- Ba-Abbad, M. M., Benamour, A., Ewis, D., Mohammad, A. W., & Mahmoudi, E. (2022). Synthesis of Fe₃O₄ Nanoparticles with Different Shapes Through a Co-Precipitation Method and Their Application. *JOM*, 74(9), 3531–3539. <https://doi.org/10.1007/s11837-022-05380-3>
- Bae, E., Park, H. J., Park, J., Yoon, J., Kim, Y., Choi, K., & Yi, J. (2011). Effect of chemical stabilizers in silver nanoparticle suspensions on nanotoxicity. *Bulletin of the Korean Chemical Society*, 32(2), 613–619. <https://doi.org/10.5012/bkcs.2011.32.2.613>
- Balali-Mood, M., Naseri, K., Tahergorabi, Z., Khazdair, M. R., & Sadeghi, M. (2021). Toxic mechanisms of five heavy metals: Mercury, lead, chromium, cadmium, and arsenic. *Frontiers in Pharmacology*, 12, 643972.

- Bao, K., Zhang, A., Cao, Y., & Xu, L. (2024). Achievements in Preparation of Cyclodextrin-Based Porous Materials for Removal of Pollutants. *Separations*, *11*(5), 143.
- Barbier, E. (2019). *The water paradox: Overcoming the global crisis in water management*. Yale University Press. <https://books.google.com/books?hl=en&lr=&id=efOFDwAAQBAJ&oi=fnd&pg=PP1&dq=70%25+Of+The+Earth%27s+Surface+Is+Covered+With+Water+Unfortunately,+only+less+than+1%25+of+this+water+is+fit+for+human+consumption+&ots=yevHjbKh0K&sig=hBf4TGpW1ob2NDA8dbxhECjiLF0>
- Bardajee, G. R., & Hooshyar, Z. (2013). A novel biocompatible magnetic iron oxide nanoparticles/hydrogel based on poly (acrylic acid) grafted onto starch for controlled drug release. *Journal of Polymer Research*, *20*, 1–13.
- Barragán, E. U. P., Guerrero, C. F. C., Zamudio, A. M., Cepeda, A. B. M., Heinze, T., & Koschella, A. (2019). Isolation of cellulose nanocrystals from *Typha domingensis* named southern cattail using a batch reactor. *Fibers and Polymers*, *20*, 1136–1144.
- Basu, A., Ali, S. S., Hossain, S. S., & Asif, M. (2022). A review of the dynamic mathematical modeling of heavy metal removal with the biosorption process. *Processes*, *10*(6), 1154.
- Beatty, M. A., & Hof, F. (2021). Host–guest binding in water, salty water, and biofluids: General lessons for synthetic, bio-targeted molecular recognition. *Chemical Society Reviews*, *50*(8), 4812–4832.
- Beebe, N. H. (2024). *A Complete Bibliography of Publications in the Journal of Mathematical Chemistry*. <https://www.netlib.org/tex/bib/jmathchem.pdf>
- Beg, M. D. H., Najwa, K., & Akindoyo, J. O. (2020). Chemistry of cellulose. In *Industrial Applications of Biopolymers and their Environmental Impact* (pp. 180–199). CRC Press. <https://www.taylorfrancis.com/chapters/edit/10.1201/9781315154190-7/chemistry-cellulose-beg-najwa-akindoyo>
- Bhaladhare, S., & Das, D. (2022). Cellulose: A fascinating biopolymer for hydrogel synthesis. *Journal of Materials Chemistry B*, *10*(12), 1923–1945.
- Bhatnagar, A., & Sillanpää, M. (2010). Utilization of agro-industrial and municipal waste materials as potential adsorbents for water treatment—A review. *Chemical Engineering Journal*, *157*(2–3), 277–296.

- Bhatnagar, A., Sillanpää, M., & Witek-Krowiak, A. (2015). Agricultural waste peels as versatile biomass for water purification—A review. *Chemical Engineering Journal*, *270*, 244–271.
- Biehl, P., Von der Lühe, M., Dutz, S., & Schacher, F. H. (2018). Synthesis, characterization, and applications of magnetic nanoparticles featuring polyzwitterionic coatings. *Polymers*, *10*(1), 91.
- Biswas, S., Meikap, B. C., & Sen, T. K. (2019). Adsorptive removal of aqueous phase copper (Cu 2+) and nickel (Ni 2+) metal ions by synthesized biochar–biopolymeric hybrid adsorbents and process optimization by response surface methodology (RSM). *Water, Air, & Soil Pollution*, *230*, 1–23.
- Bizymis, A.-P., Giannou, V., & Tzia, C. (2022). Improved properties of composite edible films based on chitosan by using cellulose nanocrystals and beta-cyclodextrin. *Applied Sciences*, *12*(17), 8729.
- Blanco, A., Monte, M. C., Campano, C., Balea, A., Merayo, N., & Negro, C. (2018). Nanocellulose for industrial use: Cellulose nanofibers (CNF), cellulose nanocrystals (CNC), and bacterial cellulose (BC). In *Handbook of nanomaterials for industrial applications* (pp. 74–126). Elsevier. <https://www.sciencedirect.com/science/article/pii/B9780128133514000055>
- Breida, M., Younssi, S. A., Ouammou, M., Bouhria, M., & Hafsi, M. (2019). Pollution of Water Sources from Agricultural and Industrial Effluents: Special Attention to NO₃⁻, Cr (VI), and Cu (II). *Water Chemistry*, *39*. <https://books.google.com/books?hl=en&lr=&id=7Jj8DwAAQBAJ&oi=fnd&pg=PA39&dq=Water+can+be+polluted+by+both+organic+and+inorganic+matter%3B+some+of+the+inorganic+pollutants+include+heavy+metals,+anions+and+ligands+above+permissible+limits.+Their+main+sources+are+industrial+effluents+and+agricultural+runoffs&ots=O-X1sGz7lu&sig=uxPor6QYzjIE7py0fq3DKf77Uxk>
- Budnyak, T. M., Błachnio, M., Slabon, A., Jaworski, A., Tertykh, V. A., Deryło-Marczewska, A., & Marczewski, A. W. (2020). Chitosan Deposited onto Fumed Silica Surface as Sustainable Hybrid Biosorbent for Acid Orange 8 Dye Capture: Effect of Temperature in Adsorption Equilibrium and Kinetics. *The Journal of Physical Chemistry C*, *124*(28), 15312–15323. <https://doi.org/10.1021/acs.jpcc.0c04205>
- Bujdák, J. (2020). Adsorption kinetics models in clay systems. The critical analysis of pseudo-second order mechanism. *Applied Clay Science*, *191*, 105630.
- Burke, N. A. D., Stöver, H. D. H., & Dawson, F. P. (2002). Magnetic Nanocomposites: Preparation and Characterization of Polymer-Coated Iron Nanoparticles. *Chemistry of Materials*, *14*(11), 4752–4761. <https://doi.org/10.1021/cm020126q>

- Burks, T., Uheida, A., Saleemi, M., Eita, M., Toprak, M. S., & Muhammed, M. (2013). Removal of chromium (VI) using surface modified superparamagnetic iron oxide nanoparticles. *Separation Science and Technology*, 48(8), 1243–1251.
- Busetty, S. (2019). Environmental treatment technologies: Adsorption. *Handbook of Environmental Materials Management*, 1367–1397.
- Bushra, R., Mohamad, S., Alias, Y., Jin, Y., & Ahmad, M. (2021). Current approaches and methodologies to explore the perceptive adsorption mechanism of dyes on low-cost agricultural waste: A review. *Microporous and Mesoporous Materials*, 319, 111040.
- Can, M. M., Coşkun, M., & Firat, T. (2012). A comparative study of nanosized iron oxide particles; magnetite (Fe₃O₄), maghemite (γ-Fe₂O₃) and hematite (α-Fe₂O₃), using ferromagnetic resonance. *Journal of Alloys and Compounds*, 542, 241–247.
- CelluForce Inc. : Quotes, Address, Contact.* (n.d.). Retrieved August 10, 2024, from <https://www.azonano.com/suppliers.aspx?SupplierID=2384>
- Cellulose Nanocrystals (CNC) | CelluRods™ by CelluForce.* (n.d.). Retrieved August 10, 2024, from <https://celluforce.com/cellulose-nanocrystals-cnc/>
- Chakraborty, R., Asthana, A., Singh, A. K., Jain, B., & Susan, A. B. H. (2022). Adsorption of heavy metal ions by various low-cost adsorbents: A review. *International Journal of Environmental Analytical Chemistry*, 102(2), 342–379. <https://doi.org/10.1080/03067319.2020.1722811>
- Chan, Y. Y., Pang, Y. L., Lim, S., & Chong, W. C. (2021). Facile green synthesis of ZnO nanoparticles using natural-based materials: Properties, mechanism, surface modification and application. *Journal of Environmental Chemical Engineering*, 9(4), 105417.
- Chaudhary, M., Singh, L., Rekha, P., Srivastava, V. C., & Mohanty, P. (2019). Adsorption of uranium from aqueous solution as well as seawater conditions by nitrogen-enriched nanoporous polytriazine. *Chemical Engineering Journal*, 378, 122236.
- Cheang, T., Zhou, H., Lin, W., Wang, Y., Chang, X., Gao, F., & Zhang, Y. (2022). Adsorption performance and mechanism of chromium on β-cyclodextrin-modified molybdenum disulfide. *Journal of Materials Science*, 57(42), 19694–19703. <https://doi.org/10.1007/s10853-022-07865-7>
- Chen, J. (2021). The interaction of flotation reagents with metal ions in mineral surfaces: A perspective from coordination chemistry. *Minerals Engineering*, 171, 107067.

- Chen, Y., Zhang, L., Yang, Y., Pang, B., Xu, W., Duan, G., Jiang, S., & Zhang, K. (2021). Recent Progress on Nanocellulose Aerogels: Preparation, Modification, Composite Fabrication, Applications. *Advanced Materials*, 33(11), 2005569. <https://doi.org/10.1002/adma.202005569>
- Chilukoti, G. R., & Mandapati, R. N. (2022). Characterization of Cellulosic Leaf Fiber from the Typha Angustifolia Plant. *Journal of Natural Fibers*, 19(7), 2516–2526. <https://doi.org/10.1080/15440478.2020.1819511>
- Chiroma, T. M., Abdulkarim, B. I., & Kefas, H. M. (2007). *The Impact of Pesticide Application on Heavy Metal (Cd , Pb and Cu) Levels in Spinach*. 11, 117–122.
- Chu, K. H. (2021). Revisiting the Temkin Isotherm: Dimensional Inconsistency and Approximate Forms. *Industrial & Engineering Chemistry Research*, 60(35), 13140–13147. <https://doi.org/10.1021/acs.iecr.1c01788>
- Cid-Samamed, A., Rakmai, J., Mejuto, J. C., Simal-Gandara, J., & Astray, G. (2022). Cyclodextrins inclusion complex: Preparation methods, analytical techniques and food industry applications. *Food Chemistry*, 384, 132467.
- Clarina, T., Flomina, P. J., Thangeswari, P., & Rama, V. (2018). Polpala flower extract mediated one step green synthesis and characterization of magnetite (Fe₃O₄) nanoparticles. *Asian Journal of Research in Chemistry*, 11(2), 459–462.
- Comninellis, C., Kapalka, A., Malato, S., Parsons, S. A., Poullos, I., & Mantzavinos, D. (2008). Advanced oxidation processes for water treatment: Advances and trends for R&D. *Journal of Chemical Technology & Biotechnology: International Research in Process, Environmental & Clean Technology*, 83(6), 769–776.
- Copenhaver, K., Li, K., Wang, L., Lamm, M., Zhao, X., Korey, M., Neivandt, D., Dixon, B., Sultana, S., Kelly, P., Gramlich, W. M., Tekinalp, H., Gardner, D. J., MacKay, S., Nawaz, K., & Ozcan, S. (2022). Pretreatment of lignocellulosic feedstocks for cellulose nanofibril production. *Cellulose*, 29(9), 4835–4876. <https://doi.org/10.1007/s10570-022-04580-z>
- Coudane, J., Van Den Berghe, H., Mouton, J., Garric, X., & Nottelet, B. (2022). Poly (lactic acid)-based graft copolymers: Syntheses strategies and improvement of properties for biomedical and environmentally friendly applications: A review. *Molecules*, 27(13), 4135.
- Cova, T. F., Murtinho, D., Aguado, R., Pais, A. A., & Valente, A. J. (2021a). Cyclodextrin polymers and cyclodextrin-containing polysaccharides for water remediation. *Polysaccharides*, 2(1), 16–38.

- Cova, T. F., Murtinho, D., Aguado, R., Pais, A. A., & Valente, A. J. (2021b). Cyclodextrin polymers and cyclodextrin-containing polysaccharides for water remediation. *Polysaccharides*, 2(1), 16–38.
- Dabizha, A., & Kersten, M. (2020). Exothermic adsorption of chromate by goethite. *Applied Geochemistry*, 123, 104785.
- Dąbrowski, A. (2001). Adsorption—From theory to practice. *Advances in Colloid and Interface Science*, 93(1–3), 135–224.
- Dantas, P. A., & Botaro, V. R. (2012). Synthesis and characterization of a new cellulose acetate-propionate gel: Crosslinking density determination. *Open Journal of Polymer Chemistry*, 2(04), 144–151.
- Das, A., Natarajan, K., Tiwari, S., & Ganguli, A. K. (2020). Nanostructures synthesized by the reverse microemulsion method and their magnetic properties. *Materials Research Express*, 7(10), 104001.
- Davis, C. S., Moon, R. J., Ireland, S., Foster, E. J., Johnston, L. J., Shatkin, J. A., Nelson, K., Forster, A. M., Postek, M. T., & Vladár, A. E. (2015). NIST-TAPPI workshop on measurement needs for cellulose nanomaterials. *NIST Special Publication*. <https://doi.org/10.6028/NIST.SP.1192>.
<https://nvlpubs.nist.gov/nistpubs/SpecialPublications/NIST.SP.1192.pdf>
- de Castro-Alves, L., Yáñez-Vilar, S., González-Gómez, M. A., Garcia-Acevedo, P., Arnosa-Prieto, Á., Piñeiro-Redondo, Y., & Rivas, J. (2024). Understanding adsorption mechanisms and metal ion selectivity of superparamagnetic beads with mesoporous CMK-3 carbon and commercial activated carbon. *Microporous and Mesoporous Materials*, 374, 113159.
- de Conti, M., Dey, S., Pottker, W., & La Porta, F. A. (2022). *An overview into advantages and applications of conventional and unconventional hydro (solvo) thermal approaches for novel advanced materials design*. <https://chemrxiv.org/engage/chemrxiv/article-details/62e89615659a3f1229312276>
- de Gimenez, I., & Mota, L. (2023). Cellulose-based materials crosslinked with epichlorohydrin: A mini review. *Revista Virtual de Química*, 15(1). <https://rvq-sub.sbq.org.br/index.php/rvq/article/view/4450>
- De Vargas Brião, G., Hashim, M. A., & Chu, K. H. (2023). The Sips isotherm equation: Often used and sometimes misused. *Separation Science and Technology*, 58(5), 884–892. <https://doi.org/10.1080/01496395.2023.2167662>

- Duan, X., Yang, S., Wacławek, S., Fang, G., Xiao, R., & Dionysiou, D. D. (2020). Limitations and prospects of sulfate-radical based advanced oxidation processes. *Journal of Environmental Chemical Engineering*, 8(4), 103849.
- Dudchenko, N., Pawar, S., Perelshtein, I., & Fixler, D. (2022). Magnetite nanoparticles: Synthesis and applications in optics and nanophotonics. *Materials*, 15(7), 2601.
- Dunky, M. (2021). Wood Adhesives Based on Natural Resources: A Critical Review: Part II. Carbohydrate-Based Adhesives. In K. L. Mittal (Ed.), *Progress in Adhesion and Adhesives* (1st ed., pp. 337–382). Wiley. <https://doi.org/10.1002/9781119846703.ch9>
- Dunlop, M. J., Acharya, B., & Bissessur, R. (2021). Effect of Cellulose Nanocrystals on the Mechanical Properties of Polymeric Composites. In M. T. Hameed Sultan, M. S. A. Majid, M. R. M. Jamir, A. I. Azmi, & N. Saba (Eds.), *Biocomposite Materials* (pp. 77–95). Springer Singapore. https://doi.org/10.1007/978-981-33-4091-6_4
- Dwivedi, A. D., Dubey, S. P., Hokkanen, S., & Sillanpää, M. (2014). Mechanistic investigation on the green recovery of ionic, nanocrystalline, and metallic gold by two anionic nanocelluloses. *Chemical Engineering Journal*, 253, 316–324.
- Ehiomogue, P., Ahuchaogu, I. I., & Ahaneku, I. E. (2021). REVIEW OF ADSORPTION ISOTHERMS MODELS. *Acta Technica Corviniensis-Bulletin of Engineering*, 14(4). <https://acta.fih.upt.ro/pdf/2021-4/ACTA-2021-4-16.pdf>
- El Amri, A., Bensalah, J., Idrissi, A., Lamy, K., Ouass, A., Bouzakraoui, S., Zarrouk, A., & Lebdiri, A. (2022). Adsorption of a cationic dye (Methylene blue) by *Typha Latifolia*: Equilibrium, kinetic, thermodynamic and DFT calculations. *Chemical Data Collections*, 38, 100834.
- El Gamal, M., Mousa, H. A., El-Naas, M. H., Zacharia, R., & Judd, S. (2018). Bio-regeneration of activated carbon: A comprehensive review. *Separation and Purification Technology*, 197, 345–359.
- Endres, S. C., Ciacchi, L. C., & Mädler, L. (2021). A review of contact force models between nanoparticles in agglomerates, aggregates, and films. *Journal of Aerosol Science*, 153, 105719.
- Etale, A., Onyianta, A. J., Turner, S. R., & Eichhorn, S. J. (2023a). Cellulose: A Review of Water Interactions, Applications in Composites, and Water Treatment. *Chemical Reviews*, 123(5), 2016–2048. <https://doi.org/10.1021/acs.chemrev.2c00477>
- Etale, A., Onyianta, A. J., Turner, S. R., & Eichhorn, S. J. (2023b). Cellulose: A Review of Water Interactions, Applications in Composites, and Water Treatment.

- Evans, S. K., Wesley, O. N., Nathan, O., & Moloto, M. J. (2019). Chemically purified cellulose and its nanocrystals from sugarcane baggase: Isolation and characterization. *Heliyon*, 5(10). [https://www.cell.com/heliyon/pdf/S2405-8440\(19\)36295-4.pdf](https://www.cell.com/heliyon/pdf/S2405-8440(19)36295-4.pdf)
- Fahlgren, D. (2017). *Genetic variation in common cattail (Typha latifolia) in southern Sweden*.
- Fahma, F., Febiyanti, I., Lisdayana, N., Arnata, I. W., & Sartika, D. (2021). Nanocellulose as a new sustainable material for various applications: A review. *Archives of Materials Science and Engineering*, 109(2), 49–64.
- Falciglia, P. P., Gagliano, E., Scandura, P., Bianco, C., Tosco, T., Sethi, R., Varvaro, G., Agostinelli, E., Bongiorno, C., & Russo, A. (2022). Physico-magnetic properties and dynamics of magnetite (Fe₃O₄) nanoparticles (MNPs) under the effect of permanent magnetic fields in contaminated water treatment applications. *Separation and Purification Technology*, 296, 121342.
- Farzin, A., Etesami, S. A., Quint, J., Memic, A., & Tamayol, A. (2020). Magnetic Nanoparticles in Cancer Therapy and Diagnosis. *Advanced Healthcare Materials*, 9(9), 1901058. <https://doi.org/10.1002/adhm.201901058>
- Fernandes, A., Cruz-Lopes, L., Esteves, B., & Evtuguin, D. (2023). Nanotechnology applied to cellulosic materials. *Materials*, 16(8), 3104.
- Gala, U. (2015). *Preparation, characterization and dissolution study for curcumin-resveratrol-cyclodextrin amorphous ternary system*. Creighton University. <https://search.proquest.com/openview/af83b13f3cf34255b3cb2ef4ec407a87/1?pq-origsite=gscholar&cbl=18750>
- Gautam, R. K., Mudhoo, A., Lofrano, G., & Chattopadhyaya, M. C. (2014). Biomass-derived biosorbents for metal ions sequestration: Adsorbent modification and activation methods and adsorbent regeneration. *Journal of Environmental Chemical Engineering*, 2(1), 239–259.
- Gautam, S., Kumar, P., & Patra, A. K. (2016). Occupational exposure to particulate matter in three Indian opencast mines. *Air Quality, Atmosphere and Health*, 9(2), 143–158. <https://doi.org/10.1007/s11869-014-0311-6>
- Gopmandal, P. P., & Duval, J. F. (2022). Electrostatics and electrophoresis of engineered nanoparticles and particulate environmental contaminants: Beyond zeta potential-based formulation. *Current Opinion in Colloid & Interface Science*, 60, 101605.

- Goyal, N., Sachdeva, D., & Sujit, U. (2023). Synthesis, Functionalization Strategies and Application of Different Types of Cyclodextrin-Based Nanosponges for Water Treatment. In S. Gulati (Ed.), *Nanosponges for Environmental Remediation* (pp. 117–143). Springer Nature Switzerland. https://doi.org/10.1007/978-3-031-41077-2_6
- Grishkewich, N., Mohammed, N., Tang, J., & Tam, K. C. (2017). Recent advances in the application of cellulose nanocrystals. *Current Opinion in Colloid & Interface Science*, 29, 32–45.
- Guerra, Y., Leal, L., Cabrera-Baez, M., Padrón-Hernández, E., Castro-Lopes, S., Viana, B. C., Abreu, G., Caland, J., Matos-Rodrigues, P., & Santos, F. (2023). Cation distribution, Fe²⁺/Fe³⁺ valence states and oxygen vacancies detection in the Y₂O₃:Er³⁺:Fe²⁺ compound. *Journal of Alloys and Compounds*, 960, 170607.
- Guna, V., Ilangovan, M., K., A., C.v., A. K., C.v., S., S., Y., Nagananda, G. S., Venkatesh, K., & Reddy, N. (2019). Biofibers and biocomposites from sabai grass: A unique renewable resource. *Carbohydrate Polymers*, 218, 243–249. <https://doi.org/10.1016/j.carbpol.2019.04.085>
- Guo, X., & Wang, J. (2019). A general kinetic model for adsorption: Theoretical analysis and modeling. *Journal of Molecular Liquids*, 288, 111100.
- Gupta, P. K., Raghunath, S. S., Prasanna, D. V., Venkat, P., Shree, V., Chithanathan, C., Choudhary, S., Surender, K., & Geetha, K. (2019). An update on overview of cellulose, its structure and applications. *Cellulose*, 201(9), 84727.
- Gupta, V. K., Carrott, P. J. M., Ribeiro Carrott, M. M. L., & Suhas. (2009). Low-Cost Adsorbents: Growing Approach to Wastewater Treatment—a Review. *Critical Reviews in Environmental Science and Technology*, 39(10), 783–842. <https://doi.org/10.1080/10643380801977610>
- Hădărugă, N. G., Hădărugă, D. I., Păunescu, V., Tatu, C., Ordodi, V. L., Bandur, G., & Lupea, A. X. (2006). Thermal stability of the linoleic acid/ α - and β -cyclodextrin complexes. *Food Chemistry*, 99(3), 500–508.
- Hamad, W. Y. (2017). *Cellulose nanocrystals: Properties, production and applications*. John Wiley & Sons. https://books.google.com/books?hl=en&lr=&id=bt6RDgAAQBAJ&oi=fnd&pg=PR13&dq=CNCs+are+created+when+cellulose+fibers+undergo+acid+hydrolysis,+which+separates+the+amorphous+regions+into+discrete+crystalline+domains.+CNCs+that+come+from+plant+sources+have+lengths+between+100+and+250+nm+and+lateral+diameters+between+5+and+70+nm&ots=aUk7WzqrYo&sig=4RzhRqVcsnGJ8wDvmF0HN_vupZY

- Hamimed, S., Abdeljelil, N., Landoulsi, A., Chatti, A., Aljabali, A. A. A., & Barhoum, A. (2022). Bacterial Cellulose Nanofibers: Biosynthesis, Unique Properties, Modification, and Emerging Applications. In A. Barhoum (Ed.), *Handbook of Nanocelluloses* (pp. 297–334). Springer International Publishing. https://doi.org/10.1007/978-3-030-89621-8_15
- Hamimed, S., Jebli, N., Othmani, A., Hamimed, R., Barhoum, A., & Chatti, A. (2022). Nanocelluloses for Removal of Heavy Metals From Wastewater. In A. Barhoum (Ed.), *Handbook of Nanocelluloses* (pp. 891–931). Springer International Publishing. https://doi.org/10.1007/978-3-030-89621-8_51
- Hassanzadeh-Tabrizi, S. A. (2023). Precise calculation of crystallite size of nanomaterials: A review. *Journal of Alloys and Compounds*, 171914.
- Ho, Y. S., Ng, J. C. Y., & McKay, G. (2000). KINETICS OF POLLUTANT SORPTION BY BIOSORBENTS: REVIEW. *Separation and Purification Methods*, 29(2), 189–232. <https://doi.org/10.1081/SPM-100100009>
- Hokkanen, S., Bhatnagar, A., & Sillanpää, M. (2016). A review on modification methods to cellulose-based adsorbents to improve adsorption capacity. *Water Research*, 91, 156–173. <https://doi.org/10.1016/j.watres.2016.01.008>
- Hokkanen, S., Bhatnagar, A., & Sillanpää, M. (2016). A review on modification methods to cellulose-based adsorbents to improve adsorption capacity. *Water Research*, 91, 156–173.
- Hokkanen, S., Repo, E., Suopajarvi, T., Liimatainen, H., Niinimaa, J., & Sillanpää, M. (2014). Adsorption of Ni (II), Cu (II) and Cd (II) from aqueous solutions by amino modified nanostructured microfibrillated cellulose. *Cellulose*, 21, 1471–1487.
- Hossain, N., Nizamuddin, S., & Shah, K. (2022). Thermal-chemical modified rice husk-based porous adsorbents for Cu (II), Pb (II), Zn (II), Mn (II) and Fe (III) adsorption. *Journal of Water Process Engineering*, 46, 102620.
- Hossini, H., Shafie, B., Niri, A. D., Nazari, M., Esfahlan, A. J., Ahmadpour, M., Nazmara, Z., Ahmadimanesh, M., Makhdoumi, P., Mirzaei, N., & Hoseinzadeh, E. (2022). A comprehensive review on human health effects of chromium: Insights on induced toxicity. *Environmental Science and Pollution Research*, 29(47), 70686–70705. <https://doi.org/10.1007/s11356-022-22705-6>
- Hu, X. J., Wang, J. S., Liu, Y. G., Li, X., Zeng, G. M., Bao, Z. L., ... & Long, F. (2011). Adsorption of chromium (VI) by ethylenediamine-modified cross-linked magnetic chitosan resin: isotherms, kinetics and thermodynamics. *Journal of hazardous materials*, 185(1), 306-314.

- Hu, Q.-D., Jiang, H.-L., Lam, K.-H., Hu, Z.-P., Liu, Z.-J., Wang, H.-Y., Yang, Y.-Y., Baigenzhenov, O., Hosseini-Bandegharai, A., & He, F.-A. (2023). Polydopamine-modification of a magnetic composite constructed from citric acid-cross-linked cyclodextrin and graphene oxide for dye removal from waters. *Environmental Science and Pollution Research*, 30(32), 78521–78536. <https://doi.org/10.1007/s11356-023-27679-7>
- Huang, Y. (2022). Comments on using of “pseudo-first-order kinetic model”[Sci. Total Environ. 750 (2021) 142370, 750 (2021) 141498, 761 (2021) 143229]. *Science of The Total Environment*, 826, 154291.
- Ievinsh, G. (2023). Halophytic Clonal Plant Species: Important Functional Aspects for Existence in Heterogeneous Saline Habitats. *Plants*, 12(8), 1728.
- Improving Access to Safe Drinking Water in Kenya – KIPPRA*. (n.d.). Retrieved August 6, 2024, from <https://kippra.or.ke/improving-access-to-safe-drinking-water-in-kenya/>
- Iqbal, D., Zhao, Y., Zhao, R., Russell, S. J., & Ning, X. (2022). A Review on Nanocellulose and Superhydrophobic Features for Advanced Water Treatment. *Polymers*, 14(12), 2343. <https://doi.org/10.3390/polym14122343>
- Iqbal, Z., Tanweer, M. S., & Alam, M. (2022). Recent advances in adsorptive removal of wastewater pollutants by chemically modified metal oxides: A review. *Journal of Water Process Engineering*, 46, 102641.
- Irshad, M. A., Sattar, S., Nawaz, R., Al-Hussain, S. A., Rizwan, M., Bukhari, A., Waseem, M., Irfan, A., Inam, A., & Zaki, M. E. (2023). Enhancing chromium removal and recovery from industrial wastewater using sustainable and efficient nanomaterial: A review. *Ecotoxicol Environ Saf*, 263(115231), 10–1016.
- Islam, M. A., Angove, M. J., & Morton, D. W. (2019). Recent innovative research on chromium (VI) adsorption mechanism. *Environmental Nanotechnology, Monitoring & Management*, 12, 100267.
- Ismail, M. M., Elkomy, R. G., & El-Sheekh, M. M. (2023). Bioactive Compounds from Components of Marine Ecosystem. *Marine Ecosystems: A Unique Source of Valuable Bioactive Compounds*, 3, 206–256.
- Jadhav, S. A., Brunella, V., & Scalarone, D. (2015). Polymerizable ligands as stabilizers for nanoparticles. *Particle and Particle Systems Characterization*, 32(4), 417–428. <https://doi.org/10.1002/ppsc.201400074>
- Jain, M., Yadav, M., Kohout, T., Lahtinen, M., Garg, V. K., & Sillanpää, M. (2018). Development of iron oxide/activated carbon nanoparticle composite for the

removal of Cr (VI), Cu (II) and Cd (II) ions from aqueous solution. *Water Resources and Industry*, 20, 54–74.

Jasim, S. A., Patra, I., Opulencia, M. J. C., Hachem, K., Parra, R. M. R., Ansari, M. J., Jalil, A. T., Al-Gazally, M. E., Naderifar, M., Khatami, M., & Akhavan-Sigari, R. (2022). Green synthesis of spinel copper ferrite (CuFe_2O_4) nanoparticles and their toxicity. *Nanotechnology Reviews*, 11(1), 2483–2492. <https://doi.org/10.1515/ntrev-2022-0143>

Jasmania, L., & Thielemans, W. (2018). Preparation of nanocellulose and its potential application. *International Journal of Nanomaterials, Nanotechnology and Nanomedicine*, 4(2), 014–021.

Jawaid, M., Boufi, S., & HPS, A. K. (2017). *Cellulose-reinforced nanofibre composites: Production, properties and applications*. Woodhead Publishing. <https://books.google.com/books?hl=en&lr=&id=7yYUDgAAQBAJ&oi=fnd&pg=PP1&dq=Cellulose-reinforced+Nanofibre+Composites+Production,+Properties+And+Applications&ots=qVbXPNbbyd&sig=1hl3A5J8dNIDa7ycrXAJz2izHAQ>

Joseph, B., Sagarika, V. K., Sabu, C., Kalarikkal, N., & Thomas, S. (2020). Cellulose nanocomposites: Fabrication and biomedical applications. *Journal of Bioresources and Bioproducts*, 5(4), 223–237.

Jung, H., Shin, G., Kwak, H., Hao, L. T., Jegal, J., Kim, H. J., Jeon, H., Park, J., & Oh, D. X. (2023). Review of polymer technologies for improving the recycling and upcycling efficiency of plastic waste. *Chemosphere*, 320, 138089.

Kabir, S. M. F., Sikdar, P. P., Haque, B., Bhuiyan, M. A. R., Ali, A., & Islam, M. N. (2018). Cellulose-based hydrogel materials: Chemistry, properties and their prospective applications. *Progress in Biomaterials*, 7(3), 153–174. <https://doi.org/10.1007/s40204-018-0095-0>

Kaboudin, B., Momen, T., Kazemi, F., & Ray, P. (2021). *Novel β -Cyclodextrin Functionalized Core-Shell Fe_3O_4 Magnetic Nanoparticles for the Removal of Toxic Metals from Water*. <https://chemrxiv.org/engage/chemrxiv/article-details/60c7598ebb8c1acb813dcc3a>

Kadam, D. M., Kaur, A., & Kasara, A. (2022). Characterization of natural fibre-based nano-composite materials: A review. *Journal of Agricultural Engineering*, 59(2), 159–178.

Kalam, S., Abu-Khamsin, S. A., Kamal, M. S., & Patil, S. (2021). Surfactant Adsorption Isotherms: A Review. *ACS Omega*, 6(48), 32342–32348. <https://doi.org/10.1021/acsomega.1c04661>

- Kamali Moghaddam, M. (2022). Structural and Thermal Properties of Cellulose Microfiber Isolated from *Typha Australis* by Sequential Alkali-Oxidative Treatment. *Journal of Natural Fibers*, 19(15), 10526–10538. <https://doi.org/10.1080/15440478.2021.1994094>
- Kamali Moghaddam, M. (2023). Morphologies and properties of lignocellulose fiber extracted from *Typha* leaves with potential for composite applications. *The Journal of The Textile Institute*, 1–10. <https://doi.org/10.1080/00405000.2023.2200316>
- Karale, M. A. B., & Game, M. D. (2022). GREEN CHEMISTRY FOR CHEMICAL SYNTHESIS. *METHODOLOGY*, 4, 5.
- Karchoubi, F., Ghotli, R. A., Pahlevani, H., & Salehi, M. B. (2023). New insights into nanocomposite hydrogels; a review on recent advances in characteristics and applications. *Advanced Industrial and Engineering Polymer Research*. <https://www.sciencedirect.com/science/article/pii/S2542504823000453>
- Katiyar, V., & Dhar, P. (2020). *Cellulose Nanocrystals: Emerging Bio-Precursors for Chemical Processes*. De Gruyter. <https://doi.org/10.1515/9783110648010>
- Kouli, M. E., Kourinou, M., Kokkinopoulos, I., Banis, G., Savvidou, M., Ferraro, A., ... & Hristoforou, E. (2020). A simple and rapid preparation of Fe₃O₄/β-cyclodextrin magnetic nanoparticles via microwave assisted co-precipitation compared with improved co-precipitation method. *Journal of Biological Physics and Chemistry*, 20(3), 111-121.
- Kekes, T., Kolliopoulos, G., & Tzia, C. (2021). Hexavalent chromium adsorption onto crosslinked chitosan and chitosan/β-cyclodextrin beads: Novel materials for water decontamination. *Journal of Environmental Chemical Engineering*, 9(4), 105581.
- Khalid, M. Y., Al Rashid, A., Arif, Z. U., Ahmed, W., & Arshad, H. (2021). Recent advances in nanocellulose-based different biomaterials: Types, properties, and emerging applications. *Journal of Materials Research and Technology*, 14, 2601–2623.
- Khan, A. U., Khan, A. N., Waris, A., Ilyas, M., & Zamel, D. (2022). Phytoremediation of pollutants from wastewater: A concise review. *Open Life Sciences*, 17(1), 488–496. <https://doi.org/10.1515/biol-2022-0056>
- Khan, S., Naushad, M., Govarthanam, M., Iqbal, J., & Alfadul, S. M. (2022). Emerging contaminants of high concern for the environment: Current trends and future research. *Environmental Research*, 207, 112609.
- Khili, F., Borges, J., Almeida, P. L., Boukherroub, R., & Omrani, A. D. (2019). Extraction of Cellulose Nanocrystals with Structure I and II and Their

- Applications for Reduction of Graphene Oxide and Nanocomposite Elaboration. *Waste and Biomass Valorization*, 10(7), 1913–1927. <https://doi.org/10.1007/s12649-018-0202-4>
- Kian, L. K., Jawaid, M., Ariffin, H., & Alothman, O. Y. (2017). Isolation and characterization of microcrystalline cellulose from roselle fibers. *International Journal of Biological Macromolecules*, 103, 931–940.
- Kinuthia, G. K., Ngunjiri, V., Beti, D., Lugalia, R., Wangila, A., & Kamau, L. (2020). Levels of heavy metals in wastewater and soil samples from open drainage channels in Nairobi, Kenya: Community health implication. *Scientific Reports*, 10(1), 8434.
- Klemm, D., Heublein, B., Fink, H., & Bohn, A. (2005). Cellulose: Fascinating Biopolymer and Sustainable Raw Material. *Angewandte Chemie International Edition*, 44(22), 3358–3393. <https://doi.org/10.1002/anie.200460587>
- Koemets, E. (2020). *The crystal chemistry of iron oxides and oxyhydroxides at extreme conditions: Implications for the deep Earth's oxygen cycle*. Universitaet Bayreuth (Germany). <https://search.proquest.com/openview/9636461ba639148c7eb7cd913797fc85/1?pq-origsite=gscholar&cbl=2026366&diss=y>
- Králik, M. (2014). Adsorption, chemisorption, and catalysis. *Chemical Papers*, 68(12), 1625–1638.
- Kumar, B., Smita, K., Galeas, S., Sharma, V., Guerrero, V. H., Debut, A., & Cumbal, L. (2020). Characterization and application of biosynthesized iron oxide nanoparticles using Citrus paradisi peel: A sustainable approach. *Inorganic Chemistry Communications*, 119, 108116.
- Kumari, G., Lima, E., Singh, K., Kumar, N., Guleria, A., Kumar, D., & Guleria, A. (2021). Cellulose-Based Nanoadsorbents for Wastewater Remediation. In *Removal of Refractory Pollutants From Wastewater Treatment Plants* (pp. 469–484). CRC Press. <https://www.taylorfrancis.com/chapters/edit/10.1201/9781003204442-26/cellulose-based-nanoadsorbents-wastewater-remediation-garima-kumari-eder-lima-kulvinder-singh-nitesh-kumar-anupam-guleria-dinesh-kumar-ashish-guleria>
- Kurniawan, T. W., Sulistyarti, H., Rumhayati, B., & Sabarudin, A. (2023). Cellulose Nanocrystals (CNCs) and Cellulose Nanofibers (CNFs) as Adsorbents of Heavy Metal Ions. *Journal of Chemistry*, 2023, 1–36. <https://doi.org/10.1155/2023/5037027>

- Lach, J., & Okoniewska, E. (2024). Equilibrium, Kinetic, and Diffusion Mechanism of lead (II) and cadmium (II) Adsorption onto Commercial Activated Carbons. *Molecules*, 29(11), 2418.
- Lam, E., & Hemraz, U. D. (2021). Preparation and Surface Functionalization of Carboxylated Cellulose Nanocrystals. *Nanomaterials*, 11(7), 1641. <https://doi.org/10.3390/nano11071641>
- Lead poisoning*. (n.d.). Retrieved August 6, 2024, from <https://www.who.int/news-room/fact-sheets/detail/lead-poisoning-and-health>
- Legge, T. M., & Goadby, K. W. (2023). Lead poisoning and lead absorption. *Dent*, 1(2), 3.
- Leonel, A. G., Mansur, A. A., & Mansur, H. S. (2021). Advanced functional nanostructures based on magnetic iron oxide nanomaterials for water remediation: A review. *Water Research*, 190, 116693.
- Leyva-Ramos, R., Jacobo-Azuara, A., Torres-Rivera, O. L., Guerrero-Coronado, R. M., Berber-Mendoza, M. S., & Alonso-Davila, P. (2008). Adsorption of chromium (VI) from water solution onto organobentonite. *J. Environ. Eng. Manage*, 18(5), 311–317.
- Li, M., He, B., & Zhao, L. (2019). Isolation and characterization of microcrystalline cellulose from Cotton Stalk Waste. *BioResources*, 14(2), 3231–3246.
- Li, M.-C., Liu, X., Lv, K., Sun, J., Dai, C., Liao, B., Liu, C., Mei, C., Wu, Q., & Hubbe, M. (2023). Cellulose nanomaterials in oil and gas industry: Current status and future perspectives. *Progress in Materials Science*, 101187.
- Li, Y., Li, L., Cao, L., & Yang, C. (2016). Promoting dynamic adsorption of Pb²⁺ in a single pass flow using fibrous nano-TiO₂/cellulose membranes. *Chemical Engineering Journal*, 283, 1145–1153. <https://doi.org/10.1016/j.cej.2015.08.068>
- Li, Z., & Lin, Z. (2021). Recent advances in polysaccharide-based hydrogels for synthesis and applications. *Aggregate*, 2(2), e21. <https://doi.org/10.1002/agt2.21>
- Li, Z., Wang, M., Wang, F., Gu, Z., Du, G., Wu, J., & Chen, J. (2007). γ -Cyclodextrin: A review on enzymatic production and applications. *Applied Microbiology and Biotechnology*, 77(2), 245–255. <https://doi.org/10.1007/s00253-007-1166-7>
- Lim, W.-R., Kim, S. W., Lee, C.-H., Choi, E.-K., Oh, M. H., Seo, S. N., Park, H.-J., & Hamm, S.-Y. (2019). Performance of composite mineral adsorbents for removing Cu, Cd, and Pb ions from polluted water. *Scientific Reports*, 9(1), 13598.
- Lima, É. C., Adebayo, M. A., & Machado, F. M. (2015). Kinetic and Equilibrium Models of Adsorption. In C. P. Bergmann & F. M. Machado (Eds.), *Carbon*

Nanomaterials as Adsorbents for Environmental and Biological Applications (pp. 33–69). Springer International Publishing. https://doi.org/10.1007/978-3-319-18875-1_3

- Liu, C., Crini, G., Wilson, L. D., Balasubramanian, P., & Li, F. (2024a). Removal of contaminants present in water and wastewater by cyclodextrin-based adsorbents: A bibliometric review from 1993 to 2022. *Environmental Pollution*, 123815.
- Liu, C., Crini, G., Wilson, L. D., Balasubramanian, P., & Li, F. (2024b). Removal of contaminants present in water and wastewater by cyclodextrin-based adsorbents: A bibliometric review from 1993 to 2022. *Environmental Pollution*, 123815.
- Liu, J. Y., Zhang, X., & TIAN, B. (2020). Selective modifications at the different positions of cyclodextrins: A review of strategies. *Turkish Journal of Chemistry*, 44(2), 261–278.
- Liu, J., Zhang, Z., Yu, Z., Liang, Y., Li, X., & Ren, L. (2017). The Structure and Flexural Properties of Typha Leaves. *Applied Bionics and Biomechanics*, 2017. <https://doi.org/10.1155/2017/1249870>
- Liu, K., Kang, Y., Wang, Z., & Zhang, X. (2013). 25th Anniversary Article: Reversible and Adaptive Functional Supramolecular Materials: “Noncovalent Interaction” Matters. *Advanced Materials*, 25(39), 5530–5548. <https://doi.org/10.1002/adma.201302015>
- Liu, M., Ye, Y., Xu, L., Gao, T., Zhong, A., & Song, Z. (2023). Recent Advances in Nanoscale Zero-Valent Iron (nZVI)-Based Advanced Oxidation Processes (AOPs): Applications, Mechanisms, and Future Prospects. *Nanomaterials*, 13(21), 2830.
- Liu, P., Borrell, P. F., Božič, M., Kokol, V., Oksman, K., & Mathew, A. P. (2015). Nanocelluloses and their phosphorylated derivatives for selective adsorption of Ag⁺, Cu²⁺ and Fe³⁺ from industrial effluents. *Journal of Hazardous Materials*, 294, 177–185.
- Liu, S., Yu, B., Wang, S., Shen, Y., & Cong, H. (2020). Preparation, surface functionalization and application of Fe₃O₄ magnetic nanoparticles. *Advances in Colloid and Interface Science*, 281, 102165.
- Liyanage, C. P., & Yamada, K. (2017). Impact of population growth on the water quality of natural water bodies. *Sustainability*, 9(8), 1405.
- M. Aguilar, N., Perez-Aguilar, J. M., González-Coronel, V. J., Soriano Moro, J. G., & Sanchez-Gaytan, B. L. (2021). Polymers as Versatile Players in the Stabilization, Capping, and Design of Inorganic Nanostructures. *ACS Omega*, 6(51), 35196–35203. <https://doi.org/10.1021/acsomega.1c05420>

- Ma, H., Hsiao, B. S., & Chu, B. (2012). Ultrafine Cellulose Nanofibers as Efficient Adsorbents for Removal of UO_2^{2+} in Water. *ACS Macro Letters*, 1(1), 213–216. <https://doi.org/10.1021/mz200047q>
- Ma, Y., Su, Q., Yue, C., Zou, H., Zhu, J., Zhao, H., Song, R., & Liu, Z. (2022). The effect of oxidative stress-induced autophagy by cadmium exposure in kidney, liver, and bone damage, and neurotoxicity. *International Journal of Molecular Sciences*, 23(21), 13491.
- Mabungela, N., Shooto, N. D., Dikio, E. D., Modise, S. J., Monapathi, M. E., Mtunzi, F. M., Xaba, T., & Naidoo, E. B. (2022). Multi-application fennel-based composites for the adsorption of Cr (VI) ions from water and control of Escherichia coli and Staphylococcus aureus. *Environmental Chemistry and Ecotoxicology*, 4, 171–185.
- Mahmoud, A. E. D., & Mostafa, E. (2023). Nanofiltration Membranes for the Removal of Heavy Metals from Aqueous Solutions: Preparations and Applications. *Membranes*, 13(9), 789. <https://doi.org/10.3390/membranes13090789>
- Mahmudov, K. T., Kopylovich, M. N., da Silva, M. F. C. G., & Pombeiro, A. J. (2017). Non-covalent interactions in the synthesis of coordination compounds: Recent advances. *Coordination Chemistry Reviews*, 345, 54–72.
- Mancilla, H. B., Cerrón, M. R., Aroni, P. G., Paucar, J. E. P., Tovar, C. T., Jindal, M. K., & Gowrisankar, G. (2022). Effective removal of Cr (VI) ions using low-cost biomass leaves (*Sambucus nigra* L.) in aqueous solution. *Environmental Science and Pollution Research*, 30(49), 106982–106995. <https://doi.org/10.1007/s11356-022-24064-8>
- Manoj, G. M., Shalini, M., Thenmozhi, K., Ponnusamy, V. K., & Hari, S. (2024). Recent advancements in the surface modification and functionalization of magnetic nanomaterials. *Applied Surface Science Advances*, 21, 100608.
- Manos, M. J., & Kanatzidis, M. G. (2016). Metal sulfide ion exchangers: Superior sorbents for the capture of toxic and nuclear waste-related metal ions. *Chemical Science*, 7(8), 4804–4824.
- Marcelo, L. R., De Gois, J. S., Da Silva, A. A., & Cesar, D. V. (2021). Synthesis of iron-based magnetic nanocomposites and applications in adsorption processes for water treatment: A review. *Environmental Chemistry Letters*, 19(2), 1229–1274. <https://doi.org/10.1007/s10311-020-01134-2>
- Mariana, M., HPS, A. K., Mistar, E. M., Yahya, E. B., Alfatah, T., Danish, M., & Amayreh, M. (2021). Recent advances in activated carbon modification techniques for enhanced heavy metal adsorption. *Journal of Water Process Engineering*, 43, 102221.

- Mariano, M., Chirat, C., El Kissi, N., & Dufresne, A. (2016). Impact of cellulose nanocrystal aspect ratio on crystallization and reinforcement of poly(butylene adipate- *co* -terephthalate). *Journal of Polymer Science Part B: Polymer Physics*, *54*(22), 2284–2297. <https://doi.org/10.1002/polb.24139>
- Masuku, M., Nure, J. F., Atagana, H. I., Hlongwa, N., & Nkambule, T. T. (2024). Advancing the development of nanocomposite adsorbent through zinc-doped nickel ferrite-pinecone biochar for removal of chromium (VI) from wastewater. *Science of the Total Environment*, *908*, 168136.
- Matsedisho, B., Otieno, B., Kabuba, J., Leswif, T., & Ochieng, A. (2024). Removal of Ni(II) from aqueous solution using chemically modified cellulose nanofibers derived from orange peels. *International Journal of Environmental Science and Technology*. <https://doi.org/10.1007/s13762-024-05819-x>
- Mautner, A. (2017). Efficient continuous removal of nitrates from water with cationic cellulose nanopaper membranes. *Resource-Efficient Technologies*, 1–7. <https://doi.org/10.1016/j.reffit.2017.01.005>
- Md Salim, R., Asik, J., & Sarjadi, M. S. (2021). Chemical functional groups of extractives, cellulose and lignin extracted from native *Leucaena leucocephala* bark. *Wood Science and Technology*, *55*(2), 295–313. <https://doi.org/10.1007/s00226-020-01258-2>
- Mennas, N., Lahreche, S., Chouli, F., Sabantina, L., & Benyoucef, A. (2023). Adsorption of Methylene Blue Dye by Cetyltrimethylammonium Bromide Intercalated Polyaniline-Functionalized Montmorillonite Clay Nanocomposite: Kinetics, Isotherms, and Mechanism Study. *Polymers*, *15*(17), 3518.
- Mishra, R. K. (2023). Fresh water availability and its global challenge. *British Journal of Multidisciplinary and Advanced Studies*, *4*(3), 1–78.
- Mohamad Sarbani, N. M., Hidayat, E., Naito, K., Mitoma, Y., & Harada, H. (2023). Cr (VI) and Pb (II) removal using crosslinking magnetite-carboxymethyl cellulose-chitosan hydrogel beads. *Gels*, *9*(8), 612.
- Mohamed, S. H., Hossain, M. S., Kassim, M. H. M., Balakrishnan, V., Habila, M. A., Zulkharnain, A., Zulkifli, M., & Yahaya, A. N. A. (2022). Biosorption of Cr (VI) using cellulose nanocrystals isolated from the waterless pulping of waste cotton cloths with supercritical CO₂: Isothermal, kinetics, and thermodynamics studies. *Polymers*, *14*(5), 887.
- Mohammed, N. (2017a). *Cellulose nanocrystals incorporated nanocomposites for water treatment applications*. <https://uwspace.uwaterloo.ca/handle/10012/11168>

- Mohammed, N. (2017b). *Cellulose nanocrystals incorporated nanocomposites for water treatment applications*. <https://uwspace.uwaterloo.ca/handle/10012/11168>
- Mohammed, N., Grishkewich, N., & Tam, K. C. (2018). Cellulose nanomaterials: Promising sustainable nanomaterials for application in water/wastewater treatment processes. *Environmental Science: Nano*, 5(3), 623–658.
- Mohan, I., Gorla, K., Dhar, S., Kothari, R., Bhau, B. S., & Pathania, D. (2021). Phytoremediation of Heavy Metals from the Biosphere Perspective and Solutions. In P. Singh, R. Singh, V. K. Singh, & R. Bhadouria (Eds.), *Pollutants and Water Management* (1st ed., pp. 95–127). Wiley. <https://doi.org/10.1002/9781119693635.ch5>
- Moini, N., Jahandideh, A., & Anderson, G. (2019). Inorganic Nanocomposite Hydrogels: Present Knowledge and Future Challenge. In Inamuddin, S. Thomas, R. Kumar Mishra, & A. M. Asiri (Eds.), *Sustainable Polymer Composites and Nanocomposites* (pp. 805–853). Springer International Publishing. https://doi.org/10.1007/978-3-030-05399-4_28
- Mourdikoudis, S., Kostopoulou, A., & LaGrow, A. P. (2021). Magnetic Nanoparticle Composites: Synergistic Effects and Applications. *Advanced Science*, 8(12), 2004951. <https://doi.org/10.1002/advs.202004951>
- Mudhoo, A., Mohan, D., Pittman Jr, C. U., Sharma, G., & Sillanpää, M. (2021). Adsorbents for real-scale water remediation: Gaps and the road forward. *Journal of Environmental Chemical Engineering*, 9(4), 105380.
- Mujahid, A., Afzal, A., & Dickert, F. L. (2023). Transitioning from supramolecular chemistry to molecularly imprinted polymers in chemical sensing. *Sensors*, 23(17), 7457.
- Mulwa, F., Li, Z., & Fangninou, F. F. (2021). Water scarcity in Kenya: Current status, challenges and future solutions. *Open Access Library Journal*, 8(1), 1–15.
- Munagapati, V. S., Wen, H.-Y., Gollakota, A. R., Wen, J.-C., Lin, K.-Y. A., Shu, C.-M., Reddy, G. M., Zyryanov, G. V., Wen, J.-H., & Tian, Z. (2022). Removal of sulfonated azo Reactive red 195 textile dye from liquid phase using surface-modified lychee (*Litchi chinensis*) peels with quaternary ammonium groups: Adsorption performance, regeneration, and mechanism. *Journal of Molecular Liquids*, 368, 120657.
- Musah, M., Azeh, Y., Mathew, J. T., Umar, M. T., Abdulhamid, Z., & Muhammad, A. I. (2022). Adsorption kinetics and isotherm models: A review. *CaJoST*, 4(1), 20–26.

- Mushtaq, F., Chen, X., Veciana, A., Hoop, M., Nelson, B. J., & Pané, S. (2022). Magnetolectric reduction of chromium (VI) to chromium (III). *Applied Materials Today*, 26, 101339.
- Musumba, G., Nakiguli, C., Lubanga, C., Mukasa, P., & Ntambi, E. (2020). Adsorption of lead (II) and copper (II) ions from mono synthetic aqueous solutions using bio-char from *Ficus natalensis* fruits. *Journal of Encapsulation and Adsorption Sciences*, 10(4), 71–84.
- Nagarajan, K. J., Ramanujam, N. R., Sanjay, M. R., Siengchin, Suchart., Surya Rajan, B., Sathick Basha, K., Madhu, P., & Raghav, G. R. (2021). A comprehensive review on cellulose nanocrystals and cellulose nanofibers: Pretreatment, preparation, and characterization. *Polymer Composites*, 42(4), 1588–1630. <https://doi.org/10.1002/pc.25929>
- Namasivayam, S. K. R., Prakash, P., Babu, V., Paul, E. J., Bharani, R. A., Kumar, J. A., Kavisri, M., & Moovendhan, M. (2023). Aquatic biomass cellulose fabrication into cellulose nanocomposite and its application in water purification. *Journal of Cleaner Production*, 136386.
- Nasrollahzadeh, M., Sajjadi, M., Irvani, S., & Varma, R. S. (2021). Starch, cellulose, pectin, gum, alginate, chitin and chitosan derived (nano) materials for sustainable water treatment: A review. *Carbohydrate Polymers*, 251, 116986.
- Nedylakova, M., Medinger, J., Mirabello, G., & Lattuada, M. (2024). Iron oxide magnetic aggregates: Aspects of synthesis, computational approaches and applications. *Advances in Colloid and Interface Science*, 323, 103056. <https://doi.org/10.1016/j.cis.2023.103056>
- Nguyen, M. D., Tran, H.-V., Xu, S., & Lee, T. R. (2021a). Fe₃O₄ nanoparticles: Structures, synthesis, magnetic properties, surface functionalization, and emerging applications. *Applied Sciences*, 11(23), 11301.
- Nguyen, M. D., Tran, H.-V., Xu, S., & Lee, T. R. (2021b). Fe₃O₄ nanoparticles: Structures, synthesis, magnetic properties, surface functionalization, and emerging applications. *Applied Sciences*, 11(23), 11301.
- Nidheesh, P. V., Couras, C., Karim, A. V., & Nadais, H. (2022). A review of integrated advanced oxidation processes and biological processes for organic pollutant removal. *Chemical Engineering Communications*, 209(3), 390–432. <https://doi.org/10.1080/00986445.2020.1864626>
- Niehs. (2010). *Endocrine Disruptors Fact Sheet*. May. <https://doi.org/10.1016/j.jmbbm.2010.09.004>

- Njora, B., & Yılmaz, H. (2021). Evaluation of water accessibility, distribution, water use policies and management in Kenya. *International Journal of Water Management and Diplomacy*, 1(3), 5–16.
- Noreña-Caro, D., & Alvarez-Láinez, M. (2016). Experimental design as a tool for the manufacturing of filtering media based on electrospun polyacrylonitrile/ β -cyclodextrin fibers. *International Journal on Interactive Design and Manufacturing (IJIDeM)*, 10(2), 153–164. <https://doi.org/10.1007/s12008-014-0241-4>
- Norrrahim, M. N. F., Knight, V. F., Nurazzi, N. M., Jenol, M. A., Misenan, M. S. M., Janudin, N., Kasim, N. A. M., Shukor, M. F. A., Ilyas, R. A., & Asyraf, M. R. M. (2022). The frontiers of functionalized nanocellulose-based composites and their application as chemical sensors. *Polymers*, 14(20), 4461.
- Obayomi, K. S., Bello, J. O., Yahya, M. D., Chukwunedum, E., & Adeoye, J. B. (2020). Statistical analyses on effective removal of cadmium and hexavalent chromium ions by multiwall carbon nanotubes (MWCNTs). *Heliyon*, 6(6). [https://www.cell.com/heliyon/fulltext/S2405-8440\(20\)31018-5](https://www.cell.com/heliyon/fulltext/S2405-8440(20)31018-5)
- Okasha, A. T., Abdel-Khalek, A. A., Alenazi, N. A., AlHammadi, A. A., Al Zoubi, W., Alhammadi, S., Ko, Y. G., & Abukhadra, M. R. (2023). Progress of synthetic cyclodextrins-based materials as effective adsorbents of the common water pollutants: Comprehensive review. *Journal of Environmental Chemical Engineering*, 11(3), 109824.
- Okrikata, E., & Nwosu, L. C. (2023). Heavy Metals and Pesticides as Hazardous Wastes and Strategies for Minimizing their Hazards. *Journal Homepage: Www. Ijrpr. Com ISSN, 2582, 7421*.
- Onyango, J., Babu, K., Njuguna, S., Wanzala, W., & Yan, X. (2020). Harnessing the potential of common water hyacinth as an industrial raw material for the production of quality biofuel briquettes. *SN Applied Sciences*, 2(8), 1316. <https://doi.org/10.1007/s42452-020-3109-1>
- Oskui, F. N., Aghdasinia, H., & Sorkhabi, M. G. (2019). Modeling and optimization of chromium adsorption onto clay using response surface methodology, artificial neural network, and equilibrium isotherm models. *Environmental Progress & Sustainable Energy*, 38(6), e13260.
- Ouyang, Y., Shinde, D., Mansell, R. S., & Harris, W. (1996). Colloid-enhanced transport of chemicals in subsurface environments: A review. *Critical Reviews in Environmental Science and Technology*, 26(2), 189–204. <https://doi.org/10.1080/10643389609388490>

- Pailhé, N., Wattiaux, A., Gaudon, M., & Demourgues, A. (2008). Impact of structural features on pigment properties of α -Fe₂O₃ haematite. *Journal of Solid State Chemistry*, 181(10), 2697–2704. <https://doi.org/10.1016/j.jssc.2008.06.049>
- Pakade, V. E., Tavengwa, N. T., & Madikizela, L. M. (2019). Recent advances in hexavalent chromium removal from aqueous solutions by adsorptive methods. *RSC Advances*, 9(45), 26142–26164. <https://doi.org/10.1039/C9RA05188K>
- Pandey, A., & Verma, R. K. (2018a). *Taxonomical and pharmacological status of Typha: A Review*. 3, 2101–2106.
- Pandey, A., & Verma, R. K. (2018b). Taxonomical and pharmacological status of Typha: A Review. *Annals of Plant Sciences*, 7(3), 2101–2106.
- Paniagua-Zambrana, N. Y., Bussmann, R. W., & Kikvidze, Z. (2024). *Typha angustifolia* L. *Typha latifolia* L. Typhaceae. In R. W. Bussmann, N. Y. Paniagua-Zambrana, & Z. Kikvidze (Eds.), *Ethnobotany of the Mountain Regions of Eastern Europe* (pp. 1–8). Springer International Publishing. https://doi.org/10.1007/978-3-030-98744-2_293-1
- Pathak, V., & Bhardwaj, K. K. (2021). *Industrial waste: The dark side of development*. AG Publishing House (AGPH Books). <https://books.google.com/books?hl=en&lr=&id=oiy8EAAAQBAJ&oi=fnd&pg=PA1&dq=Heavy+metal+contamination+exists+in+aqueous+wastes+of+many+industries,+such+as+metal+plating,+mining+operations,+tanneries,+radiator+manufacturing,+smelting,+alloy+industries+and+storage+batteries+industries+&ots=nbfyvyvcXq&sig=xCOfHxmnLB0aoeB8x4hWBgcymdk>
- Patro, A., Dwivedi, S., Panja, R., Saket, P., Gupta, S., Mittal, Y., Saeed, T., Martínez, F., & Yadav, A. K. (2023). Constructed wetlands for wastewater management: Basic design, abiotic and biotic components, and their interactive functions. In *Material-Microbes Interactions* (pp. 315–348). Elsevier. <https://www.sciencedirect.com/science/article/pii/B9780323951241000188>
- Pellicer, J. A., Rodríguez-López, M. I., Fortea, M. I., Gómez-López, V. M., Auñón, D., Núñez-Delicado, E., & Gabaldón, J. A. (2020). Synthesis of new cyclodextrin-based adsorbents to remove Direct Red 83: 1. *Polymers*, 12(9), 1880.
- Phan, M.-H., Alonso, J., Khurshid, H., Lampen-Kelley, P., Chandra, S., Stojak Repa, K., Nemat, Z., Das, R., Iglesias, Ó., & Srikanth, H. (2016). Exchange bias effects in iron oxide-based nanoparticle systems. *Nanomaterials*, 6(11), 221.
- Pholosi, A. (2019). *Synthesis, characterization and application of a novel biosorbent-magnetic nanomaterial cross-linked with cyclodextrin using epichlorohydrin and hexamethylene diisocyanate as adsorbents for heavy metals and organics* [PhD Thesis, Vaal University of Technology].

<http://digiresearch.vut.ac.za/bitstream/handle/10352/412/Agnes%20Pholosi's%20thesis.pdf?sequence=1>

- Pholosi, A., Naidoo, E. B., & Ofomaja, A. E. (2020). Intraparticle diffusion of Cr(VI) through biomass and magnetite coated biomass: A comparative kinetic and diffusion study. *South African Journal of Chemical Engineering*, *32*, 39–55. <https://doi.org/10.1016/j.sajce.2020.01.005>
- Phouthavong, V., Yan, R., Nijpanich, S., Hagio, T., Ichino, R., Kong, L., & Li, L. (2022a). Magnetic adsorbents for wastewater treatment: Advancements in their synthesis methods. *Materials*, *15*(3), 1053.
- Phouthavong, V., Yan, R., Nijpanich, S., Hagio, T., Ichino, R., Kong, L., & Li, L. (2022b). Magnetic adsorbents for wastewater treatment: Advancements in their synthesis methods. *Materials*, *15*(3), 1053.
- Pillai, S. B. (2024). Adsorption in Water and Used Water Purification. In J. Lahnsteiner (Ed.), *Handbook of Water and Used Water Purification* (pp. 99–120). Springer International Publishing. https://doi.org/10.1007/978-3-319-78000-9_4
- Poulson, B. G., Alsulami, Q. A., Sharfalddin, A., El Agammy, E. F., Mouffouk, F., Emwas, A.-H., Jaremko, L., & Jaremko, M. (2021a). Cyclodextrins: Structural, chemical, and physical properties, and applications. *Polysaccharides*, *3*(1), 1–31.
- Poulson, B. G., Alsulami, Q. A., Sharfalddin, A., El Agammy, E. F., Mouffouk, F., Emwas, A.-H., Jaremko, L., & Jaremko, M. (2021b). Cyclodextrins: Structural, chemical, and physical properties, and applications. *Polysaccharides*, *3*(1), 1–31.
- Pourhakkak, P., Taghizadeh, A., Taghizadeh, M., Ghaedi, M., & Haghdoost, S. (2021). Fundamentals of adsorption technology. In *Interface science and technology* (Vol. 33, pp. 1–70). Elsevier. <https://www.sciencedirect.com/science/article/pii/B9780128188057000011>
- Prasad, S., Yadav, K. K., Kumar, S., Gupta, N., Cabral-Pinto, M. M., Rezanian, S., Radwan, N., & Alam, J. (2021). Chromium contamination and effect on environmental health and its remediation: A sustainable approaches. *Journal of Environmental Management*, *285*, 112174.
- Priya, A. K., Yogeshwaran, V., Rajendran, S., Hoang, T. K., Soto-Moscoso, M., Ghfar, A. A., & Bathula, C. (2022). Investigation of mechanism of heavy metals (Cr⁶⁺, Pb²⁺ & Zn²⁺) adsorption from aqueous medium using rice husk ash: Kinetic and thermodynamic approach. *Chemosphere*, *286*, 131796.
- Qasem, N. A., Mohammed, R. H., & Lawal, D. U. (2021a). Removal of heavy metal ions from wastewater: A comprehensive and critical review. *Npj Clean Water*, *4*(1), 1–15.

- Qasem, N. A., Mohammed, R. H., & Lawal, D. U. (2021b). Removal of heavy metal ions from wastewater: A comprehensive and critical review. *Npj Clean Water*, 4(1), 36.
- Qin, D., Hu, W., & Zhang, L. (2024). Green synthesis of β -cyclodextrin conjugated Fe₃O₄/NiO nanocomposites and its synergistic effect of adsorption and photocatalytic degradation for Congo red removal. *Desalination and Water Treatment*, 317, 100136.
- Qu, J., Yuan, Y., Meng, Q., Zhang, G., Deng, F., Wang, L., Tao, Y., Jiang, Z., & Zhang, Y. (2020). Simultaneously enhanced removal and stepwise recovery of atrazine and Pb (II) from water using β -cyclodextrin functionalized cellulose: Characterization, adsorptive performance and mechanism exploration. *Journal of Hazardous Materials*, 400, 123142.
- Rahaman, M. H., Islam, M. A., Islam, M. M., Rahman, M. A., & Alam, S. N. (2021). Biodegradable composite adsorbent of modified cellulose and chitosan to remove heavy metal ions from aqueous solution. *Current Research in Green and Sustainable Chemistry*, 4, 100119.
- Rahimi Kord Sofla, M., Batchelor, W., Kosinkova, J., Pepper, R., Brown, R., & Rainey, T. (2019). Cellulose nanofibres from bagasse using a high speed blender and acetylation as a pretreatment. *Cellulose*, 26, 4799–4814.
- Raji, Z., Karim, A., Karam, A., & Khalloufi, S. (2023). Adsorption of heavy metals: Mechanisms, kinetics, and applications of various adsorbents in wastewater remediation—a review. *Waste*, 1(3), 775–805. <https://www.mdpi.com/2813-0391/1/3/46>
- Rani, B. S. J., & Venkatachalam, S. (2022). A neoteric approach for the complete valorization of Typha angustifolia leaf biomass: A drive towards environmental sustainability. *Journal of Environmental Management*, 318, 115579.
- Rani, S., Sharma, S., Bansal, M., Garg, R., & Garg, R. (2022). Enhanced Zn (II) adsorption by chemically modified sawdust based biosorbents. *Environmental Science and Pollution Research*, 1–16.
- Rápó, E., & Tonk, S. (2021). Factors affecting synthetic dye adsorption; desorption studies: A review of results from the last five years (2017–2021). *Molecules*, 26(17), 5419.
- Rasheed, T. (2022). Magnetic nanomaterials: Greener and sustainable alternatives for the adsorption of hazardous environmental contaminants. *Journal of Cleaner Production*, 362, 132338.

- Rashid, H., Mansoor, M. A., Haider, B., Nasir, R., Abd Hamid, S. B., & Abdulrahman, A. (2020). Synthesis and characterization of magnetite nano particles with high selectivity using in-situ precipitation method. *Separation Science and Technology*, 55(6), 1207–1215. <https://doi.org/10.1080/01496395.2019.1585876>
- Revellame, E. D., Fortela, D. L., Sharp, W., Hernandez, R., & Zappi, M. E. (2020). Adsorption kinetic modeling using pseudo-first order and pseudo-second order rate laws: A review. *Cleaner Engineering and Technology*, 1, 100032.
- Rezaei, B., Yari, P., Sanders, S. M., Wang, H., Chugh, V. K., Liang, S., Mostufa, S., Xu, K., Wang, J., Gómez-Pastora, J., & Wu, K. (2024). Magnetic Nanoparticles: A Review on Synthesis, Characterization, Functionalization, and Biomedical Applications. *Small*, 20(5), 2304848. <https://doi.org/10.1002/sml.202304848>
- Roohinejad, S., Oey, I., Everett, D. W., & Greiner, R. (2018). Microemulsions. In S. Roohinejad, R. Greiner, I. Oey, & J. Wen (Eds.), *Emulsion-based Systems for Delivery of Food Active Compounds* (1st ed., pp. 231–262). Wiley. <https://doi.org/10.1002/9781119247159.ch9>
- Rostami, P., Moradi, M. R., Pordsari, M. A., & Ghaemi, A. (2024). Carboxylic acid functionalized para-xylene based hypercrosslinked polymer as a novel and high performance adsorbent for heavy metal removal. *Arabian Journal of Chemistry*, 17(4), 105634.
- Rouhou, M. C., Abdelmoumen, S., Thomas, S., Attia, H., & Ghorbel, D. (2018). Use of green chemistry methods in the extraction of dietary fibers from cactus rackets (*Opuntia ficus indica*): Structural and microstructural studies. *International Journal of Biological Macromolecules*, 116, 901–910.
- Rout, P. R., Zhang, T. C., Bhunia, P., & Surampalli, R. Y. (2021). Treatment technologies for emerging contaminants in wastewater treatment plants: A review. *Science of the Total Environment*, 753, 141990.
- Roy, D., Semsarilar, M., Guthrie, J. T., & Perrier, S. (2009). Cellulose modification by polymer grafting: A review. *Chemical Society Reviews*, 38(7), 2046–2064.
- Rudzinski, W., & Plazinski, W. (2007). Theoretical description of the kinetics of solute adsorption at heterogeneous solid/solution interfaces: On the possibility of distinguishing between the diffusional and the surface reaction kinetics models. *Applied Surface Science*, 253(13), 5827–5840.
- Ruiz-Caldas, M.-X., Andrei, C. M., Evans, S., & De Lannoy, C.-F. (2020). The role of cellulose nanocrystals in stabilizing iron nanoparticles. *Cellulose*, 27(15), 8709–8724. <https://doi.org/10.1007/s10570-020-03384-3>

- saad Algarni, T., & Al-Mohaimeed, A. M. (2022). Water purification by adsorption of pigments or pollutants via metaloxide. *Journal of King Saud University-Science*, 34(8), 102339.
- Saha, P., & Chowdhury, S. (2011). Insight into adsorption thermodynamics. *Thermodynamics*, 16, 349–364.
- Salama, A., Abouzeid, R., Leong, W. S., Jeevanandam, J., Samyn, P., Dufresne, A., Bechelany, M., & Barhoum, A. (2021a). Nanocellulose-based materials for water treatment: Adsorption, photocatalytic degradation, disinfection, antifouling, and nanofiltration. *Nanomaterials*, 11(11), 3008.
- Salama, A., Abouzeid, R., Leong, W. S., Jeevanandam, J., Samyn, P., Dufresne, A., Bechelany, M., & Barhoum, A. (2021b). Nanocellulose-based materials for water treatment: Adsorption, photocatalytic degradation, disinfection, antifouling, and nanofiltration. *Nanomaterials*, 11(11), 3008.
- Saleh, T. A., Mustaqeem, M., & Khaled, M. (2022). Water treatment technologies in removing heavy metal ions from wastewater: A review. *Environmental Nanotechnology, Monitoring & Management*, 17, 100617.
- Salehi, M., Sharafoddinzadeh, D., Mokhtari, F., Esfandarani, M. S., & Karami, S. (2021). *Electrospun nanofibers for efficient adsorption of heavy metals from water and wastewater*. <https://ro.uow.edu.au/eispapers1/4568/>
- Sanka, P. M., Rwiza, M. J., & Mtei, K. M. (2020). Removal of selected heavy metal ions from industrial wastewater using rice and corn husk biochar. *Water, Air, & Soil Pollution*, 231, 1–13.
- Satyam, S., & Patra, S. (2024). Innovations and challenges in adsorption-based wastewater remediation: A comprehensive review. *Heliyon*. [https://www.cell.com/heliyon/fulltext/S2405-8440\(24\)05604-4](https://www.cell.com/heliyon/fulltext/S2405-8440(24)05604-4)
- Saxena, G., Purchase, D., Mulla, S. I., Saratale, G. D., & Bharagava, R. N. (2019). Phytoremediation of Heavy Metal-Contaminated Sites: Eco-environmental Concerns, Field Studies, Sustainability Issues, and Future Prospects. In P. De Voogt (Ed.), *Reviews of Environmental Contamination and Toxicology Volume 249* (Vol. 249, pp. 71–131). Springer International Publishing. https://doi.org/10.1007/398_2019_24
- Scanlon, B. R., Fakhreddine, S., Rateb, A., de Graaf, I., Famiglietti, J., Gleeson, T., Grafton, R. Q., Jobbagy, E., Kebede, S., & Kolusu, S. R. (2023). Global water resources and the role of groundwater in a resilient water future. *Nature Reviews Earth & Environment*, 4(2), 87–101.

- Schneider, H. (2009). Binding Mechanisms in Supramolecular Complexes. *Angewandte Chemie International Edition*, 48(22), 3924–3977. <https://doi.org/10.1002/anie.200802947>
- Schneider, H.-J. (2015). Dispersive Interactions in Solution Complexes. *Accounts of Chemical Research*, 48(7), 1815–1822. <https://doi.org/10.1021/acs.accounts.5b00111>
- Sehaqui, H., De Larraya, U. P., Liu, P., Pfenninger, N., Mathew, A. P., Zimmermann, T., & Tingaut, P. (2014). Enhancing adsorption of heavy metal ions onto biobased nanofibers from waste pulp residues for application in wastewater treatment. *Cellulose*, 21(4), 2831–2844. <https://doi.org/10.1007/s10570-014-0310-7>
- Sen, T. K., & Khilar, K. C. (2006). Review on subsurface colloids and colloid-associated contaminant transport in saturated porous media. *Advances in Colloid and Interface Science*, 119(2–3), 71–96.
- Shah, A. I., Dar, M. U. D., Bhat, R. A., Singh, J. P., Singh, K., & Bhat, S. A. (2020). Prospectives and challenges of wastewater treatment technologies to combat contaminants of emerging concerns. *Ecological Engineering*, 152, 105882.
- Shahrabadi, A., Daghbandan, A., & Arabiyoun, M. (2022). Experimental investigation of the adsorption process of the surfactant-nanoparticle combination onto the carbonate reservoir rock surface in the enhanced oil recovery (EOR) process. *Chemical Thermodynamics and Thermal Analysis*, 6, 100036.
- Shapiro, A. M. (2022). *Understanding morphological responses of Typha (cattail) species to nutrient pollution*. <https://scholarworks.uni.edu/etd/1251/>
- Sharma, H. K., & Bhasin, S. K. (2011). *Removal of Contaminants Using Plants a Review*. <http://gnanaganga.inflibnet.ac.in:8080/jspui/handle/123456789/10698>
- Sharma, S., & Malaviya, P. (2016). Bioremediation of tannery wastewater by chromium resistant novel fungal consortium. *Ecological Engineering*, 91, 419–425.
- Shchipunov, Y., & Postnova, I. (2018). Cellulose Mineralization as a Route for Novel Functional Materials. *Advanced Functional Materials*, 28(27), 1705042. <https://doi.org/10.1002/adfm.201705042>
- Sheha, R. R., & Metwally, E. (2007). Equilibrium isotherm modeling of cesium adsorption onto magnetic materials. *Journal of Hazardous Materials*, 143(1–2), 354–361.
- Sheikhi, A., Safari, S., Yang, H., & Van De Ven, T. G. M. (2015). Copper Removal Using Electrosterically Stabilized Nanocrystalline Cellulose. *ACS Applied Materials & Interfaces*, 7(21), 11301–11308. <https://doi.org/10.1021/acsami.5b01619>

- Sheikhi, A., & van de Ven, T. G. (2017). Colloidal aspects of Janus-like hairy cellulose nanocrystalloids. *Current Opinion in Colloid & Interface Science*, 29, 21–31.
- Shen, Z., Kuang, Y., Zhou, S., Zheng, J., & Ouyang, G. (2023). Preparation of magnetic adsorbent and its adsorption removal of pollutants: An overview. *TrAC Trends in Analytical Chemistry*, 117241.
- Shrestha, S., Wang, B., & Dutta, P. (2020). Nanoparticle processing: Understanding and controlling aggregation. *Advances in Colloid and Interface Science*, 279, 102162.
- Siddique, T., Dutta, N. K., & Roy Choudhury, N. (2020). Nanofiltration for Arsenic Removal: Challenges, Recent Developments, and Perspectives. *Nanomaterials*, 10(7), 1323. <https://doi.org/10.3390/nano10071323>
- Singh, J., & Mishra, V. (2021). Simultaneous removal of Cu²⁺, Ni²⁺ and Zn²⁺ ions using leftover *Azadirachta indica* twig ash. *Bioremediation Journal*, 25(1), 48–71. <https://doi.org/10.1080/10889868.2020.1843394>
- Singh, J., & Mishra, V. (2022). Development of sustainable and ecofriendly metal ion scavenger for adsorbing Cu²⁺, Ni²⁺ and Zn²⁺ ions from the aqueous phase. *Separation Science and Technology*, 57(3), 354–371. <https://doi.org/10.1080/01496395.2021.1913421>
- Siqueira, G., Bras, J., & Dufresne, A. (2010). Cellulosic bionanocomposites: A review of preparation, properties and applications. *Polymers*, 2(4), 728–765.
- Soliman, N. K., & Moustafa, A. F. (2020). Industrial solid waste for heavy metals adsorption features and challenges; a review. *Journal of Materials Research and Technology*, 9(5), 10235–10253.
- Stueber, D. D., Villanova, J., Aponte, I., Xiao, Z., & Colvin, V. L. (2021). Magnetic nanoparticles in biology and medicine: Past, present, and future trends. *Pharmaceutics*, 13(7), 943.
- Sun, L., Xu, G., Tu, Y., Zhang, W., Hu, X., Yang, P., Wu, D., Liang, Y., Wei, D., & Li, A. (2022). Multifunctional porous β -cyclodextrin polymer for water purification. *Water Research*, 222, 118917.
- Suopajärvi, T., Liimatainen, H., Karjalainen, M., Upola, H., & Niinimäki, J. (2015). Lead adsorption with sulfonated wheat pulp nanocelluloses. *Journal of Water Process Engineering*, 5, 136–142.
- Suter, E. K., Rutto, H. L., Seodigeng, T. S., Kiambi, S. L., & Omwoyo, W. N. (2024). Green isolation of cellulosic materials from recycled pulp and paper sludge: A Box-Behnken design optimization. *Journal of Environmental Science and Health, Part A*, 59(2), 64–75. <https://doi.org/10.1080/10934529.2024.2331942>

- Suter, E., Rutto, H., Seodigeng, T., Kiambi, L., & Omwoyo, W. (2024). Bagasse-Based Cellulose Nanocrystal–Magnetic Iron Oxide Nanocomposite for Removal of Chromium (VI) from Aqua Media. *Engineering Proceedings*, 67(1), 5.
- Sutherland, C., & Venkobachar, C. (2010). A diffusion-chemisorption kinetic model for simulating biosorption using forest macro-fungus, *fomes fasciatus*. *International Research Journal of Plant Science*, 1(4), 107–117.
- Syeda, H. I., Sultan, I., Razavi, K. S., & Yap, P.-S. (2022). Biosorption of heavy metals from aqueous solution by various chemically modified agricultural wastes: A review. *Journal of Water Process Engineering*, 46, 102446.
- Syeda, S. E. Z., Nowacka, D., Khan, M. S., & Skwierawska, A. M. (2022). Recent advancements in cyclodextrin-based adsorbents for the removal of hazardous pollutants from waters. *Polymers*, 14(12), 2341.
- Szczyglewska, P., Feliczak-Guzik, A., & Nowak, I. (2023). Nanotechnology–general aspects: A chemical reduction approach to the synthesis of nanoparticles. *Molecules*, 28(13), 4932.
- Tai, V. C., Che, H. X., Kong, X. Y., Ho, K. C., & Ng, W. M. (2023). Decoding iron oxide nanoparticles from design and development to real world application in water remediation. *Journal of Industrial and Engineering Chemistry*. https://www.sciencedirect.com/science/article/pii/S1226086X23004665?casa_token=U3W2xfLFHB4AAAAA:2i0WSIEaPTnC0N8p9ztSiTcu9Qtilojxu47BPVljl6Lx2HkYMCCanB39eBgUSdwLkJ2XYQJ86Q
- Tang, J., Sisler, J., Grishkewich, N., & Tam, K. C. (2017). Functionalization of cellulose nanocrystals for advanced applications. *Journal of Colloid and Interface Science*, 494, 397–409.
- Tang, Y., Yang, H., & Vignolini, S. (2022). Recent Progress in Production Methods for Cellulose Nanocrystals: Leading to More Sustainable Processes. *Advanced Sustainable Systems*, 6(3), 2100100. <https://doi.org/10.1002/adsu.202100100>
- Tapia-Orozco, N., Ibarra-Cabrera, R., Tecante, A., Gimeno, M., Parra, R., & Garcia-Arrazola, R. (2016). Removal strategies for endocrine disrupting chemicals using cellulose-based materials as adsorbents: A review. *Journal of Environmental Chemical Engineering*, 4(3), 3122–3142. <https://doi.org/10.1016/j.jece.2016.06.025>
- Tarchoun, A. F., Trache, D., Klapötke, T. M., Derradji, M., & Bessa, W. (2019). Ecofriendly isolation and characterization of microcrystalline cellulose from giant reed using various acidic media. *Cellulose*, 26(13), 7635–7651. <https://doi.org/10.1007/s10570-019-02672-x>

- Tayeb, A. H., Amini, E., Ghasemi, S., & Tajvidi, M. (2018a). Cellulose nanomaterials—Binding properties and applications: A review. *Molecules*, 23(10), 2684.
- Tayeb, A. H., Amini, E., Ghasemi, S., & Tajvidi, M. (2018b). Cellulose Nanomaterials—Binding Properties and Applications: A Review. *Molecules (Basel, Switzerland)*, 23(10), 2684. <https://doi.org/10.3390/molecules23102684>
- Tee, G. T., Gok, X. Y., & Yong, W. F. (2022a). Adsorption of pollutants in wastewater via biosorbents, nanoparticles and magnetic biosorbents: A review. *Environmental Research*, 212, 113248.
- Tee, G. T., Gok, X. Y., & Yong, W. F. (2022b). Adsorption of pollutants in wastewater via biosorbents, nanoparticles and magnetic biosorbents: A review. *Environmental Research*, 212, 113248.
- Tee, G. T., Gok, X. Y., & Yong, W. F. (2022c). Adsorption of pollutants in wastewater via biosorbents, nanoparticles and magnetic biosorbents: A review. *Environmental Research*, 212, 113248.
- Temkin, M. I. (1941). Adsorption equilibrium and the kinetics of processes on nonhomogeneous surfaces and in the interaction between adsorbed molecules. *Zh. Fiz. Chim.*, 15, 296–332.
- Tian, B., Hua, S., Tian, Y., & Liu, J. (2021). Cyclodextrin-based adsorbents for the removal of pollutants from wastewater: A review. *Environmental Science and Pollution Research*, 28(2), 1317–1340. <https://doi.org/10.1007/s11356-020-11168-2>
- Tlou, S., Suter, E., Alfred, M., Rutto, H., & Omwoyo, W. (2023). In situ capping of silver nanoparticles with cellulosic matrices from wheat straws in enhancing their antimicrobial activity: Synthesis and characterization. *Journal of Environmental Science and Health, Part A*, 58(11), 903–913. <https://doi.org/10.1080/10934529.2023.2260295>
- Trache, D., Hussin, M. H., Chuin, C. T. H., Sabar, S., Fazita, M. N., Taiwo, O. F., Hassan, T. M., & Haafiz, M. M. (2016a). Microcrystalline cellulose: Isolation, characterization and bio-composites application—A review. *International Journal of Biological Macromolecules*, 93, 789–804.
- Trache, D., Hussin, M. H., Chuin, C. T. H., Sabar, S., Fazita, M. N., Taiwo, O. F., Hassan, T. M., & Haafiz, M. M. (2016b). Microcrystalline cellulose: Isolation, characterization and bio-composites application—A review. *International Journal of Biological Macromolecules*, 93, 789–804.
- Trache, D., Hussin, M. H., Haafiz, M. M., & Thakur, V. K. (2017). Recent progress in cellulose nanocrystals: Sources and production. *Nanoscale*, 9(5), 1763–1786.

- Trache, D., Tarchoun, A. F., Derradji, M., Hamidon, T. S., Masruchin, N., Brosse, N., & Hussin, M. H. (2020). Nanocellulose: From fundamentals to advanced applications. *Frontiers in Chemistry*, 8, 392.
- Tripathi, G., Husain, A., Ahmad, S., Hasan, Z., & Farooqui, A. (2021). Contamination of water resources in industrial zones. In *Contamination of water* (pp. 85–98). Elsevier.
<https://www.sciencedirect.com/science/article/pii/B9780128240588000177>
- Trotta, F., Zanetti, M., & Camino, G. (2000). Thermal degradation of cyclodextrins. *Polymer Degradation and Stability*, 69(3), 373–379.
- Tseng, R.-L., Wu, F.-C., & Juang, R.-S. (2010). Characteristics and applications of the Lagergren's first-order equation for adsorption kinetics. *Journal of the Taiwan Institute of Chemical Engineers*, 41(6), 661–669.
- Tufail, T., Saeed, F., Afzaal, M., Ain, H. B. U., Gilani, S. A., Hussain, M., & Anjum, F. M. (2021). Wheat straw: A natural remedy against different maladies. *Food Science & Nutrition*, 9(4), 2335–2344. <https://doi.org/10.1002/fsn3.2030>
- Ullah, M. W., Manan, S., Ul-Islam, M., Revin, V. V., Thomas, S., & Yang, G. (2021). Introduction to nanocellulose. In *Nanocellulose: Synthesis, structure, properties and applications* (pp. 1–50). World Scientific.
- Urooj, T., Mishra, M., & Pandey, S. (2024). Unlocking environmental solutions: A review of cyclodextrins in pollutant removal. *Discover Environment*, 2(1), 65. <https://doi.org/10.1007/s44274-024-00090-w>
- Vallinayagam, S., Rajendran, K., Lakkaboyana, S. K., Soontarapa, K., Remya, R. R., Sharma, V. K., Kumar, V., Venkateswarlu, K., & Koduru, J. R. (2021). Recent developments in magnetic nanoparticles and nano-composites for wastewater treatment. *Journal of Environmental Chemical Engineering*, 9(6), 106553.
- Varan, G. (2023). Cyclodextrin in vaccines: Enhancing Efficacy and Stability. *Future Pharmacology*, 3(3), 597–611.
- Villabona-Ortíz, Á., Figueroa-Lopez, K. J., & Ortega-Toro, R. (2022). Kinetics and adsorption equilibrium in the removal of azo-anionic dyes by modified cellulose. *Sustainability*, 14(6), 3640.
- Vilén, A., Laurell, P., & Vahala, R. (2022). Comparative life cycle assessment of activated carbon production from various raw materials. *Journal of Environmental Management*, 324, 116356.
- Visaveliya, N. R., & Köhler, J. M. (2021). Hierarchical Assemblies of Polymer Particles through Tailored Interfaces and Controllable Interfacial Interactions. *Advanced Functional Materials*, 31(9), 2007407. <https://doi.org/10.1002/adfm.202007407>

- Vo, L. Q., Vu, A.-T., Le, T. D., Huynh, C. D., & Tran, H. V. (2024). Fe₃O₄/Graphene Oxide/Chitosan Nanocomposite: A Smart Nanosorbent for Lead(II) Ion Removal from Contaminated Water. *ACS Omega*, *acsomega.4c00486*. <https://doi.org/10.1021/acsomega.4c00486>
- Vo, T. S., Hossain, M. M., Jeong, H. M., & Kim, K. (2020). Heavy metal removal applications using adsorptive membranes. *Nano Convergence*, *7*(1), 36. <https://doi.org/10.1186/s40580-020-00245-4>
- Voisin, H., Bergström, L., Liu, P., & Mathew, A. P. (2017). Nanocellulose-based materials for water purification. *Nanomaterials*, *7*(3), 57.
- Wadhawan, S., Jain, A., Nayyar, J., & Mehta, S. K. (2020). Role of nanomaterials as adsorbents in heavy metal ion removal from waste water: A review. *Journal of Water Process Engineering*, *33*, 101038.
- Wahid, F., Zhao, X.-J., Jia, S.-R., Bai, H., & Zhong, C. (2020). Nanocomposite hydrogels as multifunctional systems for biomedical applications: Current state and perspectives. *Composites Part B: Engineering*, *200*, 108208.
- Wang, J., & Guo, X. (2023). Adsorption kinetics and isotherm models of heavy metals by various adsorbents: An overview. *Critical Reviews in Environmental Science and Technology*, *53*, 1–29. <https://doi.org/10.1080/10643389.2023.2221157>
- Wang, L., Shi, C., Pan, L., Zhang, X., & Zou, J.-J. (2020). Rational design, synthesis, adsorption principles and applications of metal oxide adsorbents: A review. *Nanoscale*, *12*(8), 4790–4815.
- Wang, L., Ji, H., Wang, S., Kong, L., Jiang, X., & Yang, G. (2013). Preparation of Fe₃O₄ with high specific surface area and improved capacitance as a supercapacitor. *Nanoscale*, *5*(9), 3793–3799.
- Warmiati, W., & Wijayanti, W. (2024). Reaction Stability Test of Hexavalent Chromium Complex with 1, 5-Diphenylcarbazide in Analysis using UV Visible Spectrophotometer. *Indonesian Journal of Chemical Research*, *11*(3), 218–222.
- Water, Sanitation and Hygiene | UNICEF Kenya*. (n.d.). Retrieved August 6, 2024, from <https://www.unicef.org/kenya/water-sanitation-and-hygiene>
- Wilcox, D. A., Buckler, K. A., Wilcox, D. A., & Buckler, K. (2017). *Controlling Cattail Invasion in Sedge / Grass Meadows*. December. <https://doi.org/10.1007/s13157-017-0971-8>
- World Water Day 2023: Access to Clean Water Remains a Challenge*. (n.d.). Greenpeace Africa. Retrieved August 6, 2024, from <https://www.greenpeace.org/africa/en/blogs/53365/world-water-day-2023-access-to-clean-water-remains-a-challenge/>

- Wu, F.-C., Tseng, R.-L., & Juang, R.-S. (2009). Initial behavior of intraparticle diffusion model used in the description of adsorption kinetics. *Chemical Engineering Journal*, 153(1–3), 1–8.
- Wu, Y., Jia, Z., Bo, C., & Dai, X. (2021). Preparation of magnetic β -cyclodextrin ionic liquid composite material with different ionic liquid functional group substitution contents and evaluation of adsorption performance for anionic dyes. *Colloids and Surfaces A: Physicochemical and Engineering Aspects*, 614, 126147.
- Xiao, W., Sun, R., Hu, S., Meng, C., Xie, B., Yi, M., & Wu, Y. (2023). Recent advances and future perspective on lignocellulose-based materials as adsorbents in diverse water treatment applications. *International Journal of Biological Macromolecules*, 126984.
- Xie, H., Du, H., Yang, X., & Si, C. (2018). Recent Strategies in Preparation of Cellulose Nanocrystals and Cellulose Nanofibrils Derived from Raw Cellulose Materials. *International Journal of Polymer Science*, 2018, 1–25. <https://doi.org/10.1155/2018/7923068>
- Xing, X., Alharbi, N. S., Ren, X., & Chen, C. (2022). A comprehensive review on emerging natural and tailored materials for chromium-contaminated water treatment and environmental remediation. *Journal of Environmental Chemical Engineering*, 10(2), 107325.
- Xu, Q., Huang, X., Guo, L., Wang, Y., & Jin, L. (2021). Enhancing removal of Cr (VI), Pb²⁺, and Cu²⁺ from aqueous solutions using amino-functionalized cellulose nanocrystal. *Molecules*, 26(23), 7315.
- Xu, X., Ouyang, X., & Yang, L.-Y. (2021). Adsorption of Pb (II) from aqueous solutions using crosslinked carboxylated chitosan/carboxylated nanocellulose hydrogel beads. *Journal of Molecular Liquids*, 322, 114523.
- Xu, Y., Atrous, A., & Stokes, J. R. (2020). A review of nanocrystalline cellulose suspensions: Rheology, liquid crystal ordering and colloidal phase behaviour. *Advances in Colloid and Interface Science*, 275, 102076.
- Xu, Y., Rashwan, A. K., Osman, A. I., Abd El-Monaem, E. M., Elgarahy, A. M., Eltaweil, A. S., Omar, M., Li, Y., Mehanni, A.-H. E., Chen, W., & Rooney, D. W. (2023). Synthesis and potential applications of cyclodextrin-based metal–organic frameworks: A review. *Environmental Chemistry Letters*, 21(1), 447–477. <https://doi.org/10.1007/s10311-022-01509-7>
- Yadav, C., Lee, J.-M., Mohanty, P., Li, X.-P., & Jang, W.-D. (2023). Graft onto approaches for nanocellulose-based advanced functional materials. *Nanoscale*. <https://pubs.rsc.org/en/content/articlehtml/2023/nr/d3nr03087c>

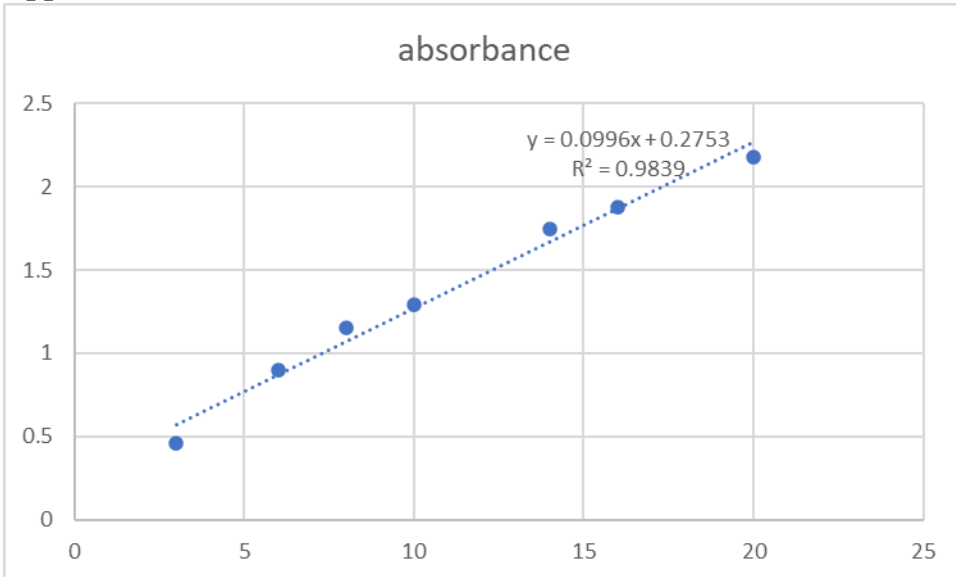
- Yadav, C., Saini, A., & Maji, P. K. (2018). Cellulose nanofibres as biomaterial for nano-reinforcement of poly[styrene-(ethylene-co-butylene)-styrene] triblock copolymer. *Cellulose*, 25(1), 449–461. <https://doi.org/10.1007/s10570-017-1567-4>
- Yaghoobi, M., Asjadi, F., & Sanikhani, M. (2023). A facile one-step green hydrothermal synthesis of paramagnetic Fe₃O₄ nanoparticles with highly efficient dye removal. *Journal of the Taiwan Institute of Chemical Engineers*, 144, 104774.
- Yamauchi, T., Shimamura, S., Nakazono, M., & Mochizuki, T. (2013a). Aerenchyma formation in crop species: A review. *Field Crops Research*, 152, 8–16. <https://doi.org/10.1016/j.fcr.2012.12.008>
- Yamauchi, T., Shimamura, S., Nakazono, M., & Mochizuki, T. (2013b). Aerenchyma formation in crop species: A review. *Field Crops Research*, 152, 8–16.
- Yang, X., Wan, Y., Zheng, Y., He, F., Yu, Z., Huang, J., Wang, H., Ok, Y. S., Jiang, Y., & Gao, B. (2019). Surface functional groups of carbon-based adsorbents and their roles in the removal of heavy metals from aqueous solutions: A critical review. *Chemical Engineering Journal*, 366, 608–621.
- Yi, Q., Lu, S., Fan, Y., Cheng, D., Wang, X., Cheng, S., & Xie, H. (2022). Preparation and adsorption performance of cellulose nanofibrils/polyvinyl alcohol composite gel spheres with millimeter size. *Carbohydrate Polymers*, 277, 118850.
- Yin, X., Xu, P., & Wang, H. (2024). Efficient and selective removal of heavy metals and dyes from aqueous solutions using guipi residue-based hydrogel. *Gels*, 10(2), 142.
- Ying, S., Guan, Z., Ofoegbu, P. C., Clubb, P., Rico, C., He, F., & Hong, J. (2022). Green synthesis of nanoparticles: Current developments and limitations. *Environmental Technology & Innovation*, 26, 102336.
- Yu, X., Tong, S., Ge, M., Wu, L., Zuo, J., Cao, C., & Song, W. (2013). Adsorption of heavy metal ions from aqueous solution by carboxylated cellulose nanocrystals. *Journal of Environmental Sciences*, 25(5), 933–943.
- Yuan, J., & Lu, W. (2024). Adsorption of Cr (VI) from aqueous solutions using inorganic clays modified magnetic chitosan adsorbent: Kinetic and thermodynamic study. *Desalination and Water Treatment*, 100442.
- Yuan, X., Li, J., Luo, L., Zhong, Z., & Xie, X. (2023). Advances in sorptive removal of hexavalent chromium (Cr (VI)) in aqueous solutions using polymeric materials. *Polymers*, 15(2), 388.
- Zadehnazari, A. (2024). Chemical synthesis strategies for metal oxide nanoparticles: A comprehensive review. *Inorganic and Nano-Metal Chemistry*, 1–40. <https://doi.org/10.1080/24701556.2024.2354926>

- Zaimee, M. Z. A., Sarjadi, M. S., & Rahman, M. L. (2021). Heavy metals removal from water by efficient adsorbents. *Water*, *13*(19), 2659.
- Zamani Kouhpanji, M. R., & Stadler, B. J. (2020). A guideline for effectively synthesizing and characterizing magnetic nanoparticles for advancing nanobiotechnology: A review. *Sensors*, *20*(9), 2554.
- Zapata-Morales, A. L., Vega-Rodríguez, S., Hernández-Morales, A., Leyva-Ramos, S., & Soria-Guerra, R. E. (2023). Efficiency of Cattail to Remove a Mixture of Pharmaceuticals in a Constructed Wetland. *Journal of the Mexican Chemical Society*, *67*(1), 1–11.
- Zhang, J., Lin, S., Han, M., Su, Q., Xia, L., & Hui, Z. (2020). Adsorption properties of magnetic magnetite nanoparticle for coexistent Cr (VI) and Cu (II) in mixed solution. *Water*, *12*(2), 446.
- Zhang, J., & Zou, W. (2019). A novel method for Isolating Nanocrystalline Cellulose from Eucalyptus Hardwood. *Journal of Analytical Sciences, Methods and Instrumentation*, *9*(3), 51–62.
- Zhang, S., Sun, B., Wang, W., Zhu, M., & Chen, J. (2006). Adsorption of Cd²⁺ and Cu²⁺ by Oxidized Cellulose from TEMPO-mediated Selective Oxidation of Alkaline Natural Cellulose Pulp. *Journal of Macromolecular Science, Part A*, *43*(11), 1895–1906. <https://doi.org/10.1080/10601320600941318>
- Zhang, X., Yelle, D. J., Kitin, P., Tong, G., & Zhu, J. Y. (2024). Producing Cellulose Microfibrils at a High Solid Content with and without Mechanical or Enzymatic Pretreatment. *Biomacromolecules*, *25*(4), 2509–2519. <https://doi.org/10.1021/acs.biomac.3c01457>
- Zhang, Y., Zhang, Y., Xu, W., Wu, H., Shao, Y., Han, X., Zhou, M., Gu, P., & Li, Z. (2023a). Preparation methods of cellulose nanocrystal and its application in treatment of environmental pollution: A mini-review. *Colloid and Interface Science Communications*, *53*, 100707.
- Zhang, Y., Zhang, Y., Xu, W., Wu, H., Shao, Y., Han, X., Zhou, M., Gu, P., & Li, Z. (2023b). Preparation methods of cellulose nanocrystal and its application in treatment of environmental pollution: A mini-review. *Colloid and Interface Science Communications*, *53*, 100707.
- Zhao, F., & Sillanpää, M. (2020). Cross-linked chitosan and β-cyclodextrin as functional adsorbents in water treatment. In *Advanced Water Treatment* (pp. 161–264). Elsevier. <https://www.sciencedirect.com/science/article/pii/B9780128192160000035>

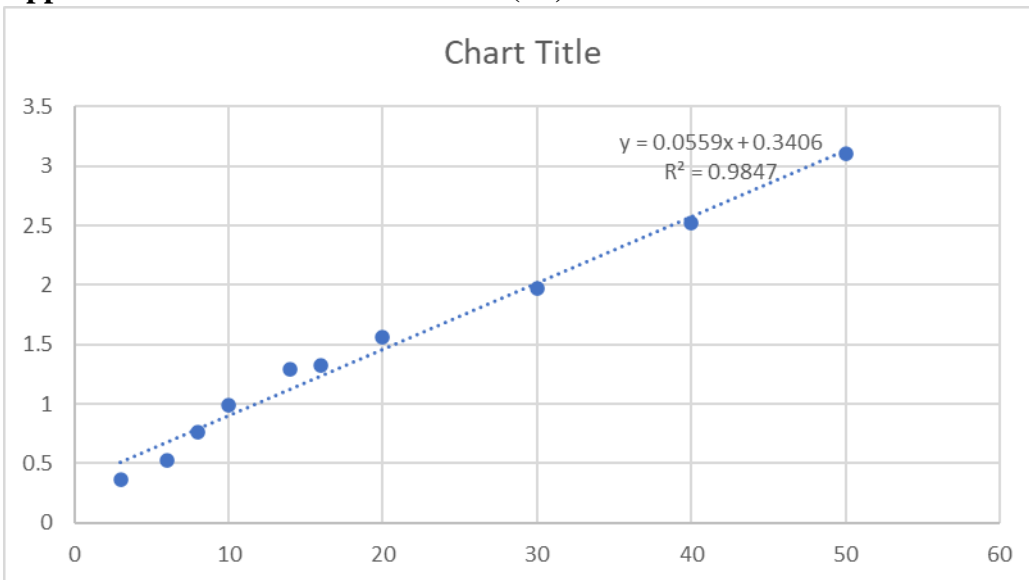
- Zhao, X., Lv, L., Pan, B., Zhang, W., Zhang, S., & Zhang, Q. (2011). Polymer-supported nanocomposites for environmental application: A review. *Chemical Engineering Journal*, *170*(2–3), 381–394.
- Zhao, Y., Shi, H., Du, Z., Zhou, J., & Yang, F. (2023). Removal of As(V) from aqueous solution using modified Fe₃O₄ nanoparticles. *Royal Society Open Science*, *10*(1), 220988. <https://doi.org/10.1098/rsos.220988>
- Zhou, Y., Fu, S., Zhang, L., Zhan, H., & Levit, M. V. (2014). Use of carboxylated cellulose nanofibrils-filled magnetic chitosan hydrogel beads as adsorbents for Pb (II). *Carbohydrate Polymers*, *101*, 75–82.
- Zhuang, F., Huang, J., Li, H., Peng, X., Xia, L., Zhou, L., Zhang, T., Liu, Z., He, Q., & Luo, F. (2023). Biogeochemical behavior and pollution control of arsenic in mining areas: A review. *Frontiers in Microbiology*, *14*, 1043024.
- Zielińska-Jurek, A., Reszczyńska, J., Grabowska, E., & Zaleska, A. (2012). Nanoparticles preparation using microemulsion systems. *Microemulsions-an Introduction to Properties and Applications*, 229–250.
- Zimmermann, T., Pöhler, E., & Schwaller, P. (2005). Mechanical and Morphological Properties of Cellulose Fibril Reinforced Nanocomposites. *Advanced Engineering Materials*, *7*(12), 1156–1161. <https://doi.org/10.1002/adem.200500157>
- Zubair, N. A., Moawia, R. M., Nasef, M. M., Hubbe, M., & Zakeri, M. (2022). A Critical Review on Natural Fibers Modifications by Graft Copolymerization for Wastewater Treatment. *Journal of Polymers and the Environment*, *30*(4), 1199–1227. <https://doi.org/10.1007/s10924-021-02269-1>

APPENDICES

Appendix 1: Calibration curve of Cr (VI) : time studies



Appendix 2: Calibration curve of Cr (VI) : time studies: concentration studies



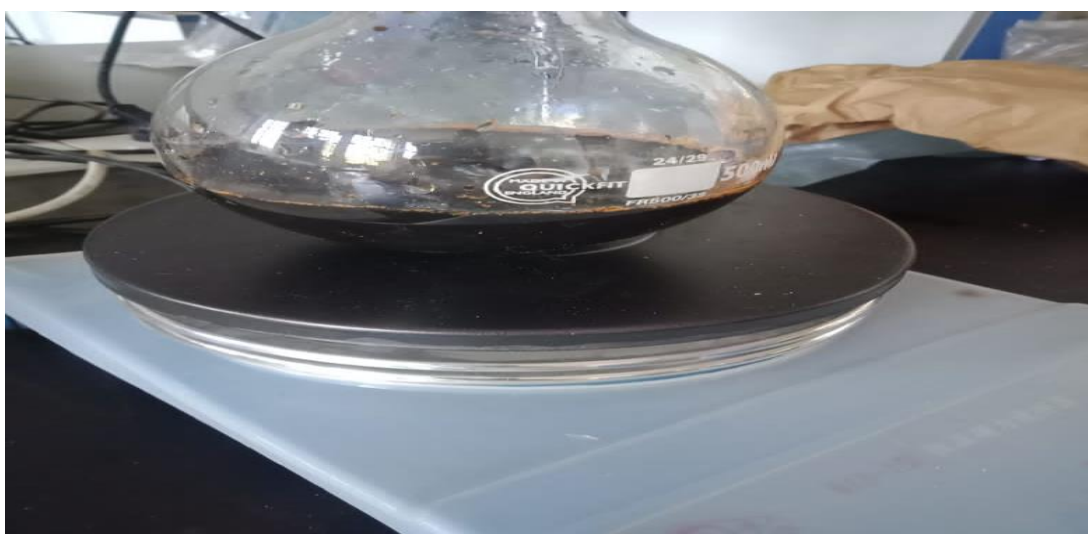
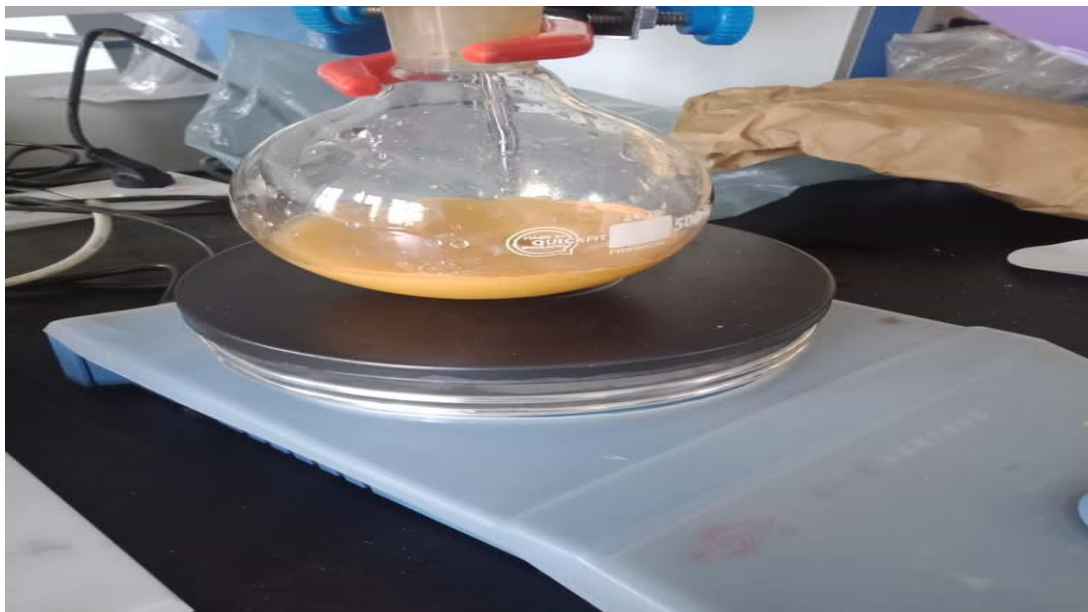
Appendix 3: Prepared adsorbents for characterization



Appendix 4: Adsorption studies



Appendix 5: preparation of Iron oxide nanoparticles



Appendix 6: Published paper 1 abstract

Isolative Synthesis and Characterization of Cellulose and Cellulose Nanocrystals from *Typha angustifolia*

Lynda S. Mesopirri¹, Evans K. Suter^{1,2}, Wesley N. Omwoyo^{1,2*}, Nathan M. Oyaró¹, Simphiwe M. Nelana²

¹Department of Mathematics and Physical Science, Maasai Mara University, Narok, Kenya

²Biotechnology and Chemistry Department, Vaal University of Technology, Vanderbijlpark, South Africa

Email: *wesleyomwoyo@mmarau.ac.ke

How to cite this paper: Mesopirri, L.S., Suter, E.K., Omwoyo, W.N., Oyaró, N.M. and Nelana, S.M. (2024) Isolative Synthesis and Characterization of Cellulose and Cellulose Nanocrystals from *Typha angustifolia*. *Open Journal of Applied Sciences*, 14, 2443-2459. <https://doi.org/10.4236/ojapps.2024.149161>

Received: July 18, 2024

Accepted: September 8, 2024

Published: September 11, 2024

Copyright © 2024 by author(s) and Scientific Research Publishing Inc.

This work is licensed under the Creative Commons Attribution International License (CC BY 4.0).

<http://creativecommons.org/licenses/by/4.0/>



Abstract

The application potential of cellulosic materials in natural composites and other fields needs to be explored to develop innovative, sustainable, lightweight, functional biomass materials that are also environmentally friendly. This study investigated *Typha angustifolia* (*Typha* sp.) as a potential new raw material for extracting cellulose nanocrystals (CNCs) for application in wastewater treatment composites. Alkaline treatments and bleaching were used to remove cellulose from the stem fibres. The CNCs were then isolated from the recovered cellulose using acid hydrolysis. The study showed a few distinct functional groups (O-H, -C-H, =C-H and C-O, and C-O-C) in the Fourier Transform Infrared (FTIR) spectra. A scanning electron microscope (SEM) revealed the smooth surface of CPC and CNCs, which resulted from removing lignin and hemicellulose from powdered *Typha angustifolia*. Based on the crystalline index, the powdered *Typha angustifolia*, CPC, and CNCs were 42.86%, 66.94% and 77.41%. The loss of the amorphous section of the *Typha* sp. fibre resulted in a decrease in particle size. It may be inferred from the features of a *Typha* sp. CNC that CNCs may be employed as reinforcement in composites for wastewater treatment.

Keywords


Typha angustifolia, Cellulose, Acid Hydrolysis, Chemically Purified Cellulose, Cellulose Nanocrystals

Appendix 7: Published paper 2 abstract

JOURNAL OF ENVIRONMENTAL SCIENCE AND HEALTH, PART A
<https://doi.org/10.1080/10934529.2024.2424084>



Preparation and characterization of β -cyclodextrin capped magnetic nanoparticles anchored on cellulosic matrix for removal of Cr(VI) from mimicked wastewater: Adsorption and kinetic studies

Lynda S. Mesopir^a, Evans K. Suter^{a,b}, Wesley N. Omwoyo^{a,b} , Nathan M. Oyaro^a, and Simphiwe M. Nelana^b

^aDepartment of Mathematics and Physical Science, Maasai Mara University, Narok, Kenya; ^bBiotechnology and Chemistry Department, Vaal University of Technology, Vanderbijlpark, South Africa

ABSTRACT

Hexavalent Chromium (Cr(VI)) is essential in many industrial processes. However, it finds its way into water bodies, posing health problems, including lung cancer and the inhibition of DNA and RNA in biological systems. Several chemical and traditional water purification methods have been developed in the past, but most are expensive, tedious and ineffective. This study aimed to prepare and characterize a low-cost hybrid adsorbent, β -Cyclodextrin capped magnetic nanoparticles anchored on a cellulosic matrix (CNC-Fe₃O₄NP-CD). The characterization techniques confirmed the integration of CNCs, Fe₃O₄NP and CD into the prepared CNC-Fe₃O₄NP-CD nanocomposite adsorbent. The adsorbent was employed in batch adsorption experiments by varying adsorption parameters, including solution pH, adsorbent dosage, initial Cr(VI) concentration, and contact time. From the findings, the nanocomposite adsorbent achieved a maximum Cr(VI) removal efficiency of 97.45%, while the pseudo-second-order kinetic model best fitted the experimental data with high linear regression coefficients ($R^2 > 0.98$). The Elovich model indicated that the adsorption process was driven by chemisorption on heterogeneous surface sites, with initial sorption rates surpassing desorption rates. These findings established that CNC-Fe₃O₄NP-CD presents high efficiency for Cr(VI) removal under acidic pH, offering the potential for optimization and application in real-world wastewater treatment.

ARTICLE HISTORY

Received 15 September 2024
Accepted 28 October 2024

KEYWORDS

Typha angustifolia;
adsorption; wastewater
treatment; hexavalent
chromium; nanocomposite;
kinetics